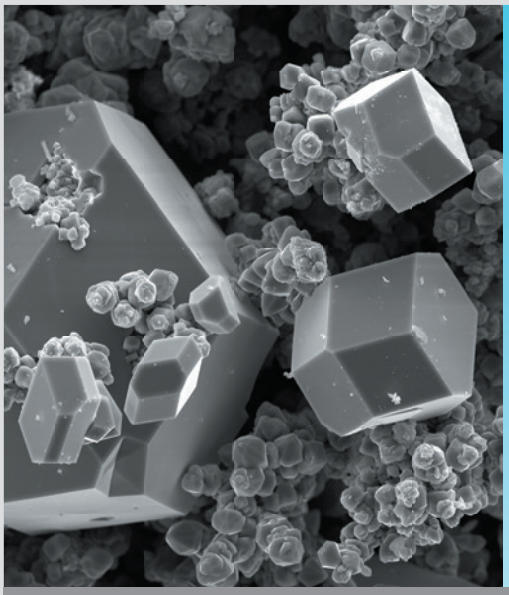

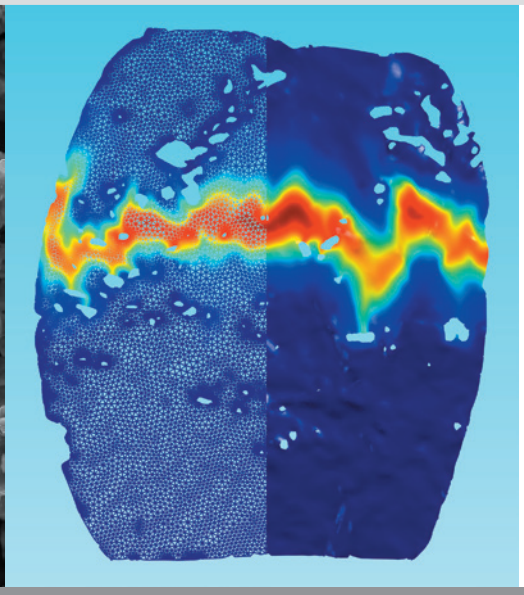

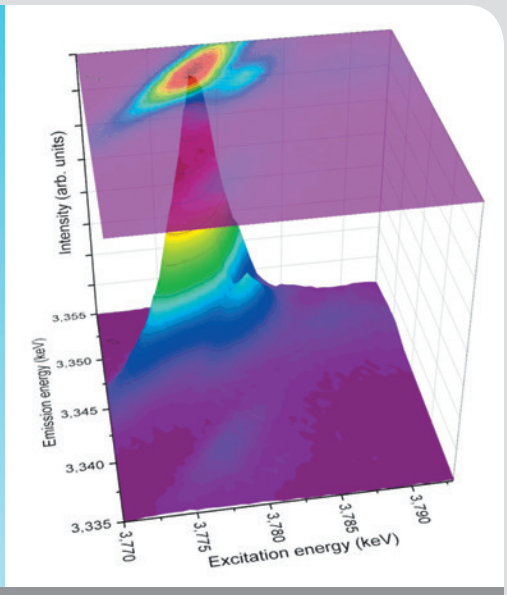

KIT SCIENTIFIC REPORTS 7709

Annual Report 2014

Institute for Nuclear Waste Disposal
Institut für Nukleare Entsorgung

H. Geckeis, M. Altmaier, S. Fanghänel (eds.)

KIT Scientific Publishing

H. Geckeis, M. Altmaier, S. Fanghänel (eds.)

Annual Report 2014

Institute for Nuclear Waste Disposal
Institut für Nukleare Entsorgung

Cover illustration

left: ESEM image of magnetite crystals grown during corrosion of fine grained steel in saturated NaCl (CaSO4) "M3" brine (662 days, 150 °C, 6 bar), size of large crystal about 150 µm.

middle: Modelled transport of a solute pulse front through a single fractured drill core. Due to the complex 3D flow field within the fracture the tracer migration is governed by heterogeneous hydrodynamic dispersion. Wireframe (left part) depicts the numerical mesh used in the simulation. Colors represent tracer concentrations (blue: high concentration, red: low concentration)

right: 3d4f RIXS map of Pu(VI) in aqueous solution recorded at the ANKA INE-Beamline for radionuclide research

Karlsruhe Institute of Technology
KIT SCIENTIFIC REPORTS 7709

Annual Report 2014

Institute for Nuclear Waste Disposal
Institut für Nukleare Entsorgung

by
H. Geckeis, M. Altmaier, S. Fanghänel (eds.)

KIT Scientific Publishing

Report-Nr. KIT-SR 7709

Impressum

Scientific Publishing

Karlsruher Institut für Technologie (KIT)
KIT Scientific Publishing
Straße am Forum 2
D-76131 Karlsruhe

www.ksp.kit.edu

Print on Demand 2015

ISSN 1869-9669

Foreword

Prof. Dr. Horst Geckeis

Director of the Institute for Nuclear Waste Disposal

2014 was another very important and successful year for the Institute for Nuclear Waste Disposal. In spring 2014 the R&D activities of INE within the Helmholtz Program "Nuclear Waste Management and Safety as well as Radiation Research (NUSAFE)" were reviewed for the third time in the course of the "Program Oriented Funding (POF)" evaluation. The members of the international review panel stated clearly that the research results as well as the proposed research strategy in the field of nuclear waste management are "outstanding and on a world-class level" (extracted from: NUSAFE evaluation report). This very positive rating of INE research stated by internationally accepted experts provides an ideal basis and a strong motivation to start into the new POF period starting from beginning 2015 and running for 5 years.

The scientific report in hand again shows features of INE research activities: Projects are strongly embedded into national and international collaborative projects and range from applied technology development to very fundamental science partly applying state-of-the-art spectroscopic techniques and theoretical approaches. Topics span from aquatic environmental radionuclide science, waste conditioning, separation chemistry and radiation protection issues. INE-scientists are involved in teaching activities and the organization of international workshops and conferences on various topics related to our research. Numerous publications in peer-reviewed international journals and presentations at international conferences document their visibility.

In addition, INE has expanded its portfolio to two new research fields. Dr. Eva Schill will set up a working group for research activities in the field of "Geoenergy". Prof. Dr. Sascha Gentes heads the group "Decommissioning of Conventional and Nuclear Facilities" at the Institute for Technology and Management in Construction and will be integrated with part of his nuclear decommissioning activities into the INE research program. Both research fields together with the investigations related to nuclear waste disposal and radiation protection are perfectly in line with the German "Energiewende" policy. Our research contributes to various aspects of a safe nuclear phase-out strategy in Germany and to the safe utilization of regenerative geoenergy sources such as geothermal energy.

By the end of 2014 Dr. Klaus Gompper the long-standing deputy director of INE and head of the department "Scientific/Technical Coordination, Analytical Chemistry" left the institute. Dr. Gompper can look back on a successful career and I would like to thank him for his support and tireless dedication to our institute.

His successor is Prof. Dr. Thorsten Schäfer who was appointed as KIT Professor within the Department of Civil Engineering, Geo and Environmental Sciences in 2014. Prof. Schäfer is teaching in the field of environmental geology and at INE he is heading the department of Geochemistry.

Since 2013 KIT-INE is founding member of the "Deutsche Arbeitsgemeinschaft für Endlagerforschung (DAEF)". As a major event, the first international conference "Key Topics in Deep Geological Disposal", was organized in 2014 with INE being part of the local organizing team. This conference provided an excellent and comprehensive overview of all central aspects in the field of deep geological disposal. The interdisciplinary approach with experts from scientific, technical and sociotechnical disciplines represented an ideal platform for a fruitful exchange and new ideas.

Finally, I would like to express my gratitude to our numerous partners, visitors and collaborators. Last, but not least, I extend a sincere thank you to the entire staff of INE for their dedication in both scientific activities and in administrative and technical support.

Table of contents

1 Introduction to the Institute for Nuclear Waste Disposal (INE)

The Institute for Nuclear Waste Disposal, **INE**, (Institute for Nuclear Waste Disposal) at the Karlsruhe Institute of Technology **KIT** performs R&D focusing on

(i) Long-term safety for nuclear waste disposal
(ii) Immobilization of high-level radioactive waste (HLW)
(iii) Separation of minor actinides from HLW
(iv) Radiation protection

In 2014 two new research activities were integrated into the portfolio of INE. A new department for '**decommissioning** of nuclear and conventional facilities' and a new working group '**geoenergy**' will be set up at INE.

All R&D activities of KIT-INE are integrated into the program Nuclear Safety Research within the KIT-Energy Center. INE contributes to German provident research for the safety of nuclear waste disposal, which is the responsibility of the Federal Government.

Following the decision taken by Germany to phase out the use of nuclear energy, the safe disposal of long-lived nuclear waste remains as a key topic of highest priority. Projections based on scheduled operation times for nuclear power plants (Amendment to the German Atomic Energy Act, August 2011) in Germany, indicate that a total of about 17,770 tons of spent nuclear fuel will be generated. About 6,670 tons have been shipped to France and the UK until 2005 for reprocessing, to recover plutonium and uranium. The resulting high-level radioactive waste (HLW) was vitrified and was/will be transferred back to Germany. Consequently, two types of high-level, heat producing radioactive waste have to be disposed of safely: spent fuel and vitrified high-level waste from reprocessing (HLW glass). The disposal of low- and intermediate level waste present in much larger quantities likewise needs to be addressed.

Over the last decades, a consensus within the international scientific/technical community was established, clearly emphasizing that storage in deep geological formations is the safest way to dispose of high-level, heat producing radioactive waste. Disposal concepts with strong passive safety features ensure the effective protection of the population and the biosphere against radiation exposure over very long periods of time. The isolation and immobilization of nuclear waste in a repository is ensured by the appropriate combination of redundant barriers (multi-barrier system).

Long-term safety research for nuclear waste disposal at KIT-INE establishes geochemical expertise and models to be used in the disposal Safety Case, focusing primarily on the detailed scientific description of aquatic radionuclide chemistry in the geochemical environment of a repository. Work concentrates on the disposal of spent fuel and HLW-glass in the relevant potential host rock formations currently considered: rock salt, clay and crystalline rock formations. Actinides and long-lived fission products play a central role, as they dominate HLW radiotoxicity over long periods of time. Long-lived anionic fission products are likewise investigated as significant contributors to the maximum radiation dose projected for relevant scenarios.

Thermomechanical studies are performed at INE, in order to describe the evolution of the constructed repository after closure. Relevant long-term scenarios for nuclear repositories in deep geological formations have to take into account possible radionuclide transport via the groundwater pathway. Possible groundwater intrusion into emplacement caverns is assumed to cause waste form corrosion and eventually radionuclide release. Radionuclide mobility is then determined by the various geochemical reactions in complex aquatic systems: i.e. dissolution of the nuclear waste form (HLW glass, spent fuel), radiolysis phenomena, redox reactions, complexation with inorganic and organic ligands, colloid formation, surface reactions at mineral surfaces, precipitation of solid phases and solid solutions.

Prediction and quantification of all these processes require fundamental thermodynamic data and comprehensive process understanding at the molecular scale. Radionuclide concentrations in relevant aqueous systems typically lie in the nano-molar range, which is exceedingly small in relation to main groundwater components. Quantification of chemical reactions occurring in these systems require the application and development of advanced sophisticated methods and experimental approaches, to provide insight into the chemical speciation of radionuclides at trace concentrations. Innovative laser and X-ray spectroscopic techniques are continuously developed and applied to this end. A specialized working group performing state-of-art theoretical quantum chemical calculations for actinide chemistry support both interpretation of experimental results and optimized experiment design.

The long-term safety of a nuclear waste repository must be demonstrated by application of modeling tools on real natural systems over geological time scales. Geochemical models and thermodynamic databases are developed at INE as a basis for the description of radionuclide geochemical behavior in complex natural aquatic systems. The prediction of radionuclide migration in the geosphere necessitates coupled modeling of geochemistry and transport. Transferability and applicability of model predictions are examined by designing dedicated

laboratory experiments, field studies in underground laboratories and by studying natural analog systems. This strategy allows to identify and analyze key uncertainties and continuously optimize the developed models.

Within the R&D topic **immobilization of high-level radioactive waste**, INE contributes to the decommissioning of nuclear facilities. The core process technology for the Vitrification Plant (VEK) on the site of the former Karlsruhe Reprocessing Plant (WAK; located at KIT Campus North) has been developed by INE. The vitrification technology developed at INE is highly competitive on an international level. INE was involved in designing and building core components of a vitrification plant being currently built within cooperation with a German industrial consortium in China.

The Partitioning & Transmutation (P&T) strategy is pursued and developed in many international research programs and is very controversially discussed. INE research activities in this field are focused on the partitioning step, i.e. **separation of minor actinides from HLW**. The R&D aims to develop efficient separation processes for minor actinide for subsequent transmutation into short-lived or stable fission products. INE develops highly selective extracting agents and performs experiments to derive kinetic and thermodynamic data to assess and optimize extraction reactions. R&D spans experimental, analytical and theoretical work, dedicated to understanding extraction ligand selectivity on a molecular scale. INE contributed as well to an interdisciplinary project coordinated by the National Academy of Science and Engineering (ACATECH) to critically discuss the use of P&T under the specific German boundary conditions.

The R&D topic **radiation protection** at INE focuses on the assessment of radiation exposures to human beings by estimating doses either from external radiation fields or from incorporation of radionuclides. The strategy driving this work is to provide techniques and models for an individualized dosimetry, which goes beyond the current approach of applying reference models in dose assessments. R&D is extended to simulate and to assess radiation exposure to workers in nuclear waste disposal facilities. Work is performed in close cooperation with the KIT safety management SUM.

INE laboratories are equipped with all necessary infrastructures to perform radionuclide/actinide research, including hot cells, alpha glove boxes, inert gas alpha glove boxes and radionuclide laboratories. State-of-the-art analytical instruments and methods are applied for analysis and speciation of radionuclides and radioactive materials. Advanced spectroscopic tools exist for the sensitive detection and analysis of radionuclides. Trace element and isotope analysis is made by instrumental analytical techniques such as X-ray fluorescence spectroscopy (XRF), atomic absorption spectroscopy (AAS), ICP-atomic emission spectroscopy (ICP-AES) and ICP-mass spectrometry (Quadrupole-ICP-MS and high resolution ICP-MS). Methods available for surface sensitive analysis and characterization of solid samples include X-ray diffraction (XRD), atomic force microscopy (AFM) and laser-ablation coupled with ICP-MS. A modern X-ray photoelectron spectrometer (XPS) and an environmental scanning electron microscope (ESEM) are installed. INE has direct access to a TEM instrument on the KIT Campus North site (Institute for Applied Materials, IAM). For actinide detection down to 10^{-15} M KIT-INE has access to the Accelerator Mass Spectrometry (AMS) at the Vienna Environmental Research Accelerator (VERA).

Laser spectroscopic techniques are developed and applied for sensitive actinide and fission product speciation such as time-resolved laser fluorescence spectroscopy (TRLFS), laser photo acoustic spectroscopy (LPAS), laser-induced breakdown spectroscopy (LIBS) and Raman spectroscopy. Structural insight into actinide species is obtained by extended X-ray fine structure (EXAFS) spectroscopy at the INE-Beamline at the Karlsruhe synchrotron source ANKA. The INE-Beamline, in the direct vicinity of INE hot laboratories and in combination with the other analytic methods, represents a world-wide unique experimental and analytic infrastructure, which both profits from and contributes to INE's leading expertise in the field of actinide chemistry and spectroscopy. INE's synchrotron-based instrumentation is currently augmented by installing the CAT-ACT beamline at ANKA, a state-of-the-art X-ray absorption spectroscopy beamline jointly funded, constructed, and operated by KIT institutes IKFT/ITCP for CATalysis research and INE for ACTinide/radionuclide research. The CAT-ACT beamline is foreseen to become fully operational towards the end of 2016. Quantum chemical calculations are performed on INE's computing cluster, which is equipped with 17 nodes and 76 processors. A 400 MHz-NMR spectrometer adapted to measuring radioactive liquid samples adds to the analytical and speciation portfolio of INE. Additional facilities at INE include a non-radioactive vitrification test facility (PVA) used to investigate and to simulate vitrification processes for hot plants. The INE CAD workstations enable construction and planning of hardware components, process layout and flow sheets. The institute workshop is equipped with modern machine tools to manufacture components for specific experimental and analytical devices in hot laboratories.

In 2014 the **Institute for Nuclear Waste Disposal** had **120 employees** working in the seven departments, which reflect the R&D and organizational tasks of the institute (Figure 1): (i) safety of nuclear waste disposal, (ii) geochemistry, (iii) radiochemistry, (iv) actinide speciation, (v) vitrification of high-level waste, (vi) radiation protection research and (vii) scientific/technical coordination and analytical chemistry.

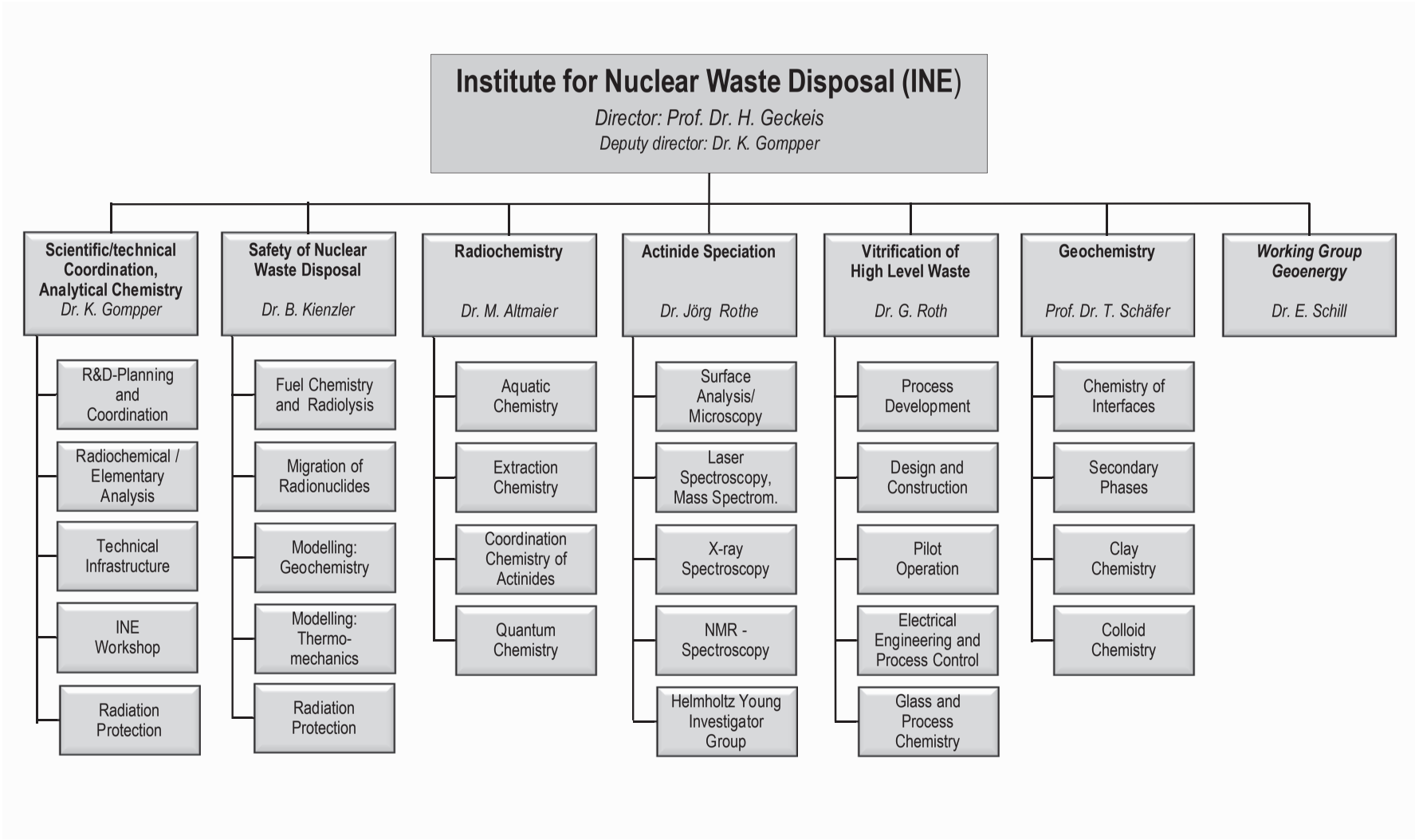

Fig. 1: Organizational chart of the Institute for Nuclear Waste Disposal (INE)

2 Education and training

Teaching of students and promotion of young scientists is of fundamental importance to ensure high-level competence and to maintain a leading international position in the fields of nuclear and radiochemistry. INE scientists are strongly involved in teaching at KIT Campus South and the Universities of Heidelberg, Berlin, Jena and Strasbourg as well as the Baden-Wuerttemberg Cooperative State University.

Prof. Dr. **Horst Geckeis**, director of INE, holds a professorship for radiochemistry at KIT Campus South, Department of Chemistry and Biosciences. He teaches fundamental and applied radiochemistry for chemistry students in bachelor, master and diploma courses. A radiochemistry module consisting of basic and advanced lectures on nuclear chemistry topics and laboratory courses has been set up for diploma and master students in Karlsruhe.

Prof. Dr. **Petra Panak**, heading a working group on actinide speciation at INE, holds a professorship of radiochemistry at the University of Heidelberg. A basic course in radiochemistry is offered for bachelor and/or master students. An advanced course comprised of the chemistry of f-elements and medical applications of radionuclides is also offered. The advanced radiochemistry lectures are supplemented by scientific internships at the INE radioactive laboratories.

Nearly 40 students from Karlsruhe and Heidelberg participated in two 3-week radiochemistry laboratory courses in 2014 held at KIT Campus North in the FTU radiochemistry and hot laboratories at INE. Some students are intensifying their knowledge in nuclear/radiochemistry topics during scientific internships at INE. Obviously students became interested in nuclear chemistry topics and appreciate the various semester courses.

Dr. **Tonya Vitova** gave lectures at the KIT Campus South, Department of Chemistry and Biosciences, in the field of instrumental analytics and Dr. **Eva Schill** and Dr. **Marika Vespa** at the Department of Civil Engineering, Geo and Environmental Sciences in the field of geophysics, general geology and analytical methods in applied mineralogy. Dr. **Volker Metz** gave lectures at the Department of Mechanical Engineering in the field of reactor physics. Prof. Dr. **Sascha Gentes** Head of Deconstruction and Decommissioning of Conventional and Nuclear Buidlings at the Institute for Technology and Management in Construction (TMB) at the Department of Civil Engineering, Geo- and Environmental Sciences at KIT Campus South gave lectures in the field of Decommissioning and civil engenieering.

Lectures and practical units taught by Prof. Dr. **Thorsten Schäfer** at the Freie Universität Berlin, Institute of Geological Sciences, Department of Earth Sciences, focused in 2014 on a master degree course on laboratory and field methods in hydrogeology, including performance and analysis of tracer tests using conservative, weakly sorbing tracers and colloids, pumping tests and determination of hydraulic parameters (Applied Hydrogeology III).

Dr. **Andreas Bauer** is lecturing Clay Mineralogy at the University of Jena. His lecture deals with the mineralogical characterization of these fine materials and the importance of quantifying surface reactions. In the second part of the lectures sound, practical advice on powder X-ray diffraction in general is provided, as well as a useful set of step-by step instructions for the novice.

Dr. **Andreas Geist** gave lectures at the École européenne de chimie, polymères et matériaux in Strasbourg concerning the solvent extraction of metal ions.

Dr. **Frank Becker** gave lectures at the Baden-Wuerttemberg Cooperative State University (DHBW). The lectures comprised principles of statistics and measurements, atomic physics and nuclear physics.

Moreover INE was involved in many schools and workshops concerning the education and teaching of students and young scientists:

- 3rd ITU-INE Research Fellow Day, February 6, 2014
- 4th PhD workshop on Reactive Transport Modeling and Experiments, March 8-9, 2014
- ThUL (Theoretical User Laboratory) workshop on Actinide Chemistry, June 2-6, 2014
- 8th European Summer School on Separation Chemistry and Conditioning as well as Supra-molecular, Intermolecular, Inter-aggregate Interactions, July, 7.-9, 2014
- European Nuclear Safety and Security School Training Courses: Introduction to the back-end of the nuclear fuel cycle, November 24, 2014
- Joint ITU-INE Workshop: Synchrotron-based spectroscopy for actinide science, December 5, 2014

Through this close cooperation with universities, students are educated in the field of nuclear and actinide chemistry, which most universities can no longer offer. Hence, INE makes a vital contribution to the intermediate and long perspective of maintaining nuclear science competence. Moreover INE is involved in the education of trainees (chemical lab technicians, industrial mechanics and product designers) as well as student internships like BORS and BOGY.

PhD students

In 2014 26 PhD students worked at INE on their doctoral dissertations; 3 of them were awarded their doctorate. Topics of the theses are listed below:

- Structural study on Cm(III) and Eu(III) complexes with ligands relevant to partitioning

- The effects of porosity clogging on transport properties of porous materials under geochemical perturbation
- Sorption of trivalent actinides on iron oxides
- Development of body models for *in-vivo* measurements in radiation protection
- Comparative NMR studies of extraction agents for the separation of trivalent actinides
- Advanced spectroscopic and microscopic structural investigations of nuclear waste glass forms
- Interaction of human serum transferrin with actinides and lanthanides
- Technetium interaction with inorganic ligands and retention processes in the sulfide system
- Release and speciation of actinides by the fabrication and dissolution of Mo- and Zr-based nuclear fuel oxides
- Redox-speciation of repository relevant and redox-sensitive elements in aqueous solutions by capillary electrophoresis coupled to ICP-MS
- Study of repository relevant carbon compounds and their influence on the ^{14}C- respectively actinide immobilization
- Investigation of the solubility and complexation of trivalent actinides: hydrolysis and complexation with organic ligands
- Influence of anions on the lanthanide/actinide interaction with mineral surfaces
- Characterization of actinide species in systems relevant for safety assessment of a nuclear waste repository by high-resolution X-ray emission/absorption spectroscopy
- Characterization of bonding differences by high-resolution X-ray emission and inelastic X-ray scattering techniques
- Bentonite erosion and colloid mediated radionuclide transport in advection controlled systems
- Development of methods for the individual dosimetry of the staff in disposal facilities
- Investigation of solubility and complexation of Plutonium and Neptunium in highly reducing aquatic systems
- Description of radionuclide sorption at clay minerals at high ionic strength
- Impact of fracture geometry and colloid transport on permeability evolution of potential crystalline geothermal reservoir rocks.Redox behavior, solubility and sorption of Pu(III/IV) in the presence of ISA
- Effect of supersaturation index and precipitation kinetics on the incorporation of trivalent actinides/ lanthanides in sulfate/carbonate minerals and CSH phase
- Tc migration in advection/diffusion controlled natural systems: Influence of ferrous iron pool
- Spectroscopic and thermodynamic investigations of the complexation of An(III) and Ln(III) with hydrophilic Bis-triazinylpyridines
- Investigation of the retention of actinides, lanthanides and long-lived fission products on stable solid phases within the system $Mg - Na \pm Cl \pm CO_2 - H_2O$
- Technetium redox processes and Tc(IV) solubility studies

3 National and international cooperation, conferences and workshops

INE R&D involves numerous national and international collaborations and projects. These are described in the following.

National

INE is involved in various bi- and multilateral collaborations with national research centers, universities and industrial partners on different topics. The projects are partly supported by the German Federal Ministry for Economics and Technology (BMWi), the Federal Ministry for Education and Research (BMBF), the Federal Ministry for the Environment, Nature Conservation, Building and Nuclear Safety (BMUB), the German Research Foundation (DFG) and the Helmholtz Association (HGF).

The work of KIT-INE within **VESPA** (ended in June 2014) is highlighting the key relevance of geochemical research for evaluating radionuclide retention and mobilization in the frame of nuclear waste disposal. Based upon new systematic experimental studies, a significant increase of understanding regarding the behavior of long-lived fission and activation products, i.e. ^{14}C, ^{79}Se, ^{129}I and ^{99}Tc, in relevant systems has been obtained. Fundamental site- and host-rock independent thermodynamic data derived within VESPA allow a better modeling and prediction of radionuclide chemistry in aquatic systems. The retention of radionuclides on several relevant mineral phases was analyzed and quantified. As a result of the work performed by KIT-INE within VESPA, the long-term safety of different repository concepts and scenarios can be assessed on a decisively improved scientific level.

Within the national **THEREDA** project, INE generates and appraises thermodynamic data – complex formation constants, solubility data – for selected radionuclides from experiments and literature data that are incorporated into a centrally managed and administered database of evaluated thermodynamic parameters. This database is generated in a cooperation of INE, Gesellschaft für Anlagen- und Reaktorsicherheit (GRS), Helmholtz-Zentrum Dresden-Rossendorf (HZDR), TU Bergakademie Freiberg, and AF-Consult Switzerland Ltd. Thermodynamic data are required for environmental applications in general and radiochemical issues in particular. This database is developed to a national (reference) standard and will be the basis for performance assessment calculations for a national nuclear waste repository. More information about this project can be obtained from the web page: www.thereda.de.

The national **HATT** project focuses on the migration of radionuclides in natural clay formations and in saline systems. Within this project not only the mechanism of radionuclide sorption onto clay is studied, but also the influence of organic matter naturally occurring in the clay stone on the radionuclide migration is a matter of interest. Because of special geochemical conditions in Lower Cretaceous Clays in North Germany regarding groundwater or pore water, retardation processes at higher ionic strengths are of special interest. Additionally, the influence of borate, a component of the high-radioactive waste, on the solubility of actinides is another important issue of the project. Besides INE, the members of this collaborative project are GRS, HZDR, University of Mainz, University of Potsdam, Technical University of Munich, University of Dresden and University of Saarland.

The bilateral GRS-INE project **KOLLORADO-*e*** started in March 2013 with a duration of three years as a successor of the KOLLORADO-2 project, focusing on the erosion stability of compacted bentonite (geotechnical barrier) as a function of the contact water chemistry/hydraulics and the formation of near-field colloids/nanoparticles as potential carriers for actinides/radionuclides. Both, a detailed experimental program quantifying the bentonite erosion and investigating the influence of surface roughness/charge heterogeneity on nanoparticle mobility and actinide bentonite nanoparticle sorption reversibility, as well as approaches to implement the acquired process understanding in reactive transport modeling codes comprise the project activities.

The general aim of the BMWi joint project on the **Comparison of Constitutive Models III** is to check the ability of numerical models to describe correctly relevant deformation phenomena in rock salt under various influences, and thus increase confidence in numerical simulations and thereby enhance acceptance of results. Another aim is to identify possibilities for further model development and improvement.

The BMBF funded joint research project **ImmoRad** (fundamental investigations for the immobilization of long-lived radionuclides through interaction with secondary mineral phases in deep geological nuclear waste repositories) started in February, 2012. ImmoRad concentrates on application-based fundamental research on retention processes in deep geological environments. Within this project, structural incorporation/entrapment or formation of solid solutions of radionuclides into host minerals in aquatic environments is studied. National (KIT-INE, HZDR, University Frankfurt, University of Bonn) and international partners (PSI-LES; Switzerland and University Oviedo; Spain) collaborate within this project.

The project **"Untersuchungen zum grundlegenden Verständnis der selektiven Komplexi-**

erung von f-Elementen (f-Kom)“ funded by the German Federal Ministry of Research and Education in the field of Basic Energy Research 2020+ aims at establishing a fundamental understanding of the separation of actinides from nuclear waste. The participating project partners from KIT-INE, KIT-CS, Universität Erlangen, Universität Heidelberg and Forschungszentrum Jülich are combining their expertise and activities in synthesis, spectroscopy, technology and theory, in order to be able to describe and ultimately predict and optimize liquid-liquid extraction separation processes for actinides at the molecular scale. The project includes a strong component of education and training of young scientists in research topics related to nuclear waste disposal and promotes their networking in the European research landscape.

The BMBF funded project “Disposal options for radioactive residues: Interdisciplinary analyses and development of evaluation principles (**ENTRIA**)” aims to investigate, and to develop evaluation principles for the three options for management of spent nuclear fuel and high-level waste glass: prolonged surface storage, emplacement in deep geological formations without retrievability measures and with monitoring retrievability measures, respectively. Scientists from five German universities, major research institutions and a Swiss partner participate in ENTRIA and represent natural sciences, civil engineering, philosophy, law, and social sciences. Two major goals of the project are interdisciplinary co-operation in the field of radioactive waste management and education of young scientists. Within the project, KIT-INE is responsible for work packages on developing radionuclide source terms and developing individual dosimetry for personnel with respect to the three options. Moreover, KIT-INE contributes to interdisciplinary publications and workshops naming specific challenges and target conflicts of importance when deciding about management options.

The collaborative project **EDUKEM**, aiming at an improved understanding of uranium chemistry in saline systems and establishing targeted experimental techniques, was started in December 2014 with a projected 3 year duration. Work of KIT-INE within EUDKEM focusses on the aquatic chemistry and thermodynamics of hexavalent and tetravalent uranium in relevant saline solutions. Based upon new solubility studies, spectroscopic evidence and literature, a comprehensive description of U(IV) and U(VI) solubility and speciation in key saline systems relevant for nuclear waste disposal in salt-based repositories will be established.

The Helmholtz young investigator group (HYIG) **“Advanced synchrotron-based systematic investigations of actinide (An) and lanthanide (Ln) systems to understand and predict their reactivity”** started in July 2011 and systematically investigates the electronic and coordination structure of actinides and chemical homologue lanthanide systems with novel synchrotron-based high-resolution X-ray emission/inelastic scattering techniques (XES/RIXS). Using advanced spectroscopic methods to secure the knowledge of actinide redox speciation and the electronic structure can improve predicting actinide environmental behavior and provide benchmark data for the improvement of quantum chemical codes. The utility of high-energy resolution X-ray absorption near edge structure (HR-XANES) studies in studies of actinide elements was the motivator for installing and commissioning a multi-analyzer Johann type XES spectrometer (MAC-spectrometer) at the INE-Beamline for actinide research at the ANKA synchrotron radiation facility, Karlsruhe, Germany. A number of systems for the determination of actinide redox states in liquids and solid crystalline and amorphous systems were investigated. Finally, results from characterization of U and Pu oxidation states in a highly active glass sample from the "Verglasungseinrichtung Karlsruhe" (VEK), which vitrified high-level liquid nuclear fuel reprocessing waste, and a glass simulate containing variable U or Pu loadings were obtained.

In the frame of emergency measures for the salt mine **Asse**, the sorption properties of the overlaying rocks need to be quantified. Presently, an exploration borehole was drilled in the overlaying rocks. On behalf of the Federal Office for Radiation Protection (BfS), drill cores were sampled and characterized. The rock samples cover different layers, such as shell limestone, red sandstone, sulfate dominated rocks and cap rock of the salt dome. The samples were packed and stored under inert gas. The preparation steps for the characterization were also performed under inert gas. The characterization covered different information such as porosity, the specific surface areas, main and trace element compositions as well as the mineralogical compositions. These data provide the basis for interpretation of the results of the planned sorption studies.

International

The international Colloid Formation and Migration (**CFM**) project focuses on the stability of the bentonite buffer/backfill in contact with water conducting features and the influence of colloids on radionuclide migration in crystalline host rocks coordinated by NAGRA (National Cooperative for the Disposal of Radioactive Waste, Switzerland). The project uses the experimental set-up in the controlled zone at the Grimsel Test Site (Switzerland). Additional partners involved are from Japan (JAEA, AIST, CRIEPI), South Korea (KAERI), Finland (POSIVA Oy and Helsinki University), Switzerland (NAGRA, PSI-LES), Spain (CIEMAT), Sweden (SKB, KTH), United Kingdom (NDA RWMD) and United States (LANL). INE plays a decisive role in the laboratory program and is also mainly carrying out the field activities.

Within the framework of the strategy of the German Federal Government for the internationalization of science and research to foster the bilateral

cooperation with Korea in the area of science and technology (WTZ) KIT-INE has started a two year project from 1.10.2014 entitled "Molecular-scale investigation of interaction mechanisms between uranium and iron-bearing minerals under diverse geochemical conditions of groundwater (**Bio-FeRad**)" with KAIST (Korean Advanced Institute of Science and Technology), group of Prof. Woojin Lee including student exchange and two bilateral workshops.

EURATOM 7thFramework Program

An additional 7th framework Collaborative Project (CP) continued this year, namely "Cation diffusion in clayrocks" (**CatClay**), which began in June 2010. The aim of CatClay is to improve understanding of the phenomena governing migration of radionuclides in clayrocks as potential host rocks for the deep geological disposal of nuclear waste. The project focuses on the diffusion-driven transport of cationic species, Sr^{2+}, Zn^{2+}, Co^{2+} and Eu^{3+}, which are more or less strongly sorbed on clay mineral surfaces. CatClay, coordinated by CEA, combines model and experimental developments from the partners, ANDRA, BRGM, CEA, SCK·CEN, PSI-LES, Appelo Hydrochemical Consultant and KIT-INE.

INE continues to be a core member in **TALISMAN** (Transnational Access to Large Infrastructure for a Safe Management of ActiNide), the follow-up project to the European "Network of Excellence for Actinide Sciences" (ACTINET-I3), which will run until January 2016. TALISMAN aims to reinforce networking and facilitating the use of existing European infrastructures in actinide sciences in order to keep a leading position in the field of nuclear energy. TALISMAN pooled facilities are accessible as a multi-site user facility for selected joint research activities (JRP). The pooled facilities offer includes: CEA (France), CHALMERS (Sweden), EC-JRC-ITU, HZDR-IRE, KIT-INE (all Germany), Micro-XAS beamline at the Swiss Light Source, PSI, Paul-Scherrer-Institut (Switzerland) and NNL, National Nuclear Laboratory (United Kingdom). These pooled facilities are laboratories licensed and equipped with infrastructure and know-how for handling radioactive material at various levels of activity and under controlled conditions, with access to analytical techniques and characterization methods.

TALISMAN pooled facilities are the sites of JRP's proposed by European institutions and organizations. These research projects potentially address all the major fields of basic actinide sciences, keeping in mind the potential applications for the production of nuclear fission energy and the safety of nuclear waste disposal, and include:

- Actinide separation chemistry
- Actinides in the geological environment
- Actinide materials

Further, these activities are complemented by two so-called Joint Research Activities (JRA). The objective of these JRA is to improve the quality of the services offered to the users. One JRA is dedicated to the implementation of spectroscopic databases giving each user access to reference data. The second JRA is continuing to develop the fundamental understanding of actinides in order to give more elaborated modeling based tools for the analyses and the understanding of experimental results acquired within the JRPs (ThUL; Theoretical User Laboratory).

Within the EURATOM 7th FP, INE coordinated the Collaborative Project INE "Fast/Instant Release of Safety Relevant Radionuclides from Spent Nuclear Fuel (CP **FIRST-Nuclides**)". The CP was started in January 2012 and ended in December 2014. Quantification and understanding of the release mechanisms of gaseous and readily soluble radionuclides from high burn-up UO_2 fuel was investigated experimentally and models were developed to predict the time-dependent mobilization of the different radionuclides on the fuel rod/fuel element scale as function of the time period between disposal and canister failure. INE performed experiments under reducing conditions and determined the combined release of soluble radionuclides and fission gasses. These results are highly acknowledged by scientists as well as by international implementers and regulators of high-level waste disposals independent on the respective host rocks.

ASGARD (Advanced fuelS for Generation IV reActors: Reprocessing and Dissolution; 1/2012–12/2015) is a EURATOM FP7 Large Scale Integrated Project focusing on advanced/novel nuclear fuels fabrication and their respective reprocessing issues. ASGARD seeks integration between reactor, fuel and recycling communities, which today is lacking. In some cases this results in discrepancies between the reactor design on one hand, and the technological feasibility of fabricating, dissolving and reprocessing the selected fuel on the other hand. ASGARD is an integrated effort of 16 institutions from 9 European countries. It is coordinated by Chalmers Technical University.

SACSESS (Safety of ACtinide SEparation proceSSes; 3/2013–2/2016) is a EURATOM FP7 Collaborative Project dealing with safety aspects of hydrometallurgical and pyrometallurgial actinide separation processes developed in previous EURATOM projects. SACSESS provides a structured framework to enhance the fuel cycle safety associated to P&T. In addition, safety studies are performed to identify weak points to be further studied. These data are used to optimize flow sheets and process operation conditions. 26 Partners from 10 countries (plus JRC-ITU and Japan) contribute to SACSESS. The project is coordinated by CEA; KIT is in charge of the hydrometallurgy domain.

Recent safety assessments of nuclear waste repositories in crystalline formations have shown that the

formation and stability of colloids may have a direct impact on the overall performance of the repository. The main aim of the 7th framework collaborative project **BELBaR** is to increase the mechanistic understanding of the processes that control bentonite erosion, clay colloid stability, and ability to transport radionuclides. The final outcome is to examine how colloids and related phenomena can be considered in the long-term safety case and to make recommendations on the quantitative and qualitative approaches that a safety case could pursue to adequately address this potentially very significant issue. BELBaR coordinated by SKB consists of a consortium of 14 partners from Sweden, Finland, Spain, Czech Republic, Great Britain, Russia and Germany with KIT-INE leading WP3 on "Colloid radionuclide & host rock interaction".

The 7th FP Collaborative Project (CP) "**CAST** (CArbon-14 Source Term)" was started in 2013. The CP is coordinated by NDA (UK) and has a duration until 2017. KIT-INE participates in 3 work packages: "Steels", "Zircaloy" and "Dissemination". INE's contribution to the project covers the determination of the inventory of ^{14}C in irradiated stainless steel and zircaloy-4 as well as the speciation of ^{14}C compounds. The analytical set-up was implemented in a glove box. The set-up together with the detection technique was tested and the recovery for inorganic and organic ^{14}C compounds quantified. The description of the system and the analytical procedure for gaseous and dissolved ^{14}C species quantification was provided to the project.

Besides those research oriented cooperations, KIT-INE has direct contracts comprising specific investigations with a series of national and international organizations. These include the HMGU (DE) and BfS (DE), the waste management organizations ONDRAF·NIRAS (BE), SKB (SE) and the consultant company Amphos S:L. (ES).

KIT-INE contributes actively to international organisations, such as the Thermodynamic Database Project of the Nuclear Energy Agency (NEA).

Conferences and workshops

INE has organized a series of workshops and conferences or has contributed significantly to the organization:

- TrePro III – Workshop on Modeling of Coupled Reactive Transport Processes, Karlsruhe, March 5-7, 2014.
- 16th International Symposium on Solubility Phenomena and Related Equilibrium Processes (ISSP-16), Karlsruhe (Germany), July 21-25, 2014
- 7th EC FP – FIRST-Nuclides Final Workshop, Karlsruhe, Germany, September 1-2, 2014
- 27th Spent Fuel Workshop, Akademie Hotel Karlsruhe, Germany September 3-5, 2014.
- Key Topics in Deep Geological Disposal, DAEF Symposium, Cologne, Germany, September 24-26, 2014.

4 Fundamental studies: Process understanding on a molecular scale

Fundamental studies on radionuclide chemistry and geochemistry ensure a detailed understanding and reliable quantitative prediction of aqueous chemistry. In order to allow a comprehensive assessment of radionuclide behavior and mobility in aquatic systems relevant for nuclear waste disposal, studies with actinides and long-lived fission products are performed. The investigated aqueous systems cover from dilute solutions to highly saline salt brine systems and establish essential site-independent data and process understanding. Work is focusing both on detailed experimental investigations using the unique facilities available at KIT-INE and subsequently developing reliable chemical models and consistent thermodynamic data. This combined approach allows a systematic and reliable evaluation of key processes such as radionuclide solubility, radionuclide speciation, radionuclide retention and transport processes in relevant near- and far-field scenarios. The work summarized in this section is related to the (i) chemistry and thermodynamics of actinides and fission products in aqueous solution, (ii) radionuclide sorption on mineral phases, (iii) radionuclide diffusion in clays, and (iv) retention of radionuclides by secondary phase formation. The studies aim at identifying relevant radionuclide retention/retardation mechanisms on a molecular level and their robust thermodynamic quantification in support of the Nuclear Waste Disposal Safety Case. Fundamental studies on aqueous radionuclide chemistry are giving support to the applied studies (see Chapter 6) performed at KIT-INE.

4.1 Chemistry and thermodynamics of actinides and fission products in aqueous solution

M. Altmaier, N. Banik, A. Baumann, M. Böttle, K. Dardenne, D. Fellhauer, D. R. Fröhlich, X. Gaona, M. Herm, K. Hinz, P. Lindqvist-Reis, R. Marsac, V. Metz, P. J. Panak, J. Rothe, J. Schepperle, A. Skerencak-Frech, Th. Rabung, D. Schild, E. Yalcintas

In co-operation with:

C. Apostolidis[a], P. Di Bernardo[b], R. Janicki[c], S. Kalmykov[d], M. Skripkin[e], A. Vasiliev[d], O. Walter[a], P. Zanonato[b]

[a]JRC-ITU, European Commission, Karlsruhe, Germany; [b]Universitá di Padova, Padova, Italy; [c]Faculty of Chemistry, University of Wrocław, Wrocław, Poland; [d]Lomonosov Moscow State University, Moscow, Russia; [e]St. Petersburg University, St. Petersburg, Russia

Introduction

Aquatic chemistry and thermodynamics of actinides and fission products is a highly relevant research field contributing to the safety and performance assessment of repositories for nuclear waste. Reflecting this key importance and continuing the strong tradition on aquatic chemistry and thermodynamics at KIT-INE, the research activities developed at KIT-INE within this field focus on systems relevant for waste disposal in terms of the investigated radionuclides, oxidations states, complexing ligands and geochemical boundary conditions. The outcome of this research has direct impact on fundamental and applied repository science ranging from the radionuclide source term to processes in the far field.

Fission products are one of the most important elements studied in the field of aquatic chemistry at KIT-INE. The work on solubility and hydrolysis of Tc(IV) was successfully completed in 2014, and will be extended to carbonate, nitrate and sulphide systems within the context of a new PhD thesis. Actinides (especially Pu and Np) under reduced oxidation states (+III and +IV) likewise received high attention in 2014, which is reflected in three of the contributions summarized in this section. Understanding the impact of temperature on the aquatic chemistry of radionuclides is relevant for certain scenarios in the disposal of high-level/heat-generating waste. Three of the highlighted contributions explore the effect of temperature on actinide and lanthanide aqueous complexes and solid phases. In line with this high relevance, the collaborative project ThermAc3 was granted by the German Ministry of Education and Finances (BMBF) and will combine experimental work, estimation approaches and quantum chemical methods to tackle the impact of temperature on actinide aqueous chemistry.

In the international frame, KIT-INE participates in the chairing and scientific review work of two ongoing NEA-TDB activities. The state-of-the-art report on "Aquatic actinide chemistry in saline systems" and the "Update book on the chemical thermodynamics of actinides and fission products". KIT-INE research on aquatic chemistry is likewise integrated in activities of the IUPAC. Members contribute to the Committee on Solubility and Equilibrium data, which held its Annual Meeting in conjunction with the International Symposium on Solubility Phenomena (ISSP 16) organized in Karlsruhe by KIT-INE.

Thermodynamic description of Tc(IV) in Tc^{4+}-Na^+-K^+-Mg^{2+}-Ca^{2+}-H^+-Cl^--OH^--H_2O systems: application to repository-relevant conditions

Technetium-99 is a β-emitting radionuclide produced in nuclear reactors by the fission of ^{235}U and ^{239}Pu. Due to its significant inventory in spent fuel, long half-life ($t_{½}$ ~211000 a) and redox-sensitivity, ^{99}Tc is a very relevant radionuclide in Performance Assessment calculations of repositories for radioactive waste dis-

posal. Under sub-oxic/oxidizing conditions, technetium exists as the highly soluble and mobile pertechnetate anion (TcO_4^-). In reducing environments, Tc(IV) prevails forming sparingly soluble hydrous oxides ($TcO_2{\cdot}xH_2O$(s)). The later redox state is expected to dominate the aqueous chemistry of Tc in the reducing conditions predicted for deep geological repositories. In this framework, an appropriate understanding of the solubility and hydrolysis of Tc(IV) in dilute to concentrated saline systems is required for an accurate assessment of technetium source term in repositories for radioactive waste disposal.

The solubility of Tc(IV) was investigated from undersaturation conditions in 0.1-5.61 m NaCl, 0.1-4.58 m KCl, 0.25-5.15 m $MgCl_2$ and 0.25-5.25 m $CaCl_2$ solutions in the pH_m range 1.5-14.6. Experiments were performed at 22 ± 2°C in Ar gloveboxes with < 2 ppm O_2. Strongly reducing conditions (pe + pH < 4) were fixed for each independent batch solubility sample with $Na_2S_2O_4$, $SnCl_2$ or Fe powder. All investigated systems were equilibrated for up to 600 days. m_{Tc}, pH_m and E_h values were monitored at regular time intervals. Thermodynamic equilibrium was established after repeated measurements with constant m_{Tc} and pH_m. After attaining equilibrium conditions, the redox speciation of Tc in the aqueous phase was quantified for selected samples using solvent extraction with TPPC and XANES analysis. Solid phases of selected batch experiments were also characterized by XRD, SEM-EDS and quantitative chemical analysis. Additional solubility experiments were conducted in "simulated systems", based on reported ground water and cementitious pore water compositions with complex mixtures of NaCl-KCl-$MgCl_2$-$CaCl_2$.

Solid phase characterization and solubility data indicate that $TcO_2{\cdot}1.6H_2O$(s) is the solid phase controlling the solubility of Tc(IV) in all the evaluated systems. The combination of solvent extraction and XANES analysis confirms the predominance of Tc(IV) in the aqueous phase, independently of the salt system and concentration. The solubility of $TcO_2{\cdot}1.6H_2O$(s) decreases with a well-defined slope of -2 in acidic dilute systems. The same slope is retained in concentrated brines, although a very significant increase in the solubility (up to 4 orders of magnitude) is observed with increasing ionic strength. The newly derived chemical model, based on these solubility data in combination with spectroscopic evidences reported in the literature [1], explains this increase considering the formation of the previously unreported trimeric technetium species $Tc_3O_5^{2+}$. In the near-neutral pH region, the pH-independent behavior of the solubility is consistent with the chemical reaction $TcO_2{\cdot}1.6H_2O$(s) ⇔ $TcO(OH)_2$(aq) + 0.6 H_2O with a $\log_{10}$ $^*K^\circ_{s,TcO(OH)2}$ in good agreement with the current NEA-TDB data selection [2]. The amphoteric behavior of Tc(IV) is confirmed by the formation of the species $TcO(OH)_3^-$ in dilute NaCl and KCl systems with $pH_m \geq 11$ (Figure 1). The same speciation is retained in concentrated alkaline NaCl and KCl solutions, although a decrease in solubility compared to dilute systems takes place due to ion interaction processes. Changes in the aqueous speciation are observed in concentrated alkaline $MgCl_2$ and $CaCl_2$ brines, where the formation of $Mg_3[TcO(OH)_5]^{3+}$ and $Ca_3[TcO(OH)_5]^{3+}$ ternary species are proposed based on the slope analysis of the corresponding solubility curves and the comparison with previous observations available for An(IV) and Zr(IV) [3, 4] in concentrated $CaCl_2$ solutions. The formation of these species has been validated by quantum chemical calculations performed at KIT-INE [5].

Based on the newly generated experimental data, comprehensive chemical, thermodynamic and activity models using both SIT and Pitzer approaches are derived for the system Tc^{4+}-Na^+-K^+-Mg^{2+}-Ca^{2+}-H^+-Cl^--OH^--H_2O at 25°C. These data complement and significantly extend the current thermodynamic selection of the OECD Nuclear Energy Agency (NEA–TDB) [2]. Tc(IV) solubility investigated in "simulated systems" is in good agreement with qualitative predictions based on pure simplified systems. Further investigations combining solution chemistry and quantum chemical calculations on the systems Tc(IV)-CO_3-H_2O, Tc(IV)-NO_3-H_2O and Tc(IV)-S(-II)-H_2O are currently on-going at KIT-INE.

Interaction of Np(V) with borate in alkaline NaCl and $MgCl_2$ solutions

Borate can be present in a nuclear waste repository as part of the emplaced waste inventory or as a component of intruding brines in the case of rock-salt formations. The interaction of Nd(III) and Cm(III) with borate in NaCl, $CaCl_2$ and $MgCl_2$ solutions was recently investigated at KIT-INE [6], showing a weak aqueous complexation accompanied by the formation of a new Nd(III)-borate solid phase at $pH_c \leq 9$ with significantly lower solubility than $Nd(OH)_3$(am). A much weaker interaction was observed for Th(IV) and U(VI), likely due to the stronger hydrolysis of +IV and +VI actinides. The case of +V actinides (with the lowest Z_{eff} and thus weakest hydrolysis) is studied

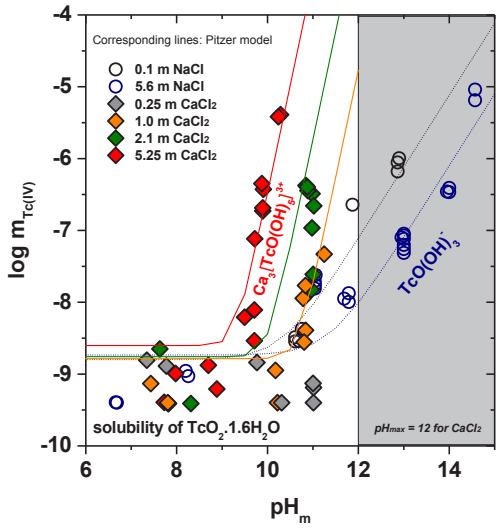

Fig. 1: Experimental solubility data of Tc(IV) in dilute to concentrated NaCl and $CaCl_2$ systems. Dashed lines corresponding to calculated Tc(IV) solubility in NaCl and $CaCl_2$ media using thermodynamic data derived in this work.

with Np in this contribution.

All experiments were conducted under inert gas (Ar) atmosphere at 22 ± 2°C. Np(V) solubility was investigated in independent batch experiments from undersaturation conditions with ~8-14 mg of freshly precipitated $^{237}NpO_2OH(am)$ solid phase per sample. Samples were prepared in 0.1-5.0 M NaCl and 0.25-3.5 M $MgCl_2$ with 0.04 M ≤ $[B]_{tot}$ ≤ 0.16 M and 8 ≤ pH_m ≤ 9. All systems were equilibrated for up to 270 days; pH_m and m_{Np} (LSC) were monitored at regular time intervals. After attaining equilibrium conditions, selected solid phases were characterized by XRD, XPS and SEM-EDX. Additional UV-Vis/NIR experiments with ~1´10^{-4} M $^{237}Np(V)$ per sample were performed in 0.25-3.5 M $MgCl_2$ solutions with 8 ≤ pH_m ≤ 9.

A slight increase in Np(V) solubility is observed in NaCl solutions with with 8 ≤ pH_m ≤ 9 and $[B]_{tot}$ = 0.04 M, indicating the formation of a rather weak Np(V)-borate complex in solution (Figure 2). Complex formation is further confirmed by UV-Vis/NIR, where a red shift and peak broadening is observed in $MgCl_2$ systems. Similar to previous observations made for Nd(III), a distinct decrease in solubility occurs in dilute to concentrated NaCl solutions with higher boron concentration ($[B]_{tot}$ = 0.16 M) and pH_m ≤ 9 (Figure 2). A similar decrease in Np(V) solubility occurs in dilute $MgCl_2$ systems, but not in concentrated $MgCl_2$ brines where a strong competition of Mg^{2+} for borate complexation is expected.

The decrease in solubility observed in NaCl and $MgCl_2$ is accompanied by a clear change in the color of the solid phase (from greenish to white) and the slope of the solubility curve (log m_{Np} vs. pH_m). The newly formed solid phase shows distinct XRD patterns (Figure 3), confirming its crystalline character in contrast to the amorphous $NpO_2OH(am)$. XPS further indicates the stoichiometric participation of boron and Na^+/Mg^{2+} in the secondary phase formation. This solid phase transformation constitutes a new potential radionuclide retention mechanism for the highly mobile Np(V).

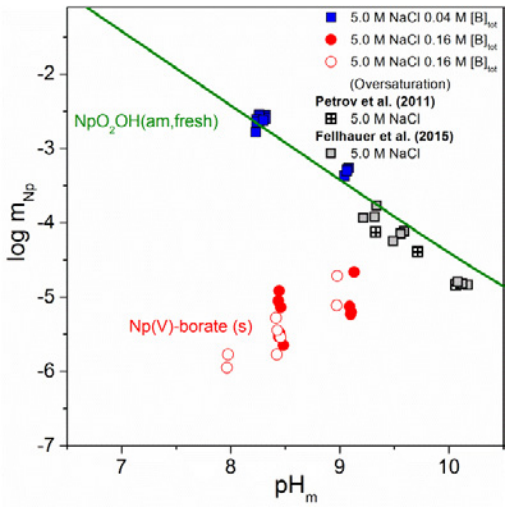

Fig. 2: Experimentally measured Np(V) solubility in 5.0 M NaCl in absence [7–8] and presence of borate ($[B]_{tot}$ = 0.04 and 0.16 M) [this work]. Solid line corresponding to the solubility of $NpO_2OH(am,fresh)$ in 5.0 M NaCl calculated according with NEA-TDB selection [2].

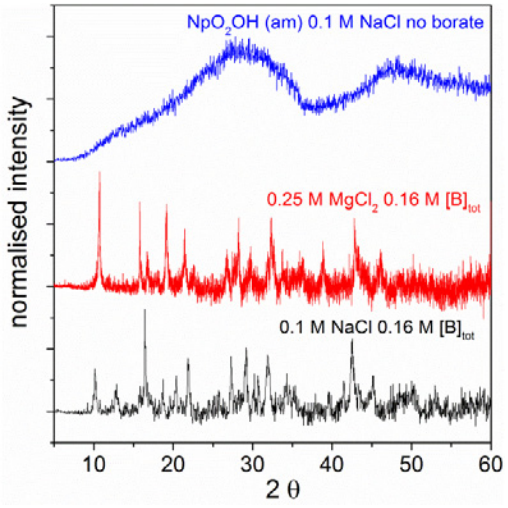

Fig. 3: Diffractograms of solubility-controlling Np(V) solid phases in the absence and presence of borate ($[B]_{tot}$ = 0.16 M).

Formation and stability of mixed Nd-OH-Cl(s) phases in concentrated chloride brines

An appropriate knowledge of the solubility controlling solid phases is mandatory in source term estimations and for accurate geochemical calculations. $An^{III}/Ln^{III}(OH)_3(s)$ phases are normally considered as solubility limiting solid phases of trivalent actinides/lanthanides in dilute to concentrated saline systems in the absence of complexing ligands. The successful synthesis of ternary An^{III}/Ln^{III}-OH-Cl(s) phases has been reported in structural studies, but no thermodynamic data has been derived so far for these systems [9–10]. The formation and stability of these solid phases can have relevant implications in the source term of repository concepts where high chloride concentrations are expected.

In a first part of this work, the transformation of $Nd(OH)_3(s)$ into a ternary Nd-OH-Cl solid phase was experimentally assessed in NaCl (5.61 m), $MgCl_2$ (0.25-5.15 m) and $CaCl_2$ (3.91 m) systems as a function of pH (7.5 ≤ pH_m ≤ 9.6) and temperature (T = 22 and 80°C). Experiments at T = 22°C were performed under argon atmosphere, whereas those at T = 80°C were conducted with autoclaves in presence of air. Note that in $MgCl_2$ solutions, the maximum pH_m (pH_{max} ~ 9) is limited by brucite or $Mg_2(OH)_3Cl{\times}4H_2O(s)$ precipitation.

Solid phase characterization (XRD and SEM-EDS) shows a clear transformation of the initial solid phase into $Nd(OH)_2Cl(s)$ in $MgCl_2$ systems at T = 22 and 80°C. The transformation is enhanced at high m_{Cl^-} and low pH_m (~ 8), whereas it does not occur in 2.67 m $MgCl_2$ and pH_{max} (~ 8.9). No solid phase transformation takes place either in 5.61 m NaCl (pH_m = 9.3) and 3.91 m $CaCl_2$ (pH_m = 9.6), indicating that these

m_{Cl^-} and/or pH_m conditions are outside the thermodynamic stability of $Nd(OH)_2Cl(s)$.

In a second part of the studies, the thermodynamic properties of $Nd(OH)_2Cl(s)$ were assessed. Batch solubility experiments were performed under argon atmosphere at room temperature using the $Nd(OH)_2Cl(s)$ phase previously synthesized at T = 22°C. Experiments were performed from undersaturation in 5.61 m NaCl, 2.67 m, 3.87 m, 5.15 m $MgCl_2$, 3.91 m $CaCl_2$ and $7.5 \leq pH_m \leq 13$. In a complementary set of experiments, $Nd(OH)_3(s)$ and $Nd(OH)_2Cl(s)$ were mixed and equilibrated under pH-unbuffered conditions with analogous background electrolyte and salt concentrations.

The comparison of $Nd(OH)_2Cl(s)$ and $Nd(OH)_3(s)$ solubility under virtually the same conditions [this work, 11] shows significantly lower m_{Nd} (up to 1.5 log_{10}-units) in equilibrium with $Nd(OH)_2Cl(s)$ in 2.67-5.15 m $MgCl_2$ and 3.91 m $CaCl_2$ at $pH_m \leq 8.8$ (see exemplarily Figure 4). On the contrary, no differences in aqueous concentrations in experiments with $Nd(OH)_2Cl(s)$ and with $Nd(OH)_3(s)$ are observed in 5.61 m NaCl within $7.5 \leq pH_m \leq 13$. The combination of the experimental solubility data determined in this work in $MgCl_2$ and $CaCl_2$ solutions with the Pitzer activity model derived in [11] allows the quantification of log_{10} $*K°_{s,0}$ for $Nd(OH)_2Cl(s)$. pH measurements in the "mixing experiments" give direct insight of log_{10} $*K'_{s,0}$ based on the thermodynamic equilibrium $Nd(OH)_2Cl(s) + H_2O \Leftrightarrow Nd_{aq} \Leftrightarrow Nd(OH)_3(s) + Cl^- + H^+$ and corresponding equation log_{10} $*K'_{s,0}(Nd(OH)_2Cl(s)) = log_{10}$ $*K'_{s,0}(Nd(OH)_3(s)) - pH_m + log_{10}$ m_{Cl^-}, provided that $pH_m^{mix} \leq pH_{max}$ in $MgCl_2$ solutions. The combination of both datasets permits an accurate quantification of the solubility product of $Nd(OH)_2Cl(s)$.

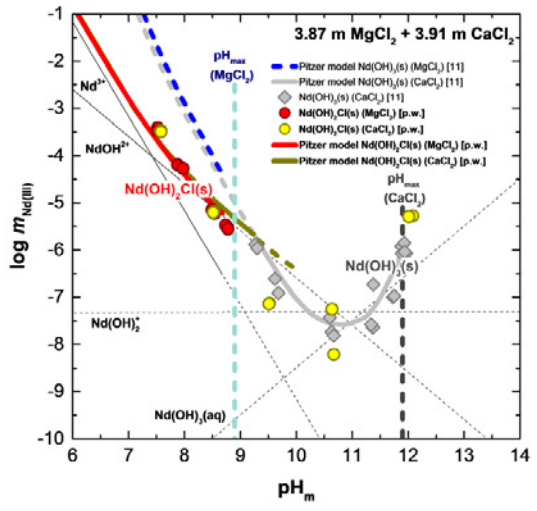

Fig. 4: Experimentally measured solubility of Nd(III) in 3.87 m $MgCl_2$ and 3.91 m $CaCl_2$. Reference solubility data of $Nd(OH)_3(s)$ [11] is included for comparison. Thick solid lines corresponding to the solubility of $Nd(OH)_2Cl(s)$ ($pH_m \leq 9.2$) and $Nd(OH)_3(s)$ ($pH_m > 9.2$) calculated with the thermodynamic and (Pitzer) activity models reported in [11] and derived in this work. Thin lines show the aqueous speciation underlying $Nd(OH)_2Cl(s)$ solubility curve in the respective systems.

The newly characterized solid phase can play a relevant role in controlling the solubility of An^{III}/Ln^{III} in repository systems with high chloride concentrations. Although kinetically slow, the transformation $An^{III}/Ln^{III}(OH)_3(s) \rightarrow An^{III}/Ln^{III}(OH)_2Cl(s)$ is enhanced at $m_{Cl^-} \geq 5.34$ m and $pH_m \leq 8.8$.

Impact of weak and strong donor ligands on the An=O bonds in actinyl(VI) complexes

The hexavalent state is the prevalent oxidation state for uranium in aqueous systems under oxic conditions, where it occurs as a linear, dioxo uranyl cation, UO_2^{2+}. In perchloric acidic solution this ion is coordinated by five equatorial aqua ligands, while a number of monomeric and oligomeric hydrolysis species form under near-neutral to hyperalkaline pH conditions. Under strongly oxidizing conditions also neptunium and plutonium form linear NpO_2^{2+} and PuO_2^{2+} cations. The linear geometry is a result of the participation of the 5f orbitals in the actinyl multiple bonds. These bonds are strong and rather unreactive, making the oxo groups weak Lewis bases. However, the reactivity and the Lewis basicity of the oxo groups depend strongly on the ligands in the equatorial plane and their binding to the metal. This is well reflected in the exchange rate of the actinyl oxo atoms, which is extremely slow (5×10^{-9} s^{-1}) in acidic solution but relatively fast (1 s^{-1}) in alkaline solution [12]. Thus, by s-donation, hydroxide ligands are able to polarize the actinyl bond through cis-destabilization and thereby increase the Lewis basicity of the oxo groups. Carbonate, fluoride, and acetate are additional potential ligands to actinyls in groundwaters [2], with a similar effect as the hydroxide ion of increasing the reactivity and the basicity of the actinyl oxo groups [13].

This Lewis basicity not only affects the exchange rate of the actinyl oxygens but also the actinyl bond length and the frequency of the symmetric (Raman active) stretching vibration, n_1. Thus, an increase of the basicity of the oxo groups by hydroxide or carbonate coordination at high pH increases the actinyl An=O distance but decreases n_1 [13]. We recently determined the X-ray crystal structures and measured the Raman spectra of several actinyl(VI) salts crystallized from aqueous solution at different pH, with or without carbonate ions. A linear correlation between n_1 and the actinyl An=O bond distance was established, showing that compounds with hydroxide and carbonate ligands have significantly longer actinyl bonds and smaller n_1 frequencies compared to compounds with water and nitrate ligands (Figure 5). Indeed, in $Cs_2[(UO_2(NO_3)_2(OH)_2]$, which has a coordination of both weak (nitrate) and strong (hydroxide) ligands, intermediate values were obtained for n_1 and the U=O distance compared to the compounds with only weak or strong ligands.

The near linear relation between n_1 and the An=O bond distance established in Figure 5 may be used for prediction of one or the other of the two parameters. Moreover, according to the bond valence method applied for hexavalent and neptunium [14-15], predic-

tion of An-O bond distances for the equatorial ligands is possible knowing the An=O bond distance, the latter of which may be estimated from n_1.

Np(V) complexation with propionate in 0.5 - 4 M NaCl solutions at 20-85°C

In the present study, the complexation of Np(V) with propionate is studied by spectrophotometry as a function of NaCl concentration, ligand concentration, and temperature. Ionic strength effects are treated with the specific ion interaction theory (SIT) [21]. Using this approach, the temperature dependent thermodynamic stability constants and $\Delta_r H^0_m$ and $\Delta_r S^0_m$ of the complexation reaction are determined.

The absorption spectra of Np(V) in presence of propionate in [NaCl] = 0.51 m for T = 23°C and pH_c = 5 shows 1:1 Np(V)-propionate complex formation. Generally, as the concentration of propionate increases, the intensity of the absorption band of free NpO_2^+ at 980 nm decreases and the maximum of the absorption band is shifting to higher wavelength. According to the peak deconvolution performed within the present study, the absorption band of the Np(V)-propionate complex has its maximum at ~984 nm. Spectral changes with increasing propionate concentration while keeping I and T constants are similar for all temperatures. NpO_2^+-Cl^- complexation has no significant effect on the spectra, as shown by Neck et al. [22] at room temperature up to I =1.0-3.0 m. The data analysis revealed that only the 1:1 complex is observable both for pH_c = 5 and 7 within the range of $[Prop]_{tot}$ investigated. Therefore, data for pH_c = 5 and 7 were treated together (i.e. two series for pH_c = 7 with I = 0.51 m, T = 23 and 85°C). Results for T = 23°C are compared to T = 85°C (both in [NaCl] = 0.51 m solution), to show the effect of temperature on the complexation reaction. Comparison to the plot at T = 23°C and [NaCl] = 3.20 m demonstrates the effect of ionic strength (see Figure 6). The slopes (n = 1.05 ± 0.05 at 23°C; 0.99 ± 0.11 at 85°C; 1.04 ± 0.15 for I = 3.2 m) confirm the formation of a 1:1 NpO_2^+-propionate complex. The y-intercept, log β, is determined as 1.04 ± 0.06 at 23°C and increases with temperature (1.36 ± 0.13 at 85°C) and with ionic strength (1.34 ± 0.15 at 3.2 m).

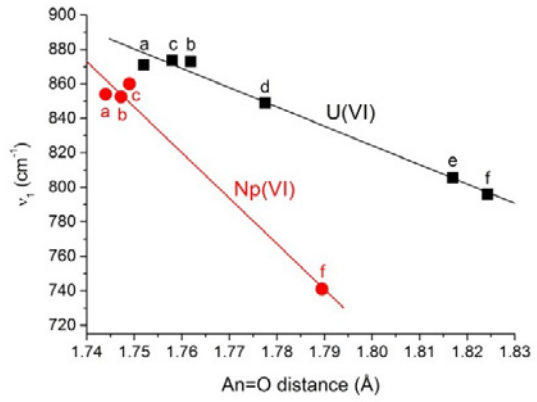

Fig. 5: The symmetric stretching n_1 vs. An=O bond length in hexavalent actinyl compounds: a) $[AnO_2(H_2O)_5](ClO_4)_2$ [16]; b) $[AnO_2(H_2O)_2(NO_3)_2]$ [17] c) $Cs[AnO_2(NO_3)_3]$; d) $Cs_2[(UO_2(NO_3)_2(OH)_2]$; e) $Na_4[(UO_2(CO_3)_3]$ [18]; f) $[Co(NH_3)_6]_2[AnO_2(OH)_4]$ $3H_2O$ [19-20].

By systematically varying the background electrolyte concentration, in this case the NaCl concentration, at constant T and applying an appropriate model for activity coefficients (γ) it is possible to extrapolate the conditional equilibrium constants β to zero ionic strength (β^0) standard conditions.

$$\beta_0 = \beta \times \frac{\gamma(NpO_2(Prop))}{\gamma(NpO_2^+) \times \gamma(Prop^-)}$$

From the slope, $\Delta\varepsilon$ is obtained as -0.17 ± 0.03 and the y-intercept (log β^0) equals to 1.26 ± 0.03. Log β^0 and $\Delta\varepsilon$ are in agreement with previously determined values for NpO_2-actetate complexation at 25°C [23]. Using $\varepsilon(Cl^-; NpO_2^+)$ = 0.09 ± 0.05 and assuming $\varepsilon(Na^+; Prop^-)$ = 0.08 ± 0.01 by analogy with acetate, $\varepsilon(Na^+ + Cl^-; NpO_2(Prop))$ would not be significantly different from to zero, which is expected for a non-charged species in accordance with SIT.

Temperature effect on the NpO_2^+ complexation by propionate was investigated between 20 and 85°C, for [NaCl] = 0.51 m at pH_c = 5 and 7. Log $\beta(T)$ are corrected to I = 0 for each temperature by applying the SIT as described in the previously to obtain log β^0(T). As a first approach, heat capacity was hypothesized to be zero as observed. $\Delta_r H^0_m$ and $\Delta_r S^0_m$ can be obtained from an Arrhenius plot on the basis of the van't Hoff equation. The NpO_2(Prop) complex formation reaction significantly increases over about half an order of magnitude when increasing temperature from 20°C to 85°C. A linear relationship is observed, confirming the initial hypothesis of zero heat capacity. $\Delta_r H^0_m$ and $\Delta_r S^0_m$ are calculated as 10.9 ± 1.2 kJ mol^{-1} and 62 ± 4 J mol^{-1} K^{-1}, respectively. Both values are positive, showing that the formation of the NpO_2(Prop) complex is endothermic and entropy driven. Positive $\Delta_r H^0_m$ and $\Delta_r S^0_m$ are likely due to dehydration effects of NpO_2^+ and $Prop^-$ ions.

The present study shows that the stability constant for the formation of the 1:1 NpO_2^+-propionate complex with log β^0 (23°C) = 1.26 ± 0.03, increases both with ionic strength (0.5 < NaCl < 3.2 m) and temperature (20 < T < 85°C). The magnitude of $\Delta_r S^0_m$ is consistent with a bidentate coordination mode, which is also shown by EXAFS [24] analysis, leading to the replacement of two water molecules in the first coordination shell of NpO_2^+ by the propionate ligand. The newly derived thermodynamic data ($\Delta_r H^0_m$, $\Delta_r S^0_m$, log $\beta^0(T)$) for Np(V)-propionate complexation are a valuable contribution to thermodynamic databases which are the basis of a reliable safety assessment for nuclear waste disposal scenarios.

Potentiometric and calorimetric studies on Eu(III)-lactate complex formation

The thermodynamics of the complexation of Eu(III) with lactate are studied in dilute to concentrated NaCl solutions ([NaCl] = 0.10 - 5.61 m, T = 25°C) by potentiometric and microcalorimetric measurements. The formation of three complexed species is observed. The conditional stability constants (log β'_n) for the formation of the $[Eu(Lac)_n]^{3-n}$ (n = 1, 2, 3) complexes as

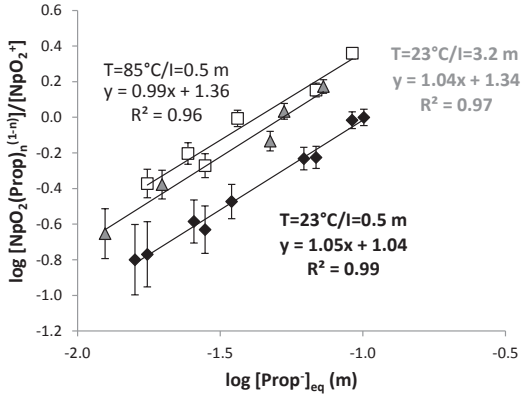

Fig. 6: Slope analysis of the Np(V)-propionate complex formed at 23 and 85°C for [NaCl] = 0.51-3.2 m.

well as for the protonation reaction of lactate ($\log \beta'_{HLac}$) are determined as a function of the ionic strength by potentiometric titrations. The $\log \beta'_n$ values are extrapolated to zero ionic strength with the SIT approach, yielding the thermodynamic constants ($\log \beta^0_{HLac} = 3.88\pm0.11$, $\log \beta^0_1 = 3.48\pm0.14$, $\log \beta^0_2 = 6.16\pm0.23$, $\log \beta^0_3 = 7.77\pm0.29$,). These values are in good agreement with literature data. [25] Furthermore, using the data given by the NEA-TDB, the following binary ion-ion interactions coefficients are determined: $\varepsilon(Na^+,Lac^-) = 0.01 \pm 0.04$, $\varepsilon(EuLac^{2+},Cl^-) = 0.09 \pm 0.03$, $\varepsilon(EuLac^{2+},Cl^-) = 0.02 \pm 0.05$ ($\varepsilon(EuLac_3,Na^+/Cl^-) \approx 0.00$) [26].

The conditional reaction enthalpies ($\Delta_rH'_n$) and entropies ($\Delta_rS'_n$) of the formation of the $[Eu(Lac)_n]^{3-n}$ (n = 1, 2, 3) species as well as of the protonation reaction of lactate are determined at different ionic strengths by microcalorimetric titrations. Using the SIT approach the conditional thermodynamic values are extrapolated to $I_m = 0$, yielding the standard state data. The results are given in Table 1. Additionally, the differences of the partial molal enthalpy specific ion interaction coefficients ($\varepsilon_L(i,k)$) for the different complexation reaction and the protonation reaction are determined ($\Delta\varepsilon_{L,HLac} = (-1.1\pm0.2)\cdot10^{-3}$, $\Delta\varepsilon_{L,1} = (-0.8\pm0.1)\cdot10^{-3}$, $\Delta\varepsilon_{L,2} = (-1.1\pm0.4)\cdot10^{-3}$, $\Delta\varepsilon_{L,3} = (-2.9\pm0.8)\cdot10^{-3}$).

Tab. 1: Thermodynamic functions (Δ_rH_n, $T\Delta_rS_n$) for the overall formation of $[Eu(Lac)_n]^{3-n}$ (n = 1, 2, 3) and for the protonation of lactate (n = HLac) at different ionic strengths (NaCl).

I_m	Δ_rH_{HLac}	Δ_rH_{01}	Δ_rH_{02}	Δ_rH_{03}
0.00	0.51 ± 0.09	0.95 ± 0.07	-0.87 ± 0.11	-8.73 ± 0.16
0.10	-0.28 ± 0.06	-1.36 ± 0.06	-4.78 ± 0.09	-14.70 ± 0.11
0.51	-1.13 ± 0.10	-2.64 ± 0.08	-6.40 ± 0.10	-16.53 ± 0.13
2.09	-2.92 ± 0.07	-4.12 ± 0.09	-9.11 ± 0.08	-19.35 ± 0.12
5.61	-6.63 ± 0.08	-8.06 ± 0.09	-14.49 ± 0.12	-33.80 ± 0.14

I_m	$T\Delta_rS_{HLac}$	$T\Delta_rS_{01}$	$T\Delta_rS_{02}$	$T\Delta_rS_{03}$
0.00	22.6 ± 2.6	20.8 ± 2.4	34.3 ± 4.3	35.6 ± 5.9
0.10	20.7 ± 2.3	14.3 ± 2.1	23.8 ± 4.0	20.5 ± 6.3
0.51	19.4 ± 2.1	11.6 ± 1.9	19.5 ± 3.8	16.1 ± 5.5
2.09	18.0 ± 2.3	9.60 ± 2.0	15.2 ± 3.9	12.5 ± 5.7
5.61	16.5 ± 2.6	6.90 ± 2.5	11.4 ± 4.1	-1.1 ± 5.7

The results show a distinct change of the thermodynamic functions with the concentration of the background electrolyte. In general, the reaction enthalpies decrease with increasing ionic strength. This change is pronounced in the range of very low to medium ionic strength ($I_m = 0.0 – 1.0$ m). At very high ionic strength ($I_m > 2.0$) the effect is still observable but less distinct. The ionic strength dependency of the thermodynamic functions follows the general trend observed for the change of activity coefficients. It is attributed to a weakening of the binding of the first hydration shell of the ions with increasing ionic strength. Thus, less energy is required for the dehydration step in the complexation/protonation reaction and the overall enthalpy decreases. Particularly for the protonation reaction and the first complexation step this effect leads to a change of the reaction enthalpy from endothermic values at $I_m = 0$ to exothermic values at $I_m > 0$. The entropy functions ($T\Delta_rS_n$) show a similar dependency of the NaCl concentration. The values decrease considerably with the ionic strength. This results from a decreasing gain of entropy due to the release of water ligands into the bulk solution during the dehydration step at higher ionic strengths. The results show, that the main driving force of the complexation of Eu(III) with lactate changes with the ionic strength. At low I_m the reaction is primarily entropy driven, while at high I_m the main driving force is the exothermic reaction enthalpy.

References

[1] Vichot, L. et al. *Radiochimica Acta*, **91**, 263-271, (2003).

[2] Guillaumont R. et al. *Chemical Thermodynamics* **Vol. 5**, Elsevier, Amsterdam, (2003).

[3] Brendebach, B. et al. *Inorganic Chemistry*, **46**, 6804-6810, (2007).

[4] Altmaier, M. et al. *Radiochimica Acta*, **96**, 541-550, (2008).

[5] Schimmelpfennig, B. et al. *Section 9.6 in this report* (2015)

[6] Hinz, K. et al. *New Journal of Chemistry*, **39**, 849-859 (2015).

[7] Petrov, V.G. et al. *Migration Conference*, Beijing, China (2011).

[8] Fellhauer, D. (2015), *Personal communication.*

[9] Zehnder, R. A. et al. *Inorg. Chem. 49*, 4781–4790 (2010).

[10] Bukin, V. I. Dokl. Akad. Nauk SSSR 207, 1332–1335 (1972).

[11] Neck, V. et al. *Pure Appl. Chem.* **81**, 1555–1568 (2009).

[12] G. Gordon et al. *J. Inorg. Nucl. Chem*. **19**, 189-191 (1961).

[13] C. Nguyen-Trung et al. *Inorg. Chem.* **31**, 5280-5287 (1992).
[14] P. Burns et al. *Can. Mineral*. **35**, 1551-1570 (1997).
[15] S. Wang et al. *Inorg. Chem*. **50**, 2527-2533. (2011).
[16] M. Grigor'ev et al. *Radiochem.*, **52**, 375-381 (2010).
[17] P. Lindqvist-Reis et al. *Dalton Trans*., **42**, 15275-15279 (2013).
[18] I. Cisarova et al. *Acta. Crystallogr*. **E75**, 32-3 (2001).
[19] D. Clark et al. *Inorg. Chem*., **38**, 1456-1466 (1999).
[20] D. Clark et al. *Inorg. Chem*., **52**, 3547-3555 (2013).
[21] Ciavatta, L. *Annali di Chimica*, **70**, 551-567 (1980).
[22] Neck, T. et al. *Radiochim. Acta*, **69**, 39-47 (1995).
[23] Rao, L. et al. *J. Solution Chem*, **39**, 1888–1897 (2010).
[24] Vasiliev, A. et al. *Dalton Trans*. (2015, in press)
[25] Barkleit, A. et al. *Dalton Trans*., **43**, 11221-11232, (2014).
[26] Hummel, W. et al. *Chemical Thermodynamics* **Vol. 9**, Elsevier, Amsterdam, (2005).

4.2 Sorption on mineral surfaces

N. L. Banik, H. Geckeis, F. Heberling, J. Lützenkirchen, C. Marquardt, R. Marsac, T. Rabung, T. Schäfer, D. Schild, A. Schnurr

In co-operation with:

R. A. Buda[a], J. V. Kratz[a], T. Preocanin[b], N. Kallay[b] and P. J. Eng[c]

[a]Institute for Nuclear Chemistry, University of Mainz, 55099 Mainz, Germany; [b]Laboratory of Physical Chemistry, Department of Chemistry, Faculty of Science, University of Zagreb, Horvatovac 102a, 10001 Zagreb, Croatia; [c] GeoSoilEnviroCars, University of Chicago, 5640 South Ellis, Chicago, IL 60637, USA

Introduction

In performance safety calculations for nuclear waste repositories radionuclide retention onto mineral surfaces is a key aspect, which has to be considered. To understand the (sorption) reactions and mechanisms at the mineral-water interface fundamental studies are essential.

In this annual report, we want to highlight the work regarding to An/Ln retention onto clay minerals. Besides laboratory experiments quantifying the retention of radionuclides onto clay minerals under different experimental conditions, also the modeling of these results is essential. By combination of a top down / button up approach and a quantitative description of sorption reactions by the means of thermodynamic constants relevant sorption data can be provided for performance assessment.

A basis for understanding radionuclide retention processes is the sound knowledge on the processes occurring at the water-mineral interface. A fundamental study on the charging behavior of hematite (001) surface in aqueous NaCl solutions is also included in this report.

Modeling plutonium sorption and redox speciation in presence of kaolinite

Plutonium exhibits a particularly complex redox chemistry with thermodynamically stable redox states from +III to +VI depending on the redox environment. The chemical behavior of Pu, e.g. complexation by organic and inorganic ligands, solubility as well as sorption to minerals strongly depends on the Pu redox state. In particular mineral surfaces are known to affect Pu redox speciation and a mixture of different Pu redox states is almost systematically found, e.g. [1]. Accordingly, interpretation of Pu sorption data is a challenge even for simplified laboratory experiments.

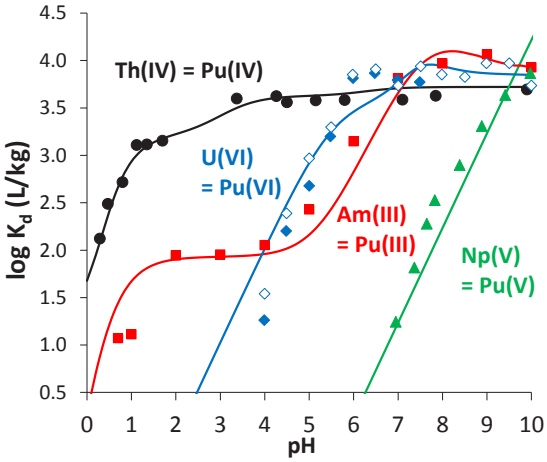

Fig. 1: Experimental sorption data (log K_d, in L/kg) for Am(III) [7], Th(IV) [1], Np(V) [8] and U(VI) [9] versus pH in 0.01 (open symbols) or 0.1 M $NaClO_4$ (closed symbols) without $CO_{2(g)}$.

In a recent study on Neptunium sorption to illite [2], we have demonstrated that the prevailing redox state at the mineral surface may differ from the one in solution: the stability field of the strongly adsorbed Np(IV) is enlarged at the illite surface compared to the solution. Such behavior is well predicted by thermodynamic calculations including surface complexation. The work on the Np(IV)-illite system is here extended to the four oxidation states of Pu and to another clay mineral: kaolinite.

Thermodynamic constants from the NEA [3] are used taking the specific ion interaction theory (SIT) [4]. PHREEQC [5] and PhreePlot [6] are used for speciation calculations (including sorption) and constructing predominance (pH-pe) diagrams, respectively.

Am(III), Th(IV), Np(V) and U(VI) are used as analogues for the corresponding Pu redox states. Previously published sorption data on kaolinite in 0.01 or 0.1 M $NaClO_4$ in the absence of $CO_{2(g)}$ [1,7-9] are shown in Figure 1. These data are used to calibrate a non-electrostatic surface complexation scheme and cation exchange model previously developed for kaolinite [10]. The modeling results are shown in Figure 1 as solid lines. A linear free energy relationship (i.e hydrolysis versus surface complexation constants) is found ($R^2 = 0.99$) supporting the consistency between the determined surface complexation constants, which will be applied for the different Pu redox states in the following.

The areas of Pu predominance are shown in the pH-pe diagram of the solution is shown in Figure 2a (in black). Note that the speciation for each redox state (i.e. the different hydrolyzed species) does not appear. By accounting for sorption in the Nernst equation, the Pu predominance pH-pe diagram at the kaolinite surface is constructed and superimposed to the one for the aqueous solution in Figure 2a (in red). The stability field of the strongly adsorbing Pu(IV) is clearly enlarged at the kaolinite surface. Therefore, Pu(IV) is predicted to be stable at the kaolinite surface under conditions where Pu(III), Pu(V) or Pu(VI) prevail in

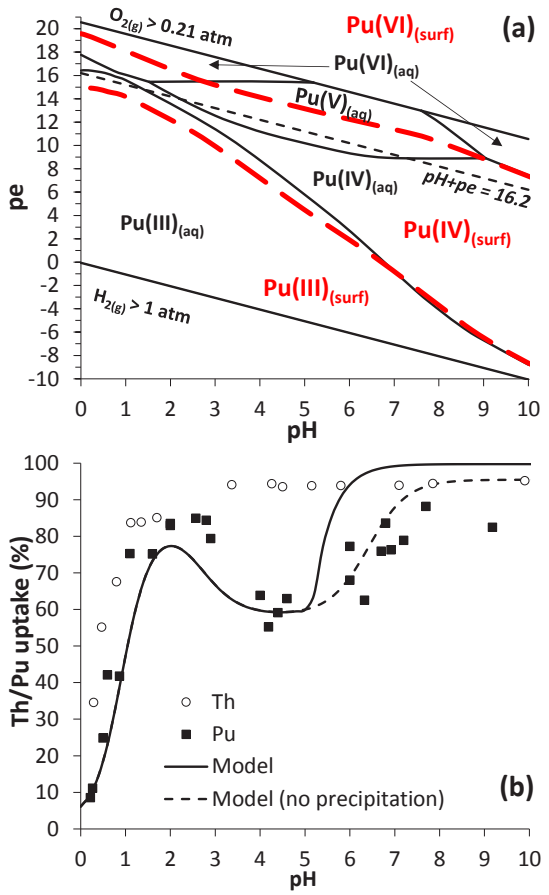

Fig. 2: (a) pH-pe predominance plot for Pu in solution (black) and at the surface of kaolinite (red). pH+pe = 16.2 is shown as a dashed black line. (b) Experimental Th and Pu uptake in 0.1 M $NaClO_4$ under ambient atmosphere [1]. The predicted Pu uptake for pH+pe = 16.2 is shown when considering (solid line) or not (dashed line) the precipitation of $PuO_{2(am,hydr)}$ as an uptake process.

the aqueous solution. For 0 < pH < 10, Pu(V) never prevails at the kaolinite surface because of its much weaker sorption behavior then Pu(VI) and Pu(IV).

Banik et al. [1] studied the adsorption of Pu (added as Pu(IV) to yield $[Pu]_{tot} = 6.9\times10^{-9}$ M) to a kaolinite suspension (solid to solution ratio: 4 g/L) in 0.1 M $NaClO_4$ salt concentration under ambient atmosphere. Pu uptake was determined after centrifugation at 3,000 g. The pattern of Pu uptake is very uncommon. Uptake is systematically lower than Th(IV) and non-monotonic for 3 < pH < 7 (Figure 2b). Redox state analysis for Pu in the aqueous solution after contact with kaolinite and subsequent phase separation was performed at pH = 1, 4 and 9, resulting in:

i. for pH = 1, 38% of $Pu(III)_{(aq)}$ and 46% of $Pu(IV)_{(aq)}$,
ii. for pH = 4, 75% of $Pu(V)_{(aq)}$ and 14% of $Pu(IV)_{(aq)}$ and
iii. for pH = 9, 45% of $Pu(IV)_{(aq)}$ and 49% of Pu(IV) in form of intrinsic (or eigen-) colloids.

The calculation of the pe from Pu redox state analysis in solution (for pH = 1 and 4) yields constant redox conditions (pH + pe ≈ 16.2; dotted line in Figure 2a). The calculated percentage of Pu uptake by kaolinite is shown on Figure 2b for pH + pe = 16.2. The unusual Pu uptake pattern is well predicted for pH < 4. For pH > 4, pe cannot be calculated because only Pu(IV) was detected. The redox conditions are assumed constant (pH + pe =16.2) for the following discussion. In addition, the experimental observation of Pu(IV) colloids (not removed by centrifugation at 3,000 g) shows that the solution is oversaturated with respect to $PuO_{2(am,hydr)}$. When considering $PuO_{2(am,hydr)}$ precipitation as an uptake process (solid line), Pu uptake is overestimated, suggesting that $PuO_{2(am,hydr)}$ did not form, maybe due to the limited equilibration time. When neglecting $PuO_{2(am,hydr)}$ precipitation (dashed line), Pu uptake is well predicted although Pu(IV) eigen-colloids formation and sorption cannot currently be taken into account in PHREEQC, which suggests that Pu(IV) monomers and eigen-colloids might exhibit similar sorption behavior to kaolinite under the experimental conditions investigated in the original study [1]. Further work dedicated to tetravalent actinides eigen-colloids sorption to minerals is required to confirm this observation. The effect of carbonate is not considered in this study because of the elusive behavior of Pu above pH = 5 in the experiments of Banik et al. [1].

The present findings have important consequences for Pu mobility in the environment. In particular surface complexation mechanisms would have an impact on Pu redox speciation. In line with our previous work on Np [2], it is possible to predict Pu and Np sorption and redox speciation when (i) accounting for redox chemistry in a comprehensive way and the respective sorption behavior in case (ii) the redox potential has been experimentally determined.

Experiment and modeling of Eu(III) sorption onto montmorillonite and illite in saline solutions: Impact of different background electrolytes

The present work is a continuation of sorption investigations of trivalent Europium (Eu) onto montmorillonite (SWy-2) and illite (Illite du Puy) under saline conditions [2, 11]. Batch sorption studies were carried out with two different background electrolytes ($MgCl_2$ and $CaCl_2$) at different concentrations (varied up to $[CaCl_2]_{max}$ = 4 mol/L (M)), at fixed metal concentration ($[Eu]_{total} = 2 \times 10^{-7}$ M, labeled with ^{152}Eu for γ-counting) and constant solid to liquid ratio (S:L = 2 g/L) over a wide pH range (3-12) excluding carbon dioxide. The experimental data obtained in this study was compared to a previous study in NaCl media ($[NaCl]_{max}$ = 3.6 M). The amount of Eu sorbed onto the clay minerals reaches > 99.5% (log K_D > 5) with increasing pH (pH_c > 8) confirming nearly complete uptake even under high salinity (Fig. 3). For pH_c < 5, where cation exchange is the dominant sorption mechanism only weak sorption (< 20%) is detectable even for the lowest investigated ionic strength ([$MgCl_2$ or $CaCl_2$] = 0.06 M). Cation exchange is more strongly suppressed by Mg^{2+}/Ca^{2+} compared to Na^+ due to the

higher charge of the cation. The uptake results in $MgCl_2$ and $CaCl_2$ solutions coincide for comparable experimental conditions within the experimental error. The two-site protolysis non-electrostatic surface complexation and cation exchange (2SPNE SC/CE) model [12] calibrated for "low" ionic strengths ($[NaClO_4]$ = 0.1 M), was applied to data in the saline $MgCl_2$ or $CaCl_2$ system. Minor adjustments allow an accurate description of the data for Na-(exchanged)-clays. Use of parameters extracted for Ca-clays however, provide a better fit to the uptake data in Mg/Ca systems. It is expected that these high Mg/Ca concentrations from the background electrolyte cause via cation- exchange the formation of the Mg/Ca-clay from the initial Na-clay.

A new model for the hematite (001) charge behavior in aqueous NaCl solutions

The hematite 001 - aqueous solution interface was studied via surface diffraction techniques (in the presence of a water film) and the macroscopic charging via surface- and zeta-potential measurements (in electrolyte solutions as a function of pH). The surface

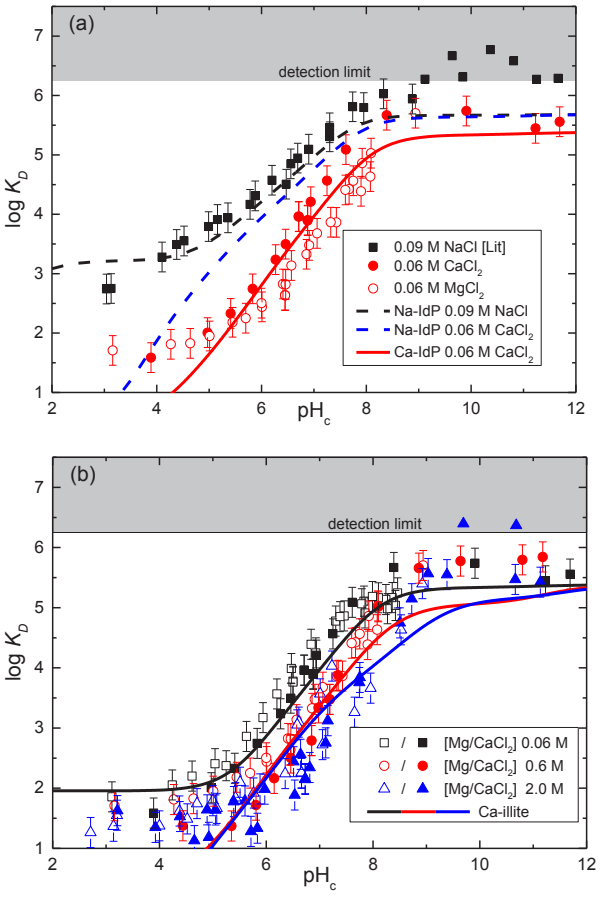

Fig. 3: (a) Sorption edge for Eu ($[Eu]_{total}$ = 2.0 x 10^{-7} M), S:L 2 g/L, on Na-illite as a function of pH_c and at 0.06 M $MgCl_2$ and $CaCl_2$ together with literature data. (b) Sorption edges with different $[MgCl_2]$ and $[CaCl_2]$ (0.06, 0.6, 2.0 M). Sorption data (symbols) are presented as the logarithm of distribution ratio (log K_D). Curves represent blind predictions using the 2SPNE SC/CE model and Pitzer equations with Na-illite (dotted lines) and "Ca-illite" (solid lines).

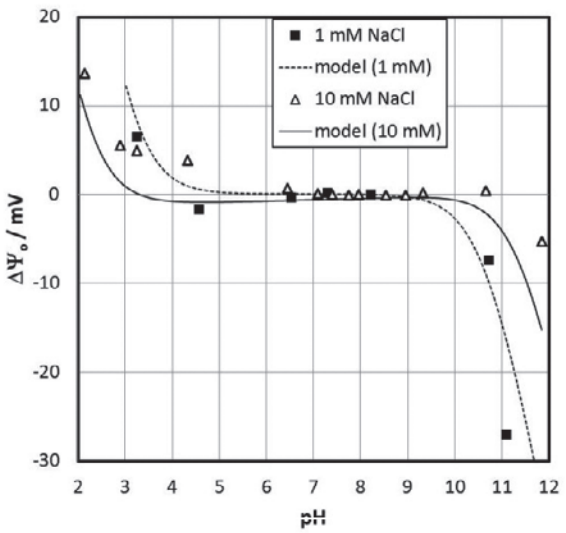

Fig. 4: Surface-potentials for a fresh hematite-(001) sample. Symbols are experimental data and lines are calculated by the proposed surface complexation model.

exhibits the typical bi-domain structure, i.e. a part that is iron terminated and another part that is oxygen terminated in agreement with previous reports [13-15]. The surface potential vs. pH curve appears to be dominated by the presence of the doubly coordinated hydroxyls. The zeta-potential vs. pH curve shows an isoelectric point at around pH 4, that is atypical for oxide particle surfaces [16], but has been frequently reported for a variety of oxide single crystal surfaces as well as "inert" surfaces and classical colloids like silver halides [19-21]. Figure 4 shows the surface potential as a function of pH at two different salt concentrations. Figure 5 shows the concomitant zeta-potentials. The point of zero surface potential, which according to Figure 4 should be at around pH 6 (in the middle of the broad plateau), is in disagreement with the isoelectric point which is found two pH units below (Fig. 5). In particular at the plateau range a strongly negative electrokinetic charge is observed.

Figure 4 and 5 include the results of calculations that are based on a rather complex interfacial model. We consider deprotonation of the surface hydroxyl groups, and have to assume that the double coordinated hydroxyls are dominant, since they yield exactly the behavior that is expected for a surface terminated by those groups. The associated surface diffraction study confirms the presence of these groups.

As stated above the isoelectric point at pH 4 has been associated with inert surfaces. For these, physical hydroxide adsorption [17-19] within the electrokinetic shear-plane is despite the ongoing debate [20-22] the most likely charging mechanism and is included here. Coupling between these two phenomena in a common model does not allow to describe the surface potentials shown in Figure 4. Various electrostatic models have been tested to this end, and none was able to consistently describe both kinds of data (i.e. surface and zeta-potentials).

Based on recent advances on ion adsorption and more specifically electrolyte layering at the interface

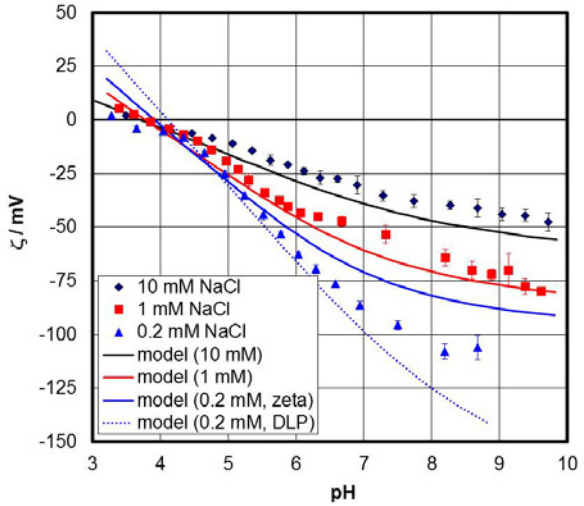

Fig. 5: Zeta-potentials for a fresh hematite-(001) sample. Symbols are experimental data and lines are calculated by the proposed surface complexation model. Two model lines are plotted for the 0.2 mM NaCl data. The one noted "zeta" points to the model-inherent slip plane distance, while the one noted "DLP" pertains to the potential at the onset of the diffuse layer.

between the gibbsite basal plane and aqueous solutions [23], we included a layer of sodium ions in the surface plane and a layer of chloride ions in the subsequent plane to account for this observation. The gibbsite basal plane is very similar to the sapphire (001) plane, which is in turn equivalent to the hematite (001) plane. Therefore, the assumption of the electrolyte layering appears justified. The revised model allows to describe both the surface and zeta-potentials as shown in Figures 4 and 5. Furthermore, and quite surprisingly the model is able to predict increasing surface potential with increasing pH [24]. This had been previously observed in some published studies, but was never discussed. The increase is at odds with the traditional models. However, these models ignore the presence of electrolyte layers on such surfaces. It appears to be a general feature on flat surfaces. Thus similar features have recently been observed in surface diffraction studies on flat calcite surfaces [25]. Furthermore, it has been hypothesized based on results from cryo-XPS experiments with hematite particles that salt (NaCl) hydrate formation on hematite (001) surfaces occurs [26], which is potentially related to or initiated by the formation of electrolyte layers as discussed here.

References

[1] Banik, N. L. et al., *Radiochim. Acta* **95** (2007), 569-575.

[2] Geckeis, H. et al.,Annual Report 2013. *KIT scientific reports* **7664** (2013).

[3] Guillaumont et al., *Chemical Thermodynamics* Vol. **5** (2003).

[4] Ciavatta, *Annali di Chimica* **70** (1980), 551-567.

[5] Parkhurst & Appelo, User's guide to PHREEQC (Version 2) (1999).

[6] Kinniburgh, D. G. and Cooper, D. M. (2009) <http://www.phreeplot.org>.

[7] Buda et al., *Radiochim. Acta* **96** (2008), 657-665

[8] Amayri et al., *Radiochim. Acta* **99** (2011), 349-357.

[9] Křepelová, Ph.D. thesis, University of Dresden, Germany (2007).

[10] Tertre et al., *GCA* **72** (2008), 1043–1056.

[11] Brewitz, W.: Eignungsprüfung der Schachtanlage Konrad für die Endlagerung radioaktiver Abfälle. GSF-T136, Neuherberg (1982).

[12] Bradbury, M. H. & Baeyens, B., *GCA* **73** (2009), 990-1003.

[13] Wang, X. G. et al., *Phys. Rev. Lett.*, 1998, **81**, 1038-1041.

[14] Trainor, T. et al., *Surf. Sci.* (2004), **573**, 204-224.

[15] Tanwar, K. S. et al., *GCA* (2009), **73**, 4346-4365.

[18] Franks, G. V. and Gan, Y., *Journal of the American Ceramic Society*, (2007), **90**, 3373-3388.

[19] Zimmermann, R. et al., *Current Opinion in Colloid & Interface Science*, (2010), **15**, 196-202

[20] D. Rothenstein, et al., *J. Am. Chem. Soc.*, (2012), **134**, 12547-12556.

[21] Selmani, A. et al., *Journal of Physics-Condensed Matter*, (2014), **26**.

[22] Cecchi, T., *Journal of Physical Chemistry C*, (2013), **117**, 25579-25585.

[23] Jungwirth, P., *Faraday Discuss.*, (2009), **141**, 9-30.

[24] Shapovalov, V. L., et al., *Physical Chemistry Chemical Physics*, (2013), **15**, 13991-13998.

[25] Siretanu, I. et al., *Scientific Reports*, (2014), **4**.

[26] Chatman, S. et al., *Journal of Colloid and Interface Science*, (2013), **391**, 125-134.

[27] Heberling, F. et al., *Phys. Chem. Chem. Phys.*, (2014), **16**, 12782-12792.

[28] Shchukarev, A. et al., *Journal of Physical Chemistry C*, (2007), **111**, 18307-18316

4.3 Retention of radionuclides by secondary phase formation

F. Heberling, N. Finck, V. Metz, M. Böttle, S. Heck, C. Garcia, L. Temgoua, S. Hofmann

In co-operation with:

E. Curtia, T. Stumpf[b]

[a]Paul Scherrer Institut, Villigen, Switzerland; [b]Helmholtz-Zentrum Dresden-Rossendorf, Institute of Resource Ecology, Bautzner Landstr. 400, 01328 Dresden, Germany.

Introduction

In the surrounding of a potential nuclear waste repository, secondary phases may form as corrosion products of HAW-glass or spent nuclear fuel, during the alteration of canister and backfill material, or in the (geo)technical and geological barriers. During the formation of secondary phases, radionuclides may be structurally incorporated into the corresponding minerals, and possibly form solid solutions. The potential of secondary phases to immobilize radionuclides and to inhibit their migration towards the biosphere can be considerable. However, despite the abundance of solid solutions in natural systems, reliable thermodynamic and kinetic models to quantitatively predict solid solution formation are hardly available. The aim of the "secondary phases group" at INE is to characterize the incorporation of actinides (e.g., Cm) as well as long-lived fission (e.g., ^{79}Se), activation and decay (e.g., ^{228}Ra) products into mineral phases on a molecular scale, using state-of-the-art spectroscopy, diffraction, and microscopy techniques, as well as computational chemistry methods (in collaboration with the computational chemistry group, cf. chapter 9.5). Based on a molecular scale process understanding and quantitative data, we develop thermodynamic solid solution models. Whenever it is indicated that thermodynamic models are not directly applicable, kinetic effects are taken into account.

Barite recrystallization in the presence of $^{226}Ra^{2+}$ and $^{113}Ba^{2+}$

$(Ba,Ra)SO_4$ is a real classic system among the solid solutions. Doerner and Hoskins [1] studied the precipitation of barite in the presence of Ra, and finally were the first to develop the concept of co-precipitation based on this system. Nevertheless, there are still ambiguities on the thermodynamic parameters necessary to describe this solid solution, even at ambient conditions. In recent years a series of studies [2-6] sought to understand the formation of $(Ba,Ra)SO_4$, starting from pre-existing barite and aqueous Ra^{2+}. In case, spontaneous equilibration between barite and aqueous Ra^{2+} could be demonstrated, and it could be shown that this reaction is fast relative to the timeframe of nuclear waste disposal, i.e. several hundred thousand years, this reaction could be implemented in performance assessment calculations. This would lead to a decrease in the $^{226}Ra^{2+}$ source term of a potential nuclear waste repository by several orders of magnitude, relative to the consideration of $RaSO_4$ as solubility limiting phase.

In this context four series of batch type recrystallization experiments were performed at INE. Each series consisted of seven batches, including two blank experiments, three multiple sampling batches to assess the recrystallization kinetics, and two batches that were only sampled after one and two years reaction period, respectively. 0.1 g/L barite from Sachtleben Chemie® (Blanc Fixe XR HR 10) were added to each batch. 0.1 mol/L NaCl was used as background electrolyte. After a nine-month pre-equilibration period, 346 Bq/mL $^{133}Ba^{2+}$ and varying concentrations of $^{226}Ra^{2+}$ were added. The experimental conditions are summarized in Table 1. The pH variation between the experimental series is due to the use of two different $^{226}Ra^{2+}$ stock solutions.

Tab. 1: Summary of the experimental conditions in the four series of barite recrystallization experiments.

	$c_0(^{226}Ra^{2+})$ (mol/L)	$c_0(^{133}Ba^{2+})$ (Bq/mL)	pH-range
A	0	346	4.72 – 5.21
B	$5 \cdot 10^{-10}$	346	3.55 – 3.57
C	$1.10 \cdot 10^{-9}$	346	3.14 – 3.17
D	$1.16 \cdot 10^{-8}$	346	4.14 – 4.18

Continuous uptake of $^{133}Ba^{2+}$ and $^{226}Ra^{2+}$ was observed during the two years reaction period (Figures 1 and 2). The uptake kinetic data is described by a new kinetic model, which is based on the homogeneous model by Curti *et al.* [7], but considers an increase of reaction time proportionally to the amount of barite that recrystallizes during each reaction step. Details about the model will be published elsewhere (Heberling *et al.* (in prep.)). It is important to note that none of the existing models, heterogeneous or homogeneous [7], is able to describe the reaction progress properly. In contrast to previous studies [2-6], our model predicts that it may take several hundred thousand years until barite equilibrates with a surrounding aqueous phase. Our results indicate that the retarded kinetics in our experiments are due to the prolonged aging time of the used barite, of about nine month, considered during the preparation of our experiments.

This may have significant implications for the implementation of $(Ba,Ra)SO_4$ formation in performance assessment calculations. In future studies

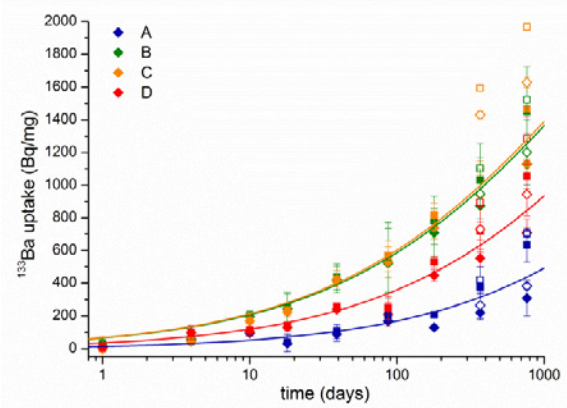

Fig. 1: ^{133}Ba uptake during the barite recrystallization experiments. The four series of experiments are color coded as shown in the legends (for sample details see Table 1). Diamonds depict the data after correction for container wall sorption, squares represent the uncorrected data. Full symbols are data from multi sampling batches and open symbols are from the batches sampled only twice. Lines indicate model calculations.

we will therefore focus on the characterization and quantification of the driving forces and the kinetic controls of barite recrystallization.

One more important aspect, with respect to kinetics, is that the recrystallization rates seem to correlate very well with the average pH in the experiments ($R^2 = 0.93$).

Due to the parallel measurements of ^{133}Ba and ^{226}Ra uptake during our experiments, the amount of ^{226}Ra taken up at each sampling time can be correlated with the amount of barite recrystallized. This provides valuable information on the thermodynamics of the uptake process. The results indicate that during an initial period the partition coefficients scatter significantly, $0.1 < D < 1.5$. However, after about 80 days of reaction time very constant values are obtained, $D = 0.54 \pm 0.08$. With the solubility products $\log_{10}(K_{SP}(BaSO_4))$ = -9.97 and $\log_{10}(K_{SP}(RaSO_4))$ = -10.26 [8] this translates to a Guggenheim Parameter, $a_0 = 1.3 \pm 0.1$. This represents the so far most precise experimental determination of this Guggenheim parameter and is in perfect agreement with the value determined by Vinograd *et al.* [5] based on DFT calculations with $a_0 = 1.0 \pm 0.4$.

TRLFS investigations on the interactions of trivalent actinides/lanthanides with celestite and strontianite

The interactions of trivalent actinides (An(III)) such as Pu, Am, and Cm with mineral phases is of crucial importance in radionuclide migration since they are responsible for the majority of radiotoxicity after 1000 years. Mixed flow experiments were coupled with time-resolved laser fluorescence spectroscopy (TRLFS) to study both the kinetics and the uptake mechanisms of trace concentrations of the dopant ions (Cm^{3+}, Eu^{3+}) interacting with the mineral phase. A previous study by Holliday *et al.* [9] showed that the anions have the most dramatic effect on the uptake of the trivalent cation by the solid mineral phase, which

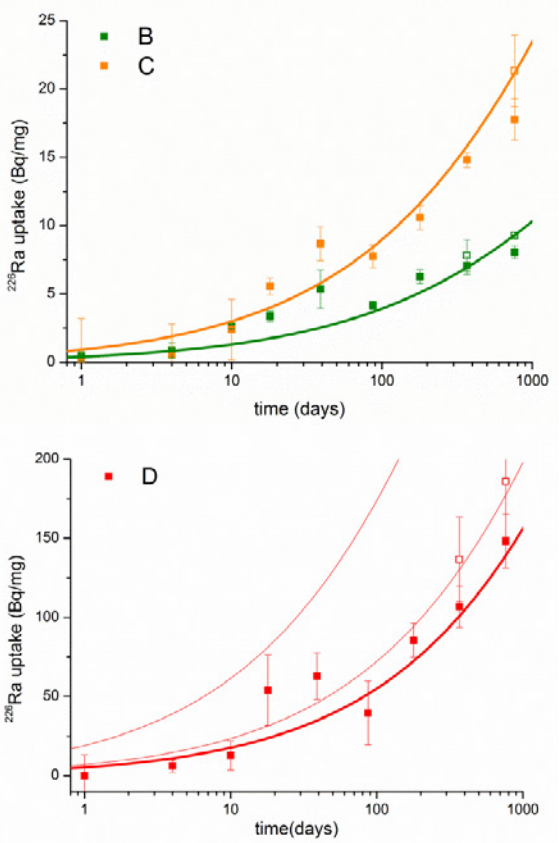

Fig. 2: ^{226}Ra uptake during the barite recrystallization experiments. Full symbols are data from multi sampling batches, open symbols are from the batches sampled only twice. Thick lines are model calculations, calculated with a Guggenheim parameter $a_0 = 1.3$, and the recrystallization rates given below. Thin lines in the graph for series D correspond to exemplary calculations with $a_0 = 1$ and an ideal solid solution, $a_0 = 0$.

was seen by comparing the much stronger CO_3^{2-} ligand having greater uptake than the weak SO_4^{2-} ligand in iso-structural strontianite and celestite, respectively. Since the precipitation rates and/or saturation index of celestite and strontianite were not similar in the work of Holliday *et al,* it was not clear if the observed uptake behaviors were only due to the nature of the anion. This study uses similar experimental conditions (precipitation rate, saturation index), so suppressing all others factors, except the nature of the anion that can influence the uptake of trivalent actinides/lanthanides by the iso-structural mineral celestite and strontianite.

Nucleation experiments. Trace amounts of Cm^{3+} or Eu^{3+} were added to solutions supersaturated with respect to celestite and strontianite, and fluorescence spectra were recorded at different times during the homogeneous nucleation of the mineral phases (Figure 3).

TRLFS data show that the same species is formed during the homogeneous nucleation and the growth of celestite. The fluorescence spectrum at 16-20 min is different from the aqua ion and shows that "early stage nuclei", as observed in LIBD experiments, show already the same Cm binding environment as the crystalline celestite. Contrary to the observations made

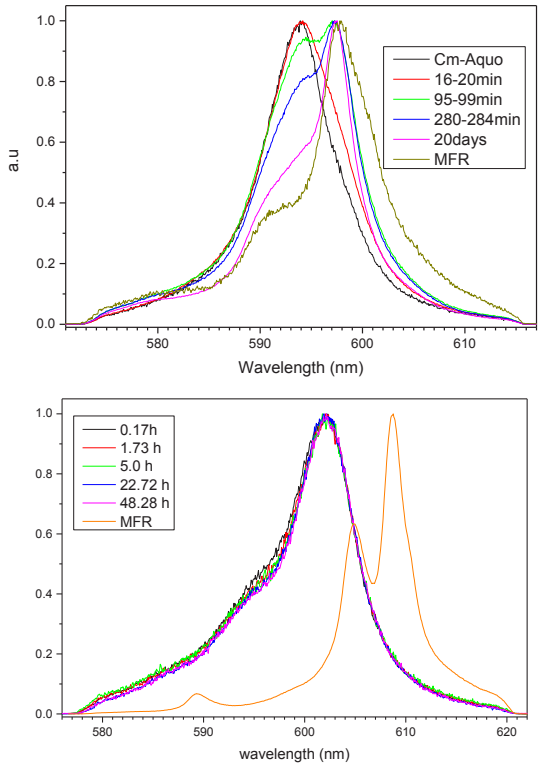

Fig. 3: Curium uptake during the nucleation of celestite (upper graph) and strontianite (lower graph)

in the celestite system, a comparison of fluorescence spectra recorded for the curium uptake during the homogeneous nucleation and the growth of strontianite in mixed flow reactors (MFR) shows the formation of different species (see Figure 3).

Additional information provided by the lifetime of the fluorescence decay indicate that the species formed during homogeneous nucleation are inner-sphere complexes with a partial loss of the hydration sphere, while only incorporated species with a complete loss of the hydration sphere are observed in the growth experiments. This first TRLFS results show clearly that the "early stage nuclei" observed in LIBD experiments having sizes < 20 nm incorporate already Cm-species within the celestite lattice while the species observed with strontianite do not totally lose its hydration sphere.

Uptake of Cm by strontianite at different growth rates. Further studies on the growth rate effect (surface reaction and 3D-nucleation) on Cm speciation via co-precipitation experiments carried out at various saturation indexes are conducted. Results of TRLFS show that the Cm environment and therefore the uptake mechanism is not influenced by the precipitation rate in the strontianite system.

Long-term interaction of Eu(III) with calcite

The interaction of trivalent actinides and lanthanides with calcite is mainly dominated by sorption processes on short time scales. However, since the crystal surface constantly recrystallizes, guest ions with suitable radii and charge can be incorporated eventually. Stumpf *et al.* could show by TRLFS of Cm(III) that two different species of the metal ion are

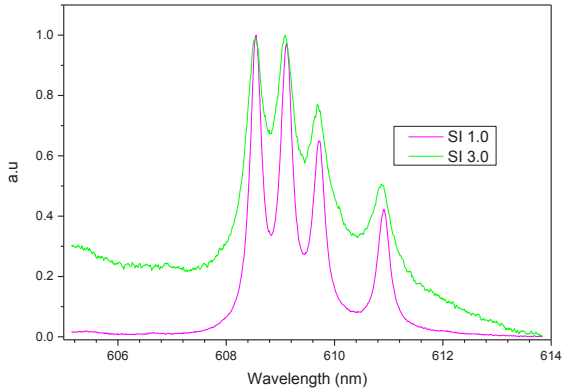

Fig. 4: High-resolution emission spectra of Cm^{3+} doped strontianite for two different supersaturation indexes (SI).

present when in contact with calcite [10]. One species could be determined as a sorption species with one H_2O left in the first coordination sphere while the other species proved to be incorporated without coordinated water and a considerable red shift in emission. Similar experiments have been conducted with Eu(III), serving as a homologue for An(III), by means of site-selective TRLFS at T < 10 K.

Experimental. Simple batch experiments were performed over a time period of more than three years with calcite powder in contact with 10^{-6} M $Eu(ClO_4)_3$ solution. The solutions were pre-equilibrated with respect to calcite in order to prevent any dissolution effects and the solution's ionic strength was adjusted by addition of 10^{-2} M $NaClO_4$. A constant solid/liquid ratio of 2 g natural microcrystalline calcite powder (MERCK) per liter was chosen. The specific surface area of the powder was determined by N_2-BET as 0.7 m^2/g. Samples were taken after 1, 10, 30, 450 and 1150 days. All samples were filtered, dried in a desiccator and cooled down to approximately 10 K prior to measurement. Site-selective TRLFS measurements allow for the determination of the Eu(III) speciation in a sample in conjunction with the characterization of single species separately regarding symmetry and hydration. The specific setup is described in detail elsewhere [9].

Results and discussion. Excitation spectra of the $^7F_0 \rightarrow {}^5D_0$ transition are presented in Figure 5. The generally broad peaks seen with all samples indicate a poorly defined Eu(III) speciation with very similar coordination and chemical environment.

With increasing reaction time, the overall full width at half maximum of the excitation peak increases with a shoulder on the left flank becoming visible first after 450 days. The main peak at λ_{exc} = 579.45 nm remains at its position over time and dominates the speciation. The shoulder around 578.8 nm is visible very clearly in the last spectrum, also with an additional small shoulder at 578.1 nm. This development over increasing contact time implies a changing speciation of europium ions from one dominating sorption species to three (overlapping) ones. Emission spectra were recorded after direct excitation at the corresponding maxima in the excitation spectra. Therefore, the single species could be characterized.

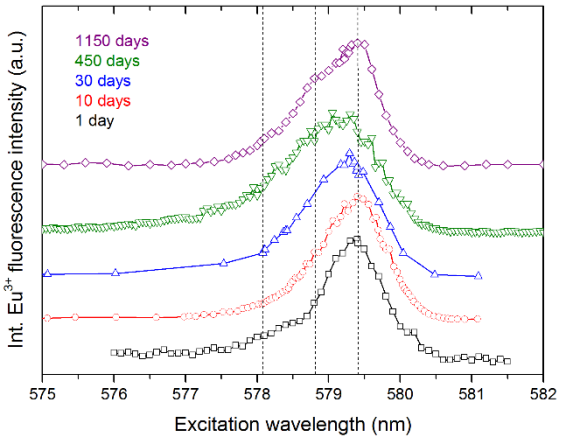

Fig. 5: Excitation spectra of all batch samples (normalized, offset in y-direction). Peaks and respective shoulders indicted by vertical lines.

Respective spectra are presented in Figure 6. Due to the broad and overlapping behavior of the $^7F_0$ transitions, the emission spectra of all species are very similar in shape and splitting of the specific bands regardless of the excitation wavelength. Therefore, only the emission spectra of the main species are shown in Figure 6.

The maximum splitting for the $^7F_1$ (3) and $^7F_2$ (5) bands, according to the maximum multiplet splitting 2J + 1, is reached for all samples. Although fivefold splitting cannot be stated clearly for the $^7F_2$ band, it can be reasonably assumed that it is full split, but not observable due to poor spectral resolution. The most striking change of the emission bands can be seen from one day to 10 days contact time. The general shape, however, only slightly changes with time, showing that the sorption species stays dominant and does not change its coordination. Fluorescence lifetime measurements, which can be correlated to number of water molecules in europium's first coordination sphere [11], confirm this trend. Lifetimes overall increase from partially hydrated Eu(III) species (4 H_2O) to species with no coordinated water.

These experiments confirm the findings of Stumpf *et al.* [10], however kinetics seem to be different with a faster incorporation seen in the literature. A likely reason for this discrepancy might be the different specific surface areas and differences in morphology of the used calcite powder. The reactivity and recrystallization rate of calcite seems to be highly dependent on these factors. Nevertheless, trivalent europium incorporates into the calcite structure, although not on a well-defined lattice site. The nature of the upcoming species at 578.1 and 578.8 nm remains to be seen after longer contact times.

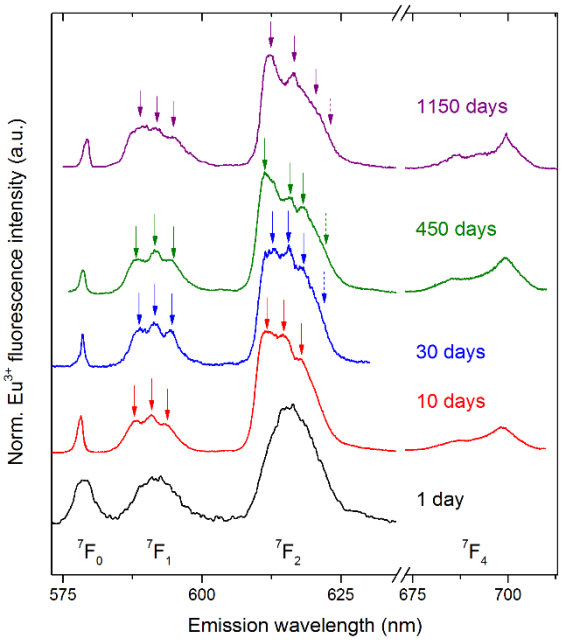

Fig. 6: Eu(III) emission spectra after direct excitation of the main species (normalized, offset in y-direction). Splitting indicated by arrows.

References

[1] H. A. Doerner and W. M. Hoskins, *J. Amer. Chem. Soc.*, **47**, 662-675 (1925).

[2] D. Bosbach, D. *et al., SKB-Report*, Swedish Nuclear Fuel and Waste Management Company, 2010.

[3] E. Curti *et al.*, *Geochim. Cosmochim. Acta*, **74**, 3553-3570 (2010).

[4] M. Klinkenberg *et al.*, *Environ. Sci. Technol.*, **48**, 6620-6627 (2014).

[5] V. L. Vinograd *et al.*, *Geochim. Cosmochim. Acta*, **122**, 398-417 (2013).

[6] N. Torapava *et al.*, *J. Radioanal. Nucl. Chem.*, **301**, 545-553 (2014).

[7] E. Curti *et al.*, *Geochim. Cosmochim. Acta*, **69**, 1721-1737 (2005).

[8] W. Hummel *et al.*, *Radiochim. Acta*, **90**, 805-813 (2002).

[9] K. Holliday *et al.*, *Dalton Transac.*, **41**, 3642-3647 (2012).

[10] T. Stumpf *et al.*, *J. Colloid Interface Sci.*, **249**, 119-122 (2002).

[11] R. M. Supkowski and W. de W. Horrocks Jr., *Inorg. Chim. Acta*, **340**, 44-48 (2002).

5 Applied studies: radionuclide retention in the multi-barrier system

Radionuclide retention in the multi-barrier system covers a wide variety of investigations using specific materials, approaches, methods, analytical techniques and models. The investigations presented in the following chapter cover the quantification of radionuclide mobilization and immobilization from highly radioactive materials and from Portland cement and sorel-based materials. Investigations by means of x-ray spectroscopy on spent nuclear fuel and vitrified high-level waste are presented in chapter 9. In the scope of emergency measures for the Asse salt mine, samples of overlaying rock were characterized in preparation for sorption studies. Experiments on the colloidal impact on radionuclide migration investigated bentonite erosion and the characterization of colloids formed in the presence of lanthanides. Modeling studies are performed on different levels: Process modeling covers the colloidal impact on radionuclide migration taking into account the metal-humic complexation under saline conditions. Coupled reactive modeling is applied for diffusion-sorption processes in clay and for migration processes in natural fractured crystalline rock samples. Simulations of larger scales comprise thermo hydro mechanic (THM) processes in the near field of a HLW disposal in rock salt and flow and transport phenomena in fractures of crystalline host rocks.

5.1 Highly radioactive waste forms

E. Gonzalez-Robles, M. Herm, N. Müller, M. Böttle, E. Bohnert, V. Metz, B. Kienzler

Introduction

The fast release of radionuclides from spent nuclear fuel (SNF) into water occurs by two main processes [1,2]: i) short term release of the so-called instant release fraction (IRF); ii) long-term release dominated by the dissolution of the UO_2 grains, which is referred as matrix contribution. The IRF is due to local segregation of parts of the radionuclide inventory in the gap between cladding and pellet or between pellets, in pellet fractures as well as on fuel grain boundaries. The segregated radionuclides are: fission gases (Kr and Xe), volatile elements iodine, cesium, selenium and some other elements or isotopes such as ^{99}Tc, ^{107}Pd and ^{126}Sn [1]. The degree of segregation of the various radionuclides is highly dependent on the fuel temperature which depends on the in-reactor fuel operating parameters such as burn-up, linear power rate, and ramping processes. In the case of the fission gases, the gas release occurs by diffusion to grain boundaries, grain growth accompanied by grain boundary sweeping, gas bubble interlinkage and intersection of gas bubbles by cracks in the fuel [3].

Synthesis of the EURATOM FP7 Collaborative Project FIRST-Nuclides

In order to achieve a better comprehension of the IRF, high burn-up spent nuclear fuels discharged from commercial light water reactors have been extensively studied within the EURATOM FP7 Collaborative Project, “Fast / Instant Release of Safety Relevant Radionuclides from Spent Nuclear Fuel (CP FIRST-Nuclides)”. The project was implemented by a Consortium with ten beneficiaries from Belgium (SCK-CEN), France (SUBATECH), Germany (KIT-INE and JÜLICH), Hungary (EK), Spain (Amphos21 and CTM), Sweden (Studsvik), Switzerland (PSI) and the Joint Research Centre of the European Commission (JRC-ITU). KIT-INE coordinated the project, which was performed from January 1, 2012 until December 31, 2014.

Based on experimental studies on twelve types of PWR and BWR spent nuclear fuels, comprising analyses of aqueous and gaseous concentrations of twenty isotopes released from the studied SNF in combination with comprehensive characterizations of the physico-chemical properties of theses SNF samples, a significantly broadened knowledge on IRF is achieved in the course of FIRST-Nuclides. Leaching experiments with the high burn-up spent nuclear fuels were performed in a standard leachant guaranteeing comparable results. Measured data cover the dissolution based radionuclide release for different type of SNF samples (cladded pellets, fragments, powders) under aerobic, anaerobic and reducing conditions in the standard leachant. The data include cumulative gap and grain boundary releases for cesium and iodine isotopes up to one-year leaching time as well as the relevant release rates. Release rates for other radionuclides, including fission gases and radionuclides incorporated in the UO_2 matrix, redox sensitive elements, and IRF of selenium were also determined. Results on the chemical state of Se were obtained by micro X-ray absorption near-edge structure spectroscopy. One important improvement of FIRST-Nuclides in comparison to previous studies was the clearance of the fuel owners to publish operational data during irradiation of the SNF in the LWR, such as burn up, power rating and calculated fission gas releases of the studied SNF samples. Releases from non-standard SNFs were also investigated, such as from extremely high burn up TRISO fuel and from leaking VVER fuel assemblies.

The huge amount of experimental and operational data acquired within FIRST-Nuclides provides an excellent basis for an improved understanding of the IRF.

In the following a short summary of major findings and conclusions is given:

- The determined rates of the gap and grain boundary releases do not confirm the approach

of Johnson et al. [4]. Initial ^{137}Cs and ^{129}I release rates are found in the same range as reported earlier; however the observed time behavior of the IRF does not follow the expected decrease during the first days of the experiments. In contrast, the shapes of the time-dependent release rate curves showed a different trend.

- For the first time fission gas release (FGR) was monitored during the leaching experiments up to one year. The initial gas release rate of a clad pellet is lower by a factor of 10 in comparison to gas release rate of a fragment, however, after some 100 days leaching experiment, the FGR rates are in the same range. The IRF(FG) and IRF(^{129}I) are also found in the same range after some time (see following sub-chapter).
- Release rate of radionuclides, which are predominantly incorporated in the UO_2 matrix were analyzed, too. IRF(^{90}Sr) under reducing conditions is about one order of magnitude below the rate obtained under oxidizing conditions.
- For redox sensitive elements, such as U, the release rate under reducing conditions is by two orders of magnitude below the rate observed under oxidizing environments. The cumulated IRF(Tc) under reducing conditions is by a factor of 100 lower as in the case of oxidizing conditions.

In addition to experiments modeling studies on fast radionuclide release from SNF were performed by the partners. A model is available for predicting the wetting of SNF and the time behavior of radionuclide release. The model suggests that transport in fractures is relatively rapid (within a few days) and that mass transport of soluble radionuclides out of fuel samples from micro-cracks should occur in less than 100 days. For evaluation and interpretation of the results, operational parameters have been made available. All data of the FIRST-Nuclides as well as the previously published data are compiled in a database available for application in safety analyses.

The final workshop of the CP FIRST-Nuclides was organized in connection with the 27th Spent Fuel Workshop by INE and held in Karlsruhe. The Annual workshop proceedings, the database, the final scientific report, as well as all deliverables of the project can be retrieved from the web page: www.firstnuclides.eu.

Fast radionuclide release from a PWR fuel rod segment (50.4 GWd/tHM) under hydrogen overpressure

Within CP FIRST-Nuclides we determine the concentration of the Xe and Kr in the gas phase as well as the concentration of ^{137}Cs, ^{129}I, ^{90}Sr, ^{99}Tc and ^{238}U in solution in two experiments performed with a cladded SNF pellet and SNF fragments under strongly reducing conditions.

Spent nuclear fuel samples

The studied SNF samples were taken from the SBS1108 N0204 fuel rod segment, which was irradiated in the pressurized water reactor Gösgen nuclear power plant in Switzerland. The irradiation was carried out in four cycles for a period of time of 1226 days with an average linear power rate of 260 W/cm and achieving an average burn-up of 50.4 GWd/t_{HM}. The fuel rod segment was discharged the 27th of May 1989 that implies a cooling time of 24 years before characterization and cutting of the segment. Characteristic data of the studied SBS1108 N0204 fuel rod segment are given in [5]. Based on results of a puncturing test of the fuel rod segment, the fission gas release into the plenum of the segment was previously calculated to be 8.35% [6].

Sample preparation

Two cladded fuel pellets were cut from the fuel rod segment. The complete sampling process is described elsewhere [7].

The first leaching experiment was performed with one clad pellet. The second experiment was performed with SNF fragments. Therefore, the second pellet was declad in order to get fragments and to separate the fuel from the Zircaloy (the cladding was not used in this leaching experiment).

Prior to the start of the experiments, the samples were weighed; in the case of the cladded pellet, the length and diameter of the sample were measured, too.

Experimental set-up of leaching experiments

Both tests were conducted as static leaching experiments in 250 mL stainless steel Ti-lined VA autoclaves (Berghof Company, Eningen, Germany). The autoclaves were equipped with two valves in the lid to facilitate sampling of liquid and gaseous aliquots.

The composition of the bicarbonate leaching solution used in each of the experiments is as following: 19 mM NaCl + 1 mM $NaHCO_3$ with a pH of (8.9 ± 0.2) and Eh of (-116.3 ± 50) mV. The leachant for the two experiments was prepared in a glove box under Ar atmosphere. The experiments themselves were carried out in an Ar / H_2 atmosphere with a total pressure of (40 ± 1) bar (with a partial pressure of pH_2 = 3 bar) at room temperature.

In the case of the experiment with the cladded pellet, the sample was mounted in a Ti sample holder to ensure the contact of the top and bottom surfaces of the pellet with the solution, whereas the fragments were kept in a glass basket, see figure 1.

Once the samples were placed into the autoclaves, they were closed and flushed with Ar to avoid the possible presence of air.

Afterwards, a pre-leaching test with duration of 1 day was performed by filling each autoclave with 220 mL of bicarbonate water.

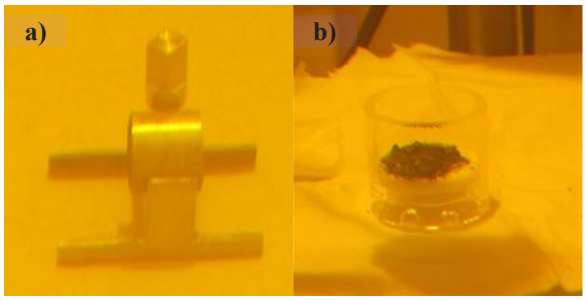

Fig. 1: a) Ti sample holder with cladded pellet; b) glass sample holder containing SNF fragments.

The solution was transferred into the autoclaves using syringes of (50 ± 1) mL under constant Ar flux to avoid air contact. This pre-leaching step was performed in order to reduce the amount of ^{135,137}Cs in solution and to remove any pre-oxidation layer potentially present at the surface of the SNF samples. After the pre-leaching, a gas sample was collected and the solution was completely purged. Then each autoclave was again replenished with 220 mL of bicarbonate solution as described above.

Gaseous (50 ± 1 mL) and liquid (15 ± 1 mL) samples were taken at certain time steps. After the sampling, the gas volume of the autoclaves was purged with Ar, and the initial conditions (40 bar of Ar + H_2 mixture) were again established. The solution was not renewed after sampling, thus the remaining leachant volume was reduced at each sampling step.

In the case of the of the cladded pellet experiment, samples were taken after 1, 7, 21, 56, 84, 176, 245 and 332 days. The leaching experiment performed with fragments is still on going; samples have been taken after 1, 7, 27, 71, 114 and 198 days.

Analyses of released radionuclides in liquid and gaseous samples

Gas samples were collected in stainless steel single-ended miniature sampling cylinders (SS-4CS-TW-50, Swagelok Company, USA) to determine the amount of Kr and Xe released during the leaching experiments and to control the gas atmosphere. These gas-sampling cylinders are characterized by a length of 159 mm, an outer diameter for tube fitting of 9.5 mm and an inner diameter for tube socket weld connection of 6.4 mm. Since the volume of the cylinders was known, the moles of released gases could be derived from the results of gas mass-spectrometry analyses.

From the liquid samples obtained during each campaign different aliquots were prepared to determine the amount of ^{90}Sr, ^{99}Tc, ^{129}I, ^{137}Cs and ^{238}U:

- An aliquot of 1 mL was acidified and measured by γ-spectrometry by means of Ge-detectors (EGC-15-185-R and GX3018, Canberra Industries Inc, Meriden, USA) to determine the amount of ^{137}Cs.
- Another aliquot of 1 mL was prepared by precipitating Cs with ammonium molybdate phosphate (AMP) to reduce the ^{135,137}Cs activity of the sample and improve the determination of ^{129}I by γ-spectrometry (Johnson et al., 2012).
- Finally, a 5 mL aliquot was acidified and, subsequently, ^{135,137}Cs was again precipitated with AMP:
  - An aliquot of 2.5 mL was analyzed by liquid scintillation counting using a Packard Tri-Carb 3110TR low activity scintillation analyzer (Perkin Elmer INC, Waltham, USA) to quantify ^{90}Sr. Prior to the LSC analysis ^{90}Sr was extracted by chromatography using a Sr-Resin crown ether (4,4'(5')-di-t-butylcyclohexano-18-crown-6), and the solution aliquots were homogenized with a LSC-Cocktail (Ultima Gold LLT, Perkin Elmer) before measurement.
  - Another aliquot of 2.5 mL was analyzed by means of Inductively Coupled Plasma Mass Spectrometry (ELAN 6100 Perkin Elmer Inc, Waltham, USA) to quantify ^{99}Tc ^{238}U dissolved in solution.

Results and Discussion

Concentration in solution

The concentration of the fission gases (Xe+Kr) in the gas phase as well as the concentration in solution of ^{90}Sr, ^{99}Tc, ^{129}I, ^{137}Cs and ^{238}U of the experiments is shown figures 2 and 3.

An increase in concentration is observed in the case of ^{129}I, ^{137}Cs and ^{90}Sr as well as in the release of fission gases both in the cladded SNF pellet experiment and in the experiment with the SNF fragments. After a relatively high initial release the concentrations of ^{99}Tc and ^{238} U decrease until approaching a virtually constant value in both experiments. Since Tc and U are redox sensitive elements, it is expected to find them in solution as Tc(IV) and U(IV) with low solubility values in the long run. However the relatively high initial release may be associated to the presence of oxidized layers

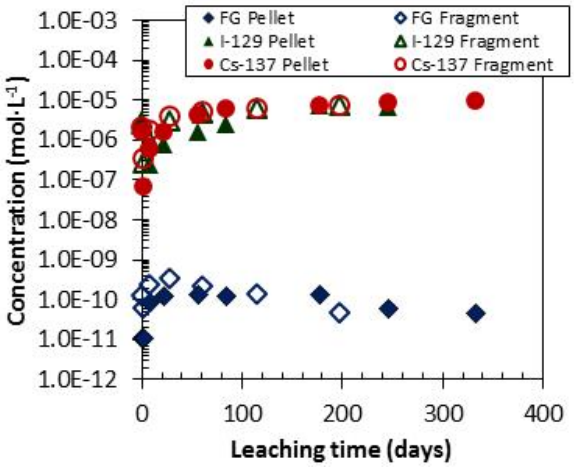

Fig. 2: Concentration as a function of leaching time in cladded pellet and fragment experiments for: ^{129}I, ^{137}Cs and normalized content of FG (Xe+Kr).

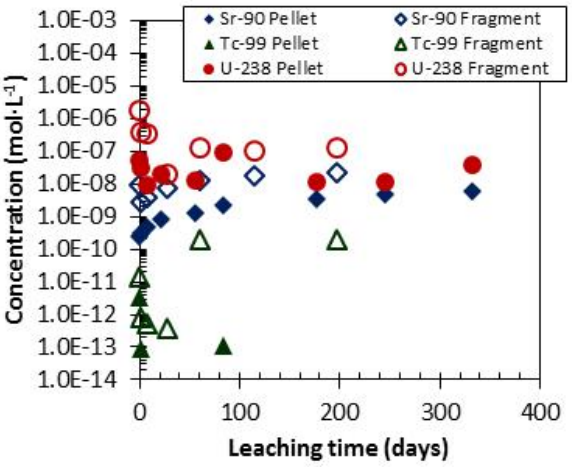

Fig. 3: Concentration as a function of leaching time in cladded pellet and fragment experiments for: ^{90}Sr, ^{99}Tc and ^{238}U.

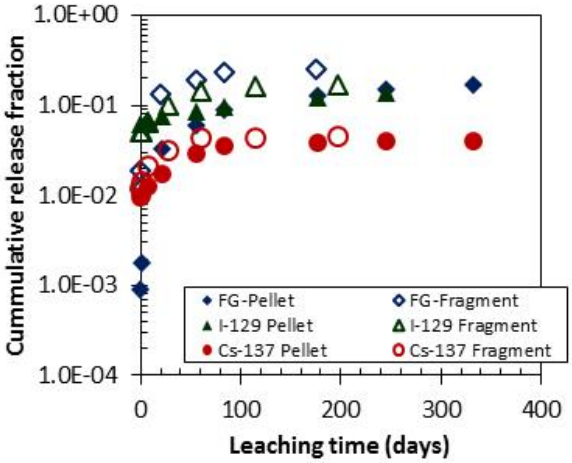

Fig. 4: Cumulative release fraction as a function of leaching time in cladded pellet and fragment experiments for: FG (Xe+Kr), ^{129}I and ^{137}Cs.

on surfaces of the samples, that release Tc(VII) and U(VI) to the solution.

Furthermore it is hypothesized that these elements are reduced as a consequence of the strongly reducing conditions present in the experiments.

Comparing the values obtained in both experiments, there is no significant difference in the initial release of ^{129}I and ^{137}Cs despite the difference in accessible surfaces of the two types of SNF samples.

In the case of ^{90}Sr, ^{99}Tc, ^{238}U as well as FG considerably higher initial concentration values are reached during the pre-leaching of the fragments experiment than in the pre-leaching of the cladded pellet. This fact may be explained by differences in the particle size of the SNF pellet on one side and that of the SNF fragments on the other side. The particle size affects the extent of oxidation on the surface of the SNF samples – in comparison with the pellet a higher extent of oxidation is expected for the fragments, which may cause a higher initial release.

Cumulative release fraction

In order to evaluate how much of the inventory has been released through the experiment, the fraction of inventory released for an element i is calculated following equation (1):

$$Fraction\ release = \frac{m_i}{m_{UO_2} x H_i} \qquad (1)$$

where m_i is the mass of element (g)i in the gas or liquid phase, m_{UO2} is the initial oxide mass (g) in the fuel sample and H_i corresponds to the fraction of inventory for the element i ($g_i \cdot g_{UO2}^{-1}$). The radionuclide inventories of the fuel rod segment are calculated by means of *webKorigen* software package (Nucleonica GmbH 2011). Based on these data, the cumulative fraction of the released inventory is calculated as the summation of the released inventory for each contact period as described in equation (2):

$$Cumulative\ release\ fraction = \sum Fraction\ release_i \qquad (2)$$

In figures 4 and 5, the cumulative release fraction as function of the leaching time for both experiments is plotted.

The cumulative fraction released from the inventory after 332 days of leaching time of a cladded pellet was: $1.5 \cdot 10^{-1}$ for FG, 1.4^{-1} for ^{129}I, $3.8 \cdot 10^{-2}$ for ^{137}Cs, $2.1 \cdot 10^{-5}$ for ^{90}Sr, $6.4 \cdot 10^{-7}$ for ^{238}U and $1.1 \cdot 10^{-8}$ for ^{99}Tc (data obtained at 85 days, the other data were under the detection limit).

In the case of the experiment carried out with the SNF fragments, the cumulative fraction released from the inventory after 198 days of leaching time was: $2.5 \cdot 10^{-1}$ for FG, $1.6 \cdot 10^{-1}$ for ^{129}I, $4.5 \cdot 10^{-2}$ for ^{137}Cs, $2.1 \cdot 10^{-4}$ ^{90}Sr, $3.9 \cdot 10^{-7}$ for ^{238}U and $1.9 \cdot 10^{-5}$ for ^{99}Tc.

The pattern of the cumulative release as a function of time is similar to the evolution of the aqueous concentration of these radionuclides with time.

Determination of the IRF

The IRF is obtained by subtracting the contribution of radionuclide dissolved into the UO_2 matrix (as indicated by the release of ^{238}U) to the value obtained for FG, ^{90}Sr, ^{129}I and ^{137}Cs. The IRF values obtained at the end of the experiments are reported in Table 1.

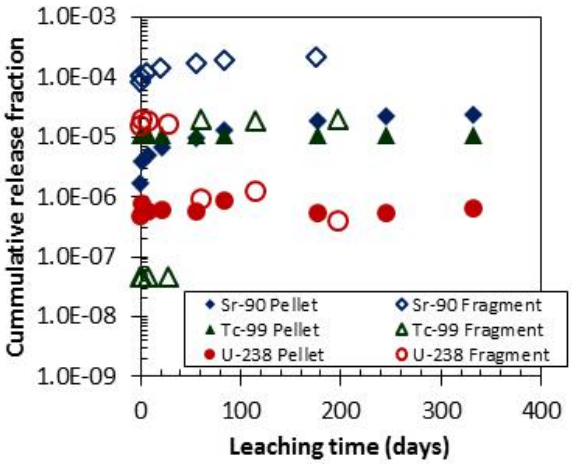

Fig. 5: Cumulative release fraction as a function of leaching time in cladded pellet and fragment experiments for: FG (Xe+Kr), ^{90}Sr, ^{99}Tc and ^{238}U.

Tab. 1: IRF (in %) obtained in cladded pellet and fragment experiments for FG, ^{90}Sr, ^{129}I and ^{137}Cs:

Experiment	FG	^{90}Sr	^{129}I	^{137}Cs
[a]Cladded pellet	14.9	2.1 x 10^{-3}	13.8	3.9
[b]Fragments	24.6	2.1 x 10^{-2}	16.4	4.5

[a]*after 332 days.*
[b]*after 198 days.*

Quantification and speciation of ^{14}C from irradiated metals

In the scope of the 7th FP Cast project (CArbon-14 Source Term), the amount and speciation of ^{14}C located in irradiated metals is quantified. First, the metal under investigation is dissolved in non-oxidizing acids (H_2SO_4/HF). An experimental set-up was installed in a glove box allowing the separation and quantification of inorganic and organic ^{14}C species both in gaseous and aqueous samples derived from these particular dissolution experiments. The analytical separation procedure involves several steps (i.e. acid stripping and wet oxidation).

The dissolution procedure, the gas and liquid sampling as well as the analytical method was tested rigorously using unirradiated Zircaloy and inorganic and organic ^{14}C compounds. It was shown that the recovery and quantification of ^{14}C was above 95%.

References

[1] Johnson, L., Ferry, C., Poinssot C., Lovera, P. *J. Nucl. Mater.*, **346**, 56-65(2005).

[2] Poinssot, C., Ferry, C., Lovera, P., Jegou C., Gras. J.-M. *J. Nucl. Mater.,* **346**, 66-77 (2005).

[3] Johnson, L., Shoesmith, D.W. "Spent Fuel", Radioactive Waste Forms for the Future, North-Holland, (1988).

[4] Johnson, L. H., Garisto, N., Stroes-Gascoyne, S., "Used-fuel dissolution sudies in Canada," in Waste Management 1985 Tucson, Arizona, March 24-28, (1985).

[5] Metz, V., González-Robles, E., Kienzler, B., *KIT Scientific Reports, Karlsruhe KIT-SR* **7676**, 55-60 (2014)

[6] González-Robles, E., Wegen, D. H., Bohnert, E, Papaioannou, D., Müller, N., Nasyrow, R., Kienzler, B., Metz, V. *Mat. Res. Soc. Symp. Proc.,* **1665**, 283-289. (2014),

[7] Wegen, D.H., Papaioannou, D., Gretter, R., Nasyrow, R., Rondinella, V.V., Glatz, J.-P. *KIT-SR* **7639**, 193-199 (2013).

5.2 Non-heat producing waste forms and natural barriers

B. Kienzler, M. Schlieker, Ch. Borkel, V. Metz, Th. Schäfer, Th. Rabung, N. Finck, F. Heberling, F. Friedrich, D. Schild, E. Soballa, E. Bohnert, V. Krepper, M. Plaschke, F. Geyer, S. Hilpp, S. Moisei-Rabung, A. Seither, C. Walschburger, J. Krullikowski, C.-H. Graser, M. Wiedemann

Full-scale cemented waste forms: Analysis of solids

Full-scale cemented waste simulates have been produced in the 1980s and exposed to salt solutions for more than 20 years in a separated gallery in the Asse salt mine. Since 1986, INE felt responsible for sampling and analyzing the leaching solutions and investigating the solid phases with respect to their radionuclide retention capacities. In 2006, four samples doped with Cs and U have been retrieved and analyzed [1]. In 2012, the remaining full-scale samples had to be removed from the Asse mine. Drill cores and by the drilling abraded solid of three samples were investigated. The solids comprise material from a $(NH_4)_2U_2O_7$ doped simulate of a low water to cement ratio (W/Z = 0.30) simulate exposed to the $MgCl_2$-rich brine (Q-brine). The other samples were doped with ^{237}Np and were exposed to saturated NaCl solution and $MgCl_2$ rich brine, respectively. The U doped sample was leached since 1984, the two other samples since 1987 and 1989.

The results obtained by detailed analyses of the element and component profiles, the mineralogical composition investigated by XRD, SEM, thermal analyses, pore structure and distribution of radionuclides corroborate well with previous findings. Both the W/Z and the type of salt solutions are the dominating factors determining the long-term stability of the simulated waste forms. During almost 30 years, the 3 full-scale samples evolved differently:

The hydrated cement of sample #36 doped with Np and leached in $MgCl_2$-rich solution was completely corroded showing no longer any mechanical stability. This sample was produced with a W/Z = 0.5, which means that a significant initial porosity was present and exchange processes with the attacking brine were not hindered. By dissolution of the embedded $NaNO_3$, the porosity increased further and finally the formation of gypsum destroyed the cement matrix. Similar situation was observed for samples #28 and #33 investigated previously.

In the case of sample #35 produced under the same conditions as sample #36 but leached in NaCl solution, the solid sample showed less corrosive attack. The sample showed degradation fronts from the outer surfaces, indicated by precipitation of solid NaCl and Friedel's salt formed by penetrating chloride. Cl^- was found throughout the whole sample. In contrast, a decrease of the nitrate concentration was observed only to a depth of some 10 cm from the leached surfaces. Most probably, the exchange processes took place mainly along micro fractures and corrosion did not affect the complete cement matrix.

Sample #25 was produced at W/Z = 0.3 and leached in in $MgCl_2$-rich solution. The solids obtained from this test showed a completely different performance. This sample had a significantly lower porosity. According to Vejmelka [2], the porosity of simulated cemented waste forms decrease by a factor of 250 comparing W/Z = 0.45 with W/Z = 0.30. At depth more than 3 to 5 cm from the surface, chloride was not found nor a decrease of the waste component nitrate was detected. Only onto the surface, which was exposed to the $MgCl_2$-rich solution, precipitates were present.

U and Np diffusion profiles were analyzed in the 3 full-scale samples. For sample concentration profiles could not be resolved even in cm range. In sample #35 a slight depletion of Np was found in a very narrow distance to the outer surface (0.3 mm). Fig. 1 shows α-autoradiography images of polished slices of a core from sample #35.

Both Np doped samples showed flat profiles over the sample volumes. Measured concentrations agreed well with the expected dopant concentrations.

The observed degradation of samples #35 and #36 indicate transport processes. In the leachant the measured ^{237}Np concentrations were ~10^{-12} mol/l. This value is by 6 orders of magnitude below the Np(V) solubility [3]. A recent study of Np(V) sorption onto CSH phases revealed distribution coefficients in a range of 10^5 - 10^6 l/kg [4]. Considering the mass to volume ratios of the full-scale experiments, the calculated Np concentration in the leaching solutions corresponds to the measured values. This finding indicates clearly effective sorption of Np(V) onto cement phases even in the presence of highly concentrated salt brines.

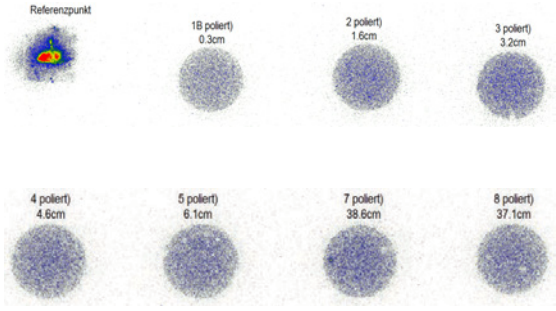

Fig. 1 α-autoradiography images of polished slices of a core from sample #35

Sorption in the Asse Overlaying Rocks
Part 1: Characterization of Rock Samples

In the scope of a BfS funded project on sorption of radionuclides onto rocks of the overlaying layers at the Asse salt mine, 26 rock samples were obtained during the drilling of the exploration drillhole RM15. The rock samples covered different layers, such as shell limestone, red sandstone, sulfate dominated rocks and cap rock of the salt dome. The samples were packed and stored under inert gas. All preparation steps were performed in an inert gas glove box. The rock samples were characterized using different methods in order to interpret the sorption behavior.

The characterization methods investigated the mass loss after drying as measure of the porosity, the specific surfaces, main and trace element compositions (Fig. 2) as well as the mineralogical compositions by XRD.

Thin sections were prepared for analysis of the connected porosity and for SEM-EDX analysis. Further investigations cover the clay components, organic components and the cation exchange capacity. Direct sampling of groundwater at the exploration drillhole RM15 was not possible. For this reason, artificial porewater was prepared by equilibration of rock materials with water. The solutions as well as the gas phase were analyzed and equilibrium CO_2 partial pressures determined. With respect to the redox conditions, differentiation of Fe(II)/Fe(III) was analyzed by coupled ion chromatography - Inductively Coupled Plasma Mass Spectrometry (IC-ICPMS).

By XRD measurements, following phases could be identified: In the shell limestone samples petrographically described by limestone, lime marl, clay stone and clay marl stone the minerals calcite, quartz, chlorite, mica and some feldspars were identified. The red sandstone pertographically characterized by claystone, siltstone and sandstone, dolomite and hematite are present. In the depth below 396 m the phase composition changed significantly. In this layers magnesite, halite, gypsum, bassanite and amphibole minerals exist.

The clay fractions analyzed with XRD showed a relatively constant composition for all rock samples. Carbonate phases were not present.

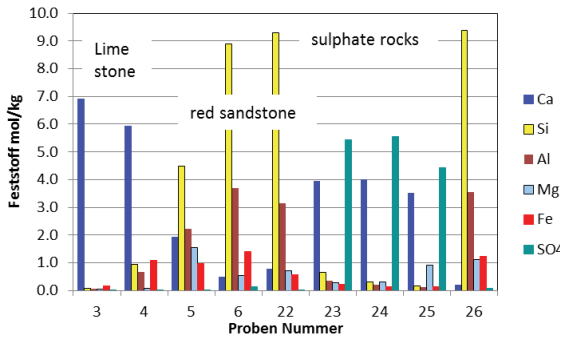

Fig. 2: Main element concentration of some rock samples

Fig. 3: Thin section of a red sandstone sample (007_KIT).

Identified phases are quartz, chlorite, mica and feldspars. Hematite was not detected in the clay fractions. The sulfate containing rocks showed the presence of Celestine, which was corroborated by SEM-EDX measurements. Swellable clays such as smectites could not be found in any of the rock samples.

Scanning electron microscopic analyses were performed using thin sections of the rock samples. As an example, a thin section of sample # 007_KIT, red sandstone, 225 m depth is shown in Fig. 3.

SEM-EDX analysis revealed a heterogeneous mineral distribution showing some spots, which were analyzed in detail (Fig. 4). This structure contains very high sulfur and strontium concentrations and very low concentrations of the divalent cations Ca, Mg or Fe. In some parts of the light structure shown in Fig. 3, up to 12 atom% of barium was found. In this part, Sr was not present.

Autoradiography measurements of this thin section showed a hot spot at the location of this structure. It is supposed that the hot spot can be attributed to radium accumulated in the $BaSO_4$ mineral. RFA analysis resulted in up to 3 - 5 ppm uranium in the sample 007_KIT.

Fe concentration was in the range of 4 -6 wt.%. By XRD, the pure iron phase hematite was identified. SEM-EDX analyses revealed also Ti / Fe oxides, Zr silicates and Ca phosphates with small concentrations of La and Ce.

The specific surfaces of the red sandstone sample are relatively large, surmounting 20 m^2/g. Furthermore, in the upper limestone specific surfaces of some 7 m^2/g were found. The porosity of the samples after drying was below 6%, only one sample (004) showed a porosity of about 10%.

Trace elements needs to be considered for planning of the sorption studies in order to select isotopes, which do not interfere with the natural trace elements. Following trace elements have been determined: Co, Ni, Cu, Zn, Ga, Rb, Sr, Y, Zr, Nb, Cs, Ba, W, Pb, Th, U. The mass concentration of Th and U is relatively low, higher in the sandstone samples. The Th concentration is about a factor of 3 above the U concentration in the solids.

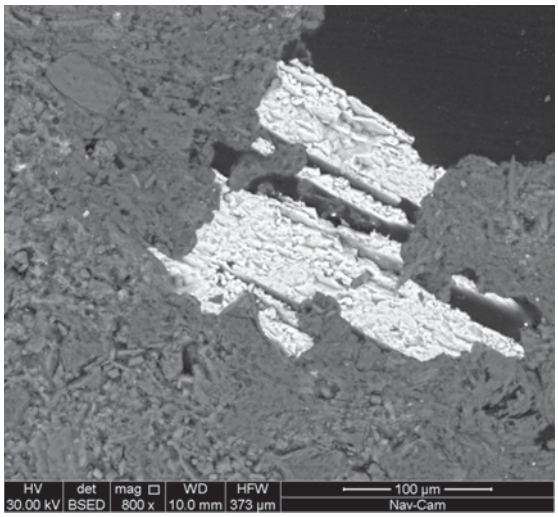

Fig. 4: Barium-sulfate structure in a red sandstone sample (007_KIT).

The main and secondary mineral phases were analyzed in the rock samples. Partly, trace elements form separate phases, such as Ba/Sr sulfates. These unexpected Sr/$BaSO_4$ phases were detected by XRD, SEM- and EDX-analysis.

The clay fraction consists mainly of mica, albite and orthoklas. Expandable clays such as smectite could not be found in any of the rock samples. In the red sandstone samples,

References

[1] B. Kienzler, V. Metz, B. Brendebach, N. Finck, M. Plaschke, T. Rabung, J. Rothe, and D. Schild, *Radiochim. Acta* vol. 98, pp. 675-684, 2010.

[2] P. Vejmelka, G. Rudolph, W. Kluger, and R. Köster, *Forschungszentrum Karlsruhe KfK* 4800, 1990.

[3] V. Neck, M. Altmaier, R. Müller, V. Metz, and B. Kienzler, "Teil 3: Löslichkeitsexperimente zur Absicherung der thermodynamischen Datenbasis," *FZK-INE, Karlsruhe FZK-INE* 007/03, 2003.

[4] X. Gaona, E. Wieland, J. Tits, A. C. Scheinost, and R. Dähn, *Applied Geochemistry,* vol. 28, pp. 109-118, 1// 2013.

Retention of Cm(III) and Eu(III) by $Mg(OH)_2$(cr) in the system Mg^{2+}-Na^+-Cl^--OH^--H_2O

In long-term safety analyses, intrusion of aqueous solutions into a repository has to be taken into account. Under reducing conditions, which develop after the closure of a deep repository, actinides are expected to prevail in tri- and tetravalent redox states, e.g. Am(III), Cm(III), Np(IV), Pu(III/IV), U(IV). There is currently a strong interest in the application of $Mg(OH)_2$-based materials as engineered barrier materials in disposal rooms and access galleries of repositories in rock salt. These materials comprise of brucite $Mg(OH)_2$ and Mg-oxychloride $Mg_2(OH)_3Cl{\cdot}4H_2O$(cr), and may provide favorable chemical conditions with respect to low actinide solubility and significant actinide retention capacities in case of water access. For disposal systems in rock salt, potentially intruding water as well as fluid inclusions and brine pockets are characterized by high ionic strengths, mostly dominated by high Na^+, Mg^{2+} and Cl^- concentrations.

For the Asse II salt mine (Lower Saxony, Germany) and the Waste Isolation Pilot Plant (WIPP, New Mexico, USA), where low and intermediate level radioactive waste products are emplaced, $Mg(OH)_2$-based material and MgO(cr) are proposed as engineered barriers and geochemical buffer, respectively [1]. In case of an intrusion of aqueous solution into the WIPP, MgO(cr) will transform into $Mg(OH)_2$(cr) [2]. In NaCl or $MgCl_2$ dominated brines, $Mg(OH)_2$(cr) buffers at pH_m of about 9 and scavenges carbonate, potentially produced by microbial degradation of organic waste constituents [3].

We study the retention mechanisms of trivalent europium and curium by brucite in $MgCl_2 \pm NaCl \pm NaClO_4$ solutions (ionic strength $0.15 \leq I \leq 15$ mol·(kg(H_2O))$^{-1}$) using recrystallization and co-precipitation experiments. The structure of Eu(III)-bearing brucite and the speciation of Cm(III) and Eu(III) sorption species were analyzed by means of Extended X-ray Absorption Fine Structure Spectroscopy (EXAFS) and Time-Resolved Laser Fluorescence Spectroscopy (TRLFS). The brucite / brine systems were doped with $4.6{\cdot}10^{-6}$ mol·g^{-1} Eu(III) and $1{\cdot}10^{-7}$ mol·L^{-1} Cm(III), respectively. In presence of brucite, the specific pH_m values were fixed in a disposal relevant range of $9.0 \leq pH_m \leq 9.6$. The aim of this study is to combine spectroscopic (EXAFS, TRLFS) and macroscopic approaches by using co-precipitation and recrystallization experiments to obtain a better understanding of the retention mechanism.

Brucite (BioUltra, ≥ 99.0 %) was purchased from Fluka and characterized by Raman spectroscopy (Senterra, Bruker/Olympus), SEM-EDX (Quanta 650 ESEM, Fei), TGA-DSC (STA409C/CD TG-DSC, Netzsch) and XRD (D8 Advance diffractometer, Bruker AXS). The molar H^+ concentration of the suspensions was determined with combination pH electrodes (Orion Ross, Thermo Scientific). To convert the operational measured pH_{exp} values, the approach of Altmaier et al. [4] was applied. Eu(III) concentrations were determined by ICP-MS (X-Series II, Thermo Scientific). Cm(III) fluorescence spectra were collected using a Nd:YAG laser (Continuum Surelite II 10 Hz) pumping a dye laser (Narrowscan Dye Laser, Radiant Dyes). Eu(III) L_3-edge EXAFS spectra were recorded at the INE-Beamline for actinide science at the ANKA synchrotron light source in fluorescence-yield detec-

tion mode using a silicon drift detector (Vortex, SII Nano Technology) [5].

A strong retention of Eu(III) (R_s >> 210 ml·g^{-1}) was observed in previous results of macroscopic sorption experiments. Since the Eu(III) concentration decreased to below the ICP-MS detection limit of $3 \cdot 10^{-10}$ mol·L^{-1} within less than a week, the reported R_s value represents a lower limit for the retention by brucite. Long-term studies of recrystallized and co-precipitated brucite in $MgCl_2$ ± NaCl ± $NaClO_4$ were monitored by TRLFS from 30 minutes up to two years and 47 days, respectively. The emission spectra show a slow evolution of the Cm(III) sorption species over several months.

During an interval of several months, TRLFS analyses show a distinct change in the speciation of Cm(III) retained by recrystallized brucite and co-precipitated Cm(III)-brucite in $MgCl_2$ ± NaCl ± $NaClO_4$ solutions. Emission spectra recorded between four months and two years are virtually the same, indicating the achievement of an equilibration between Cm(III) and brucite. After more than four months, a strong red-shift to a wavelength of 609.4 nm was observed in emission spectra of recrystallization experiments with relatively low ionic strengths (e.g. 1.53 mol·(kg(H_2O))$^{-1}$), which is interpreted as an incorporation of Cm(III) into the brucite structure. At increasing ionic strengths, a decreased red-shift of the Cm(III) species was observed in Cm(III) / brucite / brine systems. Systems at low ionic strength ($0.15 \leq I \leq 1.2$ mol·(kg(H_2O))$^{-1}$) seem to have faster kinetics than experiments at elevated ionic strengths ($1.2 \leq I \leq 5.2$ mol·(kg(H_2O))$^{-1}$) (Fig. 5). A decreasing amount of water molecules in the first coordination shell of Cm(III) (1.7 ± 0.4 H_2O) was observed in lifetime measurements within two years. Considering the quenching by OH^- to be half as efficient as quenching by H_2O [7] this corresponds to about four hydroxyl groups.

EXAFS investigations of co-precipitation experiments at ionic strengths of 1.2 and 5.2 mol·(kg(H_2O))$^{-1}$ indicate an incorporation of Eu(III) into a distorted octahedral brucite structure. No significant effect of the ionic strength on the incorporation mechanism was observed. Eu(III)-TRLFS studies of co-precipitated brucite indicate the presence of at least two species with lifetimes of 126 ± 16 µs (8.0 ± 0.8 H_2O) and 296 ± 20 µs (3.0 ± 0.1 H_2O). Ongoing Cm(III)-TRLFS studies of co-precipitated brucite at $0.15 \leq I \leq 5.2$ mol·(kg(H_2O))$^{-1}$ show very strong red-shifts up to 617 nm (major species, λ_1) and 607 to 610 nm (minor species, λ_2) within the first three hours. Within the monitoring period of 47 days, λ_1 decreases and λ_2 become the major species. Concurrent TRLFS and EXAFS results of both recrystallization and co-precipitation experiments lead to the conclusion that Cm(III) is incorporated into distorted MgO_6 octahedra of the brucite structure. The incorporation is inhibited with increasing ionic strength.

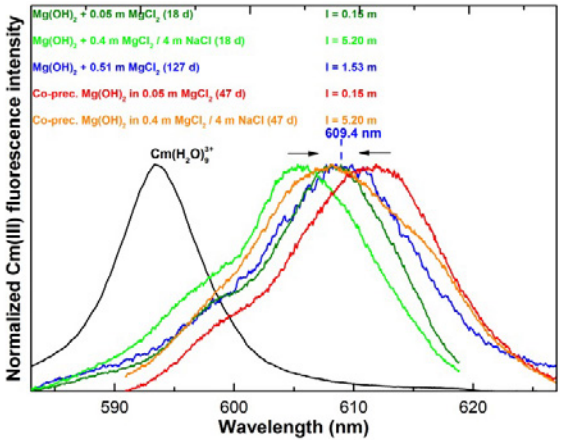

Fig. 5: Emission spectra of recrystallization and co-precipitation Cm(III) / brucite / brine systems at 0.15 ≤ I ≤ 5.2 mol·(kg(H_2O))$^{-1}$ within four months. Both, recrystallization and co-precipitation experiments, emission maxima shift slowly to the equilibrium at 609.4 nm.

These results indicate that high ionic strengths inhibits the kinetics of lanthanide / actinide retention, however a similar incorporation of lanthanides and actinides is observed at $0.15 \leq I \leq 5.2$ mol·(kg(H_2O))$^{-1}$.

Acknowledgement

The ANKA synchrotron light source is gratefully acknowledged for provision of beam time. The research leading to these results have been financially supported in part from the Federal Ministry of Education and Research (BMBF) project VESPA.

References

[1] Brush, L.H. et al., Denver *Annual Meeting, Geological Society of America*, **36**, 296 (2004).

[2] Schüssler, W. et al., *Geochim. Cosmochim. Acta suppl.*, Goldschmidt Conference Abstracts, Davos, Switzerland, **A690** (2002).

[3] Monastra, V., Grandstaff, D.E., Mat. Res. Soc. Symp. Proc., 556, 625-632 (1999).

[4] Metz, V. et al., Radiochim. Acta., 92, 819-825 (2004).

[5] Altmaier, M. et al., Geochim. Cosmochim. Acta, 67(19), 3595-3601 (2003).

[6] Kimura, T., Choppin, G.R., J. Alloy. Compd., 213, 313-317 (1994).

[7] Supkowski, R.M., Horrocks, W.D., Inorg. Chim. Acta, 340, 44-48 (2002).

5.3 Colloid impact on radionuclide migration

N. L. Banik, M. Bouby, N. Finck, S. Heck, R. Marsac, J. Lützenkirchen, C. M. Marquardt, T. Schäfer

In co-operation with:

K. H. Johannesson

Department of Earth and Environmental Sciences, Tulane University, 6823 St. Charles Avenue, New Orleans, LA 70118, USA

Introduction

In addition to naturally occurring nano suspended material (humic substances, iron and aluminosilicate oxi/hydroxide...), corrosion and alteration processes may increase the nanoparticles (NPs) population via the formation of intrinsic colloids, secondary phase products or degradation of the engineered barrier system (EBS). All these NPs may potentially contribute to the migration of radioactive waste material towards the biosphere.

In our current activities, from the near-field to the far-field, by combining laboratory and *in-situ* migration experiments, the development and the use of highly sensitive and sophisticated analytical techniques (see chapter 9 and 10), we aim to

1) detect the presence and identify the formation of the relevant NPs in repository specific areas,
2) determine their stability as a function of geochemical parameters,
3) elucidate the thermodynamics and kinetics of their interaction with radionuclides (RNs),
4) quantify the NP mobility and their interaction with mineral surfaces.

The final goal is to implement our experimental data into hydro-chemical (see chapter 5.5) and reactive transport modeling (see chapter 5.6) codes to state on the NPs relevance concerning radionuclides migration under natural geochemical conditions. This year, in this chapter, we report on

a) the modeling of the metal ion complexation by humic substances under saline conditions
b) a two year old bentonite erosion experiment under quasi stagnant flow conditions,
c) the characterization of clay colloids mobilized from an hectorite bulk solid synthesized in presence of numerous lanthanide elements.

Modeling metal ion - humic acids complexation under saline conditions

The development of geochemical models able to predict the speciation of radionuclides in concentrated brines and especially their complexation with organic substances such as humic and fulvic acids (HA and FA, respectively) is required. This work aims at this objective in the frame of the BMWi "Actinidenverbund"- project.

Relatively few experimental studies were dedicated to metal ion complexation by HA under highly saline conditions. Experimental results are available, e.g. for Am(III)/Cm(III) [1,2], Ni(II)/Co(II) [3] and Pu(IV) [4] at $4 < pHc\ (-\log m_{H+}) < 6$ and in $0.1\ M < [NaCl/ClO_4] < 6\ M$. These studies consistently show a decrease in the apparent metal ion (M)-HA complexation constant ($\log {}^{HA}\beta$) with increasing ionic strength (I) up to 1 M. Above 1 M, $\log {}^{HA}\beta$ remains constant or increases with *I*.

To account for M-HA complexation in speciation codes, $\log {}^{HA}\beta$ must be extrapolated to $I = 0$. This is often done by using the specific ion interaction theory (SIT [5]). However, as discussed elsewhere [1,4] due to conformational changes of HA with *I*, the obtained SIT parameters are hardly physically meaningful: they are merely adjustable parameters. Because HA are large charged molecules, their conformation is related to their charging behavior, as for any other polyelectrolytes, and consequently the M-HA complexation is subject to electrostatic effects [6,7]. Thus the use of electrostatic models to account for the final HA conformation due to charge effects is thought to be useful in the extrapolation of $\log {}^{HA}\beta$ values to infinite dilution. Finally this will allow to predict $\log {}^{HA}\beta$ values at a given *I*. This study aims to test, in combination with the SIT (for $I < 4$ M), the applicability of two humic-ion binding models; Model VII [6] and NICA-Donnan [7], at high 1:1 background electrolyte concentrations. To our knowledge, the applicability of the NICA-Donnan model for $I > 1$ M has only been established in the case of HA proton titrations. Model VII is not applicable above $I = 1$ M. Model VII considers the HA molecules as impermeable entities whereas NICA-Donnan considers them as permeable spheres. These conceptual differences result in totally different equations for the electrostatic potential calculation (Ψ, in V): Model VII calculates a surface potential (Ψ_0) whereas NICA-Donnan calculates the potential in the Donnan volume (Ψ_D). However, both models consistently invoke a Boltzmann factor, which includes Ψ (i.e. Ψ_0 or Ψ_D), to calculate $\log \beta$ values in various pH and *I* conditions. Calculations were done (see Fig.1) to obtain the evolution of Ψ_0 and Ψ_D with *I* at pH $(-\log a_{H+}) = 5.5$. For $I < 1$ M, Ψ_D is systematically ~60 mV below Ψ_0, thus the NICA-Donnan model involves a larger contribution of electrostatic effects to the overall M-HA complexation than Model VII. However, the variation of Ψ with *I* is almost the same for both models (see Fig.1 where the Ψ_D y-axis scale is shifted from ~ 60 mV compared to Ψ_0).

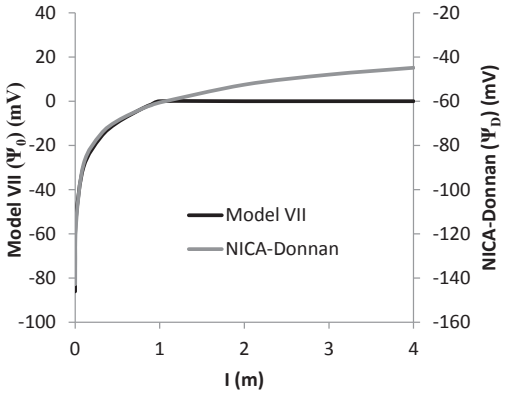

Fig. 1: Surface potential (Ψ_0) and Donnan potential (Ψ_D), both in mV, calculated for Model VII and NICA-Donnan, respectively, for pH (= -log a_{H+}) = 5.5 versus the ionic strength. Above I = 1 M, Ψ_0 is set equal to 0

For $1 < I < 4$ M, Ψ_D increases only slightly ($-60 < \Psi_D < -40$ mV). Consequently, any variation in the calculated log β values for $I > 1$ M is attributed to ionic strength effects on the metal ion aqueous speciation more than electrostatic effects on the M-HA complexation which are predicted to be only small.

The aqueous speciation is calculated by the speciation code (i.e. using the thermodynamic database and SIT) and is independent to the humic-ion binding model. In their present form, the equations inherent to Model VII cannot be used for $I > 1$ M: Ψ_0 would become positive, which is very unlikely for HA, especially in $NaCl/ClO_4$. However, by suppressing the electrostatic effects in Model VII for $I > 1$ M (i.e. $\Psi_0 = 0$; Fig.1), both models are expected to yield similar results as a function of the ionic strength.

Szabò et al. [4] measured Pu(IV)-HA binding isotherms at pH = 4 and for $0.02 < [NaClO_4] < 3.5$ M. They determined log $^{HA}\beta(Pu^{4+})$ which refers to the complexation of the free aqueous Pu^{4+} ions to HA and requires the calculation of the corresponding side reaction coefficient (noted α_{Pu} [4]) using SIT. Pu(IV)-HA complexation under the experimental conditions of Szabò et al. [4] is predicted by Model VII, using the Pu(IV)-HA binding parameters determined in previous work [8] and the same thermodynamic database [9]. The simulated binding isotherms are obtained by using the equations given in [4] and shown Fig. 2 with the experimental data. For $I < 1$ M, log $^{HA}\beta(Pu^{4+})$ decreases with increasing I. Within Model VII and applying SIT, this can be attributed to the evolution of both Ψ_0 and α_{Pu} with I. Above $I = 1$ M, the increase in log $^{HA}\beta(Pu^{4+})$ is exclusively controlled by α_{Pu} because Ψ_0 is set equal to 0 (see Fig. 1). Results of the simulation agree nicely with the experimental data. Additional examples (e.g. using NICA-Donnan or for other metal ions) and theoretical aspects will be discussed in more details [10]. This study shows that electrostatic models for HA can help to predict log $^{HA}\beta$ values versus I and, therefore, simulate the speciation of relevant radionuclides in concentrated brines.

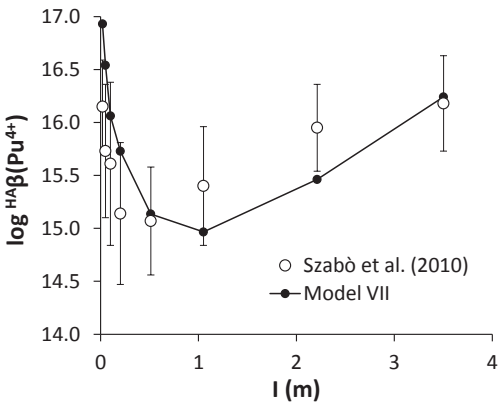

Fig. 2: Experimental log $^{HA}\beta(Pu^{4+})$ literature values at pH = 4 [4] as a function of I ($NaClO_4$) compared with Model VII predictions.

Bentonite erosion under quasi stagnant flow conditions (t_{reac} = 2a)

The main mineral component in bentonites belongs to the smectite clay group. Smectites are 2:1 phyllosilicates. In contact with water smectites hydrate and swell. A *gel* is formed able to penetrate available pore spaces (open rock fissures, joints, …). Under specific (ground) water conditions, i.e low concentration of dissolved ions, the gel can take a *sol* character. Erosion processes can thus occur at the gel front and colloidal particles can be released. Accordingly, the interaction of the eroded material with radionuclides may play an important role in the safety assessment. The aim of this work is to simulate erosion processes under dynamic conditions and tocomplete literature data [11] in the frame of the CP-BELBaR project.

Raw, Na- and Ca-exchanged MX80 bentonite samples or mixture of both have been compacted in pellets. The pellets are placed in double-side reactors (see Fig. 3) to perform erosion experiments in duplicate where one side of the compacted clay pellet is eroded by using a synthetic low ionic

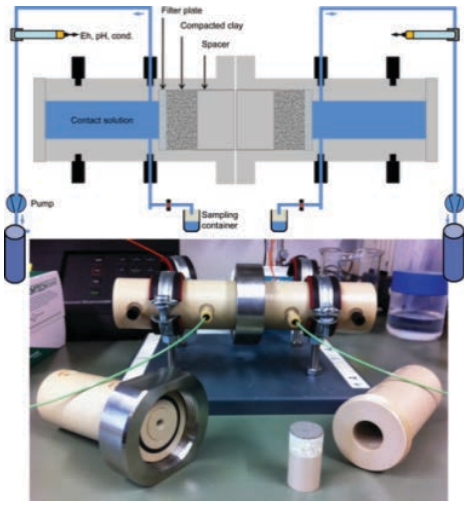

Fig. 3: Experimental set-up designed for the erosion test with two reactors assembled together

strength carbonated water (SGW) to simulate the potential effect of glacial melt water on the bentonite stability. The SGW composition is: Na^+ (28.4 mg/L), Ca^{2+} (1.49 mg/L), F^- (2.8 mg/L), Cl^- (2.64 mg/L), $S0_4^{2-}$ (4.13 mg/L) and Si (14.1 µg/L), HCO_3^-: 10^{-3} M, initial pH: 8.4. The contact solution (SGW) is not re-circulating. Samples are regularly taken and analyzed since the beginning of the experiment running now for two years.

The pH (8.3 ± 0.3) and flow rate (3.0 ± 0.1) µL·min^{-1} are constant and the experiments are very reproducible. Material is clearly produced (eroded) and identified as clay according to the concentrations of Si, Al, Mg and Fe recorded (Fig. 4). A clear effect of the initial bentonite pellet composition is evidenced. The highest erosion is seen in presence of Na-exchanged MX80 pellets while no erosion is observed when using Ca-exchanged ones or only limited when using raw MX80 pellets. When effective, the colloid production presents a maximum after ~25 days to reach a colloid concentration of ~500 mg/L. Afterwards, the clay colloid concentration is decreasing to level off after 6 months at approx. < 2 mg·L^{-1}. Interestingly, in agreement with literature data and other works, instant releases of sodium, sulphate and chloride are clearly evidenced and attributed to the dissolution of accessory minerals present in the raw bentonite (like gypsum or halite) followed by cation exchange processes.

The size (PCS determination) of the eroded material from the cation exchanged MX80 pellets with 120-150 nm is comparable to those of bentonite clay colloids obtained after "classical" delamination and centrifugation cycles. The colloids mobilized from the raw MX80 pellets appear larger with 170-200 nm. A closer inspection is necessary to detect the presence of eventually smaller nanoparticles.

Cs, Eu and U(VI) sorption tests were performed on the eroded material collected after ~ 1 month. No Cs sorption on the eroded material could be quantified independent of the source material. At a first glance, the Eu and U sorption might be slightly favored on the eroded material coming from the compacted pellets made of MX80 after the cation exchange (Na or Ca). This difference is not more than ~6 % for U whereas it reaches ~ 16% for Eu. Nevertheless the Eu (22-38%) and U(VI) (17-23%) sorption levels are rather low under the present experimental conditions due to the presence of carbonated water.

The present data have to be examined in more details and modeled by using appropriate codes. They tend nevertheless to indicate that, on one side, the size of the material mobilized will probably not allow it to migrate over long distances but, on the other side, its rather low sorption capacities under such kind of geochemical conditions does not allow it to delay the migration of some relevant elements behaving like Cs, Eu or U presently investigated. Further work is in progress.

Colloid release from synthetic REE- Hectorite

Hectorite, a Mg-rich smectite, has already been identified in some glass alteration layers [12]. Recent studies have reported the analyses of NPs mobilized from a hectorite suspension in the presence of Lu, Eu or Y [13-15] by application of the Asymmetrical Flow Field-Flow Fractionation (AsFlFFF) method coupled to ICP-MS. AsFlFFF gives information's on the size of the nanoparticles released (according to their elution time in s from the fractionator) and on their elemental composition (from the ICP-MS). In all studies reported so far, only one single element was co-precipitated with the hectorite during the synthesis. However, upon HLW glass corrosion numerous RNs of various sizes and oxidation states may be released and thus possibly present during the neo-formation of this secondary phase. In this study, hectorite was crystallized from a brucite precursor phase co-precipitated in presence of 3 (La, Eu and Yb) or 5 (Ce, Tb, Ho, Er, Lu) lanthanides simultaneously. The NPs were isolated from the bulk after centrifugation and analyzed by AsFlFFF/ICP-MS to investigate the influence of the lanthanide cation size on the incorporation. The corresponding isolated colloidal hectorite suspensions are named 3LnsCopHec and 5LnsCopHec, respectively.

The mean ICP-OES Si/Mg Mol ratio suggests the

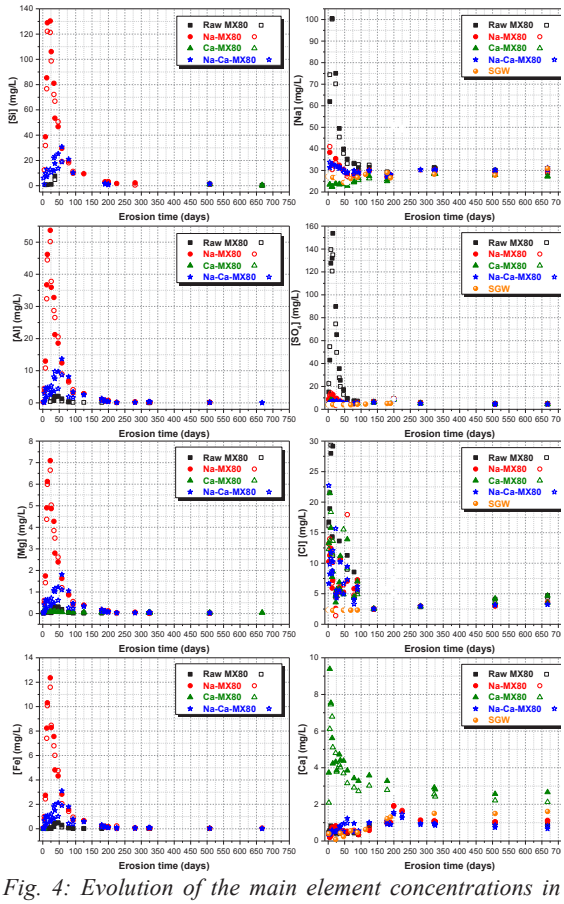

Fig. 4: Evolution of the main element concentrations in the effluent water samples collected from each reactor as determined by ICP-OES and ICP-MS.

presence of hectorite particles. The Mg- and lanthanides-ICP-MS fractograms are presented Fig. 5. Mg is the fingerprint of the hectorite colloids while the 3 (Fig. 5, upper part) or the 5 lanthanides (Fig. 5, lower part) are followed as co-precipitated elements. First, for both syntheses, the results evidence the presence of multimodal size distributions of hectorite particles as seen by the elution peak maxima and shoulders at ~400-450 s, ~700-750 s and ~900-1050 s. This corresponds to nanoparticles varying from 10 nm up to 300 nm. Secondly, it is obvious that the Mg and the different lanthanide fractograms are closely correlated over the complete size range (or elution time) giving a clear hint that there is an association between the lanthanides and the hectorite colloids.

The hectorite colloids recoveries calculated from the Mg recovery are (59±4)% and (68±4)% for the suspensions 3LnsCopHec and 5LnsCopHec, respectively, similar to earlier works [13-15]. The elemental recoveries are: La (45±4)%, Eu (58±4)%, Yb (63±4)% for the suspension 3LnsCopHec and Ce (39±2)%, Tb (65±4)%, Ho (67±1)%, Er (67±4)% and Lu (68±4)% for the suspension 5LnsCopHec. The similar recoveries between Mg and the lanthanides in both systems investigated is an indication of their structural association to hectorite colloids. For both suspensions, the two largest lanthanide cations investigated, respectively La and Ce, showed lower recoveries. In addition higher amounts of La and Ce are recovered in the void peak as "free species" (La (8±1)%, Ce (35±1)%). Finally, the examination of the Mg/REE element mole ratios, which are rather constant for the smallest lanthanides investigated, whatever the suspension considered (Yb, Lu, Er, Ho, Tb) is a indication of their strong association with the hectorite colloids, which might indicate their homogeneous incorporation. Eu in the suspension 3LnsCopHec appears incorporated too, even if in a more heterogeneous way, in agreement with [14]. On the opposite, La and Ce appears incorporated but in less proportion and even more heterogeneously. All data presented here indicate a REE cation size dependent selectivity. This agrees with literature data on REE pattern in natural clay samples [16,17].

In conclusion, these new results agree with previous ones [13-15] and tend to demonstrate that various lanthanides may be incorporated, more or less homogeneously according to their size, but all simultaneously. The hectorite particles extracted are seen as miniatures of the bulk solid. Due to their size they will probably not migrate over long distances from their source and thus may act as a RNs sink. This will be true as long as they will be chemical stable under the relevant geochemical conditions. This point remains to be elucidated.

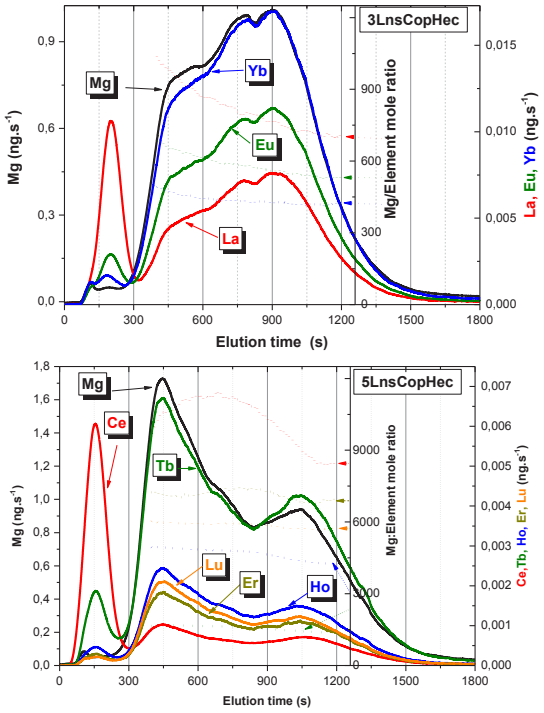

Fig. 5: Mg- and lanthanides-ICP-MS-fractograms obtained after injection of the supernatants (100 µL). Mean of two measurements, smoothed data.

References

[1] Czerwinski et al., *Radiochim. Acta,* **72**: 179 (1996)
[2] Wall et al., *Radiochim. Acta,* **90**: 563 (2002)
[3] Kurk & Choppin, *Radiochim. Acta,* **88**: 583 (2000)
[4] Szabò et al., *Radiochim. Acta,* **98**: 13 (2010)
[5] Ciavatta, *Annali di Chimica,* **70**: 551 (1980)
[6] Tipping et al., *Environ. Chem.,* **8**: 225 (2011)
[7] Benedetti et al., *Environ. Sci. Technol.,* **29**: 446 (1995).
[8] Marsac et al., *GCA* **131**: 290 (2014).
[9] R. Guillaumont et al., *Chemical Thermodynamics Vol. 5*, Elsevier, Amsterdam, (2003)
[10] Marsac et al., in preparation
[11] N. Albarran et al., Applied Clay Science, **95**: 284 (2014)
[12] G. Ledergerber et al., *J. Nucl. Mat.,* **153**: 189 (1988)
[13] M. Bouby et al., *Min. Mag.*, **76**: 2709 (2012)
[14] N. Finck et al., *Min. Mag.,* **76**: 2723 (2012)
[15] H. Geckeis et al., Annual Report 2013, *KIT Scientific reports* 7664.
[16] I.T. Uysal et al., *Chem. Geol.* **193**: 167 (2003)
[17] S. Severmann et al., *GCA* **62**: 1851 (2004)

5.4 Thermomechanical modeling

Pudewills, Alexandra

Part I. Numerical analysis of a drift intersection in a waste repository in rock salt

During the last decades, a large and detailed experimental and theoretical database of the geomechanical behavior of rock salt has been elaborated by several working groups ([1],[2]). Considering this knowledge, different advanced constitutive models for the numerical simulations have been developed. In the frame of a joint project within its research program "Improvement of tools for the safety assessment of underground repositories", the five project partners performed benchmark calculations of different real underground structures in rock salt in Germany. The aim of these projects was to evaluate the ability of the models to correctly describe the relevant deformation phenomena in rock salt under various influences, (i.e. transient and steady-state creep, the evolution of dilatancy and damage, short-term failure and long-term creep failure, post-failure behavior).

Last year the intersection between the planned main drifts in a waste repository was analyzed. The current concepts for design and construction of a waste repository in rock salt contain a number of storage panels to which the access will be provided by a system of large transportation- or access-drifts along the various directions crossing one another. The intersections are an important issue to the layout design of a repository. Therefore the stability of such intersections is an essential requirement for the proper activities during the waste container transportation and disposal in underground drifts.

The objectives of this numerical simulation was to predict deformations and stability of rock salt at the intersection of main drifts caused by excavation, and to determine the three-dimensional extension of the Excavation Disturbed Zone (EDZ) in the surrounding rock. The structural stability of the excavation intersections is a prerequisite for the operation of a repository during the ventilation, waste transportation and emplacement in underground. The 3D simulations were conducted using primarily the finite element code ADINA [3]. The model parameters for the numerical simulation have been evaluated based on the available laboratory experiments on rock salt. The computational studies include key parameters such as rock strength, rock creep behavior as well as the assumed intersection angle. The rupture of rock salt can be allowed only by tension. The tensile cracking failure is assumed if the maximum principal stress exceeds a given tension limit. When the calculated tensile stress reaches the critical value, the associated element is immediately removed. To analyze the 3D crack propagation in a salt pillar at the large drift intersection *the virtual crack extension method* [4] implemented in ADINA code was employed. This method is applicable to finite element solutions for intensively cracked structures and no particular special crack tip formulation is required. Two cases were considered: firstly, a rectangular intersection of equal large drifts (a) and secondly, a particular case of bifurcated drifts with a wedge-shaped salt pillar in between (b). Figure 1 shows both investigated drift intersections together with the assumed modeling domains (red dashed lines).

As well known, sharp intersection corners are re-

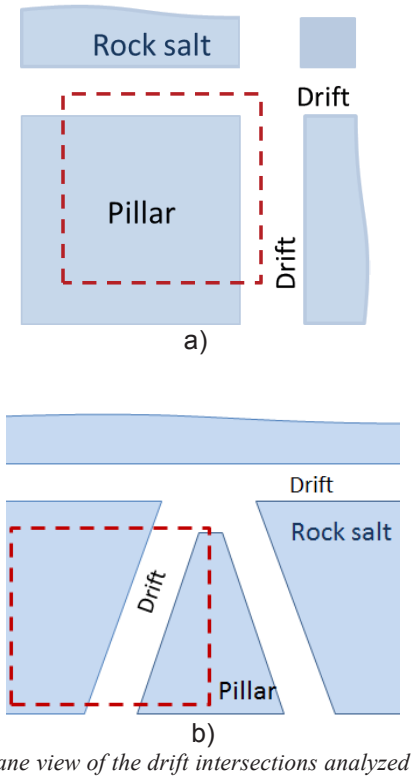

Fig. 1: Plane view of the drift intersections analyzed and the domains considered for numerical modeling (dashed lines)

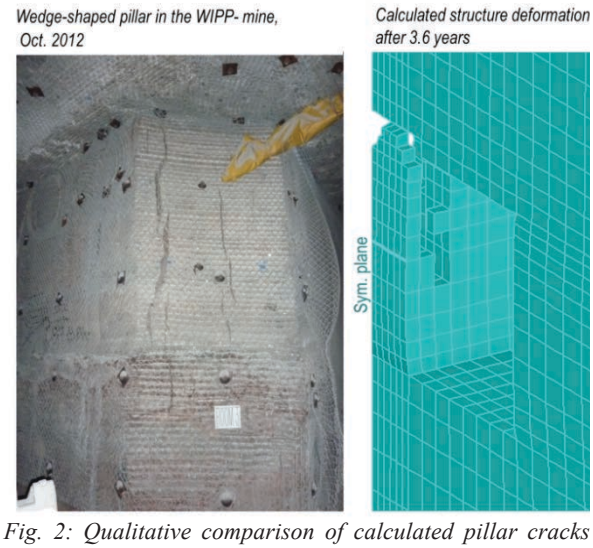

Fig. 2: Qualitative comparison of calculated pillar cracks after 1,323 days and a photograph taken in the WIPP mine.

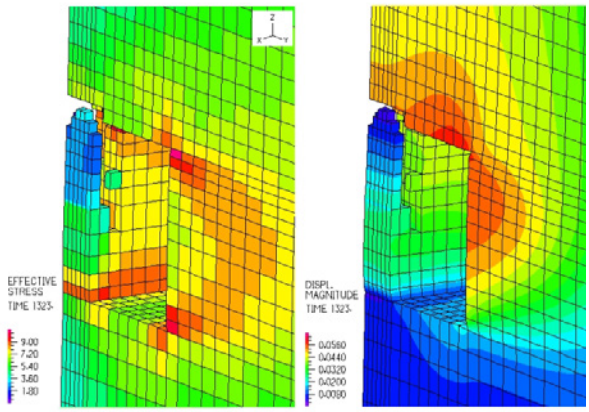

Fig. 3: Distribution of effective stress and displacement magnitude fields in rock salt at the intersection 1,323 days after drift excavation (intersection angle is 60°).

gions of high stress concentrations, which need an efficient supporting strategy or have to be rebuilt often to avoid the structural instability. The analyses were conducted under various conditions, including rock-salt creep and strength behavior, lithostatic pressure and intersection angle. The assumed angle was 60° and subsequently reduced to 50°. One important aspect is the simulation of 3D-crack propagation in the wedge pillar without a substantial support (see Figures 2 and 3). From all the simulations only some illustrative computation results will be presented.

The calculation results show a similar rock splitting as the photograph of the real salt pillar. However, a direct comparison is not possible due to lacking of *in-situ* information. The distribution of effective and mean principal stress shows that the highest values are obtained near the drift entrance and the cracks develop in 0.3 - 1 m horizontal distance from intersection.

If the intersection angle is reduced to about 50° the closure of the drift and the deformation of the salt pillar between the access drifts increases considerably. In fact, with time the 3D-crack propagation will affect the entire pillar high.

Summary of numerical results

The predictive capabilities of the constitutive model for rock salt have been improved to describe the rock failure deformations at different kinds of underground intersections. This model is able to simulate the main behavior of the rock salt such as transient and steady state creep, dilatancy and material damage. The use of virtual crack extension (VCE) technique is an efficient and accurate approach to fracture mechanics calculations in finite element analysis.

The 3D modeling of the complex structures was an important test of the numerical tools used for future rock salt benchmark calculations. The results from the present study provide valuable data for the prediction of EDZ development, extension and for future planned constructions.

In addition, the work reveals the necessity of future development and improvement of the constitutive model for rock salt in order to describe the post failure behavior and the influence of the elevated temperature.

References

[1] Hampel, A., Günther, R.-M., Salzer, K., Minkley, W., Pudewills A., Leuger B., Zapf D., Staudtmeister K., Rokahr R., Herchen, K, Wolters, R., Lux, K.-H., Schulze, O., Heemann, U. & Hunsche U. 2010. Bencharking of Geomechanical Constitutive Models for Rock Salt", *Proc. 44th US Rock Mechanics Symposium*, Salt Lake City/Utah/USA, 27-30 June 2010, American Rock Mechanics Association (ARMA).

[2] Hampel, A., Salzer, K., Günther, R.-M., Minkley, W., Pudewills, A., Leuger, B., Zapf, D., Staudtmeister, K., Rok-ahr, R., Herchen, K., Wolters, R. & Lux, K.-H. 2012. Joint Projects on the Comparison of Constitutive Models for the Mechanical Behavior of Rock Salt - II. Overview of the models and results of 3-D benchmark calculations. in P. Bérest, M. Ghoreychi, F. Hadj-Hassen & M. Tijani (eds.), *Mechanical Behavior of Salt VII, Proc. 7th Conference*, Paris, 16-19 April 2012: 231-240. London: Taylor & Francis Group (Balkema).

[3] Adina R & D Inc., ADINA (Automatic Dynamic Incremental Nonlinear Analysis). 2014. *Report ARD* 01-9, Watertown, MA, US.

[4] Hellen, T.K. 1975. On The method of Virtual Crack Extensions, *Int. J. Num. Meth. Engng.,* **9**: 187 -207.

[5] Parks, D.M. 1977. The Virtual Crack Extension Method for Nonlinear Material Behaviour,*Comp. Meth. Appl. Mech. Engng.*, **12**: 353-364

Part II. Analysis of the flow field and solute transport in the near zone of CFM 06.002 and monitoring boreholes

The Colloid Formation and Migration (CFM) project at the Grimsel Test Site (GTS) [1]; (www.Grimsel.com/gts-phase-vi/cfm-section/cfm-introduction), aims to investigate and quantify the impact of colloids on the transport of radionuclides in a fracture taking into account the repository relevant spatial and temporal conditions.

In CFM-experiment the near field geochemical conditions is monitoring by sampling the fluid from the shear zone near to the bentonite source emplacement in the CFM 06.002 borehole.

Three observation / monitoring boreholes were drilled in the near vicinity (~40 mm distance) of the injection borehole CFM 06.002. The Figure 1 shows the layout of the monitoring boreholes in the plane of shear zone close to the existing CFM 06.002. In the *in-situ* test series CFM 11.001, 11.002 and 11.003 the monitoring boreholes were included in the flow pathway around the injection-well CFM06.002. However, it seems that the drilling process of the monitoring boreholes has affected the hydraulic properties of the shear zone in the migration dipole.

In order to study the flow field and transport properties near the injection hole CFM 06.002 and the new monitoring boreholes CFM-11.001-003, computational fluid dynamics (CFDs) simulations with ADINA-F code [1] were performed. The finite element model and boundary conditions are shown in Figure 2. The 2D-model is composed of two domains in the plane of the shear zone, namely the saturated porous material of the shear zone (zone 1) and the open holes filled with groundwater in which the hydraulic head is nearly constant (zone 2). The model extension covers a domain of 1 m x 1 m and at the outer side of the geometry a groundwater flow velocity of 10^{-5} m/s was assumed. The ability of the model to calculate the fluid flow in porous media and also in open boreholes allows to simulate different flow situations, expected

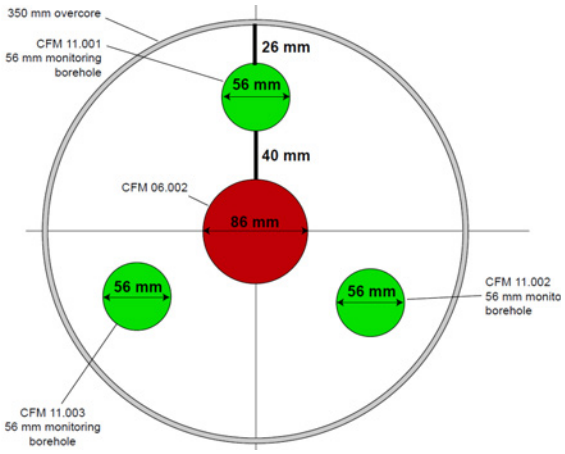

Fig. 1: Layout of monitoring boreholes (CFM 11.001 to 11-03) around the injection borehole, CFM 06.002, in the migration shear zone

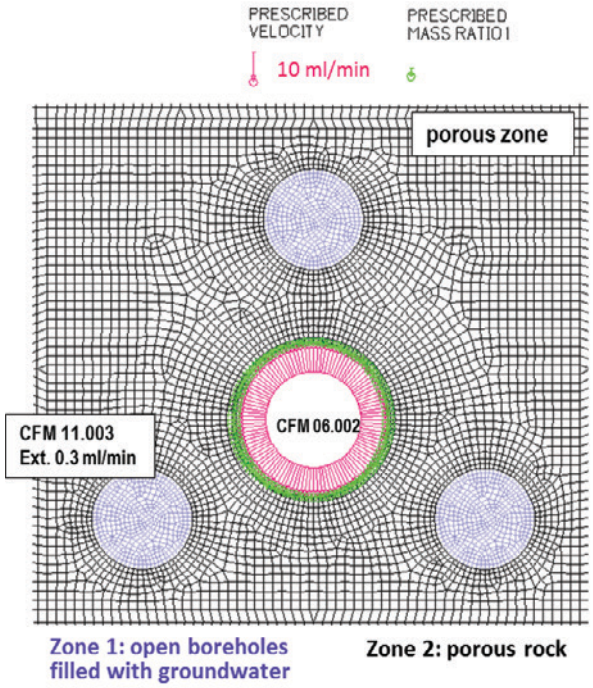

Fig. 2: Detail of the finite element mesh near the injection and monitoring wells used for simulation of groundwater flow field and solute transport.

near the main injection and monitoring holes. The model presented here was used to perform generic studies and to calculate the flow field and the transport behavior around and into the open monitoring boreholes over a short time scale.

From all performed numerical studies, we will illustrate the following case only:

- in the main borehole CFM 06-002 filled with groundwater a tracer solute was injected according an input function with the flow rate of 10 ml/min.
- all the monitoring boreholes stay open but from the borehole CFM 11-003 a small amount of groundwater was extracted (~ 0.3 ml/min) for further geochemical analysis.

Figure 3 shows the calculated fluid velocity field, the pressure field, and the distribution of the tracer at different times after injection of a hypothetical tracer in the CFM-06.002 borehole. The assumed injection function is also plotted in this figure. It can be observed that the influence of extraction of a small amount of fluid (~ 0.3 ml/min) from monitoring well CFM-11.003 is insignificant for the expected long-term migration through the planned large dipole experiment.

References

[1] Blechschmidt, I. et al., GTS Phase VI - CFM Status Report on Field Work 2004-2005, Arbeitsbericht NAB 06-361, Nagra, Wettingen, Switzerland, 2006.

[2] Adina R & D Inc., ADINA (Automatic Dynamic Incremental Nonlinear Analysis), *Report ARD* 01-9, Watertown, MA, USA, 2012.

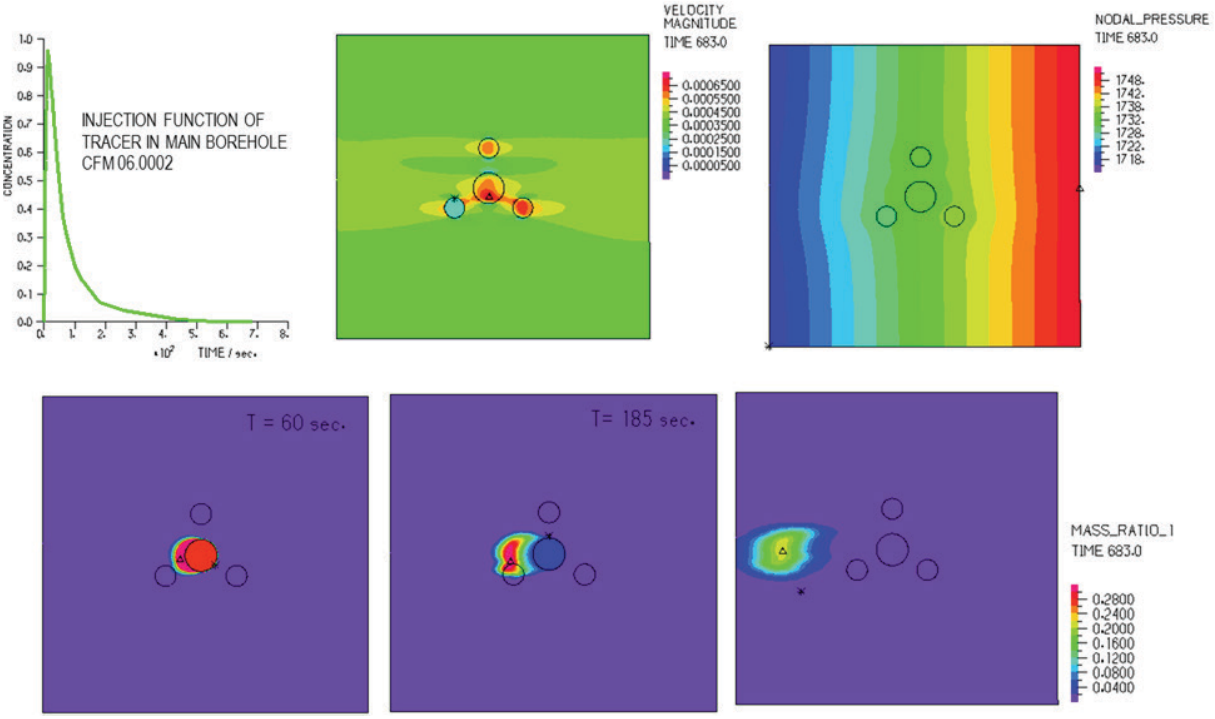

Fig. 3: Calculation results for the analyzed case: Injection of tracers in central borehole CFM06-002 and extraction at 0.3 ml/min from monitoring holes CFM 11.003. The assumed injection function and distribution of fluid velocity and pore water pressure, respectively (upper plots) and the tracer distribution after different times (lower plots).

5.5 Reactive transport modeling

F. Huber, V. Montoya, B. Kienzler, T. Schäfer

in co-operation with:

B. Baeyens[a], Ch. Bruggemann[b], M. Glaus[a], T. Kupcik[c], N. Maes[b], M. Marques Fernandes[a], J. Molineo[d], A. Sainz[d], B. Shafei[d], Y.Totskiy[c]; M. Trumm[c], L. Van Laer[b]

[a] Paul Scherrer Institut (PSI-LES), Villigen, Switzerland; [b] SCK CEN, Mol, Belgium; [c]KIT-INE, Karlsruhe, Germany, [d]Amphos 21, Barcelona, Spain

Introduction

Research activities on reactive transport modeling have been focused on simulations of radionuclides migration experiments in different scenarios representatives of nuclear waste repository concepts in clay and crystalline formations. The simulations include sorption processes, aqueous speciation and advective-dispersive transport in fracture media and diffusive transport in clays. This kind of calculations provides the scientific basis for the performance assessment of various repository design options.

The simulations are included in the framework of two different FP7 European projects: CATCLAY and BELBaR. The reactive transport simulations have been conducted with different codes depending on the system: PHREEQC v. 3 [1] and COMSOL Multiphysics ® 5.0 [2]. Additionally, the interface iCP [3] has been used and tested taking advantage that KIT-INE is part of the Consortium where this tool has been developed. One of the advantages of using these codes is that all them are in continuous development.

iCP [3] is an interface developed in Java® that couples two simulator programs: COMSOL Multiphysics® [2] and the geochemical code PHREEQC [1]. One of the characteristics of iCP is that the program is not in charge of the numerical calculations, and it is only used as an interface to couple and maximize the synergies between COMSOL and PHREEQC. This interface provides a numerical platform that can efficiently simulate a wide number of multiphysics problems coupled to geochemistry (i.e. liquid flow, solute and heat transport, elastic and plastic mechanical deformations and geochemical reactions). In this sense, iCP is an extraordinary tool to be used in reactive transport modeling which can account *inter alia* for multiphase flow, pore-scale simulations, and fractured rocks hydrogeology coupled with mineral dissolution/ precipitation, porosity changes, cation exchange or surface complexation mechanisms.

In 2014, KIT-INE, PSI, CEA and GRS organize the TRe-Pro III 2014 Workshop *"Modelling of Coupled Transport Reaction processes"* in Karlsruhe.

Modeling of diffusion-sorption processes in Na-illite

Diffusion experiments with Co(II), Zn(II), HTO, and $^{36}Cl^-$ at trace concentrations in a compacted purified Na-illite sample are modeled with PHREEQC's multicomponent diffusion module with the final aim to compare the results with the ones obtained by the iCP approach.

Diffusion cells an experimental setup used are described in Glaus et al. [4]. In the experiments, tracer concentration decrease was observed in the inlet reservoirs due to the combined effect of in-diffusion and sorption.

PHREEQC v.3 [1] option to calculate multicomponent diffusion in free pores and in the diffuse double layer (DDL) was used which allows calculating each solute species having its own tracer diffusion coefficient, and keeping electro-neutrality conditions. Solute species can be transported in coexisting charged and uncharged regions as may exist in clays. The composition of the DDL is calculated with the Donnan approximation.

Modeling of HTO diffusion in the clay gives the accessible porosities and the geometrical factors (the ratio of pore tortuosity and constrictivity, δ/τ^2), which apply in principle for all the neutral and cationic species. As anions are repelled from the vicinity of the negatively charged clay surfaces, a fraction of the porosity is not accessible for chloride (*anion exclusion*). In the model, half of the porosity is not accessible for chloride due to anion exclusion, and assumed equal to the amount of DDL-water. With this assumptions and taking into account the diffusion coefficient in water D_w (HTO) = 2.24 10^{-9} m^2/s, D_w (Cl^-) = 1.30 10^{-9} m^2/s, the experimental results at pH = 5 and I = 0.1 M have been modeled. Diffusion of $^{36}Cl^-$ in the Na-illite is slower attributed to the smaller diffusion coefficient of this tracer and to the less accessible porosity for anions in the clay.

More interesting is the modeling of strongly sorbing radionuclide species like the divalent cations Co(II) and Zn(II) which can be bound to the compacted Na-illite surfaces. Specifically, it has been studied if these cations can be mobile or immobile under the same conditions of the diffusion experiments performed for HTO and Cl^- (pH = 5 and I = 0.1 M).

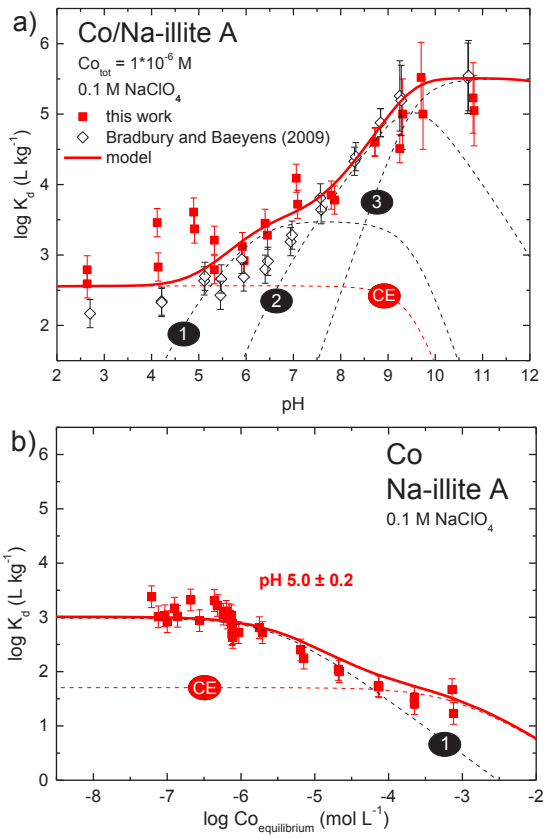

Fig. 1: Top: pH edge of Co(II) in Na-Illite at I = 0.1 M $NaClO_4$. Experiments (squares) and model (lines). Dotted lines represent the different surface species. (In red) the exchange reaction, (in black) the surface complexation species ($\equiv S^SOCo^+$, $\equiv S^SOCoOH$, $\equiv S^SOCo(OH)_2^-$). Bottom: Co sorption isotherm on Na-illite A at pH 5 in 0.1 M $NaClO_4$ with the modelled sorption and the contribution of individual Co species.

In this case, the understanding of transport processes of cobalt and zinc in compacted clay systems can be achieved through the inclusion of sorption models (based on experimental data obtained from dispersed systems) in the reactive transport simulation of diffusion processes in Na-Illite.

New sorption data (both sorption edge and isotherm) for the interaction of Co(II) and Zn(II) with purified Na-Illite has been obtained in this work and compared with data available in the literature when possible (see Fig 1 and Fig 2). A similar two site protolysis non-electrostatic surface complexation and cation exchange (2SPNE SC/CE) model like the one described in Bradbury & Baeyens [5] has been obtained for which the site types, site capacities and protolysis constants were fixed. Thus, surface complexation constants for the strong sites and cation exchange in the 2SPNE SC/CE sorption model for Co(II) and Zn(II) have been obtained.

Finally, with the sorption data now available, the 2SPNE SC/CE sorption model has been incorporated into the complete reactive transport model allowing cobalt and zinc migration to be calculated/predict. As first approximation, a non-electrostatic sorption model has been incorporated.

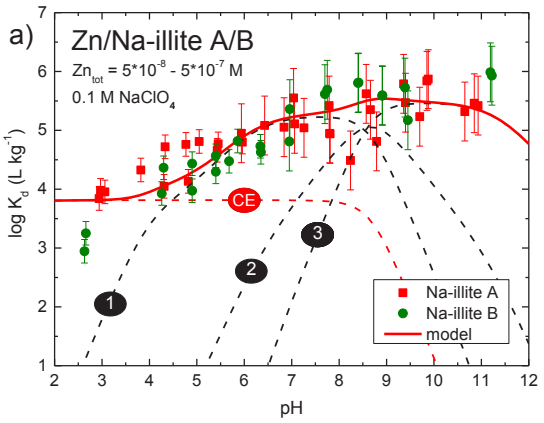

Fig. 2: pH edge of Zn(II) in Na-Illite at I = 0.1 M $NaClO_4$. Experiments (squares) and model (lines). Dotted lines represent the different surface species. (In red) the exchange reaction, (in black) the surface complexation species ($\equiv S^SOZn^+$, $\equiv S^SOZnOH$, $\equiv S^SOZn(OH)_2^-$).

A much faster decrease of concentration of Zn(II) and Co(II) is observed in comparison to HTO and $^{36}Cl^-$ (see Fig 3). This difference is mainly attributed to the higher concentration gradient due to sorption processes for cations [6]. If we look to the chemical processes under the conditions where the model is tested (pH = 5 and low cation concentration) and the sorption model described previously, we can see that the most important mechanism of retention is the exchange with the Na-Illite and surface complexation of the free divalent cation. At present no competition with other cations of the system has been incorporated in the model, but it is expected that competition between other cations present in the pore water (by the dissolution of the Na-illite) will occur [6]. Future work will be comparison with the results obtained with iCP and COMSOL.

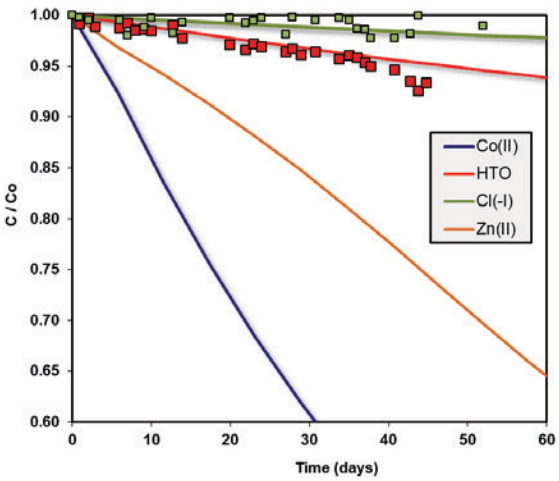

Fig. 3: Calculated decrease of the reservoir concentrations for Co(II) (blue line), Zn(II) (orange), HTO (red) and Cl(-I) (green) and the related experimental data (squares).

Modeling far field retention processes in fractured crystalline rocks

Mass transport processes in fractured systems are strongly coupled to the heterogeneous flow fields arising from the complex geometrical properties of the fractures and their distribution in fractured network systems. Consequently, flow and transport modeling of these systems is a complicated task where predictions of solute transport from experimental observations (µm-cm scale) and their upscaling for large- scale models (m-km range) is a modelers challenge. Geometrical features like fracture geometry and aperture distribution need to be considered in the models to accurately capture complex flow patterns, which govern mass transport behavior in advective controlled systems. One way to obtain these geometrical features is e.g. µ-computed tomography (µCT) as a non-invasive technique yielding digital datasets on the fracture geometry that can be directly used in 3D computational fluid dynamic (CFD) simulations. This approach has been successfully applied by Huber et al. [8] to model experimental results of conservative solute and nanoparticle transport experiments in a single fracture drill core from Äspö, Sweden. Up to now, this approach was only able to consider complex geometries, to solve the fluid flow and to take into account non-reactive mass transport processes but had to neglect geochemical processes like e.g. sorption/desorption, reduction, dissolution etc. due to the limitation of the CFD codes like ANSYS Fluent or COMSOL Multiphysics [2]. Using the above described tool iCP [3], it is possible to use highly complex geometrical models and thus complex flow fields in combination with geochemical processes and reactions. One drawback of iCP is the increasing numerical and computational demands when coupling CFD simulations with geochemical reactions. It is therefore wise to start with lower dimensional models in 1D and 2D, especially to setup and test the geochemical conceptual model before conducting a full 3D reactive transport model.

The first system to which iCP is currently applied focus on Tc migration experiments in a single fractured drill core. Following the approach by Huber et al. [8] the drill core used in the experiments was scanned with a µCT (30µm voxel resolution) to obtain information on fracture geometry and aperture distribution. Figure 4 shows the core as installed in the glove box in conjunction with a µCT slice of the core.

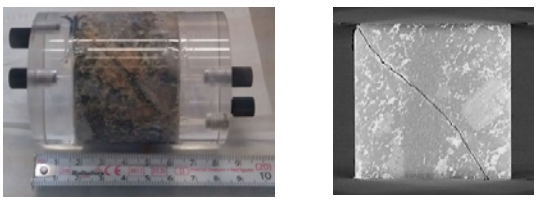

Fig. 4: (left): Drill core (right) µCT slice of the core.

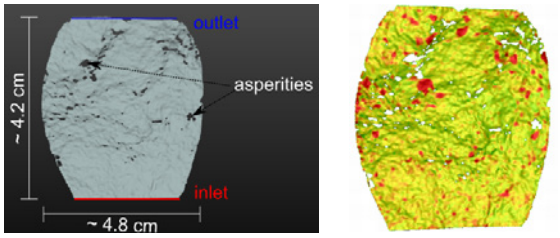

Fig. 5: (left): Rendered fracture (right) Aperture distribution.

The µCT slice of Fig. 4 shows the fracture suture as a black irregular line running from the upper left top to the lower right bottom. Out of the µCT dataset a 3D digital model has been prepared using the software Mimics© and 3matic© (both Materialise, Belgium) by greyscale threshold segmentation extracting only the connected void space (fracture). The geometry of the fracture reconstructed by the µCT dataset is shown in Figure 5 (left).

It can be clearly seen that the fracture possess heterogeneous, rough and slightly bended surfaces with several locations in the upper half of the fracture where both surfaces interconnect each other (asperities) meaning that the fracture is closed at this points. A heterogeneous distribution of the aperture (opening width of the fracture) has been derived from the 3D model which is shown in Figure 5 (right). The highest aperture is 0.8093 mm (mid to high apertures are indicated in Figure 5 with yellow to red colors, respectively). A mean aperture 0.192 mm with a standard deviation of 0.0637 mm has been obtained (mid to low apertures are represented by yellow to green colors, respectively). The total fracture surface area was determined to be 42.35 cm^2 and the total volume of the fracture void space is 0.415 ml. Before setting up the first iCP model, the fracture midplane was computed out of the 3D digital model and projected to a 2D plane. Subsequently this 2D plane was imported in COMSOL to build the model geometry and the mesh (~45k triangular elements). After applying the boundary conditions at the inlet (pressure inlet), outlet (pressure outlet) and wall the laminar steady state flow is solved. The 2D model offers the possibility to investigate the effect of the flow field on the Tc transport, namely Navier-Stokes (NS) flow [9] and Cubic Law (CL) flow [10] (by interpolating the aperture distribution from the µCT dataset on the geometry). Figure 6 depicts both normalized flow fields. While the CL flow

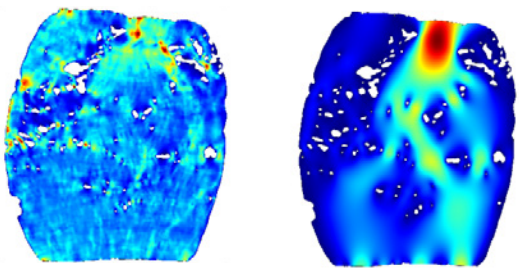

Fig. 6: (left): CL flow field (right) NS flow field.

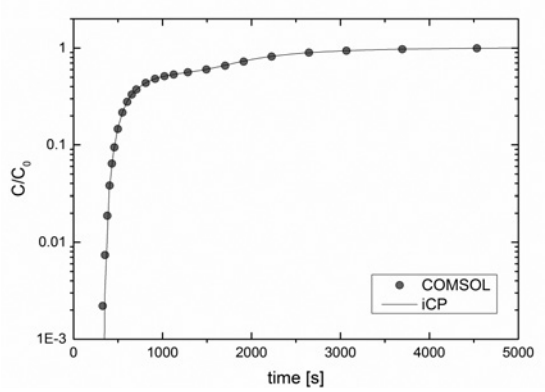

Fig. 7: Comparison between COMSOL and iCP breakthrough curves.

field is fully controlled by the apertures rather than the overall geometry of the fracture, the NS flow field clearly reflects the dependency on the fracture geometry and asperities. In consequence, the resulting flow fields are very different compared to each other.

Before solving a complex reactive transport simulation using iCP with the 2D model, a first test simulation verifying the correctness of the coupling between COMSOL and PhreeqC [3] was conducted. For this, a generic conservative tracer step injection transport simulation with a normalized concentration was solved on the 2D NS flow model both in COMSOL only and with iCP. The results of this test case are shown in Figure 7. It can be clearly seen that the results of both simulations agree very well to each other verifying the iCP coupling between the COMSOL and PhreeqC simulation. As already indicated above, the iCP approach poses higher demands in terms of numerical stability and computational time. This becomes obvious when comparing the simulation times of the test case. While COMSOL only needs around 16 min for the simulation, the iCP model simulation time was ~7h (both run on an 8 core workstation).

It is clear that iCP simulation times last longer since the model needs to be solved both in COMSOL for the transport steps and in PhreeqC for the chemistry steps. Moreover, it turned out that due to the complex geometry of the 2D model, COMSOL solver tolerance has to be fixed at $1x10^{-12}$ for the solute tracer transport within iCP instead of $1x10^{-6}$ (which is normally sufficient if only COMSOL is used) leading to much more iterations and thus simulation time. Without such a tolerance threshold numerical overshoots have been observed spoiling the accuracy of the simulation. To enhance the numerical robustness of the coupling approach will be one of the main focuses within the iCP developments in the future. The first reactive transport simulations using the 2D model incorporating experimentally determined sorption and reduction kinetics for Tc are conducted at the moment.

Generally speaking, the iCP approach opens up possibilities for reactive transport modelling to challenging systems, which have been unavailable in the past due to their high degree of spatial complexity.

References

[1] Parkhurst, D. L., Appelo, C. A. J. U.S. Geological Survey Techniques and Methods, 2013, book 6, chap. A43, 497 p.

[2] COMSOL, 2014. Comsol Multiphysics. Version 5.0, Available at: www.comsol.com.

[3] Nardi A. et al. Computers & Geosciences, 69, 2014, 10-21.

[4] Glaus et al., 2014, Geochim. Cosmochim. Acta, submitted.

[5] Bradbury M. H. and Baeyens B. Geochim. Cosmochim. Acta 2009, 73, 1004.

[6] Appelo et al. 2010, Geochim. Cosmochim. Acta 74, 1201.

[7] Tournassat C. et al. American Journal of Science, 2013; 313, 395.

[8] Huber et al. 2012. Journal of Contaminant Hydrology, 133, 40–52.

[9] Batchelor, G.K., 1967. Cambridge University Press, Cambridge.

[10] Witherspoon, P.A., et al., 1980. Water Resources Research, 16,: 1016-1024.

6. Separation of long-lived minor actinides

Recycling transuranium elements (TRU = Np, Pu, Am, Cm) from irradiated nuclear fuel may provide advantages over the direct disposal of used nuclear fuel such as a more compact final HAW repository [1, 2]. This would require separating the actinides from fission products and re-using them as nuclear fuel. Most separation schemes under development in Europe are based on the PUREX process to remove uranium and plutonium (plus neptunium after slight process modification). Additional processes for separating americium and curium are DIAMEX and SANEX but also combinations of these two processes such as 1c-SANEX [3] and i-SANEX [4]. Furthermore, processes for the co-separation of all TRU have been developed such as the EURO-GANEX process [5, 6]. More recently, processes extracting only Am(III) from PUREX raffinate are being studied, such as the AmSel process [7]. i-SANEX, EURO-GANEX and AmSel processes have in common the utilization of water soluble BTP (bis-triazinyl pyridine) or BTBP (bis-triazinyl bipyridine) based stripping agents for actinide ions. The chemistry and properties of these stripping agents is under study within the FP7 EURATOM project SACSESS [8]. Some example studies from this context are discussed below.

6.1 Recyclability of SO_3-Ph-BTP

U. Müllich, D. Munzel, A. Geist

In co-operation with:

H. Galan, A. Nuñez

CIEMAT, Madrid, Spain

Introduction

SO_3-Ph-BTP (2,6-bis(5,6-di(sulphophenyl)-1,2,4-triazin-3-yl)pyridine tetrasodium salt, Figure 1, a water soluble BTP, is useful for selectively stripping An(III) from an organic phase loaded with An(III) and Ln(III) [9]. It has been used in GANEX [4,5] and in i-SANEX process tests [6,7].

These processes generate a product solution containing actinide ions and SO_3-Ph-BTP in approx. 0.5 mol/L HNO_3. Further processing of actinides may require their separation from SO_3-Ph-BTP, which in turn offers the possibility of recycling SO_3-Ph-BTP. The separation of actinide ions from the SO_3-Ph-BTP solution is possible by re-extracting them into a new TODGA solvent. The SO_3-Ph-BTP solution can then be re-used for a new stripping cycle. This in turn requires a sufficient stability of SO_3-Ph-BTP versus HNO_3 and radiation.

Both aspects – SO_3-Ph-BTP's separation from An ions and its stability – have been studied.

Separation of An ions from SO_3-Ph-BTP

Am(III) has distribution ratios < 1 under i-SANEX stripping conditions, i.e. approx. 0.5 mol/L HNO_3. By simply increasing the HNO_3 concentration to > 1 mol/L in the product solution obtained by stripping, Am(III) distribution ratios are > 1, meaning that Am(III) can be re-extracted into a fresh solvent, separating it from SO_3-Ph-BTP.

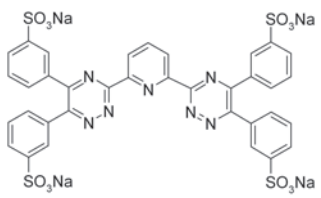

Fig. 1: SO_3-Ph-BTP.

The SO_3-Ph-BTP solution obtained after re-extracting Am(III) is not suitable for recycling it to the strip section because of a too high HNO_3 concentration (> 1 mol/L rather than 0.5 mol/L HNO_3). The HNO_3 concentration needs to be reduced, which is feasible e.g. by extracting HNO_3 into TOA (tri-*n*-octyl amine).

Solutions of TOA in 1-octanol proved to perform well for extracting HNO_3. As shown in Figure 2, significant extraction of HNO_3 is observed. For example, a solvent containing 0.5 mol/L TOA reduces HNO_3 concentration from initially 1.0 mol/L to approx. 0.5 mol/L. The organic phase HNO_3 concentration is no less than the TOA concentration. Indeed,

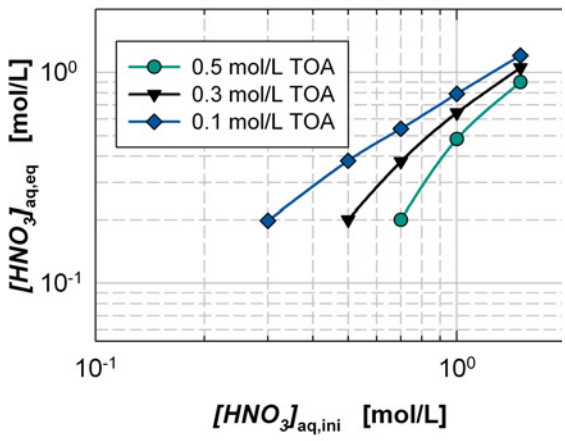

Fig. 2: Extraction of HNO_3 into TOA. Equilibrium aqueous HNO_3 concentration as a function of initial HNO_3 concentration. Organic phase, TOA (concentration as indicated) in 1-octanol. Aqueous phase, HNO_3. A/O = 1, T = (293 ± 2) K.

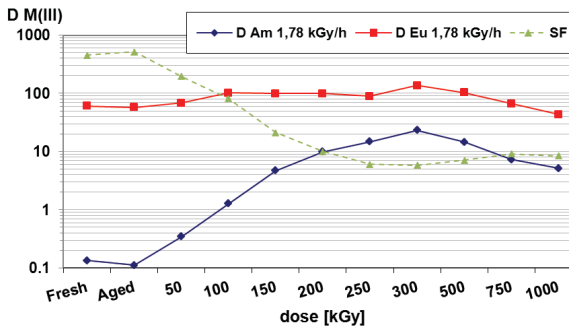

Fig. 3: Am(III) and Eu(III) extraction with fresh, aged and irradiated SO_3-Ph-BTP at different doses and dose rates. Organic phase, 0.2 mol/L TODGA + 5% 1-octanol in kerosene. Aqueous phase, 10 mmol/L SO_3-Ph-BTP + ^{241}Am(III) + ^{152}Eu(III) in 0.5 mol/L HNO_3.

TOA extracts HNO_3 by forming tri-*n*-octyl ammonium nitrate, $(HN(oct)_3^+ \cdot NO_3^-)$ in the organic phase. Additionally, 1-octanol is known to extract HNO_3 [10].

Chemical and radiolytic stability

Stability vs. HNO_3

Preliminary results indicate stability of SO_3-Ph-BTP in 0.5 mol/L HNO_3 for more than two years but its degradation in 4.1 mol/L HNO_3. To study this behavior in more detail, solutions of SO_3-Ph-BTP in 0.5-3 mol/L HNO_3 were stored. After different time intervals, Am(III) and Eu(III) distribution ratios were determined after extraction into a TODGA solvent.

Am(III) and Eu(III) distribution ratios remained virtually constant over 120 days for all HNO_3 concentrations studied. Obviously SO_3-Ph-BTP is not degraded by up to 3 mol/L HNO_3 within 120 days.

Radiolytic stability [11]

Solutions of SO_3-Ph-BTP in 0.5 mol/L HNO_3 were irradiated with varied doses ($\leq$ 1 MGy) using ^{60}Co sources at dose rates of 1.78 or 6.32 KGy/h. The complexation properties of the irradiated SO_3-Ph-BTP samples were evaluated by determining Am(III) and Eu(III) distribution ratios.

The distribution ratios obtained with fresh, aged and irradiated SO_3-Ph-BTP are compared in Figure 3.

An effect of radiolytic degradation is observed from the first irradiation step (50 KGy). Am(III) extraction increases progressively, reducing the separation factor between Am(III) and Eu(III), $SF_{Eu(III)/Am(III)}$, along the irradiation procedure. Up to 200 KGy of integrated dose the separation factor remains higher than 10. Beyond, TODGA's selectivity is approached ($SF_{Eu(III)/Am(III)} \approx 7$).

The increase in Am(III) distribution ratios upon irradiation is explained by radiolytic degradation of SO_3-Ph-BTP. Assuming that the degradation products do not interfere and taking into account the dependency of Am(III) distribution ratios on the concentration of SO_3-Ph-BTP as reported in [9], the decrease in SO_3-Ph-BTP concentration with increasing dose was estimated. Approx. 50% would be lost at a dose of 60 KGy; less than 10% would remain at 250 KGy.

Conclusions

SO_3-Ph-BTP has successfully been applied in lab-scale actinide separations processes. A further step is the recycling of SO_3-Ph-BTP. This requires its separation from actinide ions and from HNO_3, both of which have been demonstrated.

A further requirement towards its recycling is chemical and radiolytic stability. The former seems not to be an issue; SO_3-Ph-BTP maintained its performance after long-term storage in HNO_3. However, radiolytic degradation is observed. In this context, the rather high doses applied must be considered, taking into account that dose rates in the range of 0.1 KGy/h and 0.5 KGy/h are to be expected for the reprocessing of UO_2 and MOX fuels, respectively [12].

Related to the fact that SO_3-Ph-BTP is degraded by radiolysis is knowledge of the kind of degradation products generated, of their properties and of ways of how to remove them. Respective investigations are under way.

6.2 Spectroscopic studies towards the development of an AmSel process based on selective Am(III) stripping

C. Wagner, U. Müllich, P. J. Panak, A. Geist

Introduction

Combining a TODGA based solvent and an aqueous stripping phase containing SO_3-Ph-BTBP (6,6'-bis (5,6 - di(sulphophenyl) - 1,2,4 - triazin - 3 - yl) - 2,2'-ipyridine tetrasodium salt, Figure 4, in HNO_3 allows separating only Am(III) from PUREX raffinate while routing Cm(III) with the fission products [7]. Spectroscopic studies are being performed to better understand this system and to produce thermodynamic data required for process modeling.

The complexation of Cm(III) and Eu(III) with SO_3-Ph-BTBP in varied aqueous solutions has been studied using time resolved laser fluorescence spectroscopy (TRLFS) and UV/VIS spectroscopy.

Protonation

Protonation of SO_3-Ph-BTBP plays a significant role, hence the pK_a value was determined by UV/Vis in the range of pH = 0 - 7 in $HClO_4$.

Slope analysis of absorption data yields a value of 1.0, indicating monoprotonation of SO_3-Ph-BTBP in the pH range studied. A pK_a value of 2.2 ± 0.2 is calculated from the species distribution. Hence, SO_3-Ph-BTBP is present as the monoprotonated species in 0.5 mol/L HNO_3 or $HClO_4$, stressing the importance of the competition between metal ions and protons.

Complexation of Cm(III) and Eu(III)

The complexation of Cm(III) and Eu(III) with SO_3-Ph-BTBP in H_2O (pH = 3, adjusted with $HClO_4$) and in 0.5 mol/L HNO_3, $NaNO_3$, $HClO_4$ and $NaClO_4$ was studied by TRLFS: increasing concentrations of SO_3-Ph-BTBP were added to solutions of $^{248}Cm(ClO_4)_3$ or $Eu(ClO_4)_3$, and the emission spectra were recorded 15 min after each addition. The species distribution as a function of SO_3-Ph-BTBP is determined, and stability constants are derived.

As an example, Figure 5 shows the complexation of Eu(III) with increasing concentrations of SO_3-Ph-BTBP. At SO_3-Ph-BTBP concentrations in the range of 10^{-4} mol/L the 1:1 complex is the dominating species; beyond 5×10^{-4} mol/L the dominating species is the 1:2 complex. The formation of 1:1 complexes was only observed in H_2O (pH = 3); its formation was suppressed in 0.5 mol/L acid or salt solutions.

The composition of all species formed during the titration experiments was identified by slope analysis.

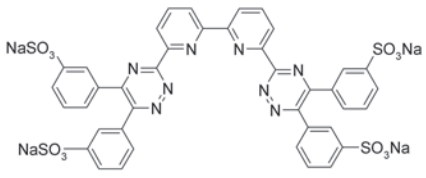

Fig. 4: SO_3-Ph-BTBP.

In any case, the 1:2 complex was identified. Conditional stability constants for the formation of the 1:2 complexes, β_{02}, were derived from the speciation diagrams. The values are compiled in Table 1.

Tab. 1: Conditional stability constants log β_{02} of the $Cm(SO_3\text{-Ph-BTBP})_2$ and $Eu(SO_3\text{-Ph-BTBP})_2$ complexes in the solutions studied.

Solution	log β_{02} Cm(III)	log β_{02} Eu(III)
H_2O (pH = 3)	10.4 ± 0.3	8.4 ± 0.3
0.5 mol/L $HClO_4$	8.5 ± 0.3	
0.5 mol/L $NaClO_4$	9.7 ± 0.2	
0.5 mol/L HNO_3	7.3 ± 0.2	7.3 ± 0.3
0.5 mol/L $NaNO_3$	9.4 ± 0.2	

The decrease by 0.7 log units when going from H_2O to 0.5 mol/L $NaClO_4$ is ascribed to a change of SO_3-Ph-BTBP's activity due to changing ionic strength. The decrease by 1.0 log units when going from H_2O to 0.5 mol/L $NaNO_3$ is explained by a combination of the above influence of ionic strength on SO_3-Ph-BTBP's activity (0.7 log units) plus the effect of nitrate complexation of Cm(III) (0.3 log units). The rather large decrease by 1.9 log units when going from H_2O to 0.5 mol/L $HClO_4$ is explained by a combined effect of increasing ionic strength on SO_3-Ph-BTBP's activity plus an effect of SO_3-Ph-BTBP protonation by the acid. An even larger decrease (3.1 log units) is observed in 0.5 mol/L HNO_3. This is in good agreement with a combination of the $NaNO_3$ effect (decrease by 1.0 log units) and the acid effect (1.9 log units).

This study contributes to a better understanding of the coordination chemistry of water-soluble BTBP molecules and generates thermodynamic stability constants, which can be implemented in calculations for process design.

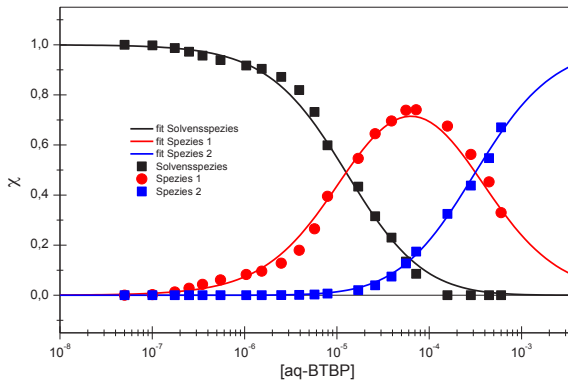

Fig. 5: Complexation of Eu(III) with SO_3-Ph-BTBP in H_2O (pH = 3). Lines calculated with log β_{01} = 4.9 and log β_{02} = 8.4.

References

[1] *Potential Benefits and Impacts of Advanced Nuclear Fuel Cycles with Actinide Partitioning and Transmutation*; NEA No. 6894, OECD, Nuclear Energy Agency (NEA), Paris: 2011.

[2] Renn, O. (ed.), *Partitionierung und Transmutation: Forschung – Entwicklung – gesellschaftliche Implikationen (acatech STUDIE),* Herbert Utz Verlag, München, 2013.

[3] Wilden, A.; Modolo, G.; Schreinemachers, C.; Sadowski, F.; Lange, S.; Sypula, M.; Magnusson, D.; Geist, A.; Lewis, F. W.; Harwood, L. M.; Hudson, M. J., *Solvent Extr. Ion Exch.* **2013,** *31* (5), 519–537.

[4] Wilden, A.; Modolo, G.; Kaufholz, P.; Sadowski, F.; Lange, S.; Sypula, M.; Magnusson, D.; Müllich, U.; Geist, A.; Bosbach, D., *Solvent Extr. Ion Exch.* **2015,** *33* (2), 91–108.

[5] Carrott, M.; Bell, K.; Brown, J.; Geist, A.; Gregson, C.; Hérès, X.; Maher, C.; Malmbeck, R.; Mason, C.; Modolo, G.; Müllich, U.; Sarsfield, M.; Wilden, A.; Taylor, R., *Solvent Extr. Ion Exch.* **2014,** *32* (5), 447–467.

[6] Malmbeck, R.; Carrott, M. J.; Geist, A.; Hérès, X.; Magnusson, D.; Miguirditchian, M.; Modolo, G.; Sorel, C.; Taylor, R. J.; Wilden, A., *Proc. Internat. Solvent Extr. Conf. (ISEC 2014)*, Würzburg, Germany, 7–11 September, 2014; pp 39–44.

[7] Wagner, C.; Müllich, U.; Panak, P. J.; Geist, A., *Sustainable Nuclear Energy Conference*, Manchester, UK, 9–11 April, 2014.

[8] Bourg, S.; Ekberg, C.; Geist, A., *45th Annual Meeting on Nuclear Technology*, Frankfurt, Germany, 6–8 May 2014, 2014.

[9] Geist, A.; Müllich, U.; Magnusson, D.; Kaden, P.; Modolo, G.; Wilden, A.; Zevaco, T., *Solvent Extr. Ion Exch.* **2012,** *30* (5), 433–444.

[10] Geist, A., *Solvent Extr. Ion Exch.* **2010,** *28* (5), 596–607.

[11] Galán, H.; Munzel, D.; Núñez, A.; Müllich, U.; Cobos, J.; Geist, A., *Proc. Internat. Solvent Extr. Conf. (ISEC 2014)*, Würzburg, Germany, 7–11 September, 2014; pp 137–143.

[12] Magnusson, D.; Christiansen, B.; Malmbeck, R.; Glatz, J. P., *Radiochim. Acta* **2009,** *97* (9), 497–50

7. Vitrification of high-level radioactive waste

G. Roth, W. Grünewald, W. Tobie, J. Knobloch, A. Salimi, S. Weisenburger, K.-H. Weiß, B. Böhland, K. Hardock, K. Meyer

7.1 VPC project

The German-Chinese VPC (Vitrification Plant China) project has been established in November 2009 with the objective to construct an HLLW vitrification plant in the Sichuan province of China on the basis of the process technology developed by KIT-INE. From German side the project is executed by an industry consortium (STEAG Energy Services, WAK GmbH, Kraftanlagen Heidelberg GmbH) with KIT-INE as nominated subcontractor responsible for design of the core process technique and key components like the waste glass melter and for input of process-chemical and glass-chemical knowhow and expertise. Besides the design work a main part of the contractual deliveries from the German consortium includes the supply of process equipment like the glass melter, HLLW receipt tank, off-gas treatment components, and canister decontamination system as well as mechanical and remote handling equipment.

The project is divided into three main phases: design (2010-2013), supply (2013/2014) and subsequent technical on-site services. The latter comprehends supervision of installation, function testing, commissioning of the supplied hardware as well as supervision of the performance of the cold and hot test. In 2014 the main part of the project for the German side was accomplished by completion of the hardware delivery as laid down in the contract. For KIT-INE the main task was the completion of the waste glass melter including its accessories.

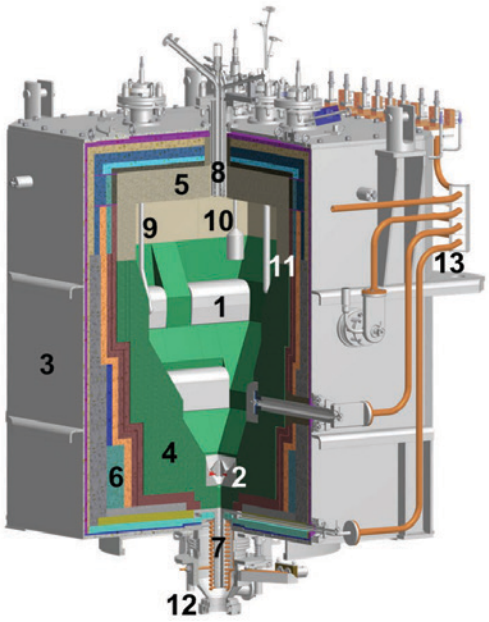

Fig. 1: Main structure of the VPC glass melter. Firmly integrated subcomponents: 1 Power electrodes, 2 bottom electrode, 3 stainless steel containment, 4 melt tank ceramic refractory, 5 melter plenum ceramics, 6 thermal insulation, 7 glass pouring pipe, Remote subcomponents: 8 feed inlet tube, 9 air bubbler, 10 glass level detection system, 11 thermo-well, 12 bottom drain housing, 13 copper tubes for power supply

1. Completion of the Glass Melter

The glass melter is composed of 19 subcomponent groups. As shown in Fig. 1 the melter consists of firmly integrated subcomponents (group 1-6) like melt tank ceramic refractories, plenum ceramics, power electrodes, bottom electrode, stainless steel containment and remotely exchangeable subcomponents (group 7-17) like bottom drain housing, HLLW- and glass frit feeding pipe, off-gas pipe, thermo-well for monitoring process temperatures, glass level detection system, and two air bubblers used for agitating the upper part of the melt and the process zone. The remaining subcomponent groups (18 - 19) are composed of service parts and tools for assembly and transportation of the melter.

The melter assembly started in April 2013 after preparation of the assembling place inside the technical hall in the building B714 of KIT-INE under supervision of KIT personnel. Until February 2014 it was completed under support of SORG company and KIT workshop.

Until mid of 2014 also the manufacturing of the remote exchangeable components including the spare parts was finalized. These components had to be shipped together with the melter and an accompanying documentation as described below.

In May the Factory Acceptance Test (FAT) for the melter was performed at INE under participation of a group of Chinese experts. This FAT mainly included the check of the remote equipment (see Fig. 2). The FAT was the precondition for accepting the shipment of the melter to China.

For shipment to China the melters interior had been completely stuffed with rigid foam material to avoid any damage of the melt tank. Additionally it has been encased in a special shock-safe containment to minimize the risk of damage during transportation. Transportation of the melter and its subcomponents to China via Hamburg and Shanghai was started by end of July 2014. Fig. 3 shows the first step of its travel after taking the melter out of the technical hall at INE by means of an air cushion technique. The total transportation distance until final destination in Guang Yuan in the Sichuan province covers about 24000 km. The melter together with the associated equipment arrived at the site of Guang Yuan on September 15. An out-

Fig. 2: Performance of the FAT. Adjustment of the feed inlet tube (see Fig. 1, position 8)

Fig. 3: VPC melter taken out of the technical hall of KIT-INE for transport to China

side check of the package after unloading in Shanghai did not reveal any damage. Also no unacceptable acceleration was recorded underway.

2. Documentation for on-site services

Besides design/planning work and supply of hardware the VPC contract also includes the creation of documents necessary for the performance of the Technical On-site Services. These documents divided into component-related descriptions and system-related descriptions include manuals for installation, functional testing, commissioning, and operation.

Equipment-related manuals

For each single process component being part of the German delivery list a description of the following items was prepared and sent to China as part of the shipment:

- Equipment installation plan & description
- Equipment functional test program incl. instructions for commissioning & function tests
- Equipment start-up manual
- Equipment operating manual
- Equipment maintenance manual

The documentation created by KIT-INE covered the core equipment of the HLLW receipt area, the glass melting area and the first part of the wet off-gas cleaning area.

Process Functional descriptions

Additional to these documents KIT-INE elaborated the Process Functional Descriptions for the core process systems HLLW reception (system 841), the glass melting system (842) and the first part of the wet off-gas treatment system (848) placed inside the melter cell V2. These documents describe among others the tasks of the system, of the respective process components and their specific task. They also include also the signal exchange between the Process Control System 876 of VPC and the respective local control cabinets. The preconditions for operation, the performance of operation, and automatic control loops are described (e.g. the automatic Feeding Vessel Cycle Sequence Chain for melter feeding). Also the various switch points of process equipment, potential process control failures and process technical failures as well as limit value exceedings are treated.

Detailed Process Functional Descriptions of core process systems provide a complete help to understand in detail the conversion of the VPC into a functional facility. The Process Functional Descriptions are indispensable for a detailed understanding of the function of the core process equipment of VPC, and also for a safe and reliable planning and performance of functional tests of the core process systems.

Operation Manuals

A further set of documentation prepared by KIT-INE for the core process systems 841, 842 and partly 848 dealt with the operation manuals for vitrification operation. Operation manuals for the core process systems represent the mandatory standard for performing cold and hot operation and for putting the VPC facility from idling to the operation mode and vice versa. They contain in detail all measures, procedures and instructions for reliable operation and for keeping the VPC facility in safe conditions. They also assure that the canisterized waste glass produced is in accordance with the predefined specification.

7.2 Immobilization of high active solid waste residues

At the end of the VEK vitrification operation with stored high-level waste solution (HAWC-WAK) a rinsing procedure was performed to reduce the remaining radioactive residuals in the process components of the VEK plant as far as feasible to ease the later D&D work. After vitrification of the bulk of the rinsing solution approximately 3000 liters of highly technetium and cesium containing rinsing solution were left which then were evenly distributed into two tanks placed in the inaccessible HLLW receipt cell V1. Prior to this transfer a sample had been taken from the rinsing solution for chemical analysis. The liquid in the two tanks subsequently underwent a drying process caused by radioactive decay heat and lasting about 1.5 years.

Basic considerations

Precondition of the further D&D work on VEK is the removal and treatment of the remaining high-active waste residues contained in process components of the V1 and V2 cell. Special attention has to be paid to the dried residues remaining from rinsing vitrification operation due the relatively high specific activity and the presence of volatile species (Cs, Tc). Conditioning processes to immobilize such materials are usually accompanied with elevated temperatures, e.g. of about 1150°C in case of vitrification. In this temperature range the loss of the volatile species from the matrix is practically complete.

Fig. 4 shows the result of a thermogravimetry measurement of a sample representing the simulated high-active solid residue using Re as surrogate for the radioactive Tc. It shows that at about 1000°C a portion of about 30% became volatile. Additionally the graph contains the curves for the species $NaNO_3$, $CsReO_4$ and $NaReO_4$, which can be expected to be mainly formed in the residue due to the thermodynamic data.

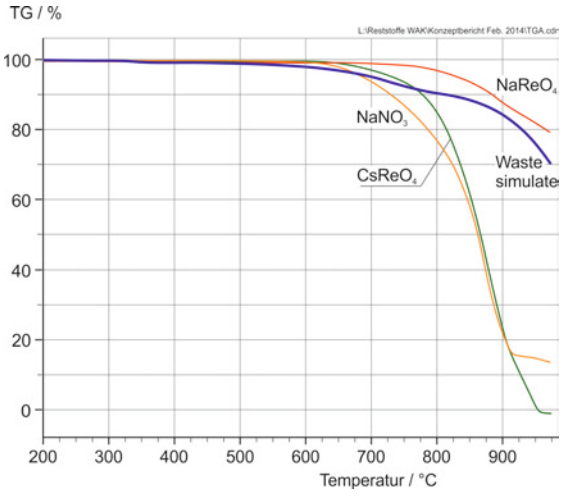

Fig. 4: Results of a thermogravimetry measurement comparing the temperature-dependent material loss of a simulated solid waste residue with that of $NaNO_3$, $CsReO_4$ and $NaReO_4$

As expected the volatilization of $CsReO_4$ dominates the material loss observed in the simulated waste sample.

The general strategy to immobilize these problematic residues was based on the following main requirements:

- Conditioning by vitrification process
- Use of an In-can melting technique
- Application of a low-temperature melting-glass

The basic process steps are illustrated in Fig. 5. The melting process is performed at moderate melting temperatures of 950°C using a barium-borosilicate glass. The melting pot is heated externally until the glass is molten. The released hot gases are routed to the dry off-gas treatment system via a second melting pot containing a cold trap (glass forming materials) to condense the volatile constituents. After filling, the first pot is moved to the Canister treatment area. The second one then is placed in the melting position and another pot is placed in the second position. Fig. 6 shows a scheme of the In-can melting technique taken into account for vitrification of high-active solid residues.

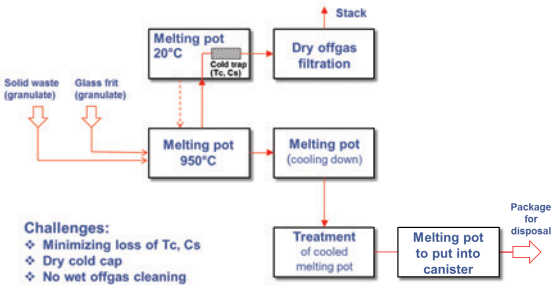

Fig. 5: Basic process to immobilize the high-active solid waste residuals

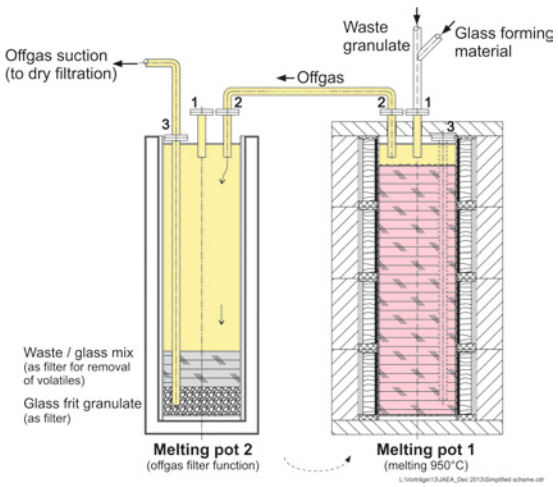

Fig. 6: Scheme of an In-can melting technique for vitrification of high-active solid residues

Drying Experiment

In respect of the later dismantling of the tanks information of the material characteristics would be helpful for the accompanying recovery of the dried high-active residues. Apart from removal aspects these characteristics are also of importance for a later conditioning step of these materials. For this purpose an experimental work was performed to simulate the drying process in a lab experiment in order to collect data about chemical composition, type and amount of different phases, solid properties and remobilization features. As basis for composing the chemical simulant the analytical result of the sample taken on March 14, 2011 before start of the drying process, was used. In the simulated solution nearly all elements were added as nitrates. Rhenium, which served as surrogate for technetium due to its similar chemical properties was added as metal. In the experiment 4.85 dm³ of simulant were dried in a stainless steel pot at temperatures of 46 - 49°C by means of a sand bed heating placed in a flue. In correspondence to the situation in the VEK tanks the surface to volume ratio of the simulated liquid at start of the experiment was adjusted to 0.64 dm²/dm³.

During the drying process samples were taken from the liquid and analyzed by use of ICP-OES and AAS. Investigations of the dried residue were carried out by means of Raman-spectroscopy, SEM-EDX, XRD und Infrared Spectroscopy. Additionally element analysis was performed by using ICP-OES und AAS.

The drying process of the simulated solution under the conditions described above lasted 8 - 9 days. During this period 1 ml samples were taken and analyzed by ICP-OES und AAS. In the course of the drying process the concentration of the most important elements Cs, Re, Na und Fe in the simulated solution at a remaining volume of only 0.34 dm³ (concentration factor of 15) were increased in the following proportions:

Tab. 1: Increase of element concentration in the remaining liquid volume

Element	Initial Concentration [g/dm³]	Concentration at 0,34 dm³ [g/dm³]	Concentration factor
Cs	3.49	57.7	16.5
Re	7.84	146.3	18.7
Na	1.27	15.4	12.1
Fe	1.67	37.7	22.6

At these relatively high concentrations only minor amounts of precipitating materials could be observed. Towards the very end of the drying process the volume had been reduced from 4.85 dm³ to approx. 0.23 dm³ (concentration factor of 21). The density accordingly increased from 1.1 to 1.67 g/dm³ while the HNO_3 molarity increased from 2.74 to over 12 mol/dm³. At this stage the extent of precipitation increased strongly. Figure 7 shows a photo of the late precipitation phase.

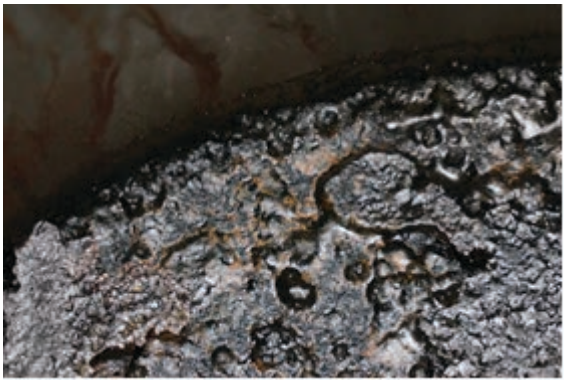

Fig. 7: Photo of the late precipitation phase of the drying process

From the drying data it can be concluded that redissolving of the dried material in each of the two the VEK tanks seems to be possible with only approx. 120-130 dm³ of HNO_3. Such a remobilization could be helpful for a subsequent conditioning process.

The dried residue consisted of three main layers:

- top layer, characterized by dark brown crusts with a bitumen-like sublayer
- intermediate single layer of bitumen-like nature with incorporated crystals
- two-layer area with a bitumen-like black upper layer of nearly liquid consistency and below a thin and very hard layer with green-colored crystals at the bottom of the stainless steel pot.

In total 20 samples from different areas of the dried residue were taken and analyzed. By means of XRD, Raman Spectroscopy, SEM-EDX und ICP-OES and AAS it could be shown that the dried residue is dominated by CsReO4 und $NaNO_3$. Cs is practically completely bonded to Re as cesium perrhenate. The remaining portion of Re not bonded as $CsReO_4$ is most probably present as iron perrhenate in the dried layer. In contrast to the expectation based on the solubility data no sodium perrhenate could be identified. Also not found was the cesium nitrate $CsNO_3$ as cesium is completely bonded to rhenium in form of $CsReO_4$.

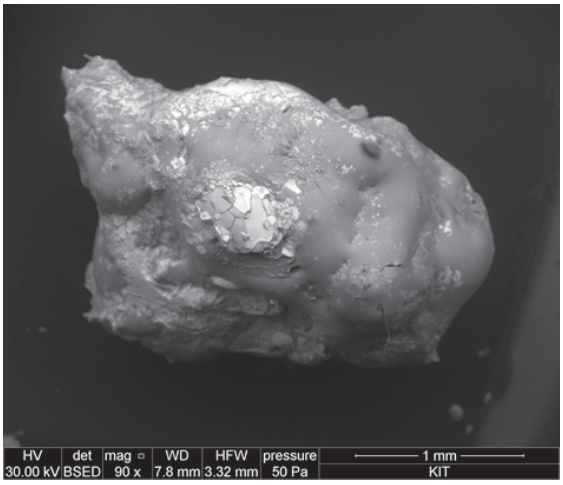

Fig. 8: Crystalline material found in the bitumen-like areas of the dried layer

The remaining metals (Ba, Cr, La, Mn, Ni) contained in the simulated solution formed nitrates in correspondence to sodium. In the bitumen-like areas of the dried layer relatively large crystalline particles of 1-3 mm size were identified (see Fig. 8). Based on SEM-EDX analysis these were found to be nitrate and perrhenate salts with $NaNO_3$ and $CsReO_4$, respectively, as main constituents. Also other elements like Fe were partly contained. The first crystals appearing during drying of the solution after about 5 days of drying time at the wall of the drying pot were identified to be barium nitrate $Ba(NO_3)_2$ by means of measurements based on infrared-spectroscopy.

All of the various nitrates of Fe, Cr, Mn und Ni contained in the dried residue exhibit low melting points - ($Fe(NO_3)3 \cdot 9H_2O$: 47°C, $Cr(NO_3)_3 \cdot 9H_2O$: 60°C, $Mn(NO_3)_2 \cdot 4H_2O$: 37°C, $Ni(NO_3)_2 \cdot 6H_2O$: 56°C. These low melting temperatures and the applied drying temperatures of 46 - 49°C probably contribute to the existence of bitumen-like, paste-like constituents.

The dried residue proved to be very hygroscopic. After one day of remaining unheated it changed from solid to a liquid material. This property has to be considered in respect of the later removal from the tanks and the subsequent conditioning step.

7.3 Shutdown of the PVA melter

In July 2014 the nonradioactive PVA test facility including the glass melter had been shut down after a long period of operation. The melter had firstly been heated up in April 1998 and had been continuously under temperature since that time. Within several alternating periods of idling and vitrification operation with HLLW simulate solution of different compositions the melter material had been exposed to severe long-term corrosion and erosion attacks by the borosilicate glass melt. Until final emptying in July 2014, the melter had been heated for more than 16 years in total. Within a total processing time of 5200 hours, almost 50 m^3 of HLLW simulate solution had been converted into about 35 metric tons of glass. Table 2 gives a complete survey of the essential life data of the melter.

Tab. 2: Total operational data of the PVA melter

Parameter	Data
Total operation time	1998 - 2014
Time of processing	5200 h
Vitrified HLLW simulate	49300 dm^3
Glass production	34900 kg
Number of canisters (400 kg)	87
Number of glass pourings	351

Major objectives of the shutdown were:
(1) Preparation for later remote dismantling, (2) inspection of the melter interior and (3) analysis of glass samples from pouring stream and from glass residuals in the melt tank after emptying

From emptying the melter after such a long operation period valuable information could be expected in respect of condition of the melt tank and the electrode material as well. The findings could be applied as basis for improvement of melter design and operation mode. Also important information was anticipated concerning the start of the glass pouring after an idling interval of 67 months since the last vitrification campaign. In case of such a long period of maintaining idling conditions (glass pool temperature approx. 950°C), an increased crystallization tendency could be expected in those areas of the glass-pouring channel, where the maximum crystal growth temperature dominated. Severe crystallization could be problematic for initiating the glass pouring.

Fig. 9: Glass pouring operation to empty the PVA test melter after 6 years of idling conditions

Fig. 10: View of the melters interior after emptying showing the lower part of the melt tank with the auxiliary electrodes

First results

The emptying operation had been intended to be completed in a continuous pouring in one batch allowing maximum glass flow rate. Following a moderate heating procedure from idling temperature to pouring conditions (glass pool temperature 1150°C), the routine operation of the glass pouring system (bottom drain) had been executed. After a comparatively short time of only 4 hours the glass flow started successfully (see Fig. 9) ending with complete discharge of the glass inventory. The heating time during regular pouring usually required about 1.5 - 2 hours. Therefore there is no indication for an increased crystallization. For further information several samples were taken from the pouring stream as well as from the melt tank glass for later analysis. First previous inspection of the melters interior after emptying indicated an intact structure of the ceramic refractory and also of the appearance of the electrodes. An example can be seen in Fig. 10 showing an image of one of the auxiliary electrodes (made of Inconel 690©) placed in the lower sloped part of the glass tank near the exit channel. The shape of the electrode appeared to not have suffered from the extensive exposure to the glass melt. Similar findings are expected for the main electrodes.

Further steps

After shutdown the melter will be subject to dismantling as a test procedure to be later applied to the radioactive VEK melter. Dismantling will take place remotely in the 1:1 scaled PVA melter cell. During disassembling inspection of the status of the materials will be documented.

Acknowledgement

The work described in chapters 8.2 and 8.3 was performed under contract with WAK GmbH.

8 Decommissioning of nuclear facilities

The process of decommissioning a nuclear facility is the last step in closing the lifecycle of a nuclear power plant. Due to political, economic and technological issues, this activity has been significantly increased worldwide, creating opportunities for highly skilled workers. By establishing an overall understanding of this complex and tedious process, the issue of addressing the education of adequate personnel is of upmost importance. The Karlsruhe Institute of Technology (KIT) provides the competences required for the decommissioning of nuclear facilities and can thus adequately face the educational necessities demanded by the industry.

M. Brandauer, S. Gentes[a]

[a] Department of Deconstruction and Decommissioning of Conventional and Nuclear Buildings, Institute for Technology and Management in Construction (TMB), Karlsruhe Institute of Technology (KIT)

Introduction

As part of the German energy transition program, the decision to completely phase-out of nuclear power generation was made abruptly in 2011, after the incident in Fukushima. As a consequence, eight operating facilities were immediately shutdown by law. These facilities were undergoing life-extension procedures at that time and were at no point concerned with decommissioning yet. This circumstance resulted in a very long transition phase that is still ongoing to date. The remaining nine facilities still in operation will now subsequently be shut down in the coming years, while a complete phase-out and final shutdown of all facilities is mandatory by the end of 2022. The final phase-out of nuclear power will, however, only be possible after the complete decommissioning of all remaining facilities.

As a result of the current situation and due to the operator's decision of opting for a direct decommissioning strategy, many large-scale facilities will be decommissioned simultaneously in Germany in the coming decades; which is going to be a significant challenge. The subject of decommissioning is, however, not a new topic in Germany. There is a substantial amount of facilities, which are already in an advanced decommissioning state. To date, three facilities have also been completely decommissioned and returned to the so-called "green-field" state, i.e. the complete demolishing of the facility and reforestation of the former site.

For this reason, decommissioning of nuclear facilities has already proven to be feasible. Nevertheless, many problems have occurred over the past decades and many lessons had to be learned. Furthermore, most of the applied techniques are still rudimentary and usually taken from other application fields, without adapting them for the new tasks. However, with the new field of research and education for the decommissioning of nuclear facilities at KIT these technical problems are addressed, advancing the development of new technologies and contributing to the education of new professionals for the upcoming challenge.

Teaching approach

Within the German excellence initiative a new professorship for the Deconstruction and Decommissioning of Conventional and Nuclear Buildings has been established in June 2008 at the KIT. It has been attributed to the Institute for Technology and Management in Construction (TMB). This professorship is one of a kind in Germany, addressing exclusively the technologies and management methods in the decommissioning of conventional and more specifically of nuclear facilities. It is headed by Prof. Dr.-Ing. Sascha Gentes and pursues the following objectives:

- setup of a scientific and technical team of experts for the decommissioning of nuclear facilities
- development of new decommissioning technologies and realization of pilot projects
- establishing a field of study for subject matter

This professorship now provides KIT's new lecture course of decommissioning of nuclear facilities opening a new field of study to students of civil engineering, mechanical engineering, and industrial engineering as well as all other interested students. The lectures give an overall introduction to decommissioning, from the shutdown of a nuclear facility, licensing application, the transition from operation to decommissioning, required technologies and stakeholders involved. This is enhanced by the institute's close cooperation with all kind of industrial partners involved in the decommissioning of nuclear facilities. Therefore, industrial guest lecturers provide practical examples of ongoing decommissioning sites. Particularly, topics like decontamination, dismantling, management methods, waste management and also the development of new technologies are given priority.

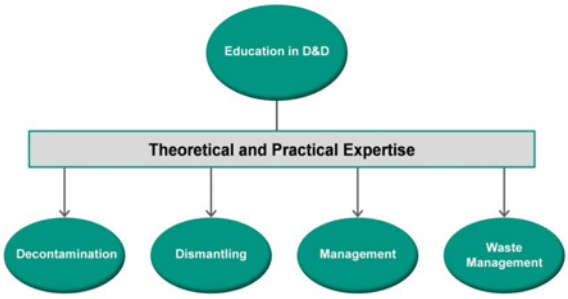

Fig. 1: KIT's decommissioning teaching structure.

Students profit from the connection between science and practical engineering providing them with up-to-date experiences of current decommissioning and dismantling projects and knowledge transfer. This concept also provides career opportunities through internships or support of bachelor and master thesis. Moreover, the institute's own technologies and current research projects for the development of new and improved decommissioning tools are an integral part of the lectures. The lecture is structured as follows:

- Fundamentals of NPPs and the current situation of Nuclear Energy in Germany
- Radiation, Radiological Protection, and Measurement Techniques
- Approval Process and Planning
- Decommissioning Principles of NPPs and Management Concepts
- Current Research and Development Projects
- Examples of current D&D Projects in Germany
- Demolition and Disassembling Techniques
- Decontamination and Surface Treatment Techniques
- Waste Management
- Major Reactor Incidents and Decommissioning approaches (e.g. Tschernobyl, Fukushima)
- Excursions to different NPPs in operation and in the decommissioning process

With this kind of lecture the students benefit from a special training unique in this form in Germany. In addition, a further course is offered at the AREVA Nuclear Professional School at the KIT. It is addressed to professionals who would like to expand their knowledge. This five-day course is an annual event. Further contribution of the professorship is the supervision of ten PhD students involved in current research projects.

Due to the high importance of this professorship it is now additionally being financed within the scope of the third program-oriented funding period lasting from 2015 to 2019 provided by the Helmholtz Association. The subject of decommissioning nuclear facilities has been aggregated to the research field "Nuclear Waste Management and Safety as well as Radiation Research". For this reason, the professorship has already been incorporated in July 2014 into the second program-oriented funding in order to allow for the preparation and integration of this subject into the upcoming research period.

Conclusion

The effort of teaching new generations of professionals for the decommissioning of nuclear facilities is an important contribution to tackle Germany's "Energiewende" and the upcoming decommissioning challenge. Both industrial and scientific insight of the subject is essential to students in order to grow into the qualified personnel that are highly required by the industry. Only then the successful decommissioning of all nuclear facilities in Germany will be achievable. Moreover, the acquired know-how, the development of adequate techniques, and the establishment of a research field of decommissioning technologies and management methods will be of crucial importance for the upcoming task of decommissioning hundreds of other nuclear facilities not only in Europe, but all around the globe. It is only with these efforts that the life cycle of nuclear power plants can finally be completed and a restoration of former sites into a safe environment for future generations will be possible.

9 Development of radionuclide speciation methods

Maintaining a state-of-the-art portfolio of advanced surface science and spectroscopy methods at INE is an important R&D activity, as these methods are crucial tools for understanding and advancing actinide and radionuclide (geo)chemistry. Radionuclide speciation methods available at INE controlled area laboratories, the KIT synchrotron source ANKA or external facilities are continuously adapted to serve the requirements of the INE in house R&D program. Access to INE facilities is also provided to the radiochemistry and nuclear science community, either through EU funded transnational access initiatives, or through direct cooperation with KIT-INE. Due to necessary reorganization following changes in the scientific and technical staff, the long-standing R&D activities in the field of laser based speciation methods at INE were primarily dedicated in 2014 to initiate necessary instrumental improvements and future system upgrades - with a focus on new instrumentation for TRLFS and LIBD investigations. In addition, the potential of remotely operated LIBS for studies of highly radioactive materials without direct or limited sample access was evaluated, e.g., for the analysis of specimen in shielded boxes or compartments of decommissioned nuclear facilities. Following initial studies of an original HLW glass fragment obtained from the WAK/VEK vitrification process, the investigation of HAW materials at the INE-Beamline was extended in 2014 to include spent nuclear fuel (SNF) particles. A major breakthrough was achieved at the beamline by the successful installation of a sealed He environment enclosing the entire beam path of the HRXES spectrometer. HR-XANES/XES measurements at the actinide $M_{5,4}$ absorption edges are now routinely possible with high efficiency and reasonable sampling time. By combining several TEM based techniques, INE researchers demonstrated in 2014 that the identification of the chemical composition and structure single actinide colloids precipitated on the surface of magnetite particles is possible with sub-nm spatial resolution. In 2014 the portfolio of methods accessible to INE researchers was extended by Accelerator Mass Spectrometry (AMS). AMS is presently one of the most sensitive analytical techniques with the possibility to perform isotope specific measurements with concentrations below ppq levels - particularly advantageous for the analysis of environmental samples which might be affected by nuclear contaminations, e.g., from the global fallout, or in the frame of field experiments employing actinide tracers. Many of the in house research activities at INE benefit from strong support by quantum chemical calculations, providing molecular structures or thermodynamic data. The systems under investigation vary from small complexes in solution to crystals or interfaces. New algorithms and the constantly improving hardware allow getting closer to a detailed description of radionuclide systems at the level of electronic structure, thus complementing spectroscopic results.

9.1. R&D projects conducted at the INE-Beamline for radionuclide research at ANKA and at external SR sources

M. Altmaier, S. Bahl, E. Bohnert, K. Dardenne, D. Fellhauer, A. Gensch, E. González-Robles, B. Kienzler, V. Krepper, V. Metz, I. Pidchenko, T. Prüßmann, J. Rothe, M. Vespa, T. Vitova

Introduction

Synchrotron radiation (SR) based speciation techniques have become key methods in actinide and radionuclide research. This development is primarily driven by the need to secure molecular-scale understanding for (geo-)chemical processes determining mobilization or immobilization of long-lived radionuclides in projected repositories for highly active, heat producing nuclear waste (HAW). Presently, final disposal in deep bedrock repositories is considered as the preferred option for the management of spent nuclear fuel (SNF) and high level waste (HLW) glass used to immobilize highly radioactive residues from nuclear fuel reprocessing. The release of actinides, fission and activation products following corrosive HAW degradation depends mainly on the oxidation state and bonding characteristics of the radionuclides in the individual waste matrices. Solving the nuclear disposal safety case requires the assessment of an envisaged disposal site on geological time scales, where speciation techniques like XAS (X-ray Absorption Spectroscopy) provide necessary input parameters for modeling geochemical reaction and transport paths for radionuclides. The INE-Beamline for radionuclide science [1] at the KIT synchrotron facility ANKA [2] is operated by KIT-INE since 2005 as a flexible experimental station for spectroscopic investigation of radioactive sample systems. The INE-Beamline is the only facility of its kind in Europe offering access to radiochemistry laboratories operating a shielded box-line in close proximity to the SR experimental station. INE's beamline scientists support *in house* and external users in planning, performing and evaluating experiments, including clearance of all relevant radiation safety and personal security issues. INE scientists also conduct various experiments at external SR sources offering capabilities not - or not yet - available at KIT.

INE-Beamline user operation in 2014

In 2014 a total of 33 *in house* and external projects were hosted at the INE-Beamline. The time available for INE internal research amounted to ~26% of all available shifts (33 days). Three days were spent for maintenance and development, 24 days were lost due to a major beamline component failure. As in the previous years, the majority of beamtime shifts in

2014 was given to external projects with (34 days) and without (24 days) PRC (ANKA Peer Review Committee) evaluation (i.e., through direct cooperation). INE projects at the beamline covered a broad X-ray spectroscopy program for characterization of radionuclide materials - with an emphasis on actinide $M_{4,5}$ edge studies applying advanced high resolution (HR) XANES techniques for speciation studies. Some of these studies are presented in more detail elsewhere in this annual report or in the recent ANKA User Report. INE *in house* projects in 2014 included various investigations of radionuclide materials or systems containing actinides, fission products and their chemical homologues, e.g., Gd / Yb-doped $NaNO_3$, Eu-transferrin complexation, Eu(III) incorporation in trihydroxides and oxyhydroxides, speciation of Nd(III) in high saline solutions, µ-focus XAFS studies of U-doped cement samples from long-term corrosion experiments in the Asse salt mine, speciation of Am(III)/illite sorption under Boom clay conditions, complexation of Np(V) with chloride at elevated temperatures and the lanthanide / actinide retention by iron (hydr)oxide phases. Investigations of HAW samples at the INE-Beamline started in 2013 with an actual HLW glass fragment obtained from VEK operation have been extended in 2014 to include genuine SNF particles.

General user research projects receive beamtime at INE-Beamline following PRC evaluation (biannually in January and June), as approved TALISMAN Joint Research Projects (both together comprising at least 30% of all available shifts) or through direct cooperation with KIT-INE. In 2014 scientists from the 15 German and international research institutions listed below conducted experiments at the beamline:

- KIT Institute for Photon Science and Synchrotron Radiation, Karlsruhe, Germany
- CEA Marcoule, France
- Ruprecht-Karls-Universität, Heidelberg, Germany
- JRC-ITU, European Commission, Karlsruhe, Germany
- CEA Saclay, France
- University of Manchester, Manchester, United Kingdom
- CEA Cadarache, France
- FZJ-IEK6, Jülich, Germany
- EPFL, Lausanne, Switzerland
- Niederrhein University of Applied Sciences, Krefeld, Germany
- University of Helsinki, Helsinki, Finland
- KIT Institute of Applied Geosciences, Karlsruhe, Germany
- National Nuclear Laboratory, Sellafield, United Kingdom
- KAIST - Korean Advanced Institute for Science and Technology, South Korea
- PSI-LES, Villigen, Switzerland

Five projects in 2014 received beamtime and were funded through the EU project TALISMAN as Joint Research Projects (JRP).

As in the previous years, a significant percentage of *in house* and PRC beamtime was used by Master and PhD students to perform experiments in the framework of their theses (more than one third of all beamtime shifts).

Round Robin Test on actinide speciation techniques

An inter-laboratory Round Robin Test (RRT) was initiated by HZDR, Institute for Resource Ecology, preceding the 2nd International Workshop on Advanced Techniques in Actinide Spectroscopy (ATAS 2014) held in November 2014 at Dresden-Rossendorf. The main goal of the RRT was the comprehensive molecular analysis of an aqueous complexing system – U(VI)-acetate (pH 1, 2, 2.5, 3.5), which was selected to be independently investigated by different spectroscopic and quantum chemical methods applied by leading laboratories in actinide or geochemical research. The RRT was subdivided into six methodical clusters encompassing XAFS spectroscopy led by INE. A first comparison of results obtained by INE (ANKA), ROBL (ESRF) and MARS (SOLEIL) beamline teams showed that the consistency of the raw data recorded at three different SR sources, beamlines and XAFS experimental stations is fully given. Molecular structures known from literature were better reproduced than within the typical EXAFS error margins.

First investigations of genuine SNF particles

Following initial radionuclide speciation studies in 2013 for an original HLW glass fragment obtained from the VEK vitrification process [3], the investigation of HAW materials was extended in 2014 to include SNF particles sampled from a fuel rod segment irradiated at the Gösgen pressurized water reactor (Switzerland) with a burn-up of ~50.4 GWd/(t HM). Determination of the oxidation states of the actinide elements U, Pu and Am was readily possible, the concentration of Cm and Np was too low for recording reliable XAFS spectra in reasonable time. The fission product Mo was detected to be present in metallic

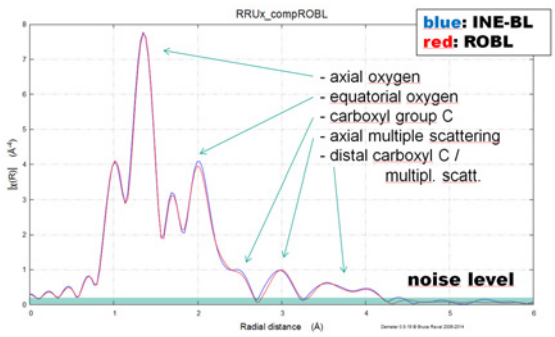

Fig. 1: Comparison of U K-EXAFS (Fourier transformation magnitude) spectra (U(VI)-acetate system, pH 3.5) recorded at the ANKA INE (blue) and the ESRF ROBL beamlines (red). The noise level is shaded in green.

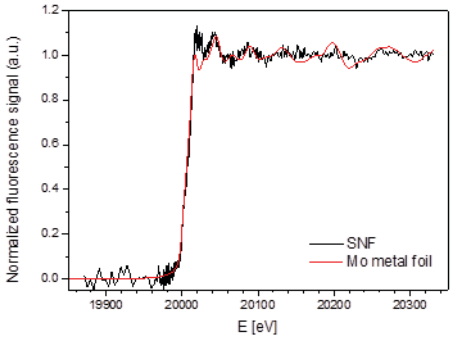

Fig. 2: Mo K-XANES spectrum obtained from a SNF particle compared to the reference spectrum of a Mo metal foil.

state, most probably incorporated in ε-phases (Fig. 2). For both types of HAW samples (HLW glass and SNF) so far no fluorescence signal of iodine, a fission product of major concern due to is assumed mobility and high radiotoxicity, was unambiguously detected. Compared to waste glass (low-Z matrix), the investigation of SNF particles is significantly hampered by the strong (re)absorption of the low-Z element emission lines by the UO_2 matrix. A new imprint technique has been meanwhile developed and successfully tested which will overcome this problem in future investigations.

Installation of the new CAT-ACT beamline at ANKA

Fig. 3: top – CAT-ACT wiggler source at its final position inside the ANKA storage ring; bottom – ACT experimental hutch during construction.

The CAT-ACT beamline at the KIT SR source ANKA is currently constructed and will be operated in a joint effort by ANKA, KIT-ITCP / IKFT and KIT-INE / JRC-ITU for research in the fields of CATalysis and ACTinide science. After installation of the control cabin in December 2013 the wiggler source, the front end and the radiation protection and experimental hutches were installed in the 2014 summer shutdown. The wiggler, a superconducting device manufactured by BINP-Novosibirsk, Russia, with 18 full periods at a period length of 48 mm, a maximum field of 2.5 T and a vacuum gap of 15 mm, was successfully tested inside the ANKA electron storage ring. Installation of the beamline optics, designed and manufactured by FMB Oxford, GB, will be finished in spring 2015. Regular operation of this new high flux / high-energy spectroscopy beamline is planned to start in 2016 and will augment the X-ray spectroscopy capabilities at ANKA, which are currently under very high demand.

U and Pu electronic structure investigations of model systems

The physics and chemistry of uranium and plutonium play a central role in the context of the safety assessment of a nuclear waste repository or envisaged processes to reduce the radiotoxicity of spent nuclear fuel. Detailed knowledge on U and Pu oxidation states and electronic structures is necessary to predict the chemical reactivity of these elements, which in turn determines U and Pu mobilization / immobilization behavior in the environment, e.g., in case of water intrusion in a deep geological repository.

The uranyl moiety UO_2^{2+} is highly symmetric. The linear dioxo cation structure has unusually short, strongly covalent bondings to two axial O atoms (U-Oax). The axial nature of the uranyl ion generally leads to an anisotropic character and a strong polarization dependency of the X-ray absorption spectroscopy signal of oriented uranyl systems, especially single crystals. Dicesium uranyl tetrachloride ($Cs_2UO_2Cl_4$) has been a model compound for experimental and theoretical studies of the electronic structure of the

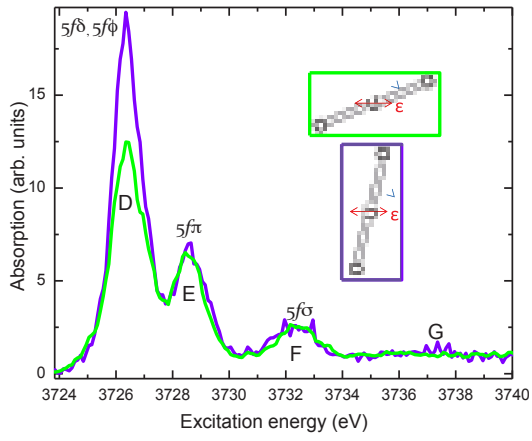

Fig. 4: U M_4-edge PD-HR-XANES spectra for two angles between the uranyl moiety UO_2^{2+} and the polarization vector ε of the incident X-ray beam.

uranyl ion for decades. Angle-resolved electronic structure information for an oriented $Cs_2UO_2Cl_4$ crystal was recently obtained with remarkable energy resolution by polarization dependent high-energy resolution M_4-edge X-ray absorption near edge structure (PD-HR-XANES). The relative energies of U 5*f*δ, 5*f*ϕ, 5*f*π, and 5*f*σ orbitals were determined and compared to predictions from Amsterdam Density Functional (ADF) theory [4].

The U M_4-edge PD-HR-XANES spectra measured for angles $\alpha = \alpha_1 + 5°$ ($0° \leq \alpha_1 \leq 45°$) and $\alpha + 40°$ orientation of the uranyl moiety with respect to the polarization vector ε of the incident X-ray beam are shown in Fig. 4. The M_4-edge ($3d_{3/2}$) electronic transitions probe unoccupied orbitals with predominant U 5*f* character. Note that the absorption resonance marked E is not resolved in the conventional U M_4-edge XANES spectrum. Previously performed DFT calculations [5] suggest that the intense first peak D describes transitions to U 5*f*δ and 5*f*ϕ orbitals. Peaks E and F are shifted by 2.2 eV ± 0.1 eV and 6 eV ± 0.1 eV to higher energy relative to peak D and probe U 5*f*π and 5*f*σ orbitals, respectively. It was estimated from optical spectroscopy data that 5*f*δ and 5*f*ϕ states should be separated by about 0.3 eV [6]. As only ~0.9 eV energy resolution is achieved in our experimental data, the splitting is manifested by an asymmetric shape of the D peak in the U M_4-edge PD-HR-XANES $\alpha = \alpha_1 + 5°$ ($0° \leq \alpha_1 \leq 45°$) spectrum. The 5*f*π orbital should be shifted by about 2.2 eV from 5*f*δ and 5*f*ϕ [6], well in agreement with our experimental observations. O K-edge XANES results report about 2.7 eV energy difference between the U 5*f*σ and 5*f*π orbitals [5], whereas ~3.8 eV is observed in the present study. The discrepancy of about 1 eV might be attributed to a different screening of the O 1*s* core-hole in the O K-edge XANES compared to the U $3d_{3/2}$ core-hole in the U M_4-edge PD-HR-XANES.

Polarization dependency is manifested mainly by a decrease in the area of the first intense absorption resonance D in case of $\alpha = \alpha_1 + 5°$ ($0° \leq \alpha_1 \leq 45°$) compared to the $\alpha + 40°$ geometry (see Fig. 4). The energy positions of the D, E and F features are not observed to be a function of ε within the sensitivity of the measurements. No significant variations of peak area for resonant features E and F are detected, as α changes only by 40°.

Literature based initial assignments of the U M_4-edge PD-HR-XANES absorption resonances are confirmed by ADF calculations [4]. ADF calculations with a $3d_{3/2}$ core-hole give a very similar pattern of energy levels for excitation to 5*f*, 6*d* and continuum final states. Peak D in the U M_4-edge PD-HR-XANES spectrum for the $\alpha = \alpha_1 + 5°$ ($0 \leq \alpha_1 \leq 45°$) geometry exhibits asymmetry, evidence for transitions to non-degenerate 5*f*δ and 5*f*ϕ orbitals with about 0.6 eV energy separation. The ground state calculation with and without spin-orbit interaction yields about 0.8 and 0.1 eV energy separation between 5*f*δ and 5*f*ϕ orbitals, respectively, essentially unaffected by the presence of the $3d_{3/2}$ core-hole. Our experimental and theoretical results suggest that spin-orbit interaction is required to reproduce the experimentally observed energy difference.

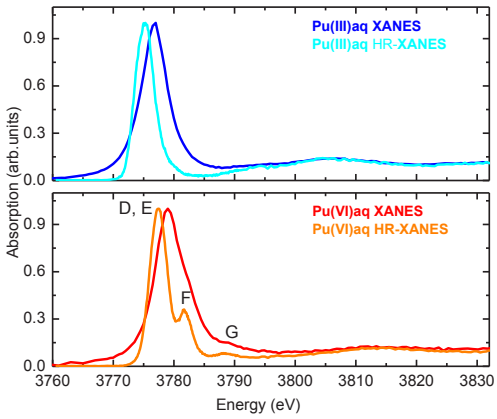

Fig. 5: Pu M_5-edge XANES and HR-XANES spectra of Pu(III) (top) and Pu(VI) (bottom) in perchloric acid.

For the first time ever aqueous plutonium species have been analyzed at the INE-Beamline applying the HR-XANES technique at the Pu M_5-edge. The Pu M_5-edge HR-XANES spectra obtained for Pu(III) and Pu(VI) species ([Pu] = 50 mM in perchloric acid solution) are plotted in Fig. 5 in comparison to conventional M_5-edge XANES spectra recorded in total fluorescence yield detection mode. The spectra exhibit narrower transition features compared to the conventional measurements due to smaller contribution of core-hole lifetime broadening effects. The main absorption peak of the Pu(VI) HR-XANES spectrum is shifted by ~2.2 eV to higher energy compared to the spectrum of Pu(III). This spectrum also exhibits additional structures not observed in the conventional measurement. Pu(VI) is bound to two axial O atoms (Pu-Oax) forming short, linear bonds (plutonyl moiety, PuO_2^{2+}) with a geometry analogous to the uranyl moiety. The Pu M_5-edge HR-XANES resembles the U M_4-edge U(VI) spectrum of $Cs_2UO_2Cl_4$ discussed above. The absorption resonances D, E and F can be assigned similarly to electronic transitions from the $3d_{5/2}$ core level to 5*f*δ/5*f*ϕ, 5*f*π, and 5*f*σ orbitals, respectively. The varying intensities and energy positions arise from differences in valence electronic configuration ($5f^0$ U(VI) and $5f^2$ Pu(VI)) but can be as well influenced by the increased nuclear charge of Pu compared to U as well as the bonding interactions with the axial and equatorial ligands. How the Pu M_5-edge HR-XANES spectrum is affected by these factors will be investigated in future systematic studies of well-defined reference systems and by quantum chemical calculations.

The HRXES experimental approach has great potential to benchmark and drive improvements in quantum chemical calculations of electronic structures of actinide elements. We anticipate a continued increase of its application for investigations of actinide compounds since highly radioactive sample system can be now studied with the Multi Analyzer Crystal spectrometer (MAC-Spectrometer) available at the INE-Beamline for radionuclide research at ANKA. The

spectrometer is intended to become the core instrumentation at the ACT experimental station of the new CAT-ACT beamline.

Instrumentation development

The MAC-Spectrometer for High Resolution X-ray Emission Spectroscopy (HRXES) commissioned in 2013 at the INE-Beamline (see Fig. 6 left) has a Johann-type geometry and can be used with up to five spherically bent analyzer crystals with 1 m bending radius (cf. INE Annual Reports 2012 and 2013). In 2014 a He-containment enclosing the MAC-Spectrometer has been designed, assembled and successfully tested at the beamline. The He-containment comprises a solid, modular bottom, which is mounted gas tight on the optical table inside the experimental hutch and a flexible top part (see Fig. 6 right) consisting of a polyethylene bag attached to the solid base enclosing the detector stage and a smaller front bag enclosing the analyzer crystals. During data acquisition the containment is constantly flushed by He gas, thereby minimizing the absorption of photons with 3 - 4 keV energy. A polyethylene window in front of the Ketek SDD with 10 µm thickness and continuous N flow on the back side prevents He penetration through the detector Be window, which would damage the thermoelectrically cooled device. In 2015 the He-Box will be additionally fitted with a second glove box sleeve and a sample transfer lock to facilitate insertion and positioning of radioactive samples.

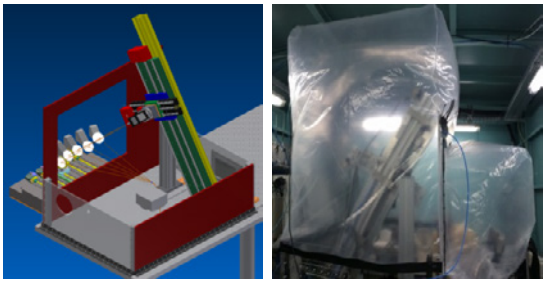

Fig. 6: A 3d-model (left) and a photograph of the MAC-Spectrometer and the He-containment.

Acknowledgements

Many thanks to H. Blank (Bonn University), A. Neumann, J. Thomas, A. Bauer and Ch. Marquardt (all KIT-INE), T. Hoffmann and G. Christill (both KIT-SUM) for invaluable technical and logistic support.

References

[1] Rothe, J. et al., *Rev. Sci. Instrum.* **83**, 043105 (2012)

[2] www.anka.kit.edu

[3] Dardenne, K. et al., *J. Nuc. Mater.* **460** 209–215 (2015)

[4] Vitova, T. et al., *Inorg. Chem.* **54**, 174-182 (2015)

[5] Denning, R. G. et al., *J. Chem. Phys.* **117**, 8008-8020 (2002)

[6] Denning, R. G., *J. Phys. Chem. A* **111**, 4125-4143 (2007)

9.2 Laser spectroscopy

C. Garcia, R. Götz, T. Hippel, F. Rinderknecht, L. Temgoua, M. Trumm, J. Laber, T. Schäfer, K. Gompper, E. Gonzalez-Robles, V. Metz

In co-operation with:

S. Büchner, C. Walther

Leibniz Universität Hannover, Institut für Radioökologie und Strahlenschutz, Hannover, Germany

Introduction

The strong need to develop new or improve already existing sensing and analytical techniques to obtain accurate information on the speciation and behavior of different lanthanide (Ln) and actinide (An) elements in the environment of a final nuclear waste repository has suffered from a considerable lack of input in the past. Researchers at KIT-INE have been striving for more than 20 years to implement different *laser based* techniques for this field of research. Among those techniques applied at INE, the focus in 2012-14 was mainly placed on the implementation and upgrade of different setups for Laser Induced Breakdown Detection (LIBD), Laser Induced Breakdown Spectroscopy (LIBS) and Time-Resolved Laser Fluorescence Spectroscopy (TRLFS). Due to necessary reorganization following changes in the scientific/technical staff dedicated to the development of laser based methods, a big effort in 2014 was the compilation and organization of all relevant information regarding past developments at INE. This step was essential to initiate necessary instrumental improvements and future system upgrades.

Developments in Laser Induced Breakdown Detection (LIBD)

During the past two decades KIT-INE has been a pioneer institution in the implementation and application of LIBD for the detection and quantification of nanoparticles in aquatic systems, mostly related to colloid formation and migration studies. The main advantage of this technique compared with other nanoparticle detection methods is its very high sensitivity for particles smaller than 100 nm. Two LIBD methods using two different detection schemes have been developed in our labs. Once a dielectric breakdown event is generated by a particle crossing the focal region of the laser beam, both the plasma-emission and the generated pressure-wave can be precisely detected by a computer-based image-detection system or by a photoacoustic sensor, respectively. In both cases a calibration with monodisperse reference particles is necessary for calculating mean size and concentration of colloids in the analyzed sample. With the 2D-optical detection method average particle diameters between 20 and 1000 nm and the concentration of the colloids are routinely determined, while the s-curve or acoustic detection method also provides information about the size distribution between 15 nm and 1000 nm.

Recent developments of our optical detection instrumentation are driven by the fact that the detection system used until now is becoming obsolete and the replacement by a new detection camera with faster data transfer capabilities is envisaged. With the new system it will be possible to acquire, integrate and process the obtained data in a much shorter period of time and, therefore, to avoid some limitation regarding the data storage capability of the present instruments. This fact is especially important when the duration of the experiments is limited as, for instance, during our groundwater field analysis at the Grimsel Test Site. Initial tests of the updated system are planned for 2015-2016 during experiments dedicated to improve the technical capabilities by studying the influence of different matrixes on the LIBD response.

Presently two different s-curve LIBD systems, one mobile and one stationary, are operative at INE. As latest implementation of the mobile setup, a system with a design similar to the first commercial LIBD launched into the market by the French Cordouan Company within a technology transfer project has been built in our lab. In 2014 this s-curve LIBD, which can be coupled to a high-pressure flow-through detection cell, has been further optimized. Other activities have been focused on tracking down sources of instabilities and running parallel calibrations with our optical and stationary LIBD systems. A new software module for controlling both s-curve detection systems has been finally implemented, allowing for automatic data processing.

Implementation of a new TRLFS system for speciation analyses at low temperature

Because of its high selectivity and sensitivity, TRLFS is routinely used as analytical technique at INE for Ln and An speciation investigations, mainly for detecting Eu(III) and Cm(III) in trace concentrations. A pulsed laser beam is used to excite the fluorescence of the sample in solid or liquid phase. The excited fluorescence signal is spectroscopically resolved by a gated detection system, providing information about the lifetime of the fluorophore. With the lifetime, the number of water molecules in the fluorophore neighborhood can be determined, giving information about the complex structure. Moreover, if the time resolved fluorescence experiments are performed at low temperatures, there is an increase of the fluorescence intensity and, additionally, the splitting of the emission peaks can be better resolved. This fact is very helpful for INE investigations, mainly in those cases

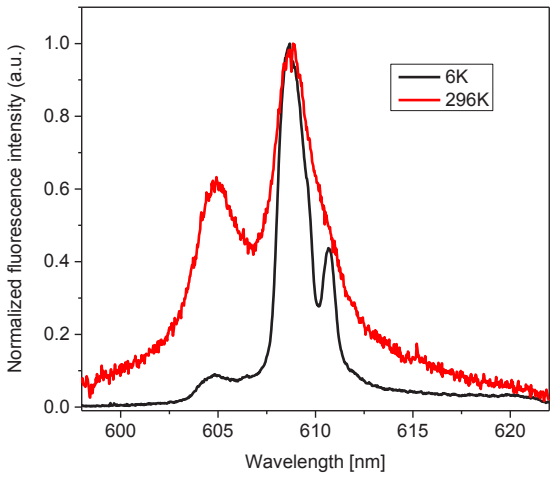

Fig. 1: Effect of temperature in the resolution of the fluorescence emission spectra of Cm(III) in strontianite measured at 6K and 296 K.

where incorporation of the An or Ln cations in the crystal lattice of mineral phases is expected.

In 2014 our efforts in this field were focused on the installation and optimization of a TRLFS setup for fluorescence excitation at low temperatures. A new dye laser (NarrowScanK, Radiant Dyes, Germany) pumped by the third or second harmonic of a Nd:YAG at 355 or 532 nm was installed in our controlled area. The dye laser beam is collected by a quartz fiber optic and focused onto the sample. The sample holder is placed inside the custom made vacuum chamber of a He cryostat (Cryovac, Germany). For the projected experiments it was important to improve the thermal contact at the interface between the cold head of the cryostat and the copper sample holder, and between the holder and the sample container. Once optimized, temperatures down to 6K were reached at the sample holder. Fig. 1 shows the differences in the spectral resolution for Cm(III) emission bands at room temperature compared to 6 K. As further upgrade steps a broadening of the excitation wavelength range and the implementation of a high degree of automation for tuning the wavelength are envisaged which will enable direct excitation spectroscopy studies.

Laser spectroscopy techniques for spatially resolved analysis of solid samples

Use of LIBS as a remote analytical sensor

Unlike LIBD, where the generated breakdown is only optically detected by a camera, in LIBS the laser generated plasma must be spectroscopically resolved by using a spectrometer coupled to the detection system, normally equipped with an intensified CCD camera. LIBS combines main advantages of using a laser probe, i.e., the possibility of *in-situ* studies with little or no sample preparation and a nearly negligible sample consumption, with those of an OES method, i.e., simultaneous multi-element analysis and good sensitivity for all relevant elements. These advantages are very important for the analysis of samples with restricted or difficult access or in case of specimen where a short operator distance may pose a significant personal hazard.

In 2014 we have accomplished a feasibility study for the Karlsruhe Reprocessing Plant (WAK) with the goal to evaluate the capabilities of LIBS as a remote analytical sensor for the characterization of HAWC residues. Analysis of these solid phases formed in the HAWC storage tanks is crucial as prerequisite for the future dismantling of the facility. Remote LIBS might help to minimize sampling times and will reduce the contamination risk when using off-field analytical techniques like ICP-MS. Considering the spatial restrictions in the access to the residues, a fiber optic LIBS configuration was chosen as the best instrumental option for the laser delivery system to the sample and the collection of the plasma emission. With the aim of supporting this project, a bench-top prototype LIBS setup was installed in the INE controlled area laboratories. The system can retrieve the spatial distribution of some elements of interest on the surface or in-depth of a solid sample by linking x, y and z position of the probe site to the obtained emission spectra. When designing this LIBS set-up we benefited from the open optical configuration installed for the new TRLFS system by using the 532 nm output of the pump laser. Initial investigations performed with this new instrument will focus on the possibility of using a fiber-optic configuration coupled to an echelle spectrometer for remote measurements with high spectral and spatial resolution.

LA-ICP-MS analysis of spent nuclear fuel

In the frame of a collaboration between KIT-INE, KIT-INR and JRC-ITU investigations of the radial distribution of isotopes in irradiated nuclear fuel pellets will be accomplished at the ITU hot cells facilities. Initial LA-ICP-MS studies have been designed and first sample preparation steps have been accomplished in 2014. The spent fuel experiments will be carried out in 2015 using a non-commercial LA-ICP-MS installed at ITU. A UV laser beam at 266 nm will be introduced via a periscope into a hot cell and focused on the sample surface. The fuel pellet section is mounted inside an ablation cell on a motorized x-y-z stage. The particles generated after the sample ablation event are carried with a Helium flow to the plasma of a double-focusing sector field ICP mass spectrometer. By correlating spatial coordinates with the obtained mass spectra, the varying distribution of fission products and actinides can be easily followed along the pellet radius. The obtained results will help to refine some models used today to predict segregation and accumulation processes of different radionuclides within the spent fuel matrix.

9.3 Microscopy and surface analytics

T. Yokosawa, E. Soballa, F. Friedrich, I. Pidchenko, X. Gaona, D. Schild

In co-operation with:

M. R. González-Siso, L. Duro, J. Bruno

Amphos 21, Barcelona, Spain

Introduction

Interaction of uranium, the main component of spent nuclear fuel, with magnetite either in the near-field due to anoxic corrosion of steel containers or with naturally occurring magnetite in the far-field was investigated by TEM complementing XAS analyses.

Plutonium is one of the main contributors to long-term radiotoxicity of spent nuclear fuel. Interaction of plutonium with magnetite was studied at reducing hyperalkaline conditions prevailing in a nuclear repository in presence of water and cement.

Prior to a potential release of radionuclides from waste forms after intrusion of water into a nuclear repository, water interacts with backfill material such as bentonite. Hydration of smectite, the main component of bentonite, causes swelling and thus a sealing effect. Analysis of the swelling behavior of smectite and ion-exchanged smectite was studied by ESEM.

TEM study of uranium co-precipitated with magnetite

For safety assessment of a deep underground nuclear waste repository it is important to know the possible processes of radionuclide mobilization and immobilization. Attenuation of radionuclide migration may occur by sorption, precipitation or incorporation into mineral phases. Magnetite will be a major product of anoxic corrosion of canister walls after a potential water intrusion into the repository.

To study possible incorporation of uranium into the magnetite structure, uranyl ions were co-precipitated with magnetite under anoxic conditions. After preparation, the low uranium concentration in the supernatant indicates presence of reduced U(IV). Samples were analyzed by SEM-EDX to identify the location of uranium. However, due to low uranium concentration this was not successful. To analyze if sorption, precipitation or incorporation of uranium occurs, TEM was applied to the samples for more detailed analyses at the nanometer scale. TEM provides the location of the trace elements in a projection of the averaged structure of the material along the electron beam direction. Therefore, it is possible to confirm if uranium precipitation has occurred or not, although it is not easy to distinguish between sorption and incorporation. TEM measurements are performed employing a FEI Tecnai G2 F20 X-TWIN operated at 200 kV, located at IAM-WBM-FML (KIT).

Figure 1a shows a high-angle annular dark field (HAADF) STEM image taken from a co-precipitated U-magnetite sample containing 10000 ppm of U. Small particles with about 5 nm diameter can be distinguished as well as large particles with 10-20 nm diameter. The small particles show relatively brighter contrast in the image than the large particles. As intensities of HAADF-STEM images become higher when either the atomic number or the sample thickness increases, the small and large particles are considered to be U and Fe oxides, respectively. Indeed, as STEM-EDX and STEM-EELS shows, the large and small particles labeled with 1 and 2 in Figure 1a consist of magnetite and U oxides, respectively (Fig. 1b, c). Additional areas with large and small particles marked in areas II and III were also confirmed to be magnetite and U oxides. Generally, the small particles detected in the HAADF-STEM images are considered to be U oxide colloids. However, these areas need to be analyzed by STEM-EDX/EELS in addition, as slightly overlapping magnetite particles may also show an

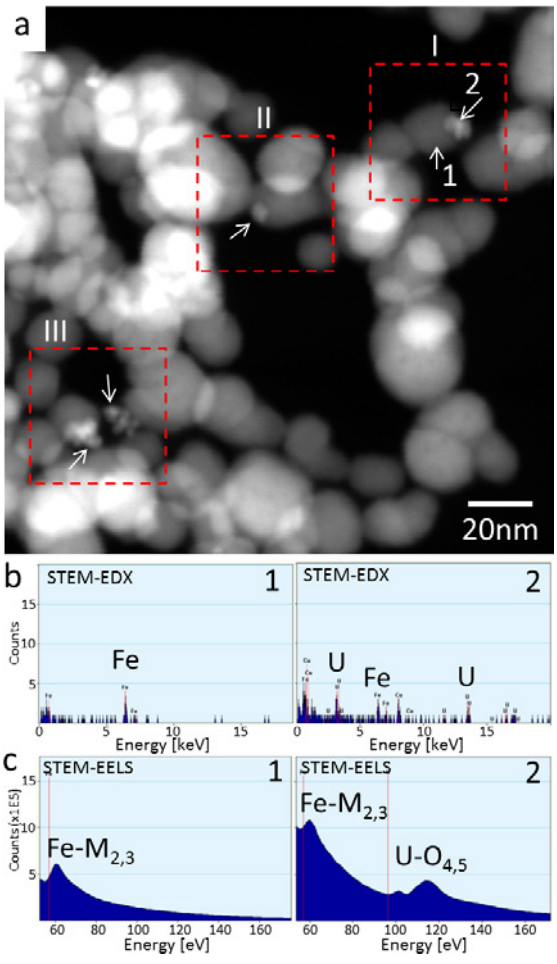

Fig. 1: (a) STEM image of U coprecipitated with magnetite: (b) STEM-EDX and (c)STEM-EELS taken from particles 1 and 2. The areas indicated by white arrows contain U oxide.

increased brightness, which is not easily distinguished from that of the U oxide. Thus, combining HAADF-STEM with EDX and/or EELS is necessary to detect U oxide colloids precipitated among magnetite particles.

Only elemental information of the sample can be gained by the techniques mentioned above. In order to reveal structural information, high-resolution (HR) TEM is performed. Figure 2 shows a HR-TEM image taken from an area where an U oxide particle was formed on the surface of the Fe oxide. The contrast of TEM images is not only attributed to the mass of the constituent atom (mass contrast), but also to interference between the transmitted and diffracted electron beams (diffraction contrast). Therefore, it is not possible to identify mineral phases based on the contrast of the TEM image. On the other hand, a crystalline phase can be identified by observing the atomic lattice fringes of the particles. The insets in the top and bottom of Figure 2 depict a zoom into the areas marked by white rectangles (1 and 2) and the corresponding Fourier-transformed images on the right hand side, respectively. The crystal lattice fringes with d ~ 0.25 nm in area 1 (large particle), and d ~ 0.27 nm, 0.32 nm in area 2 (small particle) are clearly resolved. Based on the assumption that the particles consist of UO_2 (a = 0.5471 nm, Fm-3m [1]), fluorite type crystal structure and Fe_3O_4 magnetite (a = 0.8397 nm, Fd-3m [2]), the fringes correspond to {111}UO_2 (d = 0.3159 nm), {002}UO_2 (d = 0.2736 nm), and {113}Fe_3O_4 (d = 0.2533 nm) atomic planes, respectively.

Energy-filtered (EF)TEM provides two-dimensional analysis of a TEM image of a sample with EELS by selecting electrons with a specific energy. Figure 3 depicts HAADF-STEM, HR-TEM and EFTEM images taken from area III in Figure 1a. Figures 3c, d are acquired by selecting electrons at the Fe-$M_{2,3}$ edge and U-$O_{4,5}$ edge, respectively (energy window size: 10 eV). The UO_2 colloids and magnetite particles are clearly discriminated in the images. EFTEM has an advantage

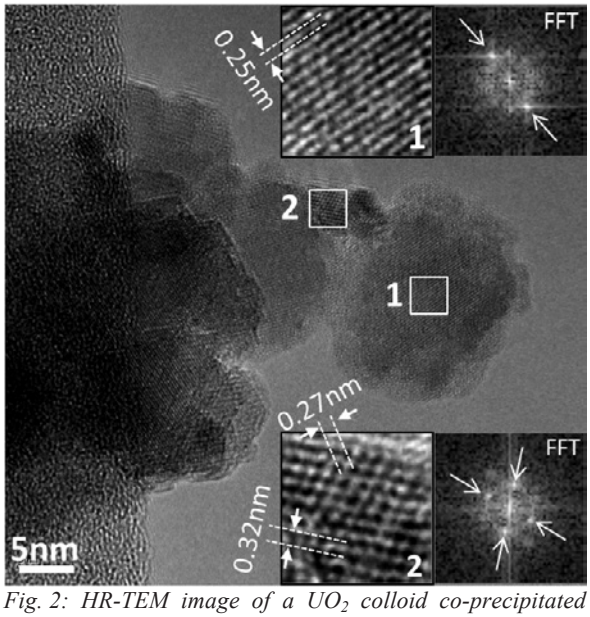

Fig. 2: HR-TEM image of a UO_2 colloid co-precipitated with magnetite particles.

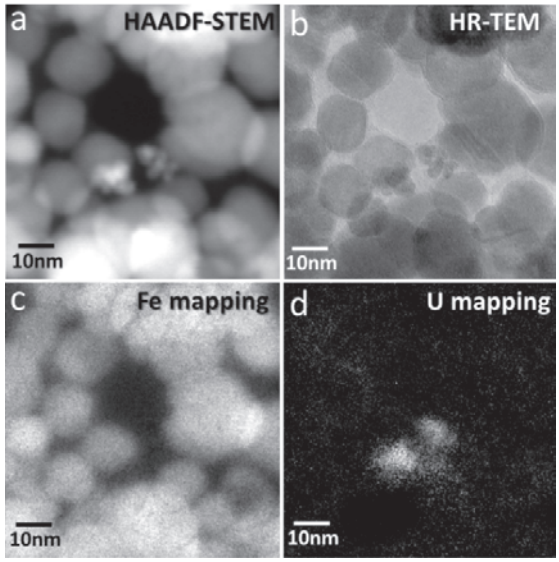

Fig. 3: Area III in figure 1 analyzed by (a) HAADF-STEM, (b) HR-TEM, and EFTEM imaging: (c) Fe mapping, (d) U mapping.

in providing two-dimensional elemental analyses on amorphous as well as crystalline phases.

In conclusion, we demonstrated by combining several TEM based techniques that we can detect and identify the elemental composition and structure of a UO_2 colloid precipitated on the surface of a magnetite particle with sub-nanometer spatial resolution. Atomic numbers of actinides are much larger than those of corrosion products. Thus, it is possible to detect actinides at trace levels incorporated in a crystalline material if atomic resolution HAADF-STEM with a probe-side aberration corrector is applied. This technique is widely used for detecting dopants in a semiconductor [3].

Plutonium redox chemistry under hyperalkaline and reducing conditions

The interaction of plutonium with the surface of magnetite was studied by XPS. Samples were retrieved from magnetite suspensions prepared under anoxic conditions with a solid-to-liquid ratio of 2 gL^{-1},

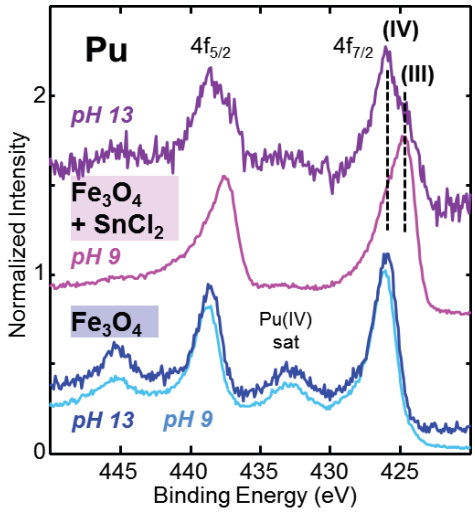

Fig. 4: Pu 4f spectra of Pu(V) added to magnetite (blue), and Pu(V) added to magnetite+$SnCl_2$ (magenta).

3E-5 M Pu(V), 0.1M NaCl, equilibrated up to 290 days, pH 9 and 13. Very reducing Eh values (pe + pH = 2) simulating repository conditions were imposed with $SnCl_2$ in a complementary series of magnetite samples prepared under analogous experimental conditions.

In case of pure magnetite systems, Pu 4f spectra show binding energies typical for Pu(IV) and satellites characteristic of PuO_2 at around pH 9 and 13 (Fig. 4). Magnetite systems in the presence of $SnCl_2$ show relevant proportions of Pu(III), both at pH ≈ 9 and pH ≈ 13. Note that formation of stable Pu(III) surface complexes has been reported under near-neutral pH conditions [4], but this is the first time that Pu(III) is detected on the surface of magnetite under hyperalkaline pH conditions resulting from water-cement interaction.

Bentonite hydration observed by ESEM

Compacted bentonite is used as an engineered barrier in high-level radioactive waste repositories in clay stone or hard rock geological formations. Hydration of bentonite clays causes swelling and formation of a clay gel-layer at the surface, which is an intermediate step to erosion. The swelling behavior of Febex bentonite, smectite content greater than 90%, was analyzed by environmental scanning electron microscopy (ESEM). The FEI Quanta 650 FEG microscope used is equipped with a precise adjustment facility of water vapor pressure inside the analysis chamber. In combination with sample stage cooling to 5°C, relative humidity up to 100% can be achieved at the sample.

A fraction < 2 µm of the untreated Febex bentonite and three interlayer cation exchanged bentonite samples were prepared: Na-, Sr-, or Li-exchanged. In addition, a Li-exchanged bentonite heated at 300°C was prepared to achieve a layer-charge reduced material. Small agglomerates in the size range around 20-30 µm with a random distribution of smectite particles were selected and the relative humidity was increased via six steps from 15 to 95%. At each step an image was taken after 15 minutes of equilibration time. The two-dimensional swelling of the bentonite was calculated from these images by image analyses (Fig. 5).

All samples show an exponential increase of swelling with increasing relative humidity. While the raw- and Na-bentonite achieved swelling percentages of up to 35%, the Sr-sample shows 29%, the Li-sample 18%, and the layer-charge reduced Li-sample only 6%. Besides the type of interlayer cation, the layer charge affects the swelling behavior of the clay.

To investigate the anisotropic swelling behavior of smectite, a thin film of oriented Na-exchanged clay platelets was prepared by sedimentation from a suspension. This film was broken and a small piece was glued vertically on a sample holder. Again, relative humidity was increased via six steps. At each step the expansion was measured in two directions: perpendicular to the film, i.e. parallel to the c-axis of the clay platelets, and along the film surface (Fig. 6). The measurements prove the anisotropic swelling behavior

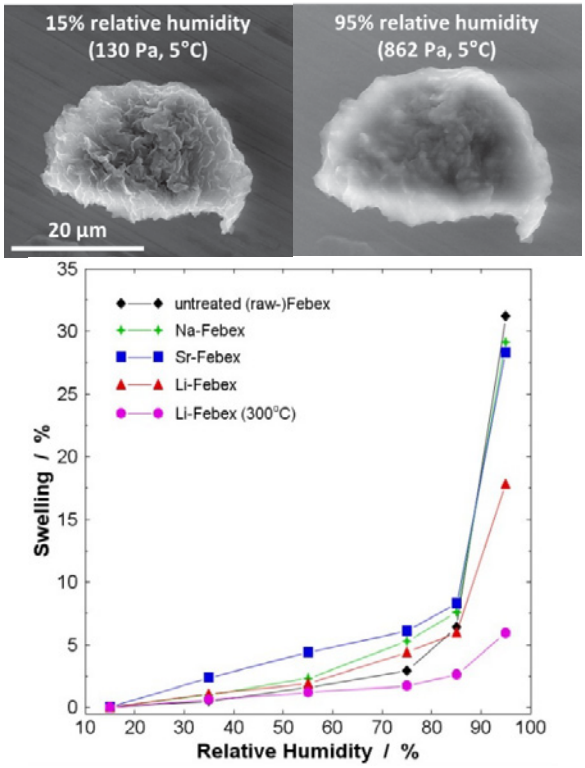

Fig. 5: ESEM images of a smectite agglomerate at different relative humidity and swelling behavior of cation exchanged smectites as determined by 2D- image analyses.

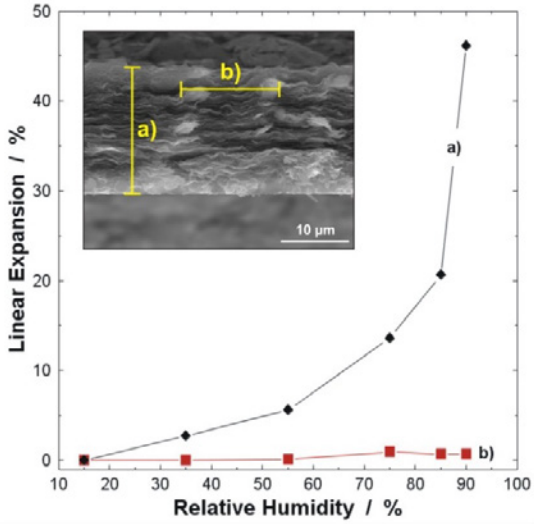

Fig. 6: ESEM image of Na-exchanged smectite film at 15 % relative humidity. Yellow marks: measurement directions (a) perpendicular and (b) parallel to the film surface of the aligned smectite platelets. Swelling occurs predominantly perpendicular to the film surface.

of the clay film, with an expansion of 46% along the c-axis and an insignificant expansion along the basal plane.

References

[1] Leinders, G. et al., *J. Nucl. Mat.* **459**: 135 (2015)

[2] Fleet, M.E., *Acta Cryst.*, **B37**: 917 (1981).

[3] Okuno, H. et al., *Appl. Phys. Lett.* **96**: 251908 (2010).

[4] Kirsch, R. et al., *Environ. Sci. Technol.*, **45**: 7267 (2011).

9.4 Accelerator mass spectrometry (AMS)

F. Quinto, M. Lagos, M. Plaschke, T. Schäfer and H. Geckeis

In co-operation with:

P. Steier

VERA Laboratory, Faculty of Physics, University of Vienna, Währinger Straße 17, A-1090 Vienna, Austria

Introduction

Accelerator Mass Spectrometry (AMS) is presently one of the most sensitive analytical techniques for the determination of actinides; that is due to the stripping process and acceleration of the ions to MeV energies providing both the destruction of molecular isobaric background and a strong reduction of tailing interferences. The Vienna Environmental Research Accelerator (VERA) has developed abundance sensitivities (AS) for ^{236}U, ^{237}Np and ^{239}Pu relative to ^{238}U at levels $\leq 10^{-15}$ [1] (Tab. 1) and detection limits (DL) at the value of 10^4 atoms per sample [2]. These features allow accurate measurements of actinide concentrations below ppq levels, particularly advantageous when limited sample size is available. Such an analytical challenge is encountered, e.g., when investigating environmental samples affected by low levels nuclear contamination, like the global fallout, or in the frame of field experiments employing actinide tracers, like the Colloid Formation and Migration Project (CFM) at the Grimsel Test Site [3].

Tab. 1: Abundance sensitivity of ^{236}U, ^{237}Np and ^{239}Pu related to the tailing from the strong directly neighboring peak of ^{238}U at VERA. Data adapted from [1].

Abundance sensitivity at AMS-VERA	
^{239}Pu/^{238}U	10^{-15}
^{237}Np/^{238}U	$< 10^{-15}$
^{236}U/^{238}U	10^{-17}

A further challenge in the determination of ^{237}Np and of ^{243}Am lays in the non-availability of pure enough isotopic tracers for mass spectrometric measurements of these nuclides. Especially when investigating actinides at the levels of 10^5 to 10^8 atoms in a sample, the use of a tracer standard may prevent the accurate determination of the wanted nuclides because it contains or produces by radioactive decay not negligible concentrations of the isotopes under investigation, or of their isobars. To overcome this limitation, at INE we have investigated the use of non-isotopic tracers, developing a new method in which different actinide nuclides can be measured sequentially without previous chemical separation from each other exploiting the exceptional AS of AMS (Tab. 1). The chemical treatment consists principally in the purification of the group of the actinides from the matrix elements with a $Fe(OH)_3$ co-precipitation employing a concentration in the final sample solution of between 20 and 70 mg/L Fe. This procedure, allowing for the first time the simultaneous mass spectrometric determination of ultra-trace levels of several actinide nuclides in presence of naturally occurring U, is especially suited to groundwater and seawater samples. We have determined global fallout derived actinides, namely ^{236}U, ^{237}Np and ^{239,240}Pu, at levels down to 10^5 atoms/sample in groundwater and seawater samples, 250 g mass, by using ^{233}U as tracer. Similarly, in the frame of the CFM Project, we have investigated groundwater background (BG) samples, 250 g mass, collected in the tailing of a tracer pulse experiment breakthrough curve (run 12-02), detecting the injected tracers down to the levels of fg/g and ag/g. In particular, the concentrations of ^{237}Np and ^{242}Pu have been determined by using ^{239}Pu as tracer and that of ^{243}Am by using ^{248}Cm as tracer.

Accuracy of the method

The count rate associated with a certain concentration of an actinide nuclide depends on both the chemical yield of the sample preparation and the ionization yield of the Cs negative ions sputtering source of AMS. In order to study these two effects, solutions of tracers were produced for each sample matrix analyzed. Seawater and groundwater samples were spiked with a multi-isotope solution obtained with known amounts of ^{233}U, ^{237}Np, ^{239}Pu, ^{243}Am and ^{248}Cm and submitted to the same chemical procedure of the samples with corresponding matrix. The so obtained "calibration samples" were repeatedly measured together with the investigated samples in order to compensate for the different chemical and ionization yields of the several actinides. Since in this experiment these two effects are not separable, we define their combination as "chemical and ionization yield" (CIY) of the actinide element. The measured CIYs appears to increase with the atomic number of the actinide element, according to literature data [4,5] and a precision between 20% and 30% is observed in their determination. Such uncertainties propagate and overwhelm the counting uncertainties of the measured nuclides; however, our method provides an unprecedented sensitivity and the advantage of the simultaneous determination of several actinides.

The method has been validated with the analysis of the Reference Material (RM) IAEA-443, radionuclides in Irish Seawater. The measured concentrations of ^{236}U, ^{237}Np, ^{239}Pu and ^{242}Pu in only 100 g mass of the RM are consistent with literature data [6,7,8] (Fig. 1). These results prove that the performed correction by the CIYs provides accurate determinations.

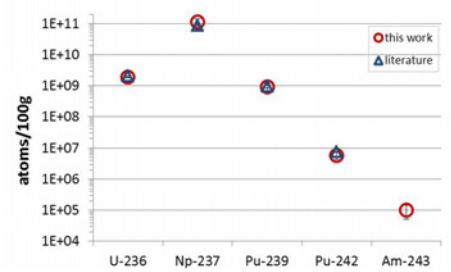

Fig. 1: Agreement between the concentrations of ^{236}U, ^{237}Np, ^{239}Pu and ^{242}Pu of the RM IAEA 443 measured in the actual study (red circles) and literature data (blue triangles). The first estimate of the concentration of ^{243}Am, provided by our method, is also shown.

Furthermore, we have measured, for the first time to our knowledge, the concentration of ^{243}Am in the RM IAEA-443. The detection of mass 243 at a level of $(1 \pm 0.5) \times 10^5$ atoms is ascribable to ^{243}Am. ^{243}Cm can be excluded, since its concentration in the RM at the time of the measurements (November 2014) was equal to ~24 atoms/100g sample – below the DL of AMS; this value is obtained from the certified content of ^{244}Cm in the RM IAEA-443 [6] and from the activity ratio ^{243}Cm/^{244}Cm measured in sediment samples from the Irish sea [9].

Environmental and CFM samples

Fig. 2 depicts the atom ratios ^{236}U/^{237}Np, ^{237}Np/^{239}Pu and ^{236}U/^{239}Pu measured in four different samples, masses between 100 and 250 g, namely the RM IAEA-443, a seawater sample from the Tyrrenian Sea (TSW), a tap water sample from Karlsruhe in Germany (KaTW), and a surface water sample from the Wildseemoor, an ombrotrophic peat bog in the German Black Forest (WSM). The actinide nuclides measured in the RM IAEA-443 and in the TSW samples originate from the liquid effluents of the Sellafield Reprocessing Plant [6] and the global fallout, respectively; in this case, the measured atom ratios represent the relative abundances of ^{236}U, ^{237}Np and ^{239}Pu in the same environmental system, seawater, relative to different contamination sources. Conversely, the atom ratios measured in the TSM, KaTW and WSM samples, originating from the same contamination source, namely global fallout, reflect the different behaviors of the investigated actinides in the three environmental systems. These results reflect the conservative behavior of U and Np in seawater with respect to Pu [10]; while in surface water rich in organic carbon (WSM sample) the atom ratios of the three nuclides are in agreement with values found in soils and peat bog samples [11,12]. In the tap water (KaTW) sample, Pu was not detectable indicating its retention in the mineral and organic phases of the overlying soil, also a higher mobility of U with respect to Np is observed relative to the surface water. ^{236}U, ^{237}Np, and Pu isotopes are [11,12] widespread over the earth surface due to the stratospheric nuclear weapons test fallout. Their ubiquity offers a unique opportunity to study the behavior of these actinides in environmental conditions, allowing gaining knowledge on the fate of U, Np and Pu originating from other contamination sources, e.g., the long-term emplacement of nuclear waste.

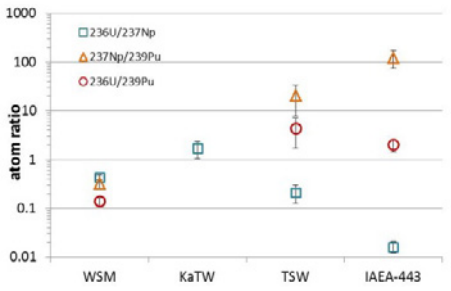

Fig. 2: ^{236}U/^{237}Np, ^{237}Np/^{239}Pu and ^{236}U/^{239}Pu atom ratios measured in four different natural water samples (see text for description) sized between 100 g and 250 g mass.

At the Grimsel Test Site, in the frame of the CFM Project, a first radionuclide tracer test under low-flow conditions has been performed in 2012 (run 12-02). In this experiment ^{237}Np, ^{242}Pu and ^{243}Am have been injected in water conducting granodiorite fractures in order to investigate the colloid mediated transport of the actinides.

In the present study we have analyzed six groundwater BG samples, where the size was limited to a mass of 500 g or to 250 g, and in which the concentration of the injected tracers was supposed to be below the detection limits of HR-ICP-MS employed for the measurements of the preceding samples and equal to 10 ppq.

The detection of the injected tracers, ^{237}Np, ^{242}Pu and ^{243}Am, was successful in the investigated samples, which were collected from 60 up to 210 days after the start of the experiment (Fig. 3). The use of non-isotopic tracers has led to a higher uncertainty in the determination of ^{237}Np and ^{243}Am than of ^{242}Pu. While the maximum relative uncertainty on the measured values of ^{239}Pu, due solely to the counting error, is equal to ~ 5%, the relative uncertainties of ^{237}Np and ^{243}Am reach ~ 16% and ~ 24%, respectively. Nevertheless, it is possible to observe for every investigated isotope a trend of concentration over the time leading

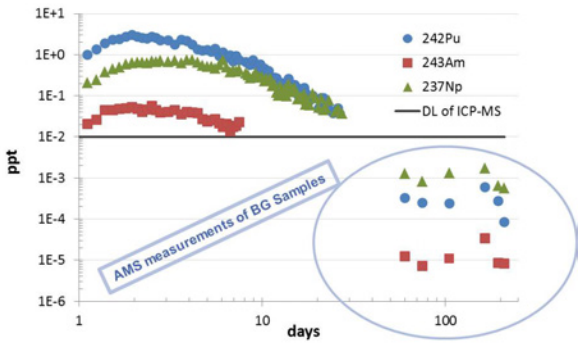

Fig. 3: ^{242}Pu (blue circles), ^{237}Np (green triangles) and ^{243}Am (red squares) concentrations in the eluent fractions of the experiment run 12-02 in the frame of the CFM Project. Above and below the black line indicating the DL of HR ICP-MS, the data obtained with the first technique and those obtained with AMS are depicted, respectively.

to a local concentration maximum at the sampling time of 165 days, as shown in Fig 3. These findings prove that the long-term release and retention of actinide tracers can be studied in samples collected up to 6 months after the starting of the experiment.

Even though AMS is, as matter of fact, a mass spectrometric technique, its extraordinary sensitivity, allowing the detection of ultra-trace levels of actinides, provides the capability to observe their behavior in a variety of environmental systems. We exploit this feature in field studies whose results are complementary to those of the fundamental research on the speciation of actinides [13].

References

[1] P. Steier et al., Presentation at the *13th International Conference on Accelerator Mass Spectrometry*, 24-29 August 2014, **37**, (Aix en Provence, France) (2014).

[2] P. Steier et al., *Nucl. Instr. Meth. Phys. Res. Sect. B,* **268,** 104-109 (2010).

[3] www.grimsel.com/gts-phase-vi/cfm-section.

[4] M. Christ et al., *Nucl. Instr. Meth. Phys. Res. Sect. B,* **331**, 225-232 (2014).

[5] K. Fifield et.al., *Nucl. Instr. Meth. Phys. Res.* Sect. B, **123,** 400-40 (1997).

[6] P. P. Povinec et al., *J. Radioanal. Nucl. Chem*., **251,** 369–374 (2002).

[7] M. K. Pham et al., *J. Radioanal. Nucl. Chem*., **288,** 603–611 (2011).

[8] S. H. Lee et al., *Appl. Radiat. Isot.,* **66,** 823-828 (2008).

[9] P. I. Mitchell et al., *Appl. Radiat. Isot*., **49,** 1283-1288 (1998).

[10] A. Sakaguchi et.al., *Earth Planet. Sci. Lett*., **333/334,** 165-170 (2012).

[11] J. M. Kelley et.al., *Sci. Total Environ.,* **237/238**, 483-500 (1999).

[12] F. Quinto et.al., *Environ. Sci. Technol.,* **47,** 5243-5250 (2013).

[13] F. Quinto et.al., *Anal. Chem.,* **87,** 5766-5773 (2015).

9.5 Computational chemistry

B. Schimmelpfennig, M. Trumm, R. Polly, P. Lindqvist-Reis, M. Vespa, X. Gaona, E. Yalcintas, M. Altmaier

Computational chemistry

There is a wide range of application for computational chemistry assisting and supporting experimental efforts at KIT-INE: from providing structures of complex chemical systems including actinides in solution or solid phase, thermodynamic data or reproducing the actual experimental spectra for EXAFS or XANES, to perform simulations and visualization of complex chemical reactions. The systems under investigation thus vary from small complexes in solution to crystals or interfaces. New algorithms and the constantly improving hardware allow getting closer and closer to a detailed description of actinide systems at the level of electronic structure.

Incorporation of Zn and Nd into Tobermorite

Cement-based materials play an important role in multi-barrier concepts developed worldwide for the safe disposal of hazardous and radioactive wastes. Cement is used to condition and stabilize the waste materials and to construct the engineered barrier systems (container, backfill and liner materials) of repositories for radioactive waste. In the past, investigations have focused on the uptake behavior of heavy metals onto cementitious materials without taking into consideration the competitive sorption behavior of the cations. The focus of a recent study was set on this competitive sorption behavior by using bulk-X-ray absorption spectroscopy (XAS) to investigate the uptake mechanism of Zn on the crystalline calcium silicate hydrates (C-S-H) phase 11 Å Tobermorite in the presence of Nd as potential competitor co-absorbing metal under strongly alkaline conditions (pH=12.5-13.3) up to 6 months reaction time. See M. Vespa *et al.* [1]. Our theoretical efforts encompass a combined dynamic and static approach helping to understand the experimental results.

For the static calculations we carried out Density functional theory (DFT) calculations with periodic boundary conditions and plane-wave basis sets as implemented in the Vienna ab initio simulation package (VASP). Electron exchange and correlation are described using the Perdew-Burke-Ernzerhof (PBE) functional. The ion cores are dealt with by the projector augmented wave (PAW) method. We employed an energy cut-off of 500 eV for the kinetic energy of the plane waves for all calculations.

We used VASP for the geometry optimizations of pure Tobermorite and the changes induced by the incorporation of Zn and Nd.

Different starting structures have been considered where the Zn ion replaces either a silicon atom in the silicon-layer (positions B and D) or a water molecule in the water layer (position W) (Fig. 1). For both B and D, four bonds to neighboring oxygen atoms are formed by Zn at a distance of 1.92 and 1.93 Å, respectively in good agreement with EXAFS data predicting 3-4 Zn-O bonds at 1.96 Å. In the water layer W different minima were found, all with bond-lengths larger 2.10 Å.

Temperature and dynamic effects can be studied using ab initio molecular dynamics with periodic boundary conditions on the DFT level as implemented in the CP2K software package. At ambient conditions 5 ps simulations have been performed for the various optimized starting structures. In addition a double-incorporation with two Zn in D positions (2D) was considered. By analysis of the radial distribution function average Zn-O bond-lengths of 1.89, 1.92, 2.13 and 1.89 Å were determined for the D, B, W and 2D starting points respectively. Using the trajectory-snapshots, EXAFS spectra were simulated using the FEFF 8.4 code. A good agreement to the measured spectra is achieved (Fig. 2.). The B trajectory shows the lowest differences compared to the experimental data (Fig. 1).

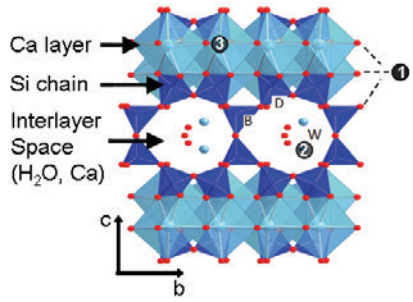

Fig. 1: The crystal structure of 11 Å Tobermorite with possible positions of Ca in the Ca layers and interlayer Ca as well as positions of structural oxygen atoms and water molecules in the interlayer. Potential sites for metal sorption and structural incorporation of Zn(II) are labeled B, D and W.

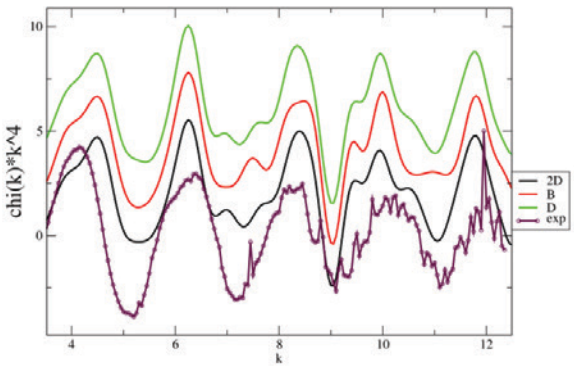

Fig. 2: Measured (purple) and simulated EXAFS of the Zn K- edge

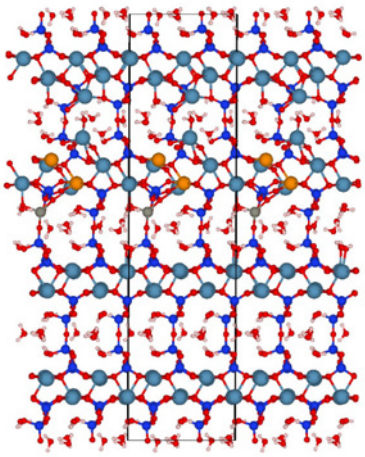

Fig. 3: Incorporation of Zn^{2+} (gray) and Nd^{3+} (orange) into Tobermorite

Furthermore, we probed different positions for the incorporation of additional Nd^{3+} ions added to the Zn^{2+} ions with static DFT calculations using VASP. We found energetically favorable positions, which have Nd-O, Nd-Si and Nd-Ca distances in good agreement with the experimental results of M. Vespa *et al.* [1] (see Fig. 3).

Tc(IV) hydrolysis species and ternary Mg/Ca-Tc^{IV}-OH complexes in alkaline $MgCl_2$ and $CaCl_2$ solutions

^{99}Technetium is a β-emitting fission product highly relevant for the safety assessment of nuclear waste repositories due to its significant inventory in radioactive waste, long half-life ($t_{½}$~211.000 a) and redox sensitivity. Due to the very reducing conditions expected under repository conditions, an appropriate knowledge of the Tc(IV) solubility and aqueous speciation in dilute to concentrated NaCl, $MgCl_2$ and $CaCl_2$ solutions is required in the context of nuclear waste disposal.

Tc(IV) hydrolizes very strongly. The anionic species $TcO(OH)_3^-$ has been shown to dominate the aqueous chemistry of Tc(IV) in dilute alkaline conditions of pH ≥ 11 [8]. In concentrated alkaline $MgCl_2$ and $CaCl_2$ solutions, solubility experiments conducted at KIT-INE (see section 5.1) hint towards the formation of higher hydrolysis species of the type $Mg_x[TcO(OH)_y]^{2+2x-y}$ and $Ca_x[TcO(OH)_y]^{2+2x-y}$. Quantum chemical calculations are well suited to identify possible Tc(IV) solvation species in alcaline solution. Since there are no ab initio calculations on $[TcO(OH)_4]^{2-}$ or $[TcO]^{2+}$ we performed pilot studies of these two species with high level Complete Active Space Self Consisdent Field (CASSCF) and Multi Reference Configuration Interaction (MRCI) calculations to determine the ground states of these species.

As a result of our multireference calculations we found that the lowest doublet and quartet state of TcO^{2+} are single reference states, respectively (see Fig. 2). We assigned the $^2\Delta$ and the $^4\prod$ quantum numbers to these states. Hence the ground states of the hydrolysis species $[TcO(OH)_y]^{2-y}$, $Ca_x[TcO(OH)_y]^{2+2xy}$ and $Na_x[TcO(OH)_y]^{2+x-y}$ are single reference states as well and therefore the application of large-scale DFT calculations is permitted to determine the structure of relevant Tc(IV) species in alkaline NaCl and $CaCl_2$ solutions involving a large number of water molecules and solvated ions in more detail (see Fig. 4).

Tab. 1: Comparison of the Nd bond distances obtained with EXAFS and DFT

	Experiment [1]	Theoretical results
Nd-O	242-245 pm	249 pm
Nd-Si	364-377 pm	341 pm
Nd-Ca	272-384 pm	391 pm

With this convincingly realistic model system we probed the species $[TcO(OH)_5]^{3-}$, $Na_x[TcO(OH)_5]^{x-3}$ and $Ca_3[TcO(OH)_5]^{3+}$. Only for the $Ca_3[TcO(OH)_5]^{3+}$ species enwrapped by one hundred water molecules a stable structure could be found. This was not possible neither for the $[TcO(OH)_5]^{3-}$ species nor for the $Na_x[TcO(OH)_5]^{x-3}$ species. This is a very strong theoretical hint for the existence of the $Ca_3[TcO(OH)_5]^{3+}$ species in alkaline $CaCl_2$ solutions and in agreement with the experimental observation [2,4] that in NaCl solutions no $Na_x[TcO(OH)_5]^{x-3}$ species could be found.

The calculations were carried out with TURBOMOLE and MOLPRO.

Violation of Badger's rule in actinyl(VI) ions

The hexavalent state is the prevalent oxidation state for uranium in aqueous systems under oxic conditions, where it occurs as a linear, dioxo uranyl cation, $[O=U=O]^{2+}$. Under oxidizing conditions also neptunium and plutonium form linear neptunyl and plutonyl cations. Their linear geometry is a result of participation of the 5f orbitals in the actinyl multiple bonds. These bonds are strong and rather unreactive, making the oxo groups to weak Lewis bases. However, the reactivity and the Lewis basicity of the oxo groups depend strongly on the ligands in the equatorial plane and their binding to the metal. By effective s-donation, hydroxide and carbonate ligands are able to

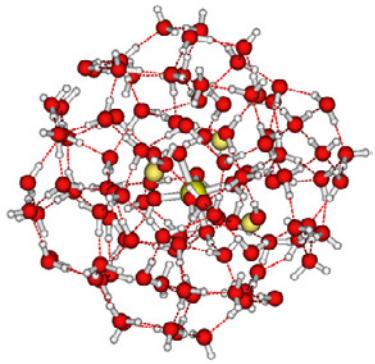

Fig. 4: $Ca_3[TcO(OH)_5]^{3+}$ species surrounded by 100 water molecules

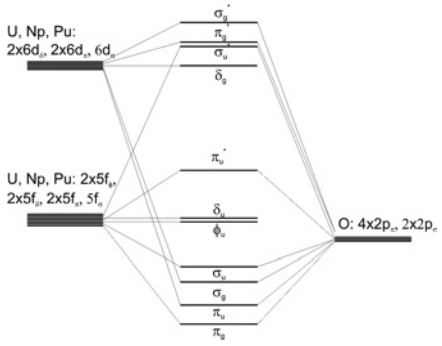

Fig. 5: Qualitative molecular orbital scheme for the AnO_2^{2+} ions

polarize the actinyl bond through cis-destabilization and thus increase the Lewis basicity of the oxo groups [2-4]. Such destabilization is reflected by an increase of the actinyl bond distance and a decrease of the symmetric actinyl stretch frequency [4]. If we instead consider a series of actinyl complexes from UO_2^{2+} to PuO_2^{2+}, for example their aqua ions $[AnO_2(H2O)_5]^{2+}$, the observed changes are counterintuitive and, in fact, violate Badgers's rule [5]. In this case the rule predicts an increase of the actinyl stretch frequency and the bond force constant on going from U to Pu as the interatomic An=O distance decreases; however, the opposite trend is observed, the stretch frequency and bond force constant decrease down the series [6]. Violation of Badgers's rule is witnessed not only for these aqua ions but also for the corresponding actinyl nitrate, carbonate, and chloride complexes [6-8]. Although it is quite obvious that the origin causing the effect must be of electronic nature, a satisfactory explanation has not yet been presented in the literature, despite the effect has been observed and reported by several researchers over the years [7-8].

A crucial role in this effect can be ascribed to the behavior of the 5f and 6d orbitals of U^{6+}, Np^{6+} and Pu^{6+} (see Fig. 5). Recent DFT calculations performed at INE on a large range of hexavalent actinyl-nitrate clusters of the type $[AnO_2(H_2O)_2(NO_3)_2]$, and $[AnO_2(NO_3)_3]^-$ revealed the same trend as observed experimentally using single-crystal X-ray diffraction and Raman and IR spectroscopy and described above [6]. This trend is seen in DFT result of the UO_2^{2+}, NpO_2^{2+} and PuO_2^{2+} ions in the gas phase. State-of-the-art multi-configurational calculations are in progress.

Investigation of An(III)/Ln(III) complexes with N-donor ligands

The theoretical investigation of Ln(III)/An(III) complexes with N-donor ligands is a challenging task for theoretical methods, because the systems under investigation are much larger in size than corresponding aquo-complexes of the metal ions. Hence molecular dynamics (MD) simulations have been performed to complement the data obtained by quantum chemical methods. Especially for An(III)-BTP systems this has never been explored before, as existing force fields are not accurate enough to correctly describe the interactions involved.

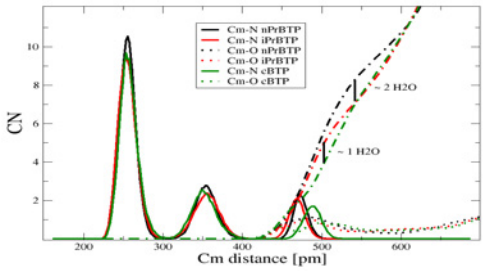

Fig. 6: Cm-N and Cm-O RDFs from the MD simulation for nPr-BTP (black), iPr-BTP (red) and campher-BTP (green).

The polarizable force field describing the interactions between all atoms and molecules in the system must be built carefully to assure a realistic description of the system's dynamics. To remain as independent from the experiments as possible, we adjusted our force fields to state-of-the-art quantum chemical ab initio reference data on the MP2 or CCSD(T) level using large, diffuse basis sets of aug-cc-pVTZ quality. Relativistic effects, necessary to correctly describe heavy metals, are accounted for by either pseudo-potentials, implicitly including those effects, or by a second order Douglas-Kroll-Hess Hamiltonian. Charges and dipole polarizabilities of all atoms are obtained by the atomic dipole-corrected hirshfeld method.

MD simulations have been performed on $[Cm(BTP)_3]^{3+}$ and $[Gd(BTP)_3]^{3+}$ in aqueous solvent, explicitly modeled by 1000 water molecules in the cubic simulation box. The 10 ns time-scale allows a good statistics of the configuration space. The resulting trajectories are in good agreement with radial distribution functions obtained by EXAFS measurements showing a Cm-N distance of 2.57 Å for the coordinating nitrogen atoms, compared to 2.56 Å from the experimental data (Fig 6).

Changes in complex stabilities were found for different alkyle side-chains. The origin of these differences was determined to be a shielding effect for the solvent molecules depending on the side chains' steric behavior. Fewer solvent molecules occupying the space between the aromatic ring system allow a less restrained torsion motion, hence allowing a more

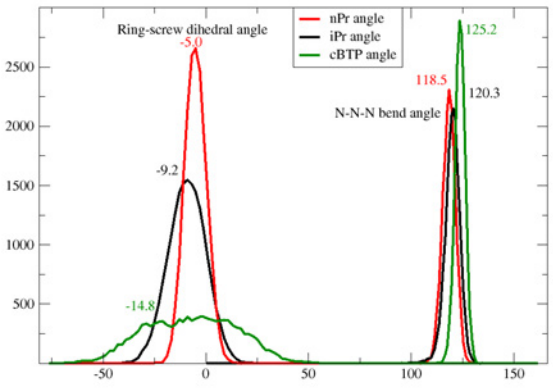

Fig. 7: ADFs for the NCCN torsion and NNN bending angles from the MD simulation for nPr-BTP (black), iPr-BTP (red) and campher-BTP (green).

flexible adjustment of the geometry. Thus varying the substituent from n-proply over i-propyl to campher, lead to an increase of the average ring torsion within the time frame of the MD simulation (Fig. 7).

In future projects these force fields will be used to shed further light on the complexation reactions of An(III)/Ln(III) with BTP-ligands. In addition, the correlation between dipole polarizabilities and complex stability constants will be further analyzed.

Structure and vibrational spectra of the Cm(III)-$HClO_4$ system

A number of researchers have previously reported that the luminescence lifetime of Eu(III) in aqueous solution decreases substantially with increasing concentration of perchlorate ions (which may be added in the form of $HClO_4$ or $NaClO_4$). We have recently shown that this is also true for Cm(III). The reason for this *luminescence quenching* is still a matter of controversy. In contrast to water molecules or hydroxide ions, both of which quench the luminescence lifetime of Eu(III) through multi-phonon coupling with OH vibrational overtones, the corresponding mechanism for perchlorate is unfavorable and does not result in quenching. It has even been proposed that the reduced Eu(III) lifetime is a consequence of an increased hydration number. Considering that the hydration number of Eu(III) may change between eight and nine depending on the temperature and the chemical environment, an increase of the hydration number from nine to eleven, corresponding to a reduction of the lifetime from about 110 to 90 µs, is not realistic. Therefore, other mechanisms should account for this additional quenching. TRLFS and vibronic sideband spectroscopic measurements at INE suggest that perchlorate ions residing the second hydration spheres of the hydrated metal ions form weak hydrogen bonds to the water molecules of the first hydration sphere, effecting their OH-vibrational manifolds. Vibrational modes calculated with DFT and RICC2 techniques concur with experimental findings: The OH stretching vibrations of the first shell water molecules are blue-shifted in the presence of perchlorate ions in the second shell by approximately 100 cm^{-1} on average.

Based on the gas-phase data, a force field for the Cm(III)-perchlorate system was generated. MD simulations for different perchlorate ion concentrations ranging from 0.3 to 9 M have been performed. For all concentrations, perchlorate ions enter the second hydration sphere to form solvent-shared ions pairs, whereas contact ion pairs (inner sphere complexes) are only formed for short very periods of time and only at perchlorate ion concentrations around 9 M. Based on the trajectories, a likely representative $[Cm(H_2O)_9](ClO_4)_3(H_2O)_{207}$ structure was chosen as a starting structure for an ab initio MD simulation (Fig. 4). In contrast to previous classical MD simulations, interactions are described here by quantum chemical DFT potentials. Employing a very short time-step of 0.25 fs, vibrational motions can be accurately described and be used to calculate IR spectra. A

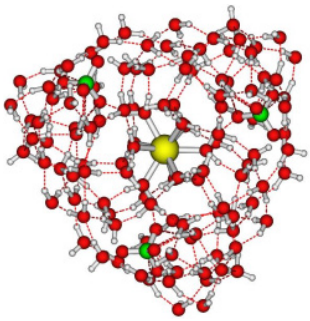

Fig. 8: Optimized $[Cm(H_2O)_9(ClO_4)_3](H_2O)_{207}$ structure.

blue-shift of ~200 cm^{-1} for the HOH···$OClO_3$ configuration as compared to that of HOH···OH_2 was determined, which is in very good agreement with the measured spectra (Fig. 9).

As a final step, the same set of calculations will be performed for the Gd(III)-perchlorate system and compared to experimental findings. In addition, the perchlorate ion in bulk water will be investigated, ensuring a detailed understanding of the influence of the metal center.

Structure and coordination of the Cm(III)-Oxalate system

In this study, we investigated the complexation with the oxalate anion in aqueous solution as a function of the ligand concentration, the ionic strength (NaCl) and the temperature (T = 20 - 90°C) by TRLFS, quantum chemical calculations and MD simulations. Four complex species $([Cm(Ox)_n]^{3-2n}$, n = 1, 2, 3, 4) are identified and their molar fractions are determined by peak deconvolution of the emission spectra.

The conditional log $K'_n(T)$ values of the first three complexes are calculated and extrapolated to zero ionic strength with the specific ion interaction theory approach (SIT). The $[Cm(Ox)_4]^{5-}$ complex forms only at high temperatures. Thus, the log $K^0_4(T)$ value was determined at T > 60°C. The log $K^0_1(25°C)$ = 6.86 ± 0.02 decreases by 0.1 logarithmic units in the studied temperature range. The log $K^0_2(25°C)$ = 4.68 ± 0.09 increases by 0.35 and log $K^0_3(25°C)$ = 2.11 ± 0.05 by 0.37 orders of magnitude. A detailed understanding of the coordination is gained by quantum

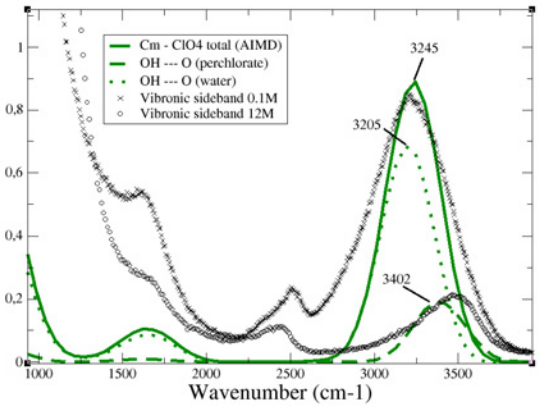

Fig. 9: Measured VBS (black) and simulated (green) IR spectra.

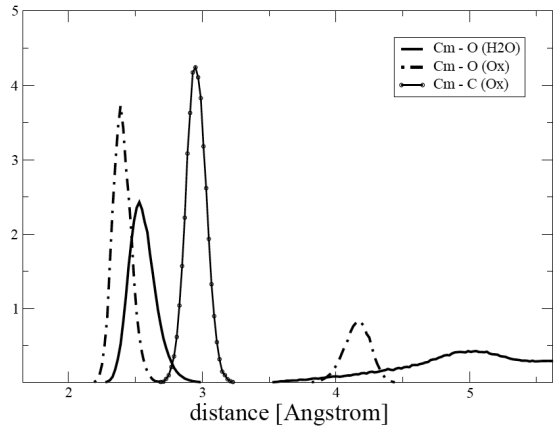

Fig. 10: RDF of the 1:3 all side-on complex from the MD simulation

chemical structure optimizations in the gas-phase.

The bond lengths and bond angles of the different Cm(III) oxalate complexes are determined by calculations on the DFT/B3-LYP/TZVP level. As expected, the side-on coordination form has shorter Cm-O bond lengths than the end-on coordination form. In a second step, binding energies are obtained from single-point MP2/aug-cc-pVTZ calculations. For all Cm-Oxalate species, the all side-on coordination has the lowest binding energy.

The influence of the solvent is investigated by MD simulations of the various complexes in a 1000 H_2O box at ambient conditions. Radial distribution functions agree with the gas-phase results. A side-on coordination is formed for all starting structures within the time-frame of the simulation with average Cm-O(Ox) bond-lengths of 2.40-2.43 Å and Cm-O(H_2O) bond-lengths of 2.51-2.57 Å (Fig. 10). The only exception being the 1:3 complex with one anion in end-on coordination which is also stable for the 10 ns simulation time, although higher in energy than it's all side-on counterpart. The formation of a 1:4 complex could not be observed, in agreement with the experimental findings for room temperature. This work has been published in 2015 [9].

References

[1] M. Vespa et al., *Physics and Chemistry of theearth* **70-71**, 32-38, (2014).

[2] P. L. Arnold, G. M. Jones, S. O. Odoh, G. Schreckenbach, N. Magnani, J. B. Love, *Nat. Chem*., 2012, **4**, 221-227.

[3] A. J. Lewis, H. Yin, P. J. Carroll, E. J. Schelter, *Dalton Trans*., 2014, **43**, 10844-10851.

[4] Vallet, V.; Wahlgren, U.; Grenthe, I., *J. Phys. Chem. A*. 2012, **116**, 12373-12380.

[5] R. M. Badger, *J. Chem. Phys*., 1934, **2**, 128-131.

[6] M. Skripkin, unpublished results, European FP7 TALISMAN project (JRP TALI-C01-07).

[7] D. L. Clark et al., *abstracts of papers of the Am. Chem. Soc.*, Volume **243**, 60-NUCL.

[8] D. D. Schnaars et al., *Inorg. Chem.,* 2013, **52,** 14138-14147.

[9] A. Skerencak et al., *Inorg. Chem.,* 2015, **54**, 1860-1868

10 (Radio-)chemical analysis

The INE analytical labs provide the advanced analytical techniques, well-developed procedures and competences in radioanalytical sample preparation and handling needed for the R&D projects of the institute. These capabilities are also requested by external clients, e.g., in the fields of nuclear waste declaration, High Level Liquid Waste (HLLW) vitrification, decommissioning of nuclear installations, quality control of radioanalytical separation materials and of radiopharmaceuticals. A special focus is in mass spectrometry techniques, which are adapted and improved for trace element analysis and speciation studies of actinides and fission products. Sector Field (SF)-ICP-MS and collision cell quadrupole CC-Q-ICP-MS are coupled to species sensitive methods, e.g., to capillary electrophoresis (CE-SF-ICP-MS) and field-flow field fractionation (FFF-Q-ICP-MS), respectively. The investigation of actinides below ppq levels in groundwater and clay deposits is carried out with newly developed analytical methods and accelerator mass spectrometry (AMS); this part of our scientific research is illustrated in chapter 9.4. Furthermore, the analytical group supports the INE infrastructure, is involved in various teaching activities and is responsible for education of chemical laboratory assistants.

M. Plaschke, A. Bauer, N. Banik, K. Bender, M. Böttle, L. Böringer, F. W. Geyer, C.-H. Graser, K. Gompper, S. Heck, S. Hilpp, A. Kaufmann, B. Kienzler, T. Kisely, M. Lagos, C. M. Marquardt, F. Quinto, T. Renz, J. A. Schäfer, T. Schäfer, A. Seither, C. Walschburger, and H. Geckeis

Routine analysis

A pool of advanced analytical techniques, well-developed procedures and competence in the fields of radioanalytical sample preparation and separation techniques, elemental and isotope analysis, chromatographic methods and nuclear spectroscopic techniques is available. Our personnel is trained in handling of nuclear samples and in the operation and maintenance of instruments adapted to glove boxes. Several analytical techniques listed in Table 1 are available both in inactive and active labs. In the reporting period over twenty thousands of samples are routinely analyzed providing the data mainly for the INE R&D projects and also for external clients.

Tab. 1: Routine analytical techniques at INE

Elemental and Isotope Analysis
Quadrupole Inductively Coupled Mass Spectrometry (Q-ICP-MS)
Collision Cell Q-ICP-MS (CC-Q-ICP-MS)
Sector Field ICP-MS (SF-ICP-MS)
Inductively Coupled Optical Emission Spectrometry (ICP-OES)
Atomic Absorption Spectrometry (AAS)
Flame Atomic Emission Spectrometry (F-AES)
X-Ray Fluorescence Spectrometry (XRF)
Nuclear Spectroscopic Methods
Alphaspectrometry
Liquid Scintillation Counting (LSC, conventional/high sensitivity)
Gammaspectrometry (with auto-sampler)
Other Methods
Ion Chromatography (IC) for cations and anions
Gas Chromatography (GC)
Carbon Analysis (TOC, DOC, TIC, NPOC)
Specific Surface Area Analysis (BET)
Differential Thermal Analysis (DTA)
Dilatometry
Fusion and Microwave Digestions
Gravimetry and Titrations

Commercial analytical services

Commercial analytical service is offered for various clients on the basis of formal contract agreements. Data are recorded, documented and quality controlled according to the requirements of the clients.

Nuclear waste treatment and decommissioning of nuclear facilities (WAK-HDB)

Samples from the WAK-HDB (Wiederaufarbeitungsanlage Karlsruhe GmbH, Hauptabteilung Dekontaminationsbetriebe) can be classified according to their origin in samples from the HDB incineration (ashes) or LAW evaporation plants (liquid concentrates), annually averaged samples, samples from decommissioning of nuclear facilities and others. Samples are processed by radioanalytical separation methods and analyzed using elemental, isotope and nuclear spectroscopic techniques. The nuclides routinely determined include (but are not limited to): ^{55}Fe, ^{63}Ni, ^{90}Sr, ^{233,234,235,236,238}U, ^{238,239,240,241,242}Pu, ^{241}Am, $^{242,243+244}$Cm.

Quality control of separation resins

INE is the first quality control lab of the TRISKEM Sr separation resin and the secondary lab for actinide separating TRU and TEVA resins. The analytical service comprises the determination of the capacity of the Sr resin, column tests, determination of possible interferences and of eluted organic material. On average, one sample batch of Sr resin is analyzed each month.

Quality control of radiopharmaceuticals

During the last years a ^{223}Ra containing alpha-radiopharmaceutical is regularly analyzed with regard to toxic heavy metal trace impurities. ^{223}Ra acts as a calcium mimic and is indicated for patients suffering from bone metastases. Due to the short penetration of the alpha emitter a highly localized tumor cell killing is achieved with minimal damage to surrounding healthy tissue. A batch of drug sample is analyzed weekly in our lab.

Mass spectrometry techniques

At INE several mass spectrometers are currently in operation including two Q-ICP-MS instruments (Perkin Elmer Elan 6100, adapted to a glove-box, and Thermo X-Series2, equipped with reaction/collision cell technology) and a SF-ICP-MS (Thermo Element XR/2, adapted to a glove box). SF-ICP-MS provides 1) detection limits for transuranium elements as low as ~10^{-14} mol/L (lower ppq range) and 2) elevated mass resolution (up to 10.000) which is beneficial for accurate determination of elements suffering from interfering species, e.g., Fe, Se or lanthanides (see next paragraph). Even lower detection limits down to 10^4 actinide atoms per sample can be obtained by Acceleration Mass Spectrometry (AMS), for that INE maintains a close cooperation with the VERA AMS facility in Vienna (cf chapter 9.4).

Lanthanide signature in overburden rock

In the context of Asse, different aspects are addressed: i) the signature of homologues (e.g. lanthanides, U, Th, Cs, Ba, Zr, etc.) in the overburden sedimentary rock, ii) the determination of in situ-Kd´s between sedimentary rock and porewater constituents and iii) the interaction between radionuclides and cement in waste barrels stored in the Asse underground mine for long term studies.

Figure 1 shows the lanthanide pattern from siltstones and limestone samples (overburden rock) treated by a sequential acid extraction procedure (0.04 mol/L NH_2OH*HCl in 25% (v/v) HOAc at pH 2.0) and measured by SF-ICP-MS. To reduce possible interfering species (i.e., lanthanide oxide species) elevated mass resolution (medium and high resolution) is combined with optimized ICP plasma parameters. The obtained CI-chondrite normalized lanthanide signature is smooth and non-fractionated. Moreover, it shows an enrichment of light lanthanides over the heavy ones (CI-chondrite normalized La/Yb ratios between 5 and 12), and negative Eu anomalies. All these features are typical for sedimentary material of continental crust origin and support the reliability of the data.

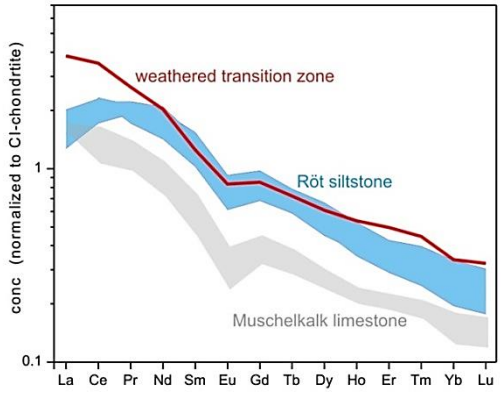

Fig. 1: Lanthanide signature of several Asse sedimentary rocks analyzed by a sequential extraction scheme (see text)

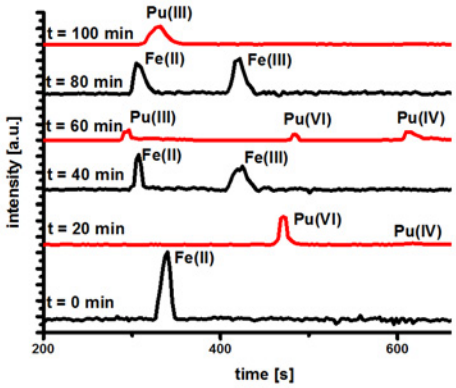

Fig. 2: Fe (black) and Pu (red) redox state analysis of a solution containing [Pu]total=$5.0\cdot10^{-10}$ M, $[Fe]_{total}$= $2.0\cdot10^{-6}$ M, 0.1M $HClO_4$, pH= 1.0, aerobic conditions

CE-SF-ICP-MS – Actinide redox speciation

Redox speciation of Pu

Detailed knowledge of the redox speciation of actinides, i.e. Pu and Np, under geochemical conditions is a prerequisite for the long-term safety assessment of a nuclear waste disposal site. Likewise, the redox speciation of Fe (being available from waste canister corrosion) can serve as an indicator for the present redox conditions. In this study, for the first time a sequential time-resolved monitoring of a Pu(VI) reduction by Fe(II) is demonstrated by CE-SF-ICP-MS. An o-phenanthroline/EDTA system was applied to "freeze" the Fe redox states for analysis and SF-ICP-MS detection has been performed in medium resolution mode to suppress interfering signals from ArO^+ and ArN^+.

For the Pu redox state analysis at trace levels, low mass resolution was adjusted to profit from the higher sensitivity in this measuring mode. One can assume that o-phenanthroline/EDTA might affect Pu redox chemistry. In order to avoid artifacts from these additives on the Pu redox speciation, measurements were performed using separate sample aliquots, with and without addition of o-phenanthroline/EDTA for Fe and Pu analysis, respectively.

Tab. 2: Redox speciation of Fe and Pu vs. time; (species below the limit of quantification (9σ) are estimated < 5 %)

Species	**t = 0 min**	**t = 40 min**	**t = 80 min**
Fe(II)	100 %	56 %	41 %
Fe(III)	< 5 %	44 %	59 %
Species	**t = 20 min**	**t = 60 min**	**t = 100 min**
Pu(III)	< 5 %	42 %	> 90 %
Pu(IV)	18 %	54 %	< 5 %
Pu(VI)	82 %	< 5 %	< 5 %

An improved CE-SF-ICP-MS setup is used to investigate the Pu(VI) reduction by Fe(II) in a 0.1 M $HClO_4$ homogeneous solution. The measured pH was 1.0 during the whole experiment. A solution containing $2.0\cdot10^{-6}$ M Fe(II) was added to a plutonium sample containing $5.0\cdot10^{-10}$ M ^{242}Pu to get a total volume of 50 mL. Two aliquots of the sample were taken every 40 minutes. The first two aliquots of 1.5 mL each

were taken immediately after Fe(II) was added to the Pu(VI) solution. To the first aliquot o-phenanthroline/EDTA was added for Fe analysis, while the second one was untreated for Pu analysis.

The electropherograms and the redox speciation of Fe and Pu are shown in Figure 2 and summarized in Table 2, respectively. The initial Fe redox speciation corresponded to 100% Fe(II) and no Fe(III) (t=0 in Figure 2 and Table 2). After 40 minutes the iron composition reached almost 50% Fe(II) and 50% Fe(III). After 80 minutes, a further oxidation of Fe(II) to Fe(III) is observed. Because Fe is in wide excess compared with Pu, a partial oxidation of Fe(II) to Fe(III) might be caused by traces of O_2 (< 1 ppm) during this experiment. Although this effect must be considered, it does not query the principle of the method.

At t=20 minutes, Pu(VI) and Pu(IV) were found at a ratio of 82 to 18%. We can conclude, that the presence of Pu(IV) is due to a proceeding reduction of Pu(VI) by Fe(II). After 60 minutes, Pu(VI) was still detected (but below the quantification limit estimated to < 5%), and Pu(IV) and Pu(III) were the predominant species. After 100 minutes the solution contained almost only Pu(III) (> 90%), while Pu(IV) and Pu(VI) were below the quantification limits. Therefore, in the present experiment, an almost complete reduction of Pu(VI) to Pu(III) in the presence of Fe(II) was observed within 100 min.

As the total Fe exceeds the Pu concentration by orders of magnitude, we can assume that the redox potential is controlled by the iron chemistry. The calculated and measured redox potentials are close to the Fe(III)/Fe(II) equilibrium in the Pourbaix diagram under these conditions. The redox potential (Eh) of the solution was measured during the experiment. The initial experimental Eh value (Eh_{exp} at t=0) was 0.634 V and it increased with time, in particular: Eh_{exp} (40 min) = 0.774 V and Eh_{exp} (80 min) = 0.817 V. This trend is consistent with the increasing Fe(III)/Fe(II) ratio measured by CE-ICP-SF-MS. Furthermore, it demonstrates, that the oxidation of Fe(II) occurred in the samples, and it was not an artifact during the CE-ICP-SF-MS measurement itself. Based on the redox state analysis of Fe by CE-ICP-SF-MS, the redox potential of the solution (denoted Eh_{calc}) was calculated using the Nernst equation:

$$E_{h,calc} = E^0_{Fe^{3+}/Fe^{2+}} + \frac{R \cdot T}{n \cdot F} log \frac{[Fe^{3+}]}{[Fe^{2+}]} \qquad (1)$$

where $E^0_{Fe^{3+}/Fe^{2+}}$ refers to the redox potential (V) in standard conditions, brackets denote activities, R is the molar gas constant (J mol^{-1} K^{-1}), T the temperature (K), n the number of electrons in the half redox reaction and F the Faraday constant (J V^{-1}). At pH = 1, the hydrolysis of both Fe(II) and Fe(III) are negligible. The activities of the iron species were calculated using the Davies equation. At t = 40 minutes the Eh_{calc} reaches the value of 0.771 V, which is in good agreement with Eh_{exp}. After 80 min, the Eh_{calc} is calculated as equal to 0.764 V, which is regarded as no alteration relative to the state after 40 minutes. We can conclude that Fe redox state analysis determined by CE-ICP-SF-MS is fairly consistent with Eh_{exp} and Eh_{calc}, within an uncertainty of Eh_{exp} of about ± 50mV. The conditional redox potential of the Pu(VI)/Pu(III) couple is +0.918V in 0.1 M $HClO_4$. Therefore, Pu(VI) reduction is thermodynamically favored under the present conditions. Furthermore, our results demonstrate that the Pu reduction proceeds with a rather fast kinetics.

Sorption studies of Np on illite

Illite is a clay mineral with strong affinity to actinides and, therefore, is considered as a suitable host rock for nuclear waste disposal. It is known that the Np mobility strongly depends on the redox state, Np(IV) and Np(V), providing low and high mobility, respectively. In a previous study Np(V) ($3.0 \cdot 10^{-8}$ < $[^{237}Np(V)]_{tot}$ < $3.0 \cdot 10^{-4}$ M) was contacted with illite (2 g/L) at different pH in 0.1 M NaCl under inert (Ar) atmosphere [1]. Although it is known from the literature that Np(V) weakly sorbs to minerals, here, a strong interaction of Np with illite was observed. Based on the Eh measurement, Np(V) prevailed in the aqueous phase. Therefore, the unexpected high sorption was attributed to the formation of Np(IV) at the illite surface, thermodynamically favored because of its strong sorption to minerals. The prevalence of Np(V) in the aqueous phase and the presence of a fraction of Np(IV) at the surface could be confirmed by liquid-liquid extraction and X-Ray absorption spectroscopy at relatively high Np concentrations ($[^{237}Np(V)]_{tot}$ > 10^{-5} M).

To confirm this result at lower concentrations, CE-ICP-SF-MS was applied. A sample with ($[Np(V)]_{tot}$ = $3.0 \cdot 10^{-8}$ M) and illite (2g/L) was kept in a Ar-glovebox for 1.2 years after its preparation. After 63 days contact time, the pH was 7.0 and the Eh_{exp}, measured in the suspension, was 0.24 V. After 1.2 years we measured a slightly increased pH of 7.4 and the same Eh_{exp} as before (Eh_{exp} = 0.24 V). Therefore, the redox conditions were constant and are clearly in the stability field of Np(V) in solution. After phase separation by ultracentrifugation (400'000 g) an aliquot of the supernatant was taken for CE-ICP-SF-MS measurement. The Np concentration in the remaining solution dropped down to $2.2 \cdot 10^{-10}$ M, because most of the Np was adsorbed on the clay miner-

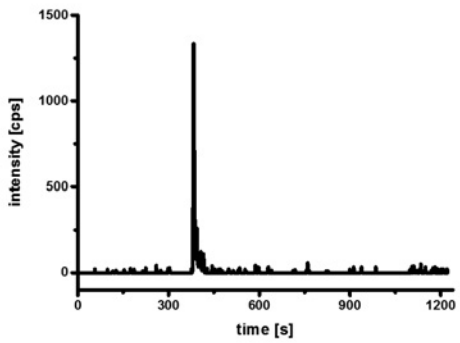

Fig. 3: Np in the supernatant of a suspension with illite; [Np]= $2.2 \cdot 10^{-10}$ M

al. The electropherogram in Figure 3 shows only one peak, which evidences the prevalence of a single Np redox state. The electrophoretic mobility was calculated as equal to $2.5 \cdot 10^{-4}$ $cm^2 V^{-1} s^{-1}$, which is a typical value for Np(V). We can conclude, that the prevalence of Np(V) in solution is also confirmed for samples with very low Np concentration. This result is in agreement with the Eh and pH conditions of the solution, confirms the results obtained in a previous study for higher $[Np(V)]_{tot}$ and, moreover, supports a surface reduction process of Np on illite clay.

References

[1] R. Marsac, N. L. Banik, J. Lützenkirchen, C. M. Marquardt, K. Dardenne, D. Schild, J. Rothe, A. Diascorn, T. Kupcik, T. Schäfer, H. Geckeis, Neptunium redox speciation at the illite surface *Geochimica Cosmochimica Acta*, submitted.

[2] V. Neck, J. I. Kim, B. S. Seidel, C. M. Marquardt, K. Dardenne, M. P. Jensen, W. Hauser, A spectroscopic study of the hydrolysis, colloid formation and solubility of Np(IV). *Radiochim Acta* 2001, **89**, 439-446.

11 Radiation protection research

Radiation Protection Research at INE is focusing on assessing radiation exposures by estimation of doses from external radiation fields or from intakes of radionuclides. The techniques applied for assessing radiation exposures are both direct measurements and numerical simulation of radiation fields. High priority in the past was devoted to the development of techniques and models for an individualized dosimetry taking into account not only the radiation fields but also the individual itself with his or her anatomical and physiological properties. By requirements by the research project ENTRIA new questions needed to be resolved, dealing with final disposal in deep geological formations with or without arrangements for retrieval and with surface storage issues. The dose rates of highly radioactive samples used in various experiments have been calculated by the available MCNP techniques and compared to measurements. Close collaborations are established with national and international partners in several research projects such as. “Strahlung und Umwelt” in Competence Alliance Radiation Research KVSF, the EU project “BOOSTER” in FP7, and the European Radiation Dosimetry Group (EURADOS e.V.).

11.1 ENTRIA: Individual dosimetry for workers in waste disposal facilities

H. Saurí Suárez, B. Pang, F. Becker, H. Geckeis

Introduction

To develop an appropriate concept for long-term and safe disposal of nuclear waste is still a challenge that cannot be solved by engineer alone. The interdisciplinary research platform ENTRIA [1] was established in order to compare three fundamental disposal options, i.e., disposal in a deep geological repository without provisions of retrieval, disposal in a deep geological repository with provisions of monitoring and retrieval as well as long-term aboveground storage, from multidisciplinary aspects.

One important aspect concerns the occupational radiation exposure of workers in disposal facilities due to stored nuclear waste. In order to estimate the personal dose, information of the representative radiation field in such a disposal facility should be determined, for which the Monte-Carlo code MCNP6 [2] will be applied in the current study.

Recalculation of the AHE experiments with ^{252}Cf as neutron source in a simulated rock salt disposal facility of nuclear waste

In order to validate the MCNP6 code for its application to simulate the radiation field in a disposal facility, the AHE experiments performed in [3-4] were recalculated. The radiation field was calculated around a model-shielding container placed in a rock salt mine gallery.

The model-shielding container was 91.2 cm in diameter and 135 cm in length. As depicted in Fig. 1, it was divided in to 4 different zones according to material and geometry. The ^{252}Cf line source (60 cm length) with a neutron source strength of $1.7 \cdot 10^{8}$ n/s was surrounded by a cylindrical stainless cask (the internal cask), which in turn was covered by a polyethylene cylinder as neutron moderator. Finally, this body was contained in a thick cast iron cask (the outer cask).

Both neutron and photon dose rates and spectra were measured in various positions with different distances to the container surfaces (see figure 2). The measurement was performed both aboveground and underground in an emplacement drift, in order to investigate the impact of the surrounding rock salt on the radiation field.

In order to define the neutron source as input parameter for the MCNP6 simulations, the neutron production spectrum of the ^{252}Cf source (zone 1 in Fig. 1) was calculated with the SOURCE 4C code [5]. In the current case, the spontaneous fission of ^{252}Cf isotope is the only contributor of neutron yield.

Tallying is the process of scoring the parameters of interest and tally cards are used to specify what type of information the user wants to gain from the Monte Carlo calculation, e.g. current across a surface, flux at a point, energy deposition averaged over a cell, etc.

In the case under consideration the flux at a point record (F5 tally in MCNP) was applied to obtain the neutron flux spectra at the detector positions depicted in Figure 2.

Fig. 3 compares the measured neutron spectra with that calculated by MCNP6 at the detector position 2, which is 2 m away from the lid surface of the shielding container. For above- and under-ground situations, the shapes of the measured neutron spectra are reproduced fairly well by the simulation results. The peak around 20 to 30 keV is caused by a dip in the neutron cross-section of Fe-56 at 24 keV, which is the most

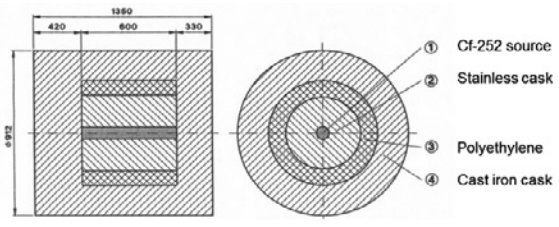

Fig. 1: Cross-section view of the model-shielding cask [3]

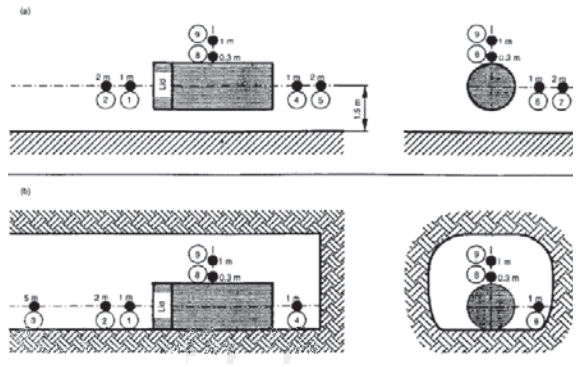

Fig. 2: Detector positions around the model shielding container (a) above-ground over a concrete surface and (b) under-ground at the end of an emplacement drift [4].

abundant isotope (91.7% in natural occurrence) of the main shielding material iron.

Due to the backscattering of neutrons from the surrounding rock salt, the neutron flux of the underground situation, in the energy range from 1 eV to 1 MeV, is generally larger than that of the aboveground situation. This enhancement of neutron flux is particularly evident at the peak around 1 to 2 keV, which is attributed to the resonance scattering of neutrons from the sodium nuclei of the rock salt. In the thermal neutron range, i.e. from 10^{-8} to 10^{-7} MeV, the neutron flux in the aboveground situation is slightly higher, which is attributed to the backscattering from the concrete surface.

However, it should be mentioned that in general the simulated neutron flux is always lower than the corresponding measured value for both aboveground and underground situations. For instance, the integral neutron flux derived from measurement at the detector position 2 is 99 $cm^{-2}s^{-1}$, while the simulated flux at the same position is only about 80 $cm^{-2}s^{-1}$. Since the error of the neutron flux derived from measurement is less than 5% [4], this deviation should be attributed to the deficiency of the modeling/simulation with MNCP6 or experimental systematic errors.

The dose conversion factors in ICRP 21 [6] were adopted in the simulations to convert the neutron flux to dose rate. Tab. 1 compares the measured and calculated neutron dose equivalent rates with the ratio indicate the ratio between the under-ground and the aboveground situations. Due to the backscattered neutrons, the dose rates in the under-ground situation can rise twice as high as in the aboveground situation. However, the calculated neutron dose rates in the current study with MCNP6 deviate partly up to higher than 30% from the measured dose rates. This relative large difference could be correlated to the deficiency in the simulated neutron flux as discussed above.

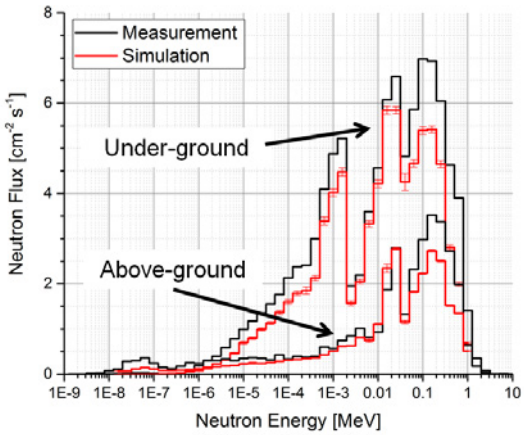

Fig. 3: Neutron spectra from measurements (black lines) and calculated by MCNP6 (red lines) at the detector position 2

Tab. 1: Comparison between measured and calculated neutron dose equivalent rates in mSv s-1.

Detector	Measurement			Calculation with MCNP6		
	Above-ground	Under-ground	Ratio	Above-ground	Under-ground	Ratio
1	26.0	40.6	1.56	18.5	28.2	1.52
2	8.8	18.4	2.09	6.0	12.1	2.00
3	-	6.4	-	1.2	3.7	-
4	47.4	79.3	1.67	39.1	56.8	1.46
5	16.5	-	-	12.1	-	-
6	23.4	50.0	2.14	17.8	32.6	1.83
7	9.4	-	-	6.9	-	-
8	67.3	87.0	1.29	48.2	57.7	1.20
9	25.5	41.1	1.61	16.7	27.0	1.62

The photons emitted from the ^{252}Cf source are negligible and were in the case of the AHE measurement well shielded. However, the neutron induced photons in the shielding material and the environment must be considered. These photons result from the capture of thermal neutrons in certain target nuclei and nuclei characteristic energy peaks are observable. However, both measurement and recalculation in the current study indicate that the photon dose rates are negligible compared to neutron dose rate. The radiation field in the emplacement drift is dominated by neutrons.

Despite of the observed deficiency, the recalculation performed in the current study demonstrates the capability of the code to simulate the representing radiation field in such a disposal facility, which is characterized by the backscattering of the radiation due to the surrounding host rock layers.

Monte-Carlo calculations of the radiation field in a horizontal emplacement gallery of an underground nuclear waste disposal

MCNP6 is now applied to calculate the radiation field of a reference deep geological repository with a POLLUX container emplaced in an under-ground gallery [7]. A typical waste inventory [8] consists of a 50 years old (counting from unloaded from reactor) mixture of 89% spent DWR-UO_2 and 11% spent DWR-MOX fuel with a burn up of 55 GWd/tHM was considered in the current study.

Modeling of the POLLUX canister with MCNP6

Due to the geometrical complexity of the POLLUX container, some simplifications were conducted in the modeling (see Figure 4). The nuclear waste stored inside the internal cask was considered as an isotropic

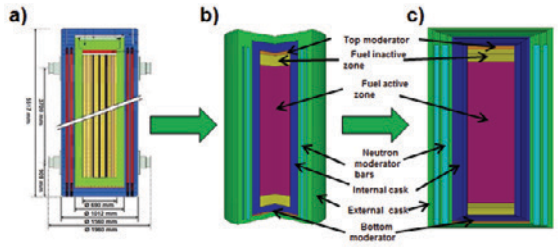

Fig. 4: Pollux geometry a) Original Model b) MCNP Model c) Geometry Splitting

volumetric source with an active and inactive zone, which represents top and bottom of the fuel assemblies. The finned elements at the outer surface were not considered. Due to the thickness of the double casks, the variance reduction technique "Geometry Splitting" in MCNP6 [2] was applied to keep the particle population penetrating the slices to be roughly constant.

Modeling of a horizontal emplacement gallery with MCNP

A rock salt gallery was chosen as the representative case, while a clay gallery covered with a concrete wall was defined as the comparative case. A third model with the walls replaced by air was also considered to represent the case of a POLLUX free in air. In order to obtain dose rates and spectra, various detector spheres filled with air were defined at different positions inside the gallery. Figure 5 shows both the gallery geometry and the detector sphere positions. The numbers in the name of the detectors indicate the distance of the respective detectors to the surfaces of the POLLUX container.

Results and discussion

Influence of the gallery in the ambient dose rate equivalent H(10)*

A comparison of the neutron dose rates between the rock salt gallery and the POLLUX in free air was shown in Figure 6. Due to the backscattered radiation, the dose rates are higher inside the gallery. The effect of the backscattered neutrons increases, when moving away from the POLLUX.

Contribution of the different particles to the total dose rate

Besides the neutrons and photons directly coming from the contained waste, interactions of neutrons with the materials of the POLLUX and the gallery produce photons with different energy levels. These secondary photons contribute also to the total dose

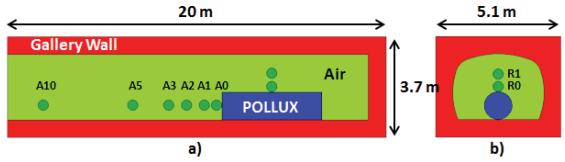

Fig. 5 MCNP6 model of a horizontal emplacement gallery a) Lateral View b) Frontal View

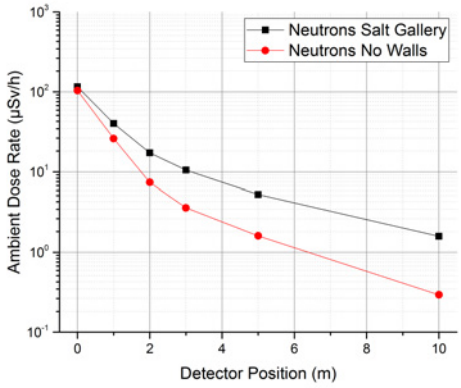

Fig. 6: Evolution of the neutrons ambient dose rate equivalent H(10) with and without salt walls*

rates. According to Figure 7, for the considered waste inventory in the current study, neutrons contribute more than 95% of the total dose rate. The dose rate due to the secondary photons is more than one order of magnitude lower than that of the neutrons. The contribution of the primary photons is negligible.

Influence of the gallery material on ambient dose rate equivalent H(10)*

The simulation of a clay gallery with concrete walls was performed to investigate the influence of the different gallery materials on the resulted dose rate.
As shown in Figure 8, the neutron dose rates in a clay

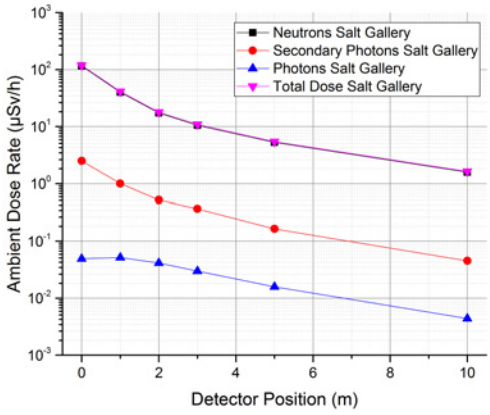

Fig. 7: Contribution from the different particle types to the total dose in a rock salt

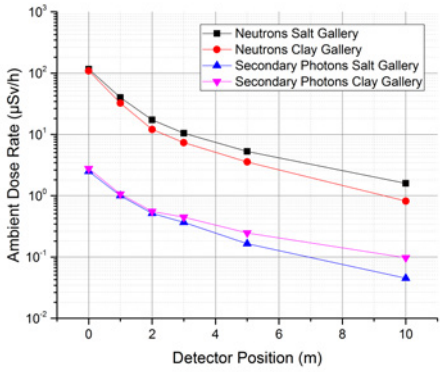

Fig. 8: Evolution of the ambient dose rate equivalent H(10) with rock salt and clay*

gallery are slightly lower than in a salt gallery, while the dose rates due to secondary photons are higher in the clay gallery. These differences should be attributed to the different scattering behavior of the materials in the salt and clay gallery.

References

[1] ENTRIA; Vorhabenbeschreibung zur Bildung einer Forschungsplattform: Entsorgungsoptionen für radioaktive Reststoffe: Interdisziplinäre Analysen und Entwicklung von Bewertungsgrundlagen

[2] Denise B. Pelowitz (editor); MCNP6 USER'S MANUAL, Version 1.0, May **2013**.

[3] H. J. Engelmann (project leader); Direkte Endlagerung ausgedienter Brennelemente DEAB (02 E 8472 7): aktives Handhabungsexperiment mit Neutronenquellen, TA 1: Berechnung der Ortsdosisleistung und Neutronenspektren vom POLLUX-Behälter, Einzelabschirmbehälter und Versuchsbehälter in einem Salzbergwerk; November 1995

[4] K. Knauf et al.; Neutron and photon spectra and dose rates around a shielding case placed in a salt mine to simulate a nuclear waste package; *Radiation Protection Dosimetry*, **70**(1-4):251-254, 1997.

[5] W. B. Wilson et al.; SOURCES 4C: A Code for Calculating (alpha,n), Spontaneous Fission, and Delayed Neutron Sources and Spectra; LA-UR-02-1839, 2002.

[6] ICRP; Data for Protection against Ionizing from External Sources – Supplement to ICRP Publication 15; ICRP Publication 21; 1973.

[7] Rocio P. Leon Vargas, Volker Mintzlaff and Joachim Stahlmann; Generische Tiefenlagermodelle mit Option zur Rückholung der radioaktiven Reststoffe; ENTRIA internal report, 2014.

[8] Peiffer McStocker, "Abfallspezifikation und Mengengerüst, Basis Ausstieg aus der Kernenergienutzung. Bericht zum Arbeitspaket 3 Vorläufige Sicherheitsanalyse für den Standort Gorleben, GRS-278," 2011

11.2 Assessment of the β/γ dose rate fields related to a spent nuclear fuel pellet

V. Romanello

Matrix dissolution of aged spent nuclear fuel is mainly controlled by radiolysis products formed by

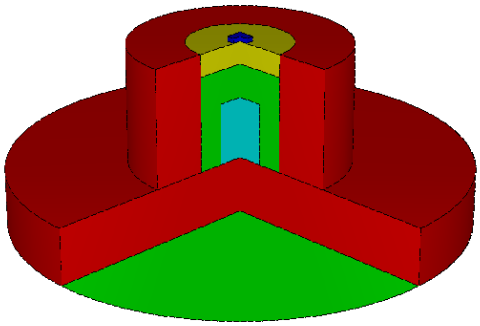

Fig. 1: MCNP model of the measurement cell

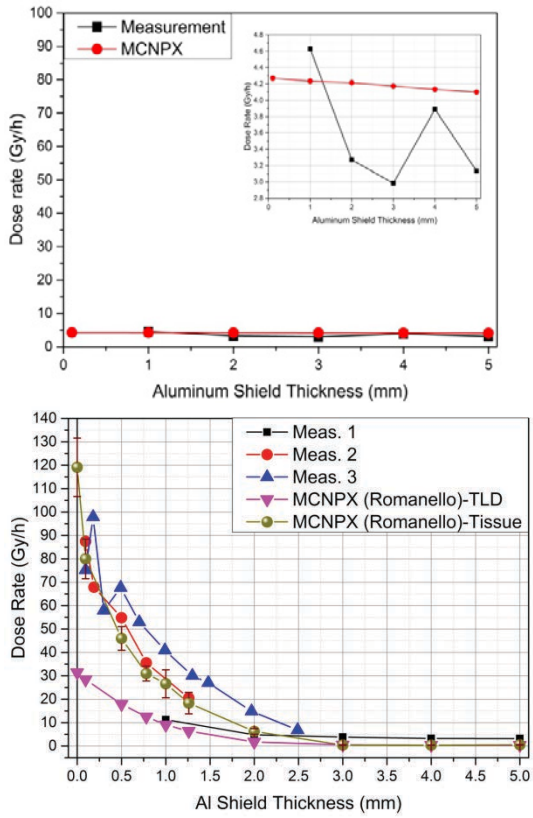

Fig. 2: Gamma and beta measurements Monte Carlo simulation assessment

radiation fields, therefore a comprehensive understanding of the radiolysis source term is required. In this frame I reproduced by Monte Carlo computer simulation the beta and gamma radiation rates associated to a Gösgen nuclear power plant (PWR) irradiated pellet measured by INE and SUM (results reported in Annual Report 2009 – Chapter 6). In particular the first task was to reproduce the pellet composition at the measurement date: for doing this I analyzed all the available data concerning reactor and fuel characteristics (materials, dimensions, burnup, irradiation time, etc.) and I simulated the full irradiation cycle both with Webkorigen and with a reactor-dedicated Monte Carlo code (Serpent-2) for comparison purposes: results were compared for consistency between them and with available experimental analysis, providing a reasonable agreement (despite some clear inconsistencies concerning plutonium concentration, attributable to experiments however).

As a second step the complete experimental setup (in a simplified configuration) was reproduced in MCNPX (Los Alamos National Laboratory developed code), consisting in a steel sleeve where the pellet was located, and an aluminum shield (increasing thicknesses were simulated, from ca. 0.1 to 5 mm) on top of which a TLD detector was deposited – the distance between the pellet surface and the TLD was kept constant (1 cm) – Fig. 1.

According to pellet composition the various beta and gamma radiations fields were calculated and used as a source term: the obtained Hp(0.07) dose rate (provided experimentally by SUM) was reproduced in a rather accurate way (considering the unavoidable experimental bias) – Fig. 2.

An estimate of the alpha, beta and gamma dose rate to a surrounding water layer (with a thickness from 10 µm to 1.5 cm) was estimated too by computer simulation.

Finally it was assessed also the alpha dose rate of a depleted uranium pellet doped with a proper plutonium composition with two different contents (i.e. 0.1% and 10%): in this case the provided composition decay was simulated and then the alpha radiation source determined; a model of the configuration (consisting of a TLD pellet encased in a Makrofol layer posed on the Pu-doped depleted U pellet) was reproduced with MCNPX and the dose rates evaluated. Comparison with measurements is still ongoing.

11.3 Simulated alpha dose at the surface of the rim zone of spent nuclear fuel pellets

F. Becker, B. Kienzler

Introduction

For light water nuclear power plants uranium oxide and/or mixed oxide (MOX) fuel is used. The nuclear fuel consists of cylindrical UO_2 tablets (pellets). These pellets are inserted in a cladding tube, usually made of a zirconium alloy, forming the fuel rod. The fuel rods are bundled in square arrangements forming the fuel elements. During irradiation in the reactor, fission products and transuranic elements (actinides) are formed. The fission products mainly cause the beta/gamma radioactivity whereas the actinides contribute to the alpha activity of the spent fuel. For the safety analysis of nuclear waste disposals, the potential radionuclide release (source term) is required. The source term depends on the dissolution of the UO_2 matrix of the spent nuclear fuel and on the related release of radionuclides. Unirradiated tetravalent UO_2 shows a low solubility as well as slow dissolution kinetics. However, investigations performed in the last decades revealed a different behavior of spent nuclear fuel: Due to the alpha-radiolysis, directly on the surface of the fuel pellets in contact with aqueous solutions, oxidizing species are formed causing oxidation of the tetravalent uranium to the hexavalent state which has significantly higher solubility. For a better understanding of the processes, deeper insight in the dose rate distribution at the surface of the spent nuclear fuel pellets and the related energy deposition is needed. As it is difficult to measure the α-particles dose rate directly, we calculated the dose rate induced by α-particles employing the code MCNPX [1].

Procedure for the simulations

Details of the following summary are published by the authors in reference [2]. For the simulations a pellet model, based on data for 48 GWd/tHM, was constructed for MCNPX. It consisted of a cylinder with a diameter of 9.2 mm and a height of 11.1 mm. The cylinder model was surrounded with a thin layer of water of 0.1 mm, to capture all of the deposited energy of the α particles. To account for the rim zone on the surface of the pellet, as shown in the top of fig. 1, the rim zone was divided in 10 segments each containing a different chemical inventory and density. This inventory was assigned as linear interpolation between experimental determined data for a pellet in the center and rim regions. The specific activity of the fuel was calculated with Korigen. α spectra of the decay of the nuclides were calculated for the 10 different inventories in the different regions of the pellet surface. They provided in turn the different source definitions for the input file of MCNPX. The cell energy deposition record (*F8 tally in MCNP) was used to obtain the total energy deposited in the water layer above each region. 10^8 "particle histories" were calculated with MCNPX in order to achieve a statistical accuracy better than 2%.

Results and discussion

In the lower part of fig. 1 the simulated dose distribution at the pellet surface with focus on the rim zone is shown. In the rim zone the local dose per emitted α-particle in a 0.1 mm thick layer of water varies between 1.4×10^{-10} and 1.9×10^{-10} Gy. Assuming an average specific α activity of 12 GBq/g results in the corresponding dose rates of 12 and 17 Gy/s, respectively. The result shows that in the rim zone the dose rate is increased about 50% in comparison to the center of the fuel pellet. This effect enhances the yield of oxidizing species close to the rim zone leading to an incongruent oxidation of UO_2 over the fuel pellet surface.

Radionuclide release from the fuel depends on dissolution processes of the UO_2 matrix, and the dissolu-

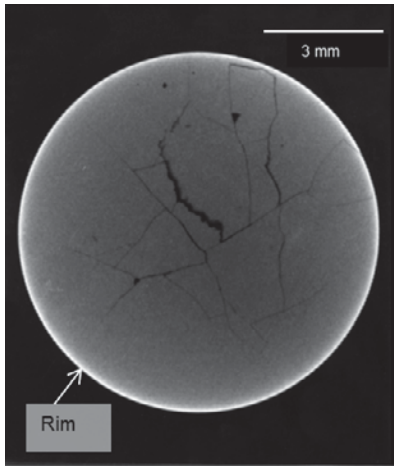

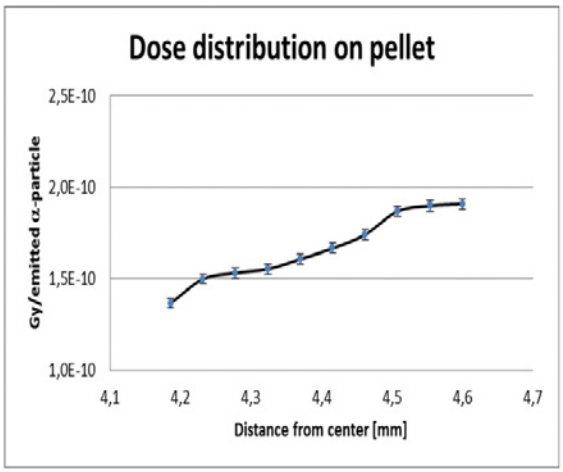

Fig. 1: α-radiography indicating the rim zone of a pellet (top) and simulated α-dose distribution on the surface of the outer region of the core and the rim zone (bottom).

tion rate of irradiated UO_2 is determined by oxidizing species formed by radiolysis of water in contact with fuel. As the dose rate and energy deposition at the pellet surface is difficult to measure, we simulated the dose rate induced by α-particles at the surface of the pellets deposited in a thin water layer. Furthermore, we took the rim zone of the fuel into consideration. As a result in the rim zone an increased α-dose level is observed. In the investigated case the local dose rate stemming from alpha particles could go up to 680 Gy/h. This is a factor 5 more than reported for similar cases with regard to β-dose rates and about a factor 200 more than for γ-dose rates [2]. The simulation shows clearly that the α-radiation field is dominant for the formation of oxidizing species in the case of water contact to spent nuclear fuel.

References

[1] D.B. Pelowitz, MCNPX User's Manual Version 2.6.0. Los Alamos National Laboratory, Tech. Rep. LA-CP-07-1473 (2008)

[2] Simulation of alpha dose for predicting radiolytic species at the surface of spent nuclear fuel pellets; *Open Chem*., 2015; **13**: 586–590, ISSN (Online) 2391-5420, DOI: 10.1515/chem-2015-0076, December 2014; Frank Becker, Bernhard Kienzler

12 Geoenergy

The focus of geoenergy research at INE concerns mainly geothermal energy research in fractured reservoir systems. In order to allow the assessment of particular hydro-mechanical and thermo-chemical processes related to fluid transport, relevant initial reservoir condition such as fracture porosity is imaged using advance gravimetric methods. A special focus is given to the reactivation potential of existing fractures during reservoir engineering, obtained from stress measurements and modeling. Possible heat sources in the mid-crustal level are investigated by magnetotelluric methods. To improve possibilities to observe changes in fluid pathways during hydro-mechanical processes, innovative experimental approaches in the development of advanced electric and electromagnetic monitoring techniques are pursued. Fundamental studies on the behavior of clay colloids in fluid flow on fractures ensure an improved characterization of fractures and further understanding of alteration processes in crystalline rock. The investigated geothermal systems cover naturally sufficiently permeable, hydrothermal systems to enhanced geothermal systems (EGS) that are stimulated either hydraulically or chemically. The work summarized in this section is related to (i) filter and stripping techniques in gravity, (ii) high-resolution magnetotellurics (iii) field experiments to develop electric and electromagnetic monitoring, (iv) laboratory experiments on colloid transport and deposition in fracture zones. The studies aims at characterizing fluid transport-related processes in the fractured environment.

Y. Abdelfettah, G. K. Darbha, F. Huber, Th. Schäfer, E. Schill, M. Stoll

In co-operation with:

S. Held[a], J. Meixner[a], P. Saillhac[b], P. Altwegg[c]

[a] AGW, Karlsruhe Institute of Technology, Germany, [b] EOST, Université de Strasbourg, France, [c] Université de Neuchâtel, Switzerland

Introduction

In Europe, major geothermal resources outside of the volcanic or metamorphic complexes in Iceland and Italy are contained within deep fractured crystalline rock at high differential stresses. Economic viable projects require about 50 L/s of flow at temperature > 130°C. There are a number of scientific challenges that limit environmentally friendly development of deep geothermal energy in these geothermal fields, today. Key issues relate mainly to sensible seismicity during enhancement of the reservoir performance and operation, as well as radioactive scaling.

The geothermal research at INE is embedded into Helmholtz Portfolio project *Environmentally friendly provision of local energy from georesources – Geoenergy*. Its scientific geothermal program addresses the issues of economically viable condition and low environmental impact by advanced exploration and monitoring methods. In this respect, fundamental research is needed in particular on the relations between fluid circulation, hydromechanics, alteration and geophysical properties such as electric resistivity. At present, the majority of the phenomena are investigated at reservoir level. This concerns innovative geophysical exploration techniques for the crystalline basement and based on this, the investigation of hydraulic condition in natural geothermal systems. Furthermore, new monitoring techniques are developed in order to study of processes related to reservoir engineering. First laboratory experiments have been started to study specific issues under controlled condition. This activity will be intensified at KIT-INE in the coming years.

INE is strongly involved in the preparation of the large-scale research infrastructure application GeoLaB. GeoLaB is planned as large-scale underground research facility for controlled high flow-rate (CHFE) experiments in fractured, crystalline basement. With the aim to investigate hydraulic, hydro-mechanic and heat transfer processes, and existing mine is envisaged to be equipped for such experiments. In this respect, exploration methods for the crystalline basement are validated and extended to larger frequency bands. This includes comparable to acoustic emission adding up to seismic monitoring, high frequency electromagnetic measurements. These ongoing developments will be completed in the following years.

Quantification of fracture porosity of geothermal reservoirs from gravity

Fracture porosity controls the performance of geothermal reservoirs and is, thus, a crucial parameter in geothermal exploration. Its determination is a major challenge, in particular, in the absence of nearby exploration wells. Negative gravity anomalies are found to be related to geothermally relevant structural features in the crystalline basement including fracture porosity along major fault zones of the Upper Rhine Graben [1].

Forward modeling of gravity anomalies based on a 3D seismic survey is used to estimate possible fracture porosity. After stripping gravity effects of geothermally irrelevant geological units from the residual anomaly, most likely only local structures related to the fault zone account for remaining anomalies. The approach includes the implementation of the Blakely algorithm [2] into a 3D forward modeling software and its application on the 3D geological models. The code allows the calculation of the gravity effects of the different individual geological units and structures of the model discretized into vertical prisms. These

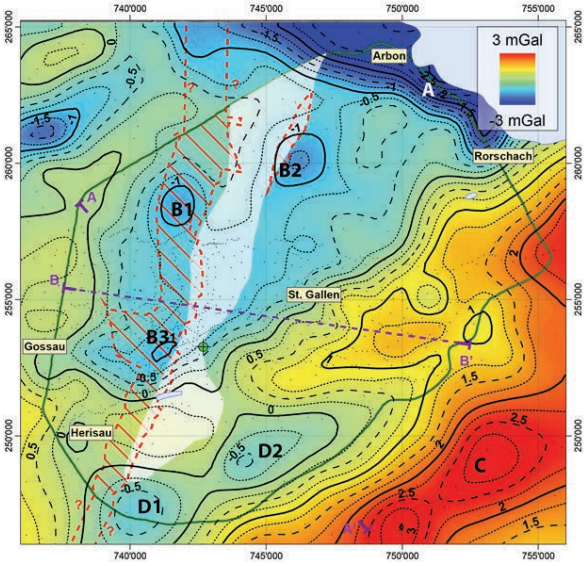

Fig. 1: Residual anomaly of the Sankt Gallen area obtained by applying polynomial regression. Black lines: 1 mGal isolines, dashed lines: 0.5 mGal, dotted lines: 0.25 mGal. Red dashed area: considered damage zone of the fault, white area: outline of the seismically top Permo-Carboniferous. Swiss coordinates (CH 1903) are used.

effects can then be subtracted from the measured data and thus, the code allows for sequential stripping.

The methodology has been tested in the Sankt Gallen geothermal project. This project targets a fault zone that affects Mesozoic sediments at a depth of about 4500 m. Spatial extension of these sediments, a major fault zone and indication for graben structures in the crystalline basement are observed in 3D seismic. Both the graben and the fault zone coincide with negative gravity anomalies (Fig. 1).

Synthetic case study on the effect of density variation and considerable gas content in the well support possible fracture porosity between about 4 and 8%.

Mid-crustal electric anomalies

Geothermal anomalies in high-enthalpy regions are often connected to granitic intrusions representing their heat source. They are typically identified by electric resistivity anomalies that originate clay minerals formed during hydrothermal alteration above the intrusion in the so-called cap layer. These layers are identified using magnetotelluric methods.

In some cases, however, specific tectonic features lead to the absence of high-enthalpy resources even near very active volcanoes. This coincides also with the absence of cap-layers. However, very low resistivity anomalies are found at mid-crustal depth (Fig. 2). Different hypotheses such as partial melting, aquatic fluids linked to fault zones [4], graphitic layers, sulphides or metamorphic processes, have been postulated to explain such mid-crustal anomalies. Against this background, high-resolution magnetotelluric and hydro-chemical data were acquired to investigate the second hypothesis.

Oxygen isotopy (Fig. 3), chlorofluorocarbon, Sr-isotopy and sulfate geothermometry indicated meteoric water origin (Fig. 3), local circulation paths and low reservoir temperatures without magmatic contribution.

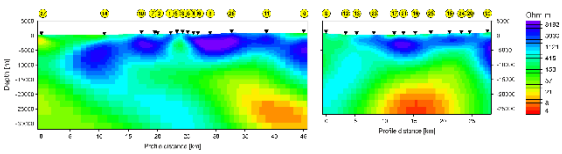

Fig. 2: 2D inversion of magnetotelluric data across the Liquiñe-Ofqui fault zone in southern Chile (left, E-W) and parallel to the fault near Mt. Villarica (right, N-S).

Similarly, the magnetotelluric data do not reveal a direct connection between the mid-crustal resistivity anomaly and Liquiñe-Ofqui fault zone.

Towards magnetotelluric monitoring of fracture re-activation

Changes in fluid pathways in the subsurface induced during geothermal reservoir engineering and production are typically inferred from micro-seismic monitoring. Micro-seismicity typically localizes shear processes at high resolution. Information on fracture connectivity or fluid content is difficult to obtain. In contrast, electromagnetic methods are of comparably lower resolution since they base on the diffusion equation. On the other hand, electromagnetic methods are sensitive to conductivity contrasts that are an indicator of fracture connectivity.

Magnetotelluric measurements before and after an injection experiment a ~3.6 km deep EGS reservoir at Paralana (South Australia) suggest transient variations in subsurface conductivity structure generated from the introduction of fluids at depth [3]. Furthermore, phase tensor representation of the time dependent MT response suggests fluids migrated in a NE direction from the injection well. Relative phase difference tensor is defined from the phase tensors at two different dates.

The relative phase difference tensor at a given frequency can be represented by an ellipse. In this way, a simple scalar can be used to represent the relative phase difference.

Preliminary results from a first field experiment using continuous monitoring reveals changes of the

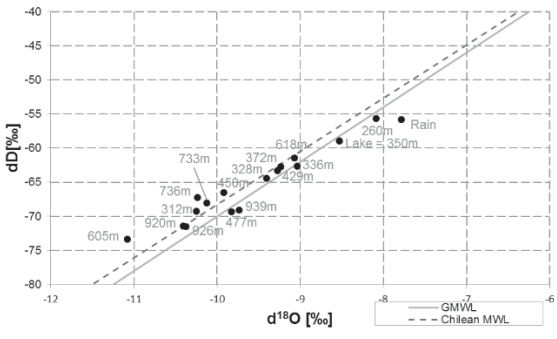

Fig. 3: Oxygen isotopic composition of geothermal springs at Mt. Villarrica, southern Chile. Global and Chilean meteoric water line are shown in grey and dashed lines, respectively. Altitudes of springs is indicated.

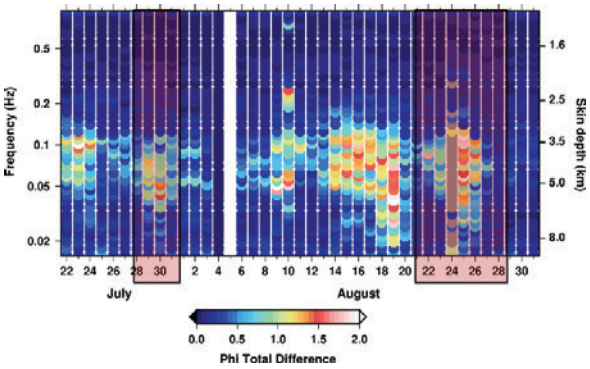

Fig. 4: Phase differences between 2014-07-22 and 2014-08-31 relative to 2014-08-04 at frequencies between 10^{-2} and 1 Hz, representing a depth range of about 1 and 8 km. Red shaded areas represent the periods of injection into the well GRT-1 and 2 at Rittershoffen.

phase differences with respect to 2014-08-05 during the injection/production periods into two different wells GRT-1 (2014-08-21 to 2014-08-29) and GRT-2 (2014-07-28 to 2014-08-01) that assess the reservoir (Fig. 4). The reference has been chosen based on data quality.

We would like to point out that there are strong changes indicated in periods before and in-between the injection/production operations. The identification of processes related to these changes is ongoing. Micro-seismic activity will be used as reference.

Particle retention on granite using a synthetic fracture flow cell

Clay coating of fracture zones modifies strongly the hydraulic and mechanical properties. On the one hand, clay may completely clog a fracture and on the other hand, it may reduce the shear strength of rock and thus, lead to more favorable condition for hydraulic stimulation [5].

In order to understand the accumulation and mobilization of clay particles in hydraulically active fractures, flow cell experiments have been carried out in the laboratory of INE. A cylindrical parallel plate type fracture flow cell (diameter 38 mm; aperture 0.75 mm) has been designed for the transport experiments. The artificial fracture of flow cell is sandwich of acrylic glass and/or granite. At the flow cell's outlet the breakthrough curves/residence time distributions are obtained continuously by means of fluorescence spectroscopy and by photon correlation spectroscopy (PCS)/ laser induced breakdown detection (LIBD) and single particle counting (SPC), respectively. All experiments are conducted at pH 5 under low ionic strength (1 mM NaCl). For post mortem analysis of the granitic fracture surface fluorescence microscopy, scanning electron microscopy and laser scanning microscopy are applied to obtain information on the colloid deposition/attachment behavior

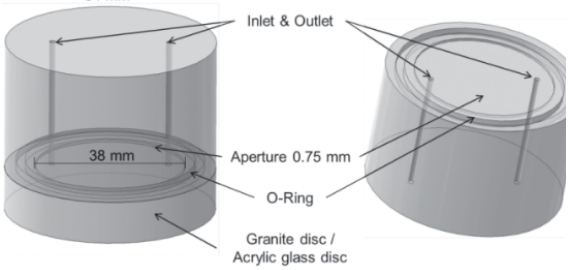

Fig. 5: Sketch of the synthetic fracture flow cell with a internal diameter of 38 mm and aperture of the synthetic fracture of 0.75 mm. The distance between in- and outflow is 29.8 mm. The upper part is made of acrylic glass (right) and the lower part of the cell is exchangeable.

and spatial distribution as a function of e.g. mineralogy and/or surface roughness [6].

In preliminary studies, the interaction of monodisperse fluorescent carboxylated polystyrene particles (25 nm and 1000 nm in diameter) with a cut granodiorite surface from Grimsel (Switzerland) is investigated both, experimentally and numerically. The results are compared to experiments using natural polydisperse clay particles mainly consisting of illite (bimodal size distribution with maxima at ~1000 nm and 20-40 nm). These particles are obtained from hydrothermal altered natural fractured granite drill cores from Soultz-sous-Forêts; France). The focus of the study is the effect of residence time, colloid size and fracture orientation on colloid retention. Long residence times is accomplished by stop-flow experiments between 1 h and 24 h. In addition to the colloids, a conservative solute tracer (Amino-G) is added to the system to characterize the flow and transport conditions. Results show earlier first arrivals and more pronounced tailings in the measured breakthrough curves for the colloids compared to the conservative tracer. A positive correlation between residence time and particle retention is observed in all experiments. The experimental findings are corroborated by 2-D and 3-D numerical simulations and highlight the influence of sedimentation processes being relevant even for low-density latex microspheres as a retention process.

References

[1] Bailllieux, P. et al., *Geothermal energy Journal*, **2**:16, (2014)

[2] Blakely, R.J., *Cambridge University Press* (1996).

[3] Peacock J.R., et al., *Geophysics*, **78**, B121-130 (2013).

[4] Brasse, H., et al., *Physics Earth Planet. Int.* **173**, 1 (2009).

[5] Evans, K. F., et al., *Geophys. J. Int.* **160**, 1 (2005)

[6] Darbha, G., Fischer, C., Luetzenkirchen, J., Schäfer, Th., *Environ. Science Tech.* **46**, 17, (2012)

13 Publications

ISI/SCOPUS

[1] Afsar, A.; Laventine, D. L.; Harwood, L. M.; Hudson, M. J.; Geist, A., *Immobilisation of Phenanthroline-Bis Triazine (C1-Btphen) on Magnetic Nanoparticles for Co-Extraction of Americium(III) and Europium(III)*, *Heterocycles* **2014**, *88*, 613-620.

[2] Afsar, A.; Westwood, J.; Harwood, L. M.; Hudson, M. J.; Laventine, D. M.; Geist, A., *The effect of alkyl substitution on the extraction properties of BTPhen ligands for the partitioning of trivalent minor actinides and lanthanides in spent nuclear fuels*, *Jordan J. Chem.* **2014**, *9*, 50-58.

[3] Altmaier, M.; Duro, L.; Grivé, M.; Montoya, V.; Buckau, G.; Kienzler, B., *RECOSY: "Understanding of Redox Phenomena Controlling the Long-term Release/Retention of Radionuclides in Nuclear Waste Disposal*, *EURADWASTE '13, 8th EC Conference on the Management of Radioactive Waste Community Policy and Research on Disposal*, Vilnius, Lithuania, **2014**

[4] Autillo, M.; Kaden, P.; Geist, A.; Guerin, L.; Moisy, P.; Berthon, C., *The influence of radioactive decay on actinide magnetic susceptibility measurements obtained using the Evans method*, *Phys Chem Chem Phys* **2014**, *16*, 8608-8614.

[5] Bach, D.; Christiansen, B. C.; Schild, D.; Geckeis, H., *TEM study of Green Rust Sodium Sulphate (GR(NA,SO_4)) Interacted with Neptunyl Ions (NpO^{2+})*, *Radiochim Acta* **2014**, *102*, 279-289.

[6] Banik, N. L.; Brendebach, B.; Marquardt, C. M., *Investigations of actinides in the context of final disposal of high-level radioactive waste: trivalent actinides in aqueous solution*, *J Radioanal Nucl Ch* **2014**, *300*, 177-183.

[7] Bauer, N.; Fröhlich, D. R.; Panak, P. J., *Interaction of Cm(III) and Am(III) with human serum transferrin studied by time-resolved laser fluorescence and EXAFS spectroscopy*, *Dalton T* **2014**, *43*, 6689-6700.

[8] Beattie, J. K.; Djerdjev, A. M.; Gray-Weale, A.; Kallay, N.; Lützenkirchen, J.; Preocanin, T.; Selmani, A., *pH and the surface tension of water*, *J Colloid Interf Sci* **2014**, *422*, 54-57.

[9] Becker, F.; Kienzler, B., *Simulation of alpha dose for predicting radiolytic species at the surface of spent nuclear fuel pellets*, *Open Chemistry* **2014**, *Band 13*.

[10] Bohler, R.; Welland, M. J.; Prieur, D.; Cakir, P.; Vitova, T.; Pruessmann, T.; Pidchenko, I.; Hennig, C.; Gueneaud, C.; Konings, R. J. M.; Manara, D., *Recent advances in the study of the UO_2-PuO_2 phase diagram at high temperatures*, *J Nucl Mater* **2014**, *448*, 330-339.

[11] Bremer, A.; Whittaker, D. M.; Sharrad, C. A.; Geist, A.; Panak, P. J., *Complexation of Cm(III) and Eu(III) with $CyMe_4$-BTPhen and $CyMe_4$-BTBP studied by time resolved laser fluorescence spectroscopy*, *Dalton T* **2014**, *43*, 2684-2694.

[12] Bube, C.; Metz, V.; Schild, D.; Rothe, J.; Dardenne, K.; Lagos, M.; Plaschke, M.; Kienzler, B., *Combining thermodynamic simulations, element and surface analytics to study U(VI) retention in corroded cement monoliths upon > 20 years of leaching*, *Phys Chem Earth* **2014**, *70-71*, 53-59.

[13] Caisso, M.; Lebreton, F.; Horlait, D.; Picart, S.; Martin, P. M.; Bes, R.; Renard, C.; Roussel, P.; Neuville, D. R.; Dardenne, K.; Rothe, J.; Delahaye, T.; Ayral, A., *Nanostructured gadolinium-doped ceria microsphere synthesis from ion exchange resin: Multi-scale in-situ studies of solid solution formation*, *J Solid State Chem* **2014**, *218*, 155-163.

[14] Carrott, M.; Bell, K.; Brown, J.; Geist, A.; Gregson, C.; Heres, X.; Maher, C.; Malmbeck, R.; Mason, C.; Modolo, G.; Müllich, U.; Sarsfield, M.; Wilden, A.; Taylor, R., *Development of a New Flowsheet for Co-Separating the Transuranic Actinides: The "Euro-Ganex" Process*, *Solvent Extr Ion Exc* **2014**, *32*, 447-467.

[15] Catrouillet, C.; Davranche, M.; Dia, A.; Bouhnik-Le Coz, M.; Marsac, R.; Pourret, O.; Gruau, G., *Geochemical modeling of Fe(II) binding to humic and fulvic acids*, *Chem Geol* **2014**, *372*, 109-118.

[16] Deschamps, E.; Weidler, P. G.; Friedrich, F.; Weiss, C.; Diabate, S., *Characterization of indoor dust from Brazil and evaluation of the cytotoxicity in A549 lung cells*, *Environ Geochem Hlth* **2014**, *36*, 225-233.

[17] Duro, L.; Bruno, J.; Grive, M.; Montoya, V.; Kienzler, B.; Altmaier, M.; Buckau, G., *Redox processes in the safety case of deep geological repositories of radioactive wastes. Contribution of the European RECOSY Collaborative Project*, *Appl Geochem* **2014**, *49*, 206-217.

[18] Duro, L.; Bruno, J.; Grivé, M.; Montoya, V.; Kienzler, B.; Altmaier, M.; Buckau, G., *Redox Processes in the Safety Case of Deep Geological Repositories of Radioactive Wastes – Contribution of the European RECOSY Collaborative Project*, *EURADWASTE '13, 8th EC Conference on the Management of Radioactive Waste Community Policy and Research on Disposal*, Vilnius, Lithuania, **2014**

[19] Fischer, C.; Kurganskaya, I.; Schäfer, T.; Luttge, A., *Variability of crystal surface reactivity: What do we know?*, *Appl Geochem* **2014**, *43*, 132-157.

[20] González-Robles, E.; Fuß, M.; Bohnert, E.; Müller, N.; Herm, M.; Metz, V.; Kienzler, B., *Study of the release of the fission gases (Xe and Kr) and the fission products (Cs and I) under anoxic conditions in bicarbonate water*, *Scientific Basis of Nuclear Waste Management*, Boston, USA, **2014**

[21] González-Robles, E.; Wegen, D. H.; Bohnert, E.; Papaioannou, D.; Müller, N.; Nasyrow, R.; Kienzler, B.; Metz, V., *Physico-chemical characterization of a spent UO_2 fuel with respect to its stability under final disposal conditions*, *MRS Online Proceedings Library*, **2014**

[22] González-Robles, E.; Wegen, D. H.; Papaioannou, D.; Kienzler, B.; Nasyrow, R.; Metz, V., *Physical Characterisation of Spent Nuclear Fuel: First Steps to Further Instant Release Fractions Investigations*, *EURADWASTE '13, 8th EC Conference on the Management of Radioactive Waste Community Policy and Research on Disposal*, Vilnius, Lithuania, **2014**

[23] Heberling, F.; Bosbach, D.; Eckhardt, J. D.; Fischer, U.; Glowacky, J.; Haist, M.; Kramar, U.; Loos, S.; Müller, H. S.; Neumann, T.; Pust, C.; Schäfer, T.; Stelling, J.; Ukrainczyk, M.; Vinograd, V.; Vucak, M.; Winkler, B., *Reactivity of the calcite-water-interface, from molecular scale processes to geochemical engineering*, *Appl Geochem* **2014**, *45*, 158-190.

[24] Heberling, F.; Eng, P.; Denecke, M. A.; Lützenkirchen, J.; Geckeis, H., *Electrolyte layering at the calcite(104)-water interface indicated by Rb^+- and Se(VI) K-edge resonant interface diffraction*, *Phys Chem Chem Phys* **2014**, *16*, 12782-12792.

[25] Heberling, F.; Vinograd, V. L.; Polly, R.; Gale, J. D.; Heck, S.; Rothe, J.; Bosbach, D.; Geckeis, H.; Winkler, B., *A thermodynamic adsorption/entrapment model for selenium(IV) coprecipitation with calcite*, *Geochim Cosmochim Ac* **2014**, *134*, 16-38.

[26] Hofmann, S.; Voitchovsky, K.; Schmidt, M.; Stumpf, T., *Trace concentration - Huge impact: Nitrate in the calcite/Eu(III) system*, *Geochim Cosmochim Ac* **2014**, *125*, 528-538.

[27] Huber, F. M.; Heck, S.; Truche, L.; Bouby, M.; Brendlé, J.; Hoess, P.; Schäfer, T., *Radionuclide desorption kinetics on synthetic Zn/Ni-labeled montmorillonite nanoparticles*, *Geochim Cosmochim Ac* **2014**, *148*, 426-441.

[28] Hudry, D.; Apostolidis, C.; Walter, O.; Janssen, A.; Manara, D.; Griveau, J. C.; Colineau, E.; Vitova, T.; Pruessmann, T.; Wang, D.; Kubel, C.; Meyer, D., *Ultra-Small Plutonium Oxide Nanocrystals: An Innovative Material in Plutonium Science*, *Chem-Eur J* **2014**, *20*, 10431-10438.

[29] Janecek, J.; Netz, R. R.; Flörsheimer, M.; Klenze, R.; Schimmelpfennig, B.; Polly, R., *Influence of Hydrogen Bonding on the Structure of the (001) Corundum-Water Interface. Density Functional Theory Calculations and Monte Carlo Simulations*, *Langmuir* **2014**, *30*, 2722-2728.

[30] Jordan, N.; Ritter, A.; Scheinost, A. C.; Weiss, S.; Schild, D.; Hubner, R., *Selenium(IV) Uptake by Maghemite (gamma-Fe_2O_3)*, *Environ Sci Technol* **2014**, *48*, 1665-1674.

[31] Kienzler, B.; Borkel, C.; Finck, N.; Heck, S.; Hilpp, S.; Schlieker, M.; Metz, V.; Plaschke, M.; Soballa, E.; Cron, T.; Miassoedov, A., *Characterization and radionuclide retention properties of heat-treated concrete*, *Phys Chem Earth* **2014**, *70-71*, 45-52.

[32] Kienzler, B.; Loida, A.; González-Robles, E.; Müller, N.; Metz, V., *Fast/Instant Radionuclide Release: Effects inherent to the experiment*, *Materials Research Society (MRS) Online Proceedings Library*, **2014**

[33] Kienzler, B.; Metz, V.; González-Robles, E.; Duro, L.; Valls, A.; Wegen, D.; Carbol, P.; Serrano-Purroy, D.; Curtius, H.; Günther-Leopold, I.; Zumbiehl, A. F.; Curti, E.; Lemmens, K.; Vandenborre, J.; Pablo, J. D.; Casas, I.; Clarens, F.; Hózer, Z.; Roth, O., *FIRST-NUCLIDES: "Fast / Instant release of safety relevant radionuclides from spent nuclear fuel"*, *EURADWASTE '13, 8th EC Conference on the Management of Radioactive Waste Community Policy and Research on Disposal*, Vilnius, Lithuania, **2014**

[34] Kratsch, J.; Beele, B. B.; Koke, C.; Denecke, M. A.; Geist, A.; Panak, P. J.; Roesky, P. W., *6-(Tetrazol-5-yl)-2,2 '-bipyridine: A Highly Selective Ligand for the Separation of Lanthanides(III) and Actinides(III)*, *Inorg Chem* **2014**, *53*, 8949-8958.

[35] Kurtukian-Nieto, T.; Benlliure, J.; Schmidt, K. H.; Audouin, L.; Becker, F.; Blank, B.; Casarejos, E.; Farget, F.; Fernandez-Ordonez, M.; Giovinazzo, J.; Henzlova, D.; Jurado, B.; Pereira, J.; Yordanov, O., *Production cross sections of heavy neutron-rich nuclei approaching the nucleosynthesis r-process path around A=195*, *Phys Rev C* **2014**, *89*.

[36] Kurtukian-Nieto, T.; Benlliure, J.; Schmidt, K.-H.; Audouin, L.; Becker, F.; Blank, B.; Borzov, I. N.; Casarejos, E.; Farget, F.; Fernández-Ordóñez, M.; Giovinazzo, J.; Henzlova, D.; Jurado, B.; Langanke, K.; Martínez-Pinedo, G.; Pereira, J.; Yordanov, O., *Beta-decay half-lives of new neutron-rich isotopes of Re, Os and Ir approaching the r-process path near N = 126*, *European Physical Journal A* **2014**, *50*, 1-8.

[37] Lin, D. H. M.; Manara, D.; Lindqvist-Reis, P.; Fanghänel, T.; Mayer, K., *The use of different dispersive Raman spectrometers for the analysis of uranium compounds*, *Vib Spectrosc* **2014**, *73*, 102-110.

[38] Lützenkirchen, J.; Abdelmonem, A.; Weerasooriya, R.; Heberling, F.; Metz, V.; Marsac, R., *Adsorption of dissolved aluminum on sapphire-c and kaolinite: implications for points of zero charge of clay minerals*, *Geochem T* **2014**, *15*.

[39] Marsac, R.; Banik, N. L.; Marquardt, C. M.; Kratz, J. V., *Stabilization of polynuclear plutonium(IV) species by humic acid*, *Geochim Cosmochim Ac* **2014**, *131*, 290-300.

[40] Martel, L.; Vigier, J. F.; Prieur, D.; Nourry, S.; Guiot, A.; Dardenne, K.; Boshoven, J.; Somers, J., *Structural Investigation of Uranium-Neptunium Mixed Oxides Using XRD, XANES, and O-17 MAS NMR*, *J Phys Chem C* **2014**, *118*, 27640-27647.

[41] Modolo, G.; Wilden, A.; Kaufholz, P.; Bosbach, D.; Geist, A., *Development and demonstration of innovative partitioning processes (i-SANEX and 1-cycle SANEX) for actinide partitioning*, *Prog Nucl Energ* **2014**, *72*, 107-114.

[42] Nargang, T. M.; Brockmann, L.; Nikolov, P. M.; Schild, D.; Helmer, D.; Keller, N.; Sachsenheimer, K.; Wilhelm, E.; Pires, L.; Dirschka, M.; Kolew, A.; Schneider, M.; Worgull, M.; Giselbrecht, S.; Neumann, C.; Rapp, B. E., *Liquid polystyrene: a room-temperature photocurable soft lithography compatible pour-and-cure-type polystyrene*, *Lab Chip* **2014**, *14*, 2698-2708.

[43] Nunez, U. C.; Eloirdi, R.; Prieur, D.; Martel, L.; Honorato, E. L.; Farnan, I.; Vitova, T.; Somers, J., *Structure of UC_2 and U_2C_3: XRD, C-13 NMR and EXAFS study*, *J Alloy Compd* **2014**, *589*, 234-239.

[44] Retegan, T.; Drew, M.; Ekberg, C.; Engdahl, E. L.; Hudson, M. J.; Fermvik, A.; Foreman, M. R. S.; Modolo, G.; Geist, A., *Synthesis and Screening of t-Bu-CyMe$_4$-BTBP, and Comparison with CyMe$_4$-BTBP*, *Solvent Extr Ion Exc* **2014**, *32*, 720-736.

[45] Rosenberg, Y. O.; Sadeh, Y.; Metz, V.; Pina, C. M.; Ganor, J., *Nucleation and growth kinetics of $Ra_xBa_{1-x}SO_4$ solid solution in NaCl aqueous solutions*, *Geochim Cosmochim Ac* **2014**, *125*, 290-307.

[46] Schoepff, V.; Almasi, I.; Amgarou, K.; Becker, F.; Carrel, F.; Carvajal, F.; Gaboriau, D. C.; Gmar, M.; Kelemen, A.; Kovacs, A.; Kovacs-Szeles, E.; Lemaire, H.; Menaa, N.; Mesterhazy, D.; Morat, L.; Morrison, C. G.; Perez-Llopis, I.; Raskob, W.; Robbe, M. F.; Szabo, S.; Testard, I.; Trybushnyi, D.; Ugolin, N.; Viau, M.; Vincze, A., *BOOSTER: Development of a Toolbox for Triage of Large Groups of Individuals Exposed to Radioactive Material*, *Ieee T Nucl Sci* **2014**, *61*, 2210-2216.

[47] Scholler, M.; Abbasi, M.; Friedrich, F., *Tranzschelia in the Americas revisited: two new species and notes on the Tranzschelia thalictri complex*, *Mycologia* **2014**, *106*, 448-455.

[48] Seiler, A.; Bauder, O.; Ibrahimkutty, S.; Pradip, R.; Pruessmann, T.; Vitova, T.; Fiederle, M.; Baumbach, T.; Stankov, S., *Growth and structure characterization of $EuSi_2$ films and nanoislands on vicinal Si(001) surface*, *J Cryst Growth* **2014**, *407*, 74-77.

[49] Selmani, A.; Lützenkirchen, J.; Kallay, N.; Preocanin, T., *Surface and zeta-potentials of silver halide single crystals: pH-dependence in comparison to particle systems*, *J Phys-Condens Mat* **2014**, *26*.

[50] Serrano-Purroy, D.; Aldave de las Heras, L.; Glatz, J.-P.; Benes, O.; Colle, J.-Y.; Sureda, R.; González-Robles, E.; de Pablo, J.; Casas, I.; Barrachin, M.; Dubourg, R.; Martínez-Esparza, A., *Interpretation of Knudsen Cell Experiments to determine the Instant Release Fraction in Spent Fuel Corrosion Scenarios by using a Mechanistic Approach: the Caesium Case Materials Research Society Symposium Proceedings*, **2014**

[51] Shinonaga, T.; Steier, P.; Lagos, M.; Ohkura, T., *Airborne Plutonium and Non-Natural Uranium from the Fukushima DNPP Found at 120 km Distance a Few Days after Reactor Hydrogen Explosions*, *Environ Sci Technol* **2014**, *48*, 3808-3814.

[52] Skerencak-Frech, A.; Fröhlich, D. R.; Rothe, J.; Dardenne, K.; Panak, P. J., *Combined Time-Resolved Laser Fluorescence Spectroscopy and Extended X-ray Absorption Fine Structure Spectroscopy Study on the Complexation of Trivalent Actinides with Chloride at T=25-200 degrees C*, *Inorg Chem* **2014**, *53*, 1062-1069.

[53] Tirumalasetty, G. K.; Fang, C. M.; Jansen, J.; Yokosawa, T.; Boeije, M. F. J.; Sietsma, J.; van Huis, M. A.; Zandbergen, H. W., *Structural tale of two novel (Cr, Mn)C carbides in steel*, *Acta Mater* **2014**, *78*, 161-172.

[54] Tits, J.; Gaona, X.; Laube, A.; Wieland, E., *Influence of the redox state on the neptunium sorption under alkaline conditions: Batch sorption studies on titanium dioxide and calcium silicate hydrates*, *Radiochim Acta* **2014**, *102*, 385-400.

[55] Vitova, T.; Mangold, S.; Paulmann, C.; Gospodinov, M.; Marinova, V.; Mihailova, B., *X-ray absorption spectroscopy of Ru-doped relaxor ferroelectrics with a perovskite-type structure*, *Phys Rev B* **2014**, *89*.

[56] Volz, D.; Wallesch, M.; Grage, S. L.; Göttlicher, J.; Steininger, R.; Batchelor, D.; Vitova, T.; Ulrich, A. S.; Heske, C.; Weinhardt, L.; Baumann, T.; Bräse, S., *Labile or Stable: Can Homoleptic and Heteroleptic PyrPHOS-Copper Complexes Be Processed from Solution?*, *Inorg Chem* **2014**, *53*, 7837-7847.

[57] Vrba, T.; Nogueira, P.; Broggio, D.; Caldeira, M.; Capello, K.; Fantinova, K.; Figueira, C.; Hunt, J.; Leone, D.; Murugan, M.; Marzocchi, O.; Moraleda, M.; Shutt, A.; Suh, S.; Takahashi, M.; Tyminska, K.; Lopez, M. A.; Tanner, R., *EURADOS intercomparison exercise on MC modeling for the in-vivo monitoring of Am-241 in skull phantoms (Part I)*, *Radiat Phys Chem* **2014**, *104*, 332-338.

[58] Wallner, A.; Belgya, T.; Bichler, M.; Buczak, K.; Dillmann, I.; Kappeler, F.; Lederer, C.; Mengoni, A.; Quinto, F.; Steier, P.; Szentmiklosi, L., *Novel Method to Study Neutron Capture of U-235 and U-238 Simultaneously at keV Energies*, *Phys Rev Lett* **2014**, *112*.

[59] Walshe, A.; Pruessmann, T.; Vitova, T.; Baker, R. J., *An EXAFS and HR-XANES study of the uranyl peroxides* $[UO_2(h^2\text{-}O_2)(H_2O)_2].nH_2O$ *(n=0, 2) and uranyl (oxy)hydroxide* $[(UO_2)_4O(OH)_6].6H_2O$, *Dalton T* **2014**, *43*, 4400-4407.

[60] Wilden, A.; Modolo, G.; Lange, S.; Sadowski, F.; Beele, B. B.; Skerencak-Frech, A.; Panak, P. J.; Iqbal, M.; Verboom, W.; Geist, A.; Bosbach, D., *Modified Diglysamides for the An(III) plus Ln(III) Co-separation: Evaluation by Solvent Extraction and Time-resolved Laser Fluorescence Spectroscopy*, *Solvent Extr Ion Exc* **2014**, *32*, 119-137.

[61] Yalçintaş, E.; Gaona, X.; Scheinost, A. C.; Kobayashi, T.; Altmaier, M.; Geckeis, H., *Redox chemistry of Tc(VII)/Tc(IV) in dilute to concentrated NaCl and* $MgCl_2$ *solutions*, *Radiochim Acta* **2014**, *103*, 57–72.

[62] Yan, M. Q.; Korshin, G. V.; Claret, F.; Croue, J. P.; Fabbricino, M.; Gallard, H.; Schäfer, T.; Benedetti, M. F., *Effects of charging on the chromophores of dissolved organic matter from the Rio Negro basin*, *Water Res* **2014**, *59*, 154-164.

Other referred publications

[63] Bahl, S.; Kutzer, A.; Roth, G.; Geckeis, H.; Vitova, T., *Investigation of Ca, Ba and Cs molybdates in a Mo bearing borosilicate glass*, *ANKA User Reports 2012/2013*, KIT, **2014**, pp. 137-138.

[64] Banik, N. L.; Marsac, R.; Marquardt, C. M.; Rothe, J., *XAFS studies of NpO^{2+} behavior on Illite*, *ANKA User Reports 2012/2013*, KIT, **2014**, pp. 24-25.

[65] Bauer, A.; Velde, B., *Geochemistry at the Earth's Surface: Movement of Chemical Elements*, **2014**

[66] Bauer, N.; Fröhlich, D. R.; Dardenne, K.; Rothe, J.; Panak, P. J., *EXAFS investigation on actinide and lanthanide transferrin complexes*, *ANKA User Reports 2012/2013*, KIT, **2014**, pp. 12-13.

[67] Bauer, N.; Fröhlich, D. R.; Dardenne, K.; Rothe, J.; Panak, P. J., *EXAFS investigation on actinide and lanthanide transferrin complexes*, *ANKA User Reports 2012/2013*, KIT, **2014**, pp. 139-140.

[68] Becker, F.; Göpfert, F.; Figueira, C.; Blunck, C., *Application of hand phantoms in simulations to determine the radiation exposure of medical staff*, *Progress in Nuclear Science and Technology* **2014**, *4*, 891-895.

[69] Becker, F.; Zhang, G., *Monte Carlo calculations for the determination of the radiation field in an interim storage facility*, *Progress in Nuclear Science and Technology* **2014**, *4*, 807-811.

[70] Bouby, M.; Geckeis, H.; Lützenkirchen, J.; Mihai, S.; Schäfer, T., *Interaction of bentonite colloids with Cs, Eu, Th and U in presence of humic acid: a Flow Field-Flow Fractionation study*, *KIT Scientific Reports, Colloid/nanoparticle formation and mobility in the context of deep geological nuclear waste disposal* (Eds.: F. Huber, U. Noseck, T. Schäfer), KIT, **2014**, pp. 32-52.

[71] Bremer, A.; Ruff, C. M.; Girnt, D.; Müllich, U.; Rothe, J.; Roesky, P. W.; Panak, P. J.; Denecke, M. A.; Geist, A., *C5-BPP as a ligand for actinide(III)/lanthanide(III) separation*, *ANKA Highlights 2012/2013*, **2014**, pp. 6–7.

[72] Bube, C.; Dardenne, K.; Denecke, M. A.; Kienzler, B.; Metz, V.; Prüßmann, T.; Rothe, J.; Schild, D.; Soballa, E.; Vitova, T., *μ-XAFS/XRF/XRD investigation of U(VI) phases in cement alteration products*, *ANKA User Reports 2012/2013*, KIT, **2014**, pp. 30-31.

[73] Curtius, H.; Dardenne, K., *Fe, Co, Ni K edge XAFS investigation on transition metal (M=Fe,Co,Ni) doted hydrotalcite [Mg_3-yMyAl$(OH)_8$Cl]-xH_2O*, *ANKA User Reports 2012/2013*, KIT, **2014**, pp. 32-34.

[74] Dardenne, K.; González-Robles, E.; Rothe, J.; Müller, N.; Christill, G.; Kienzler, B.; Metz, V.; Roth, G.; Geckeis, H., *XAFS investigation of a genuine HAWC glass fragment sampled from the Karlsruhe Vitrification Plant (VEK)*, *ANKA User Reports 2012/2013*, KIT, **2014**, pp. 117-118.

[75] Fellhauer, D.; Altmaier, M.; Neck, V.; Rothe, J.; Runke, J.; Fanghänel, T., *Solubility and speciation of Np(V) in alkaline $CaCl_2$ solutions*, *ANKA User Reports 2012/2013*, KIT, **2014**, pp. 26-27.

[76] Fernandes, T.; Dardenne, K.; Rothe, J.; Schild, D.; Soballa, E., *Characterisation of the environment of U and Th in the effluent of a uranium treatment plant*, *ANKA User Reports 2012/2013*, KIT, **2014**, pp. 134-136.

[77] Finck, N.; Bouby, M.; Dardenne, K., *Fate of Lu(III) during 2-line ferrihydrite transformation*, *ANKA User Reports 2012/2013*, KIT, **2014**, pp. 126-127.

[78] Finck, N.; Dardenne, K., *Zr(IV) co-precipitation with clay minerals*, *ANKA User Reports 2012/2013*, KIT, **2014**, pp. 141-142.

[79] Fröhlich, D. R.; Skerencak, A.; Rothe, J.; Panak, P. J., *EXAFS investigation on the formation of Am(III) chloro complexes in saline solutions at temperatures up to 200°C*, *ANKA User Reports 2012/2013*, KIT, **2014**, pp. 14-15.

[80] Fröhlich, D. R.; Skerencak-Frech, A.; Dardenne, K.; Rothe, J.; Panak, P. J., *EXAFS study of Am(III) complexation with oxalate as a function of pH*, *ANKA User Reports 2012/2013*, KIT, **2014**, pp. 122-123.

[81] Gaona, X.; Fellhauer, D.; Rothe, J.; Altmaier, M., *Solubility and aqueous speciation of An(VI) in NaCl solutions*, *ANKA User Reports 2012/2013*, KIT, **2014**, pp. 28-29.

[82] Heberling, F., *Eu^{3+} and Gd^{3+} sorption at Aragonite and Calcite*, *ANKA User Reports 2012/2013,* KIT, **2014**, pp. 124-125.

[83] Herm, M.; Gaona, X.; Dardenne, K.; Finck, N.; Altmaier, M., *Speciation of Nd(III) in $MgCl_2$-$Mg(NO_3)_3$ systems*, *ANKA User Reports 2012/2013*, KIT, **2014**, pp. 128-131.

[84] Huber, F. M.; Noseck, U.; Schäfer, T., *Colloid/nanoparticle formation and mobility in the context of deep geological nuclear waste disposal: (Project KOLLORADO-2) Final report*, *KIT Scientific Reports, Vol. 7545*, **2014**, p. 214.

[85] Kaufhold, S.; Stucki, J. W.; Finck, N.; Steiniger, R.; Zimina, A.; Dohrmann, R.; Ufer, K.; Pentràk, M.; Pentràkovà, L., *About the relation between tetrahedral charge and Fe-content of dioctahedral smectites and the role of tetrahedral iron*, *ANKA User Reports 2012/2013*, KIT, **2014**, p. 173.

[86] Lee, J.-Y.; Gaona, X.; Vespa, M.; Dardenne, K.; Rothe, J.; Rabung, T.; Altmaier, M.; Yun, J.-I., *Formation behavior of ternary Me-UO_2-CO_3 species in weakly alkaline condition (Me = Ca^{2+} and Mg^{2+})*, *ANKA User Reports 2012/2013*, KIT, **2014**, pp. 149-151.

[87] Olson, A. C.; Kozimor, S. A.; Vitova, T.; Loeble, M. W., *Identifying the Role of Covalency in Transuranic Extractants*, *ANKA User Reports 2012/2013*, KIT, **2014**, pp. 18-19.

[88] Petrov, V. G.; Dardenne, K.; Gaona, X.; Fellhauer, D. S.; Kalmykov, N.; Altmaier, M., *Solubility limiting Np(V) solid phases in NaCl solutions*, *ANKA User Reports 2012/2013*, KIT, **2014**, pp. 35-36.

[89] Pidchenko, I.; Fellhauer, D.; Prüßmann, T.; Dardenne, K.; Rothe, J.; Vitova, T., *Plutonium oxidation states speciation in perchloric acid by high-energy resolution XANES technique*, *ANKA User Reports 2012/2013*, KIT, **2014**, pp. 132-133.

[90] Pölz, S., *Personalised body counter calibration using anthropometric parameters*, *KIT Scientific Publishing*, **2014**.

[91] Prieur, D.; Vigier, J.-F.; Martel, L.; Dardenne, K.; Somers, J., *Structural investigation of uranium-neptunium mixed dioxides*, *ANKA User Reports 2012/2013*, KIT, **2014**, pp. 120-121.

[92] Prieur, D.; Vigier, J.-F.; Wiss, T.; Janssen, A.; Rothe, J.; Cambriani, A.; Somers, J., *Structural investigation of self-irradiation damaged AmO_2*, *ANKA User Reports 2012/2013*, KIT, **2014**, pp. 115-116.

[93] Prüßmann, T.; Dardenne, K.; Denecke, M. A.; Glatzel, P.; Pidchenko, I.; Rothe, J.; Vitova, T., *A multi-analyser crystal spectrometer at the INE-Beamline*, *ANKA User Reports 2012/2013*, KIT, **2014**, pp. 145-146.

[94] Prüßmann, T.; Pidchenko, I.; Banik, N.; Dardenne, K.; Rothe, J.; Vitova, T., *Pu L3 edge high energy-resolution X-ray absorption near edge structure investigations of actinide partitioning complexes*, *ANKA User Reports 2012/2013*, **2014**, pp. 143-144.

[95] Rabung, T.; Garcia, D.; Montoya, V.; Molinero, J., *Final Workshop Proceedings of the Collaborative Project "Crystalline Rock Retention Processes" (7th EC FP CP CROCK)*, *KIT Scientific Report 7656*, **2014**.

[96] Totskiy, Y.; Schäfer, T.; Huber, F.; Schild, D.; Geckeis, H.; Kalmykov, S., *Tc(VII) sorption on natural granite rocks and synthetic magnetite*, *Final Workshop Proceedings of the Collaborative Project 'Crystalline ROCK Retention Processes'. (7th EC FP CP CROCK)*, KIT Scientific Reports, **2014**.

[97] Wiedemann, M.; Finck, N.; Metz, V.; Geckeis, H., *EXAFS investigations on incorporated Eu(III) in brucite at high ionic strength*, *ANKA User Reports 2012/2013*, KIT, **2014**, pp. 147-148.

Invited oral presentations

[98] Altmaier, M., *Aquatic radionuclide chemistry and thermodynamics at KIT-INE*, *Geochemical Safety of Radioactive Waste Disposal - K3 Trilateral Workshop*, Daejeon, Korea, **2014**

[99] Becker, F., *Monitoring of Occupationally Exposed Individuals*, *Advanced WE-Heraeus Physics School: Ionizing Radiation and Protection of Man*, Physikzentrum Bad Honnef, **2014**

[100] Becker, F., *Recent Developments in Occupational Dosimetry*, *Advanced WE-Heraeus Physics School: Ionizing Radiation and Protection of Man*, Physikzentrum Bad Honnef, **2014**

[101] Gaona, X., *Redox chemistry, solubility and hydrolysis of Np: XAFS contribution to thermodynamics*, *7th Workshop on Speciation, Techniques, and Facilities for Radioactive Materials at Synchrotron Light Sources (AnXAS)*, Schloss Böttstein, Switzerland, **2014**

[102] Gaona, X., *Recent advances in aqueous chemistry and thermodynamics of neptunium*, *248th ACS National Meeting & Exposition*, San Francisco, USA, **2014**

[103] Geckeis, H., *Mineral-water interface reactions of actinides – all mechanisms understood?* , *Goldschmidt conference*, Sacramento, USA, **2014**

[104] Geckeis, H., *Introduction to research on repository safety at KIT-INE and the current situation in Germany*, *K3-Trilateral Workshop*, Daejeon, Korea, **2014**

[105] Geckeis, H., *Rückhaltung endlagerrelevanter Radionuklide im natürlichen Tongestein und in salinaren Systemen*, *11. Projektstatusgespräch zu BMWi-geförderten FuE-Projekten bei der Endlagerung radioaktiver Abfälle*, Karlsruhe, Germany, **2014**

[106] Geist, A., *Metals recycling from industrial materials - can one learn from nuclear fuels reprocessing?*, *247th ACS National Meeting*, Dallas, USA, **2014**

[107] Geist, A., *Actinide separations using N-donor compounds*, *TALISMAN Theoretical User Lab (ThUL)*, Karlsruhe, Germany, **2014**

[108] Kienzler, B., *Investigations on high level waste materials (spent fuel, glass, steel, cladding) at KIT-INE*, *K³ Workshop, INTEC, KAERI*, Daejon, South Korea, **2014**

[109] Kienzler, B., *Zement/Beton im Endlager*, *IKET-Kolloquium*, KIT IKET, **2014**

[110] Kienzler, B., *Nukleare Entsorgung – Abfälle, (End-) Lager, Sicherheit*, *Seminar über „Nukleare Energieerzeugung"*, KIT INR, **2014**

[111] Lützenkirchen, J., *Charging of some aluminum (oxy)(hydr)oxide polymorphs and relations to inert surfaces*, *University of Enschede*, Enschede, the Netherlands, **2014**

[112] Lützenkirchen, J., *Charge properties of alumina-polymorphs: Particles versus single crystals*, *University of Geneva*, Geneva, Italy, **2014**

[113] Lützenkirchen, J., *Reactivity at solid/water interfaces: a combined static/flow approach*, *University of Zagreb*, Zagreb, Serbia, **2014**

[114] Lützenkirchen, J., *Surface physico-chemistry, interfacial chemistry*, *1st EFCATS-CNRS European Summer School on Catalyst Preparation: Fundamental Concepts and Industrial Requirements*, Vogüé, France, **2014**

[115] Lützenkirchen, J., *Water at interfaces The potential effect of water structure on charging phenomena*, *7th Mid-European Clay Conference*, Dresden, Germany, **2014**

[116] Natrajan, L. S.; Woodall, S. D.; Swinburne, A. N.; Randall, S.; Geist, A.; Panak, P. J.; Beele, B. B.; Banik, N.; Adam, C.; Kaden, P.; Kerridge, A., *Monitoring redox and separation behavior of actinide ions by a combination of NMR and Emission Spectroscopy*, *Advanced Techniques in Actinide Spectroscopy 2014 (ATAS 2014)*, Dresden, Germany, **2014**

[117] Panak, P. J., *Time-resolved Laser Fluorescence Spectroscopy – a Valuable Tool for Actinide Speciation*, *16th International Symposium on Solubility Phenomena and Related Equilibrium Processes (ISSP16)*, Karlsruhe, Germany **2014**

[118] Panak, P. J., *Complexation and Extraction of An(III) and Ln(III) with Water-soluble SO_3-Ph-BTBP*, *7th Radiochemical Conference, RadChem 2014*, Marianske Lazne, Czech Republic, **2014**

[119] Plaschke, M.; Geckeis, H., *Radionuclide analysis by ICP-MS*, *IAEA-KIT Interregional Advanced Training Course on Marine Radioactivity*, Karlsruhe, Germany, **2014**

[120] Plaschke, M.; Geckeis, H., *Institut für Nukleare Entsorgung (INE) am KIT*, *Vortrag Universität Karlsruhe*, Karlsruhe, Germany, **2014**

[121] Plaschke, M.; Schäfer, T.; Lagos, M.; Quinto, F.; Geckeis, H., *Elemental and isotope analysis of nuclear samples at KIT-INE*, *Universität Wien*, Vienna, Austria, **2014**

[122] Pölz, S., *Personalised body counter calibration using anthropometric parameters: Application to the KIRAMS whole-body counter*, *Korea Institute of Radiological and Medical Sciences (KIRAMS)*, Seoul, South Korea, **2014**

[123] Quinto, F.; Hrnecek, E.; Krachler, M.; Shotyk, W.; Steier, P.; Winkler, S. R., *Determination of ^{239}Pu, ^{240}Pu, ^{241}Pu, ^{242}Pu and ^{236}U at femtogram and attogram levels: evidence for the migration of global fallout plutonium and uranium in an ombrotrophic peat bog profile*, *International Atomic Energy Agency (IAEA) Laboratories*, Seibersdorf, Austria, **2014**

[124] Quinto, F.; Hrnecek, E.; Krachler, M.; Shotyk, W.; Steier, P.; Winkler, S. R., *Assessing the mobility of global fallout ^{236}U and plutonium in an ombrotrophic peat bog profile: an application of super trace analysis with accelerator mass spectrometry*, *Helmholtz Zentrum München, Deutsches Forschungszentrum für Gesundheit und Umwelt (GmbH)*, Neuherberg, Germany, **2014**

[125] Quinto, F.; Hrnecek, E.; Krachler, M.; Shotyk, W.; Steier, P.; Winkler, S. R., *AMS measurements of ^{236}U and $^{239, 240, 241, 242}Pu$ in an ombrotrophic peat profile: evidence for post depositional migration of global fallout U and Pu*, *IRMM*, Geel, Belgium, **2014**

[126] Quinto, F.; Lagos, M.; Plaschke, M.; Schäfer, T.; Steier, P.; Geckeis, H., *AMS of actinides in groundwater: a new procedure for simultaneous trace analysis of U, Np, Pu, Am and Cm isotopes below ppq levels*, *Bilateral Exchange Meeting between CEA and KIT-INE*, Institut für Nukleare Entsorgung, Karlsruhe Institute of Technology, Karlsruhe, Germany, **2014**

[127] Quinto, F.; Lagos, M.; Plaschke, M.; Schäfer, T.; Steier, P.; Geckeis, H., *AMS of Actinides in Groundwater: Development of a New Procedure for Simultaneous Trace Analysis of U, Np, Pu, Am and Cm Isotopes*, *ETH-Zurich, Laboratory of Ion Beam Physics*, Zurich, Switzerland, **2014**

[128] Rabung, T., *Studies at KIT-INE on radionuclide retention using laser-based spectroscopic tools*, *K3 Trilateral Workshop, Geochemical Safety of Radioactive Waste Disposal*, Daejeon, South Korea, **2014**

[129] Rothe, J., *X-ray Absorption Fine Structure Spectroscopy (XAFS) with Synchrotron Radiation – an Introduction*, *Fifth National Crystallographic Symposium*, Sofia, Bulgaria, **2014**

[130] Rothe, J., *XAFS investigations of genuine nuclear waste glass and spent fuel particles at ANKA*, *Topical Session, FIRST-Nuclides Final Workshop*, Karlsruhe, Germany, **2014**

[131] Rothe, J.; Geckeis, H., *X-ray Absorption Fine Structure (XAFS) Determination of Actinide Speciation in Aqueous Media*, *Plutonium Futures 2014*, Las Vegas, USA, **2014**

[132] Schäfer, T., *Colloid/Nanoparticle mobility determining processes investigated by laser and synchrotron based techniques*, *European Geophysical Union (EGU), Session HS8.1.7 "Fate and transport of biocolloids and nanoparticles in soil and groundwater systems"*, Vienna, Austria, **2014**

[133] Schäfer, T., *Colloid/Nanoparticle mobility determining processes investigated by laser- and synchrotron based techniques*, *8th European Summer School on Separation Chemistry and Conditioning as well as Supramolecular, Intermolecular, Interaggregate Interactions*, Bonn, Germany, **2014**

[134] Schäfer, T.; Huber, F.; Temgoua, L.; Claret, F.; Darbha, G.; Chagneau, A.; Fischer, C.; Jacobsen, C., *Colloid/Nanoparticle mobility determining processes investigated by laserand synchrotron based techniques*, *Geophysical Research Abstracts 2014*, **2014**

[135] Skripkin, M.; Lindqvist-Reis, P.; Schimmelpfennig, B.; Apostolidis, C.; Walter, O., *Structure and spectral properties of $An(VI)O_2^{2+}$ nitrate complexes (An = U, Np, Pu) in solids and solutions*, *VII All-Russian Conference "The problems and perspectives of chemical and radiochemical control at nuclear power production"*, Sosnovy Bor, Russia, **2014**

[136] Vitova, T., *High Energy Resolution X-ray absorption spectroscopy and inelastic X-ray scattering investigations of actinide materials*, *V-th National Crystallography Symposium*, Bulgaria, Sofia, **2014**

[137] Vitova, T., *Structural investigations of actinide systems by high energy resolution X-ray absorption spectroscopy*, *LCLS/SSRL Annual Users' Meeting, joint SSRL/ALS Workshop Advances in Actinide Science from Synchrotron Spectroscopy*, SLAC National Accelerator Laboratory, Menlo Park, USA, **2014**

[138] Vitova, T., *High Energy Resolution X-ray absorption spectroscopy and inelastic X-ray scattering investigations of actinide materials The 16th International Nanoscience&Nanotechnology conference, NANO'2014*, Technical University Bulgaria, Sofia, **2014**

[139] Vitova, T., *Structural investigations of actinide systems by high energy resolution X-ray absorption spectroscopy*, *European Synchrotron Radiation Facility (ESRF) spectroscopy meeting*, Grenoble, France, **2014**

[140] Vitova, T., *Structural investigations of actinides and lanthanides by high energy resolution X-ray absorption/emission spectroscopy*, *Joint ITU-INE Workshop: Synchrotron-based spectroscopy for actinide science*, Karlsruhe, Germany, **2014**

[141] Bourg, S.; Ekberg, C.; Geist, A., *SACSESS and ASGARD — EURATOM FP7 projects on actinide separation from nuclear fuels*, *45th Annual Meeting on Nuclear Technology*, Frankfurt/M., Germany, **2014**

[142] Galán, H.; Munzel, D.; Núñez, A.; Müllich, U.; Cobos, J.; Geist, A., *Stability and recyclability of SO_3-Ph-BTP for i-SANEX process development*, *Proc. Internat. Solvent Extr. Conf. (ISEC 2014)*, Würzburg, Germany, **2014**

[143] González-Robles, E.; Bohnert, E.; Müller, N.; Herm, M.; Metz, V.; Kienzler, B., *Determination of the fission gas release in the segment N0204 and gas phase result of anoxic leaching experiment*, *Proceedings of 7th EC FP – FIRST-Nuclides 2nd Annual Workshop*, Antwerp, Belgium, **2014**

[144] Ho Mer Lin, D.; Manara, D.; Varga, Z.; Fongaro, L.; Nicholl, A.; Berlizov, A.; Lindqvist-Reis, P.; Fanghänel, T.; Mayer, K., *Exploring spectroscopic and morphological data as new signatures for uranium ore concentrates*, *IAEA Nuclear Forensics Conference* Vienna, Austria, **2014**

[145] Malmbeck, R.; Carrott, M.; Christiansen, B.; Geist, A.; Hérès, X.; Magnusson, D.; Modolo, G.; Sorel, C.; Taylor, R.; Wilden, A., *EURO-GANEX, a process for the co-separation of TRU*, *Sustainable Nuclear Energy Conference*, Manchester, UK, **2014**

[146] Malmbeck, R.; Carrott, M. J.; Geist, A.; Hérès, X.; Magnusson, D.; Miguirditchian, M.; Modolo, G.; Sorel, C.; Taylor, R. J.; Wilden, A., *The hydrometallurgical co-separation of neptunium, plutonium, americium and curium by the EURO-GANEX process*, *Proc. Internat. Solvent Extr. Conf. (ISEC 2014)*, Würzburg, Germany, **2014**

[147] Metz, V.; González-Robles, E.; Kienzler, B., *Characterization of PWR UOX fuel segments irradiated in the PWR Gösgen*, *Proceedings of 7th EC FP – FIRST-Nuclides 2nd Annual Workshop*, Antwerp, Belgium, **2014**

[148] Rabung, T.; Garcia, D.; Montoya, A.; Molinero, J., *CROCK: 'Investigations of Uncertainties in Radionuclide Transport Processes in the Far-field of a Repository in Crystalline Rock*, *8th EURADWASTE conference*, Vilnius, Lithuania, **2014**

[149] Wagner, C.; Müllich, U.; Panak, P. J.; Geist, A., *AmSel, a new system for extracting only americium from PUREX raffinate*, *Sustainable Nuclear Energy Conference*, Manchester, UK, **2014**

[150] Wilden, A.; Modolo, G.; Kaufholz, P.; Sadowski, F.; Lange, S.; Sypula, M.; Bosbach, D.; Magnusson, D.; Müllich, U.; Geist, A., *Spiked laboratory-scale continuous counter-current centrifugal contactor demonstration of a novel innovative-SANEX process. , Proc. Internat. Solvent Extr. Conf. (ISEC 2014)*, Würzburg, Germany, **2014**

[151] Wilden, A.; Modolo, G.; Kaufholz, P.; Sadowski, F.; Lange, S.; Sypula, M.; Magnusson, D.; Müllich, U.; Geist, A., *Spiked laboratory-scale continuous counter-current centrifugal contactor cemonstration of a novel innovative-SANEX process*, *Sustainable Nuclear Energy Conference*, Manchester, UK, **2014**

[152] Wilden, A.; Modolo, G.; Sadowski, F.; Lange, D.; Bremer, A.; Munzel, D.; Panak, P. J.; Geist, A., *Process development studies and demonstration of an r-SANEX process using C5-BPP – selective separation of trivalent actinides from lanthanides*, *Proc. Internat. Solvent Extr. Conf. (ISEC 2014)*, Würzburg, Germany, **2014**

[153] Wilden, A.; Modolo, G.; Sadowski, F.; Lange, S.; Bremer, A.; Munzel, D.; Panak, P. J.; Geist, A., *Process development studies and demonstration of an r-SANEX process using C5-BPP – selective separation of trivalent actinides from lanthanides*, *Sustainable Nuclear Energy Conference*, Manchester, UK, **2014**

Oral and poster presentations

[154] Adam, C.; Beele, B.; Kaden, P.; Geist, A.; Böringer, L.; Schäfer, J.; Panak, P., *Comparative NMR Study on Am(III) Complexes of nPr-BTP and C5-BPP*, *First Joint Student Workshop on f-Element Chemistry*, Manchester, UK, **2014**

[155] Adam, C.; Beele, B.; Kaden, P.; Schäfer, J.; Böringer, L.; Geist, A.; Panak, P., *Comparative NMR Study on Am(III) Complexes of nPr-BTP and C5-BPP*, *EUFEN3, Cost Action Meeting*, Erlangen, Germany, **2014**

[156] Adam, C.; Beele, B. B.; Kaden, P.; Geist, A.; Panak, P. J., *^{15}N NMR Study of C5-BPP complexes with Ln(III) and Am(III)*, *First Joint Student Workshop on f-Element Chemistry*, Manchester, UK, **2014**

[157] Adam, C.; Beele, B. B.; Kaden, P.; Geist, A.; Panak, P. J., *^{15}N NMR Study of C5-BPP complexes with Ln(III) and Am(III)*, *ThUL School in Actinide Chemistry*, Karlsruhe, Germany, **2014**

[158] Adam, C.; Kaden, P.; Beele, B. B.; Geist, A.; Denecke, M. A.; Panak, P. J., *Probing Bonding Modes in Actinide and Lanthanide Complexes by NMR Spectroscopy*, *First Joint Student Workshop on f-Element Chemistry*, Manchester, UK, **2014**

[159] Adam, C.; Kaden, P.; Beele, B. B.; Geist, A.; Denecke, M. A.; Panak, P. J., *Probing Bonding Modes in Actinide and Lanthanide Complexes by NMR Spectroscopy*, *ThUL School in Actinide Chemistry*, Karlsruhe, Germany, **2014**

[160] Adam, C.; Kaden, P.; Beele, B. B.; Müllich, U.; Geist, A.; Panak, P. J., *Evidence for covalence in a N-donor complex of Americium(III)*, *ITU-INE Research Fellows Day*, Karlsruhe, Germany, **2014**

[161] Altmaier, M.; Bourg, S.; Collings, P.; Dacheux, N.; Duplantier, B.; Ekberg, C.; Grolimund, D.; Natrajan, L.; Poinssot, C.; Raison, P.; Schaefer, T.; Scheinost, A.; Schimmelpfennig, B., *TALISMAN - A European Commission FP7 Project Promoting Transnational Access to Large Infrastructures for a Safe Management of Actinides*, *Pu-Futures – The Science 2014*, Las Vegas, USA, **2014**

[162] Altmaier, M.; Fellhauer, D.; Rabung, T.; Gaona, X., *Aquatic chemistry in alkaline $CaCl_2$ solutions: solubility and speciation of An(III), An(IV) and An(V)*, *NUWCEM 2014, 2nd International Symposium on Cement-Based Materials for Nuclear Waste*, Avignon, France, **2014**

[163] Altmaier, M.; Gaona, X.; Fellhauer, D.; Geckeis, H., *Application of fundamental aquatic chemistry to the Safety Case and the role of thermodynamic reference databases*, *DAEF Symposium 'Key Topics in Deep Geological Disposal'*, Cologne, Germany, **2014**

[164] Altmaier, M.; Gaona, X.; Fellhauer, D.; Kienzler, B., *Solubility and Speciation of An(IV): Recent Advances and Open Questions*, *Redupp International Workshop on Surface Reactivity and Dissolution of Nuclear Fuel Materials*, Stockholm, Sweden, **2014**

[165] Altmaier, M.; Kienzler, B.; Gaona, X.; Geckeis, H., *Studies on cement based materials (CEBAMA) and aquatic radionuclide chemistry in cementitious systems*, *Geodisposal 2014*, Manchester, UK, **2014**

[166] Altmaier, M.; Schäfer, T.; Geckeis, H., *The Institute for Nuclear Waste Disposal at KIT*, *TALISMAN – Plenary Meeting*, Marcoule, France, **2014**

[167] Altmaier, M.; Yalcintas, E.; Gaona, X.; Kobayashi, T.; Geckeis, H., *Redox chemistry, solubility and hydrolysis of Tc in acidic to hyperalkaline NaCl, $MgCl_2$ and $CaCl_2$ solutions*, *Symposium on Cement-Based Materials for Nuclear Waste*, Avignon, France, **2014**

[168] Bahl, S.; Koldeisz, V.; Kvashnina, K.; Yokosawa, T.; Pidchenko, I.; Geckeis, H.; Vitova, T., *Spectroscopic and microscopic characterization of U bearing multicomponent borosilicate glass*, *2nd International Workshop on Advanced Techniques for Actinide Spectroscopy (ATAS 2014)*, Dresden, Germany **2014**

[169] Bahl, S.; Koldeisz, V.; Pidchenko, I.; Prüßmann, T.; Rothe, J.; Roth, G.; Kvashnina, K.; Geckeis, H.; Vitova, T., *High energy resolution X-ray absorption near edge structure spectroscopy investigations of highly active genuine VEK glass*, *ANKA User Meeting 2014*, Karlsruhe, Germany, **2014**

[170] Bahl, S.; Kutzer, A.; Koldeisz, V.; Prüssmann, T.; Yokosawa, T.; Pidchenko, I.; Roth, G.; Geckeis, H.; Vitova, T., *Impact of increasing MoO_3 loading on the composition of multicomponent borosilicate glass*, *Actinide XAS 2014*, Schloss Böttstein, Switzerland, **2014**

[171] Bauer, N.; Fröhlich, D. R.; Panak, P. J., *Interaction of Cm(III), Eu(III) and Am(III) with human serum transferrin*, *First Joint Student Workshop on f-Element Chemistry*, Manchester, UK, **2014**

[172] Bauer, N.; Fröhlich, D. R.; Panak, P. J., *Interaction of Cm(III), Am(III) and Eu(III) with human serum transferrin INE/ITU Research Fellow Day*, Karlsruhe, Germany, **2014**

[173] Bauer, N.; Panak, P. J., *Interaction of human serum transferrin with Cm(III) studied by TRLFS*, *The third Joint Meeting of Working Groups WG1, WG2 and WG3 and the 5th Management Committee Meeting of COST Action CM1006: European f-Element Chemistry (EUFEN-3)*, Nuremberg, Germany, **2014**

[174] Baumann, A.; Yalcintas, E.; Gaona, X.; Altmaier, M.; Geckeis, H., *Solubility and hydrolysis of Tc(IV) in KCl solutions*, *16th International Symposium on Solubility Phenomena and Related Equilibrium Processes (ISSP-16)*, Karlsruhe, Germany, **2014**

[175] Baumann, A.; Yalcintas, E.; Gaona, X.; Altmaier, M.; Geckeis, H., *Chemistry of technetium in cementitious environments: solubility and hydrolysis of Tc(IV) in KCl solutions*, *3rd ITU-INE Research Fellows Day*, Karlsruhe, Germany, **2014**

[176] Becker, F., *BOOSTER-Projekt (BiO-dOSimetric Tools for triagE to Responders)*, *80. Sitzung des Arbeitskreises Dosimetrie (AKD)*, München, Germany, **2014**

[177] Becker, F., *Ein Vergleich von Monte Carlo Codes am Beispiel von Abschirmungsrechnungen zu Y-90*, *81. AKD*, Berlin, Germany, **2014**

[178] Becker, F., *Personendosimetrie: Dosisbegriffe und Dosisgrößen – Dosisgrenzwerte – Personendosismessung*, *ENTRIA Bearbeitertreffen* Goslar, Germany, **2014**

[179] Becker, F., *First draft of the protocol for NM measurements*, *EURADOS annual meeting, WG12 - Medical Staff Dosimetry*, Budapest, Hungary, **2014**

[180] Becker, F.; Kienzler, B., *Simulation of alpha dosimetry for predicting production of radiolytic species at the surface of spent nuclear fuel pellet*, *2nd Int. Conference on Radiation and Dosimetry in various Fields*, Nis, Serbia, **2014**

[181] Becker, F.; Kienzler, B., *Simulation of alpha dose for predicting radiolytic species at the surface of spent nuclear fuel pellets*, *Second International Conference on Radiation and Dosimetry in Various Fields of Research (RAD 2014)*, Nis, Serbia, **2014**

[182] Becker, F.; Pang, B.; Saurí-Suarez, H., *AP 4.5 „Individuelle Dosimetrie für Beschäftigte in Entsorgungsanlagen“*, *Transversalprojekt-Treffen „Interdisziplinäre Risikoforschung“*, Zürich, Switzerland, **2014**

[183] Borkel, C.; Montoya, V.; Kienzler, B., *Modeling long-term leaching experiments of full scale cemented wastes: effect of solution composition on diffusion*, *2nd International Symposium on Cement-based Materials for Nuclear Wastes, (NUWCEM 2014)*, Avignon, France, **2014**

[184] Borkel, C.; Montoya, V.; Kienzler, B., *Modelling long-term leaching experiments of full scale cemented wastes: effect of solution composition on diffusion*, *Transport Reaction Processes III, (TREPro 2014)*, Karlsruhe, Germany, **2014**

[185] Bremer, A.; Geist, A.; Panak, P. J., *Influence of the solvent on the complexation of Cm(III) and Eu(III) with nPr-BTP studied by time-resolved laser fluorescence spectroscopy*, *First Joint Student Workshop on f-Element Chemistry*, Manchester, UK, **2014**

[186] Bremer, A.; Whittaker, D. M.; Geist, A.; Panak, P. J., *Complexation of Cm(III) and Eu(III) with $CyMe_4$-BTBP and $CyMe_4$-BTPhen studied by time-resolved laser fluorescence spectroscopy*, *Joint ITU-INE Research Fellows‘ Day*, Karlsruhe, Germany, **2014**

[187] Brendler, V.; Altmaier, M.; Moog, H.; Voigt, W.; Wilhelm, S., *A thermodynamic reference database for nuclear waste disposal*, *DAEF Symposium 'Key Topics in Deep Geological Disposal'*, Cologne, Germany, **2014**

[188] Darbha, G.; Lützenkirchen, J.; Schäfer, T., *Probing the Reactivity of Clay-Edge Sites (Aluminol to Silanol) Towards Mineral Surfaces*, *Goldschmidt 2014*, Sacramento, USA, **2014**

[189] Dardenne, K.; González-Robles, E.; Rothe, J.; Müller, N.; Christill, G.; Kienzler, B.; Metz, V.; Roth, G.; Geckeis, H., *XAFS investigation of a HAWC glass fragment sampled from the Karlsruhe Vitrification Plant (VEK)*, *Actinide XAS 2014 - 7th Workshop on Speciation, Techniques, and Facilities for Radioactive Materials at Synchrotron Light Sources*, Schloss Böttstein, Switzerland, **2014**

[190] Fellhauer, D.; Altmaier, M.; Gaona, X.; Neck, V.; Lagos, M.; Wiss, T.; Runke, J.; Fanghänel, T., *Comparison of plutonium and neptunium redox behavior in reducing aqueous solution*, *Plutonium Futures – The Science 2014*, Las Vegas, USA, **2014**

[191] Finck, N.; Bouby, M.; Dardenne, K., *Fate of Lu(III) during 2-line ferrihydrite transformation*, *6th ANKA / KMNF Joint Users Meeting*, Karlsruhe, Germany, **2014**

[192] Friedrich, F.; Bender-Koch, C., *Characterization of iron sites in a fine grained illite*, *Mideuropean Clay Conference (MECC14)*, Dresden-Radebeul, Germany, **2014**

[193] Gaona, X.; Adam, C.; Rojo, H.; Böttle, M.; Kaden, P.; Altmaier, M., *Complexation of gluconate with Np(IV) in cementitious environments: characterization of Ca–GLU and Ca–Np(IV)–GLU systems*, *2nd International Symposium on Cement-based Materials for Nuclear Wastes (NUWCEM 2014)*, Avignon, France, **2014**

[194] Gaona, X.; Altmaier, M.; Marques-Fernandes, M.; Baeyens, B.; Skerencak-Frech, A.; Panak, P.; Kienzler, B.; Geckeis, H., *Aquatic chemistry and thermodynamics of radionuclides at elevated temperature conditions*, *IGD-TP Conference, Implementing Geological Disposal – Technology Platform*, Manchester, UK, **2014**

[195] Gaona, X.; Fellhauer, D.; Rothe, J.; Dardenne, K.; Altmaier, M., *Solubility and spectroscopic studies of Np(VI/VII) under hyperalkaline and oxidizing conditions*, *Plutonium Futures - The Science*, Las Vegas, USA **2014**

[196] Gaona, X.; Marques-Fernandes, M.; Baeyens, B.; Altmaier, M., *Solubility and hydrolysis of U(VI) at 80°C under acidic to hyperalkaline conditions*, *16th International Symposium on Solubility Phenomena and Related Equilibrium Processes (ISSP-16)*, Karlsruhe, Germany, **2014**

[197] Gaona, X.; Pallagi, A.; Adam, C.; Böttle, M.; Kaden, P.; Peintler, G.; Sipos, P.; Altmaier, M., *Thermodynamic description of the system Ca^{2+}-Na+-H^{+}-gluconate^{-}-OH^{-}-Cl^{-}-H_2O: SIT and Pitzer approaches*, *16th International Symposium on Solubility Phenomena and Related Equilibrium Processes (ISSP-16)*, Karlsruhe, Germany, **2014**

[198] Gaona, X.; Rojo, H.; Rabung, T.; Garcia, M.; Missana, T.; Altmaier, M., *Complexation of An(III) and An(IV) with gluconate under hyperalkaline pH conditions: solubility and TRLFS studies*, *16th International Symposium on Solubility Phenomena and Related Equilibrium Processes (ISSP-16)*, Karlsruhe, Germany, **2014**

[199] Geckeis, H.; Rabung, T.; Lützenkirchen, J.; Finck, N.; Rothmeier, M.; Radulescu, L., *Barrier function of a corroding iron based container*, *Key Topics in Deep Geological Disposal, DAEF 2014 Symposium*, Cologne, Germany, **2014**

[200] Geckeis, H.; Rabung, T.; Lützenkirchen, J.; Finck, N.; Rothmeier, M.; Radulescu, L., *Barrier function of a corroding iron based container*, *DAEF Symposium 'Key topics in Deep Geological Disposal 2014'*, Cologne, Germany, **2014**

[201] Geist, A., *EURO-GANEX, a process for the co-separation of TRU*, *Sustainable Nuclear Energy Conference 2014*, Manchester, UK, **2014**

[202] Geist, A., *Actinide separation processes developed in recent European research programmes*, *First Joint Student Workshop on f-Element Chemistry*, Manchester, UK, **2014**

[203] González-Robles, E.; Fuß, M.; E., B.; Müller, N.; M., H.; Metz, V.; B., K., *Study of the release of the fission gases (Xe and Kr) and the fision products (Cs and I) under anoxic conditions in bicarbonate water*, *Materials Research Society Symposium Proceedings Scientific Basis for Nuclear Waste Management XXXVI.*, Boston, USA, **2014**

[204] González-Robles, E.; Lagos, M.; Bohnert, E.; Müller, N.; Herm, M.; Metz, V.; Kienzler, B., *Fast radionuclide release from a PWR fuel rod segment (50.4 GWd/tHM) under hydrogen overpressure*, *Proceedings of the Spent Fuel Workshop*, Karlsruhe Germany, **2014**

[205] González-Robles, E.; Lagos, M.; Bohnert, E.; Müller, N.; Herm, M.; Metz, V.; Kienzler, B., *Leaching experiments with cladded pellet and fragments of a high burn-up nuclear fuel rod segment under argon/H_2 atmosphere*, *7th EC FP – FIRST-Nuclides Final Workshop*, Karlsruhe, Germany, **2014**

[206] Gonzalez-Siso, M. R.; Gaona, X.; Duro, L.; Schild, D.; Lagos, M.; Darbha, G.; Finck, N.; Altmaier, M.; Bruno, J., *Solubility and hydrolysis of Fe oxides in reducing alkaline to hyperalkaline conditions: Fe(0)-magnetite-$Fe(II)_{aq}$ systems*, *International Symposium on Solubility Phenomena and Related Equilibrium Processes (ISSP-16)*, Karlsruhe, Germany, **2014**

[207] Gorbunov, A.; Lindqvist-Reis, P.; Marsac, R., *Complexation in the systems $AnO_2(NO_3)_2$ - HNO_3 - H_2O as the chemical background of PUREX process*, *VII All-Russian Conference, The problems and perspectives of chemical and radiochemical control at nuclear power production*, Sosnovy Bor, Russia, **2014**

[208] Göttlicher, J.; Steininger, R.; Mangold, S.; Simon, R.; Vitova, T.; Rothe, J.; Gasharova, B.; Garbex, K., *New Perspectives of Synchrotron Radiation based Techniques for Mineralogical Research at ANKA*, *92nd Annual Meeting Deutsche Mineralogische Gesellschaft*, Jena, Germany, **2014**

[209] Graser, C.-H.; Banik, N. L.; Lagos, M.; Marquardt, C. M.; Geckeis, H., *Redox-Speziation von Np, Pu und Fe in wässriger Lösung mittels einer Kapillarelektrophorese gekoppelt an eine ICP-MS*, *24. ICP-MS Anwendertreffen*, Helmholtz-Zentrum Geesthacht, Germany, **2014**

[210] Graser, C.-H.; Banik, N. L.; Lagos, M.; Marquardt, C. M.; Geckeis, H., *Speciation of elements relevant to nuclear waste disposal by capillary electrophoresis hyphenated to inductively coupled plasma sector field mass spectrometer (CE-ICP-SF-MS)*, *DAEF Symposium 'Key Topics in Deep Geological Disposal'*, Cologne, Germany, **2014**

[211] Gyekye, P. K.; Becker, F.; Emi-Reynolds, G.; Pölz, S., *Monte Carlo investigation into scatter radiation from CT fluoroscopy gantry: Effect on staff dose*, *International Conference on Occupational Radiation Protection: Enhancing the Protection of Workers - Gaps, Challenges and Developments (IAEA-CN-223)*, Vienna, Austria, **2014**

[212] Langford Paden, P. M.; Alker, A. J.; Geist, A.; Kaden, P.; Adam, C.; Natrajan, L. S., *Development of a new ligand system for trivalent lanthanide-actinide separations*, *First Joint Student Workshop on f-Element Chemistry*, Manchester, UK, **2014**

[213] Hampel, A.; Günther, R.-M.; Salzer, K.; Minkley, W.; Pudewills, A.; Yildirim, S.; Rokahr, R.; Gährken, A.; Missal, C.; Stahlmann, J.; Herchen, K.; Lux, K.-H., *Joint Project III on the comparison of constitutive models for the thermo-mechanical behavior of rock salt: I. Overview and results from model calculations of healing of rock salt*, *Mechanical Behavior of Salt VIII (SALTMECH 8) Conference*, Rapid City, USA, **2014**

[214] Heberling, F., *X-ray surface diffraction investigations of calcite(104)*, *Lorentz Discussion 2014*, Leiden, the Netherlands, **2014**

[215] Heberling, F.; Eng, P.; Denecke, M. A.; Lützenkirchen, J.; Geckeis, H., *Rb^+ at the calcite(104)-water-interface*, *Lorentz Discussion 2014*, Leiden, the Netherlands, **2014**

[216] Heberling, F.; Vinograd, V. L.; Polly, R.; Gale, J. D.; Heck, S.; Rothe, J.; Bosbach, D.; Geckeis, H.; Winkler, B., *A thermodynamic adsorption/entrapment model for selenium(IV) coprecipitation with calcite*, *Selen2014*, Karlsruhe, Germany, **2014**

[217] Heide, B., *A Percolation Model for Calculating SSB- and DSB-yield*, *MiND-IBCT Workshop (Micro- and Nano-Dosimetry for Ion Beam Cancer Therapy), European Metrology Research Programme*, European Association of National Metrology Institutes, Wiener Neustadt, Austria, **2014**

[218] Herm, M.; Bohnert, E.; Böttle, M.; González-Robles, E.; Lagos, M.; Müller, N.; Kienzler, B.; Metz, V.; Geckeis, H., *Quantification and Speciation of ^{14}C from a Spent Nuclear Fuel*, *INE-ITU Research Fellow Day*, Karlsruhe, Germany, **2014**

[219] Herm, M.; Gaona, X.; Rabung, T.; Fellhauer, D.; Crepin, C.; Dardenne, K.; Altmaier, M.; Geckeis, H., *Complexation of nitrate with An(III) and Ln(III) in Na-, Mg- and Ca-brines: Thermodynamic and activity models*, *Plutonium Futures – The Science 2014,*, Las Vegas, USA, **2014**

[220] Herm, M.; Gaona, X.; Rabung, T.; Fellhauer, D.; Crepin, C.; Dardenne, K.; Altmaier, M.; Geckeis, H., *Solubility and spectroscopic study of An^{III}/Ln^{III} in dilute to concentrated Na-Mg-Ca-Cl-NO_3 solutions*, *16th International Symposium on Solubility Phenomena and Related Equilibrium Processes (ISSP16)*, Karlsruhe, Germany, **2014**

[221] Herm, M.; González-Robles, E.; Böttle, M.; Müller, N.; Bohnert, E.; Dagan, R.; Papaioannou, D.; Kienzler, B.; Metz, V.; Geckeis, H., *Quantification and speciation of ^{14}C from a spent nuclear fuel segment – methods and first results*, *27th Spent Fuel Workshop 2014*, Karlsruhe, Germany, **2014**

[222] Hinz, K.; Altmaier, M.; Gaona, X.; Rabung, T.; Alekseev, E.; Schild, D.; Geckeis, H., *Interaction of An(III/IV/V and VI) with borate in dilute to concentrated NaCl, $CaCl_2$ and $MgCl_2$ solutions*, *16th International Symposium on Solubility Phenomena and Related Equilibrium Processes (ISSP16)*, Karlsruhe, Germany, **2014**

[223] Hinz, K.; Altmaier, M.; Gaona, X.; Rabung, T.; Alekseev, E.; Schild, D.; Geckeis, H., *Interaction of An(III/IV/V and VI) with borate in dilute to concentrated NaCl, $CaCl_2$ and $MgCl_2$ solutions*, *248th ACS National Meeting*, San Francisco, USA, **2014**

[224] Hinz, K.; Altmaier, M.; Gaona, X.; Rabung, T.; Alekseev, E.; Schild, D.; Geckeis, H., *Interaction of An(III/IV/V and VI) with Borate in Dilute to Concentrated NaCl, $CaCl_2$ and $MgCl_2$ Solutions*, *Plutonium Futures – the Science 2014*, Las Vegas, USA, **2014**

[225] Huber, F.; Trinchero, P.; Molinero, J.; Schäfer, T., *Np(V) migration in a single fracture from Äspö, Sweden: Experiments and reactive transport modeling*, *FH-DGG - Tagung Fachsektion Hydrogeologie*, Bayreuth, Germany, **2014**

[226] Huber, F. M.; Schäfer, T., *Status update on the modelling work*, *CP BELBaR, 2nd Annual Meeting*, Meiringen, Switzerland, **2014**

[227] Kaden, P.; Adam, C.; Beele, B. B.; Müllich, U.; Trumm, S.; Geist, A.; Panak, P. J.; Denecke, M. A., *NMR spectroscopy on actinide containing samples*, *ThUL School in Actinide Chemistry*, Karlsruhe, Germany, **2014**

[228] Kienzler, B., *FIRST-Nuclides: Outcome, Open Questions and Steps Forward*, *IGD-TP Exchange Forum n°5*, Kalmar, Sweden, **2014**

[229] Kienzler, B., *TSWG JA6a: Cement-organics-radionuclide interactions*, *IGD-TP Exchange Forum n°5*, Kalmar, Sweden, **2014**

[230] Kienzler, B., *Results of the 7th FP Collaborative Project FIRST-Nuclides*, *27th Spent Fuel Workshop*, Karlsruhe, Germany, **2014**

[231] Kienzler, B.; Bube, C.; Metz, V.; Schlieker, M.; Bohnert, E.; Borkel, C., *Evolution of cement based materials in a repository for radioactive waste and their barrier function*, DAEF Symposium '*Key Topics in Deep Geological Disposal'*, Cologne, Germany, **2014**

[232] Kienzler, B.; González-Robles, E.; Metz, V., *FIRST-Nuclides: Selected Results*, *IGD-TP Geodisposal 2014*, Manchester, UK, **2014**

[233] Kupcik, T.; Glaus, M.; Van Loon, L.; Baeyens, B.; Schaefer, T., *Multitracer (HTO, ^{36}Cl, ^{85}Sr) diffusion in $Cu(en)_2$-illite and $Cu(en)_2$-montmorillonite*, *18. Koordinierungsgespräch KIT/INE –PSI/LES*, Villingen, Switzerland, **2014**

[234] Lindqvist-Reis, P.; Apostolidis, C.; Walter, O.; Janicki, R.; Marsac, R.; Skripkin, M.; Banik, N.; Rothe, J., *Structure and spectroscopic properties of actinyl(VI)-nitrate complexes in the solid state and in aqueous nitric acid*, *16th International symposium on solubility phenomenon and related equilibrium processes*, Karlsruhe, Germany, **2014**

[235] Metz, V., *Hydrogen effect on spent nuclear fuel corrosion under final disposal conditions*, *Fachtagung der Kerntechnischen Gesellschaft, KTG, zum Thema "Aktuelle Themen rund um das Brennelement"*, KIT Campus Nord, Eggenstein-Leopoldshafen, **2014**

[236] Metz, V., *Safety of a geological repository for nuclear waste – an outline of multi-barrier systems*, *European Nuclear Safety and Security School, Training Courses on "Introduction to the back-end of the nuclear fuel cycle"*, JRC-ITU, Karlsruhe, Germany, **2014**

[237] Metz, V.; González-Robles, E.; Dardenne, K.; Rothe, J.; Altmaier, M.; Kienzler, B.; Geckeis, H., *Current state of knowledge on long term behavior of highly active waste forms*, *DAEF Symposium "Key topics in deep geological disposal"*, Cologne, Germany, **2014**

[238] Metz, V.; Kienzler, B.; Altmaier, A.; Rabung, T.; Geckeis, H., *Radionuclide behaviour in a geological disposal system for nuclear waste*, *16th International Symposium on Solubility Phenomena and Related Equilibrium Processes (ISSP-16)*, Karlsruhe, Germany, **2014**

[239] Nargang, T. M.; Brockmann, L.; Nikolov, P.; Schild, D.; Helmer, D.; Keller, N.; Dirschka, M.; Kolew, A.; Worgull, M.; Giselbrecht, S.; Neumann, C.; Rapp, B. E., *Liquid polystyrene: a photocurable liquid polystyrene prepolymer as new materials for microfluidic prototyping.*, *18th International Conference on Miniaturized Systems for Chemistry and Life Sciences (MicroTAS 2014)*, San Antonio, USA **2014**

[240] Natrajan, L. S.; Woodall, S. D.; Swinburne, A. N.; Randall, S.; Geist, A.; Panak, P. J.; Beele, B. B.; Banik, N. L.; Adam, C.; Kaden, P.; Kerridge, A., *Monitoring Redox and Separation Behavior of Actinide Ions by a Combination of NMR and Emission Spectroscopy*, *ATAS*, Helmholtz-Zentrum Dresden-Rossendorf, Germany, **2014**

[241] Pidchenko, I.; Fellhauer, D.; Prüssmann, T.; Dardenne, K.; Rothe, J.; Bohnert, E.; Schimmelpfennig, B.; Vitova, T., *Plutonium oxidation state speciation in aqueous solution studied by Pu L and M edge high energy resolution XANES technique*, *2nd International Workshop on Advanced Techniques for Actinide Spectroscopy (ATAS 2014)*, Dresden, Germany, **2014**

[242] Pidchenko, I.; Fellhauer, D.; Prüssmann, T.; Dardenne, K.; Rothe, J.; Bohnert, E.; Schimmelpfennig, B.; Vitova, T., *Plutonium oxidation state speciation in aqueous solution studied by Pu L and M edge high-energy resolution XANES technique*, *Actinide XAS 2014*, Schloss Böttstein, Switzerland, **2014**

[243] Pidchenko, I.; Fellhauer, D.; Prüssmann, T.; Dardenne, K.; Rothe, J.; Vitova, T., *Plutonium oxidation state speciation in aqueous solution studied by high-energy resolution XANES technique*, *3rd ITU – INE Research Fellow Day*, Karlsruhe, Germany, **2014**

[244] Podkovyrina, Y.; Pidchenko, I.; Prüßmann, T.; Kvashnina, K.; Soldatov, A.; Vitova, T., *Speciation of uranium sorbed on magnetite/maghemite nanoparticles: HR-XANES and ab-initio calculations*, *Actinide XAS 2014*, Schloss Böttstein, Switzerland, **2014**

[245] Polly, R.; Schimmelpfennig, B.; Yalcinta, E.; Gaona, X.; Altmaier, M., *A quantum chemical study on Tc(IV) hydrolysis species and ternary Ca-Tc^{IV}-OH complexes in alkaline $CaCl_2$ solutions*, *ATAS 2014*, Dresden, Germany, **2014**

[246] Polly, R.; Schimmelpfennig, B.; Yalcintas, E.; Gaona, X.; Altmaier, M., *Tc(IV) hydrolysis species and ternary Ca-TcIV-OH complexes in alkaline $CaCl_2$ solutions*, *16th International Symposium on Solubility Phenomena and Related Equilibrium Processes (ISSP-16)*, Karlsruhe, Germany, **2014**

[247] Prüßmann, T.; Denecke, M. A.; Geist, A.; Rothe, J.; Lindqvist-Reis, P.; Banik, N. L.; Schimelpfennig, B.; Fellhauer, D.; Apostolidis, C.; Walter, O.; Batchelor, D. R.; Nagel, P.; Schuppler, S.; Vitova, T., *Comparative investigation of N donor ligand-lanthanide/actinide compexes from ligand point of view.*, *50th Symposium on Theoretical Chemistry*, Vienna, Austria, **2014**

[248] Prüssmann, T.; Denecke, M. A.; Geist, A.; Rothe, J.; Lindqvist-Reis, P.; Banik, N. L.; Schimmelpfennig, B.; Fellhauer, D.; Apostolidis, C.; Walter, O.; Batchelor, D. R.; Nagel, P.; Schuppler, S.; Kvashnina, K.; Vitova, T., *Comparative investigation of N donor ligand and lanthanide/actinide partitioning complexes from the metal and ligand point of view*, *Actinide XAS 2014*, Schloss Böttstein, Switzerland, **2014**

[249] Prüßmann, T.; Denecke, M. A.; Geist, A.; Rothe, J.; Lindqvist-Reis, P.; Banik, N. L.; Schimmelpfennig, B.; Fellhauer, D.; Apostolidis, C.; Walter, O.; Batchelor, D. R.; Nagel, P.; Schuppler, S.; Vitova, T., *Comparative investigation of N donor ligand and lanthanide/actinide partitioning complexes from ligand point of view*, *50th Symposium on Theoretical Chemistry 2014 Quantum Chemistry and Chemical Dynamics*, University of Vienna, Austria, **2014**

[250] Pudewills, A., *Numerical Analysis of a Drift Intersection in a Waste Repository in Rock*, *Mechanical Behavior of Salt VIII (SALTMECH 8) Conference*, Rapid City, USA, **2014**

[251] Pudewills, A., *Simulation of thermo-mechanical behavior of WIPP-salt and preliminary simulation of Room D in the WIPP site (Carlsbad, NM, USA) with ADINA code*, *US-German Workshop*, Albuquerque, USA, **2014**

[252] Pudewills, A.; Schäfer, T., *Numerical modelling of solute transport in a saturated shear zone at the Grimsel Test Site*, *20th Inter. Conf. on Computational Methods in Water Resource, CMWR*, Stuttgart, Germany, **2014**

[253] Quinto, F.; Lagos, M.; Plaschke, M.; Schäfer, T.; Steier, P.; Geckeis, H., *AMS of actinides in groundwater: development of a new procedure for simultaneous trace analysis of U, Np, Pu, Am and Cm isotopes*, *Plutonium Futures - The Science 2014*, Las Vegas, USA, **2014**

[254] Quinto, F.; Lagos, M.; Plaschke, M.; Schäfer, T.; Steier, P.; Geckeis, H., *AMS of actinides in groundwater samples: development of a new procedure for trace analysis of Pu, Np, Am and Cm isotopes*, *Deutsche Physikalische Gesellschaft (DPG) Frühjahrstagung*, Berlin, Germany, **2014**

[255] Quinto, F.; Lagos, M.; Plaschke, M.; Schäfer, T.; Steier, P.; Golser, R.; Geckeis, H., *AMS of actinides in ground- and sea-water: a new procedure for simultaneous trace analysis of U, Np, Pu, Am and Cm isotopes*, *Advanced Techniques in Actinide Spectroscopy (ATAS 2014)*, HZDR-Helmoltz-Zentrum Dresden-Rossendorf, Germany, **2014**

[256] Quinto, F.; Hrencek, E.; Krachler, M.; Shotyk, W.; Steier, P.; Winkler, S. R., *AMS measurements of ^{236}U and Pu isotopes in an ombrotrophic peat bog profile: evidence for post depositional migration of global fallout radionuclides*, *Deutsche Physikalische Gesellschaft (DPG) Frühjahrstagung*, Berlin, Germany, **2014**

[257] Polly, R.; Schimmelpfennig, B.; Yalcintas, E.; Gaona, X.; Altmaier, M., *A quantum chemical study on Tc(IV) hydrolysis species and ternary Ca-Tc^{IV}-OH complexes in alkaline $CaCl_2$ solutions*, *50th Symposium of theoretical chemistry*, Vienna, Austria, **2014**

[258] Rojo, H.; Gaona, X.; Rabung, T.; Garcia, M.; Missana, T.; Altmaier, M., *Nd(III)/Cm(III) complexation with gluconate in NaCl and $CaCl_2$ alkaline solutions: solubility and TRLFS studies*, *2nd International Symposium on Cement-based Materials for Nuclear Wastes (NUWCEM 2014)*, Avignon, France, **2014**

[259] Rothe, J.; Dardenne, K.; Denecke, M. A.; Prüßmann, T.; Vespa, M.; Vitova, T.; Geckeis, H., *Actinide and radionuclide speciation by X-ray absorption spectroscopy methods at ANKA – a facility report*, *AnXAS 2014, 7th Workshop on Speciation, Techniques, and Facilities for Radioactive Materials at Synchrotron Light Sources*, Schloss Böttstein, Switzerland, **2014**

[260] Rothe, J.; Dardenne, K.; Denecke, M. A.; Prüßmann, T.; Vespa, M.; Vitova, T.; Geckeis, H., *X-ray Absorption Spectroscopy for radionuclide speciation in support of the nuclear waste disposal safety case*, *IGD-TP Geodisposal 2014*, Manchester, United Kingdom, **2014**

[261] Saurí-Suarez, H.; Pang, B.; Becker, F.; Geckeis, H., *Entwicklung von Verfahren für die individuelle Dosimetrie für Beschäftigte in Entsorgungsanlagen (AP 3.4.5)*, *Großes ENTRIA-Projekttreffen*, Goslar, Germany, **2014**

[262] Schäfer, T.; Blechschmidt, I.; Brendle, J.; Hauser, W.; Heck, S.; Huber, F.; Lagos, M.; Martin, A.; Reimus, P., *The latest results on colloid associated radionuclide mobility from the CFM project, Grimsel (Switzerland)*, *FH-DGG - Tagung Fachsektion Hydrogeologie*, Bayreuth, Germany, **2014**

[263] Schepperle, J.; Fellhauer, D.; Gaona, X.; Altmaier, M.; Geckeis, H., *Solubility and hydrolysis of NpO_2(am) and PuO_2(am) in dilute to concentrated NaCl solutions*, *International Symposium on Solubility Phenomena and Related Equilibrium Processes (ISSP16)*, Karlsruhe, Germany, **2014**

[264] Schepperle, J.; Fellhauer, D.; Gaona, X.; Altmaier, M.; Geckeis, H., *Investigation of the Solubility and Complexation of Plutonium and Neptunium in reducing aquatic systems*, *3rd ITU – INE Research Fellow Day*, Karlsruhe, Germany, **2014**

[265] Schild, D.; Beele, B. B.; Schimmelpfennig, B.; Trumm, S.; Panak, P. J., *Complexation of Eu(III) with ^{n}Pr-BTP studied by XPS*, *2nd International Workshop on Advanced Techniques for Actinide Spectroscopy (ATAS 2014)*, Dresden, Germany **2014**

[266] Schimmelpfennig, B.; Trumm, M.; Panak, P. J.; Geist, A., *Development of accurate force field parameters for An(III)/Ln(III) ions in aqueous solution*, *International Workshop on Advanced Techniques in Actinide Spectroscopy (ATAS)*, Dresden-Rossendorf, Germany, **2014**

[267] Schnurr, A.; Marsac, R.; Rabung, T.; Lützenkirchen, J.; Geckeis, H., *Sorption studies of actinides/lanthanides onto clay minerals under saline conditions*, *248th ACS National Meeting*, San Francisco, USA, **2014**

[268] Schnurr, A.; Marsac, R.; Rabung, T.; Lützenkirchen, J.; Geckeis, H., *Sorption studies of actinides/lanthanides onto clay minerals under saline conditions*, *TrePro III – Workshop on Modelling of Coupled Reactive Transport Processes*, Karlsruhe, Germany, **2014**

[269] Steier, P.; Lachner, J.; Priller, A.; Quinto, F.; Sakaguchi, A.; Winkler, S.; Golser, R., *The AMS isotope Uranium-236 at VERA*, *13th Accelerator Mass Spectrometry Conference (AMS 2014)*, Aix-en-Provence, France, **2014**

[270] Temgoua, L.; Chagneau, A.; Schäfer, T.; Geckeis, H., *Influence of reaction parameters on the nucleation and growth of $SrSO_4/SrCO_3$ determining the fate of An(III)/Ln(III)*, *Goldschmidt 2014*, Sacramento, USA, **2014**

[271] Temgoua, L.; Schäfer, T.; Geckeis, H., *Influence of reaction parameters on the nucleation and growth of $SrSO_4/SrCO_3$ determining the fate of An(III)/Ln(III)*, *ImmoRad Project Meeting 2014*, Oviedo, Spain, **2014**

[272] Tits, J.; Gaona, X.; Laube, A.; Wieland, E., *Influence of the redox state on the neptunium sorption under hyperalkaline highly alkaline conditions: Batch sorption studies on titanium dioxide and calcium silicate hydrates*, *17th Radiochemical Conference*, Marianske Lazne, Czech Republic, **2014**

[273] Tits, J.; Stumpf, T.; Walther, C.; Gaona, X.; Wieland, E., *Sorption of actinides onto titanium dioxide, calcium silicate hydrates and hardened cement paste*, *2nd International Symposium on Cement-based Materials for Nuclear Wastes (NUWCEM 2014)*, Avignon, France, **2014**

[274] Totskiy, Y.; Huber, F.; Schild, D.; Schäfer, T.; Kalmykov, S.; Geckeis, H., *Tc(VII) immobilization on granitic rocks from Äspö (Sweden) and Nizhnekansky massif (Russia)*, *TRePro III – Workshop on Modelling of Coupled Reactive and Transport Processes*, Karlsruhe, Germany, **2014**

[275] Totskiy, Y.; Huber, F.; Schild, D.; Schäfer, T.; Kalmykov, S.; Geckeis, H., *Tc(VII) immobilization on granitic rocks from Äspö HRL (Sweden) and Nizhnekansky massif (Russia)*, *Goldschmidt 2014*, Sacramento, USA, **2014**

[276] Totskiy, Y.; Yalcintas, E.; Huber, F.; Gaona, X.; Schäfer, T.; Altmaier, M.; Kalmykov, S.; Geckeis, H., *A contribution from fundamental and applied technetium chemistry to the nuclear waste disposal safety case*, *DAEF Symposium 'Key Topics in Deep Geological Disposal'*, Cologne, Germany, **2014**

[277] Trumm, M.; Lindqvist-Reis, P.; Schimmelpfennig, B., *Properties of solvent-shared and contact ion pairs in aqueous Ln(III) and An(III) perchlorate solutions*, *16th International symposium on solubility phenomenon and related equilibrium processes (ISSP16)*, Karlsruhe, Germany, **2014**

[278] Trumm, M.; Lindqvist-Reis, P.; Schimmelpfennig, B., *Properties of solvent-shared and contact ion pairs in aqueous Ln(III) and An(III) perchlorate solutions*, *50th Symposium on Theoretical Chemistry*, Vienna, Austria, **2014**

[279] Vasiliev, A. N.; Banik, N. L.; Marsac, R.; Marquardt, C. M.; Kalmykov, S. N., *Study of Np(V) Complexation with Propionate and Lactate at Varying Ionic Strengths and Temperatures*, *ISSP 16*, Karlsruhe, Germany, **2014**

[280] Vespa, M.; Dardenne, K.; Denecke, M. A.; Prüssmann, T.; Rothe, J.; Vitova, T.; Geckeis, H., *New X-ray absorption spectroscopic opportunities for actinides and radionuclides experiments: INE-Beamline & CAT-ACT at ANKA*, *Deutsche Tagung für Forschung mit Synchrotronstrahlung, Neutronen und Ionenstrahlen an Großgeräten* Bonn, Germany, **2014**

[281] Wagner, C.; Müllich, U.; Geist, A.; Panak, P. J., *Water soluble BTBP ligand – a highly efficient ligand for the separation of Am(III) and Cm(III)*, *First Joint Student Workshop on f-Element Chemistry*, Manchester, UK, **2014**

[282] Wagner, C.; Müllich, U.; Geist, A.; Panak, P. J., *A new System for separation Am(III) from PUREX Raffinate*, *International solvent extraction conference (ISEC)*, Würzburg, Germany, **2014**

[283] Wallner, A.; Belgya, T.; Bichler, M.; Buczak, K.; Christl, M.; Dillmann, I.; Fifield, L. K.; Hotchkis, M.; Käppeler, F.; Krasa, A.; Lachner, J.; Lippold, J.; Plompen, A.; Quinto, F.; Semkova, V.; Srncik, M.; Steier, P.; Szentmiklosi, L.; Tims, S.; Winkler, S., *A novel method for studying neutron-induced reactions on actinides*, *13th Accelerator Mass Spectrometry Conference (AMS 2014)*, Aix-en-Provence, France, **2014**

[284] Wallner, A.; Faestermann, T.; Feldstein, C.; Golser, R.; Knie, K.; Korschinek, G.; Kutschera, W.; Ofan, A.; Paul, M.; Priller, A.; Quinto, F.; Rugel, G.; Steier, P., *Search for interstellar ^{244}Pu as a probe for recent heavy-element nucleosynthesis*, *13th Accelerator Mass Spectrometry Conference (AMS 2014)*, Aix-en-Provence, France, **2014**

[285] Wiedemann, M.; Metz, V.; Rabung, T.; Finck, N.; Geckeis, H., *Interaction of Eu(III) and Cm(III) with $Mg(OH)_2(cr)$ in the system Mg^{2+}-Na^+-Cl^--OH^--H_2O*, *16th International Symposium on Solubility Phenomena and Related Equilibrium Processes (ISSP-16)*, Karlsruhe, Germany, **2014**

[286] Will, P.; Friedrich, F.; Hochleitner, R.; Gilg, H. A., *Fraipontite in the hydrothermally overprinted oxidation zone of the Preguiça mine, Southern Portugal*, *Mideuropean Clay Conference (MECC14)*, Dresden-Radebeul, Germany, **2014**

[287] Woodall, S.; Swinburne, A.; Kaden, P.; Adam, C.; Banik, N. L.; Denecke, M. A.; Natrajan, L., *Addressing Oxidation State Selectivity in Neptunyl(VI) Chemistry*, *First Joint Student Workshop on f-Element Chemistry*, Manchester, UK, **2014**

[288] Yalcintas, E.; Gaona, X.; Altmaier, M.; Geckeis, H., *Thermodynamic description of Tc(IV) solubility and hydrolysis in dilute to concentrated NaCl, $MgCl_2$ and $CaCl_2$ solutions*, *16th International Symposium on Solubility Phenomena and Related Equilibrium Processes (ISSP16)*, Karlsruhe, Germany, **2014**

[289] Yalcintas, E.; Gaona, X.; Scheinost, A. C.; Altmaier, M.; Geckeis, H., *Aquatic chemistry and thermodynamics of Tc in dilute to concentrated saline systems*, *8th International Symposium on Technetium and Rhenium: Science and Utilization*, La Baule - Pornichet, France, **2014**

[290] Yokosawa, T.; Zandbergern, H. W., *In-situ TEM on (de)hydrogenation and oxidation/reduction of Pd at high pressures.*, *2nd Conference on In-situ and Correlative Electron Microscopy (CISCEM 2014)*, Saarbrücken, Germany, **2014**

Patents

[291] Becker, F., (Ed.: KIT), **2014**.

Others

[292] Altmaier, M.; Duro, L.; Grivé, M.; Montoya, V.; Buckau, G.; Kienzler, B., *RECOSY: "Understanding of Redox Phenomena Controlling the Long-term Release/Retention of Radionuclides in Nuclear Waste Disposal"*, *EURADWASTE '13 - 8th EC Conference on the Management of Radioactive Waste, Book of Abstracts*, Vilnius, Lithuania, **2014**

[293] Altmaier, M.; Gaona, X.; Fellhauer, D.; Buckau, G., *ReCoSy – Intercomparison Exercise on Redox Determination Methods*, *EURADWASTE '13 - 8th EC Conference on the Management of Radioactive Waste, Book of Abstracts*, Vilnius, Lithuania, **2014**

[294] Altmaier, M.; Gaona, X.; Geckeis, H., in *Online-Zeitschrift GDCh*, **2014**.

[295] Bouby, M.; Heyrich, Y.; Heck, S.; Schäfer, T., *On bentonite colloid stability and DOC effect*, *Status Report CP-BelBar (FP7 295487), Work Package 4, Deliverable 4.5*, **2014**.

[296] Bouby, M.; Heyrich, Y.; Heck, S.; Schäfer, T., *on the influence of complexing agents on clay colloid stability:Influence of organic matter (fulvic acids) on the stability of clay colloids prepared under different chemical conditions*, *Status Report CP-BelBar (FP7 295487), Work Package 4, Deliverable 4.6*, **2014**.

[297] Bouby, M.; Norrfors, K. K.; Heyrich, Y.; Heck, S.; Schäfer, T., *Understanding of radionuclide colloid interaction: Bentonite colloid size effect on the radionuclide sorption and reversibility and tetravalent actinide clay colloid interaction*, *Status Report CP-BelBar (FP7 295487), Work Package 3, Deliverable 3.6*, **2014**.

[298] Bouby, M.; Schäfer, T.; Heck, S., *On the effects of the water chemistry and clay chemistry on erosion processes*, *Status Report CP-BelBar (FP7 295487), Work Package 2, Deliverable 2.4*, **2014**.

[299] Duro, L.; Bruno, J.; Grivé, M.; Montoya, V.; Kienzler, B.; Altmaier, A.; Buckau, G., *Redox Processes in the Safety Case of Deep Geological Repositories of Radioactive Wastes – Contribution of the European RECOSY Collaborative Project.*, *EURADWASTE '13 - 8th EC Conference on the Management of Radioactive Waste, Book of Abstracts*, Vilnius, Lithuania, **2014**

[300] González-Robles, E.; Loida, A.; Müller, N.; Bohnert, E.; Herm, M.; Montoya, V.; Kienzler, B.; Metz, V., *Investigation of the Corrosion Behaviour of Spent Nuclear Fuel Fragments in High pH Solutions under H_2 Overpressure*, KIT-INE, **2014**.

[301] Herm, M.; Tanabe, H.; Sakuragi, T.; Tateishi, T.; Yamashita, Y.; Böttle, M.; González-Robles, E.; Kienzler, B.; Bottomley, P. D. W.; Serrano-Purroy, D.; Wegen, D. H.; Metz, V., *Description of the analytical procedure for gaseous and dissolved C-14 species quantification*, *CAST project report*, **2014**.

[302] Kienzler, B.; Bohnert, E.; González-Robles, E.; Herm, M.; Gaona, X.; Borkel, C., *Thermodynamic Considerations on the Speciation of ^{14}C in Spent Nuclear Fuel*, *KIT-SR 7676*, Karlsruhe Institute of Technology (KIT), **2014**.

[303] Kienzler, B.; Metz, V.; Duro, L.; Valls, E. A., *2nd Annual Workshop Proceedings of the Collaborative Project 'FIRST-Nuclides*, *KIT-SR 7676*, Karlsruhe Institute of Technology (KIT), **2014**.

[304] Kienzler, B.; Metz, V.; Duro, L.; Valls, E. A., *Final Workshop Proceedings of the Collaborative Project 'FIRST-Nuclides*, **2014**.

[305] Metz, V.; Gonzalez-Robles, E.; Kienzler, B., *Characterization of UOX fuel segments irradiated in the Gösgen pressurized water reactor*, *KIT-SR 7676*, Karlsruhe Institute of Technology (KIT), **2014**.

[306] Metz, V.; Rosenberg, Y. O.; Böttle, M.; Ganor, J., *Ra-Ba precipitation in laboratory and large-scale evaporitic systems. In "Natural Analogues for Safety Cases of Repositories in Rock Salt"*, *Salt Club Workshop Proceedings*, Nuclear Energy Agency, NEA, Paris, **2014**

[307] Montoya, V.; Kupcik, T.; Rabung, T.; Tournassat, C.; Glaus, M. A.; Schaefer, T.; Van Laer, L.; Bruggeman, C.; Maes, N.; Aertsens, M.; Frick, S.; Van Loon, L. R.; Gaboreau, S.; Robinet, J.-C.; Savoye, S.; Jacquier; Appelo, T.; Altmann, S., *Processes of cation migration in clayrocks CatClay Project, Final Scientific Report* **2014**.

[308] Podkovyrina, Y.; Pidchenko, I., *Speciation of uranium after interaction with magnetite nanoparticles using high-resolution XANES techniques*, *G-RISC(German-Russian Interdisciplinary Science Center)*, **2014**.

[309] Pölz, S.; Breustedt, B., *Verbundprojekt Strahlung und Umwelt II: Radionuklide in der Umwelt, ihr Transport in Nahrungsketten zum und im Menschen. Teilprojekt A (Arbeitspaket 3.2): Zähleffizienzkalibrierung von in vivo Messsystemen mit probanden-adaptierten anthropomorphen Phantomen* Karlsruher Institut für Technologie, **2014**.

[310] Röhlig, K. J.; Walther, C.; Bach, F. W.; Brunnengräber, A.; Budelmann, H.; Chaudry, S.; Eckhardt, A.; Geckeis, H.; Grunwald, A.; Hassel, T.; Hocke, P.; Lux, K. H.; Mengel, K.; Metz, V.; Ott, K.; Plischke, E.; Riemann, M.; Smeddinck, U.; Schreurs, M.; Stahlmann, J., *ENTRIA 2014: Memorandum zur Entsorgung hochradioaktiver Reststoffe*, *Niedersächsische Technische Hochschule, Hannover*, **2014**.

[311] Sánchez, V.; Coeck, M.; Manara, D.; Schillebeeckx, P.; Lennox; Metz, V.; Cabellos, O.; Paul; Legrady, D.; Kyrki-Rajamaki, R., *Content and curriculum of courses in open literature*, *Graduate and Executive Nuclear Training and Lifelong Education - GENTLE, Deliverable D3.1.*, European Commission, Brussels, **2014**.

[312] Wegen, D. H.; Papaioannou, D.; Nasyrow, R.; Gretter, R.; Paperini, G.; van Winckel, S.; Serrano Purroy, D.; Martínez Torrens, A.; Sureda, R.; Schubert, A.; Rondinella, V. V.; Glatz, J. P.; Metz, V., *Fast / Instant Release of Safety Relevant Radionuclides from Spent Nuclear Fuel (FIRST-Nuclides): Characterisation of spent UO_2 fuel used for experimental work in FIRST-Nuclides*, *FIRST-Nuclides Deliverable No 1.3.*, European Commission, Brussels, **2014**.

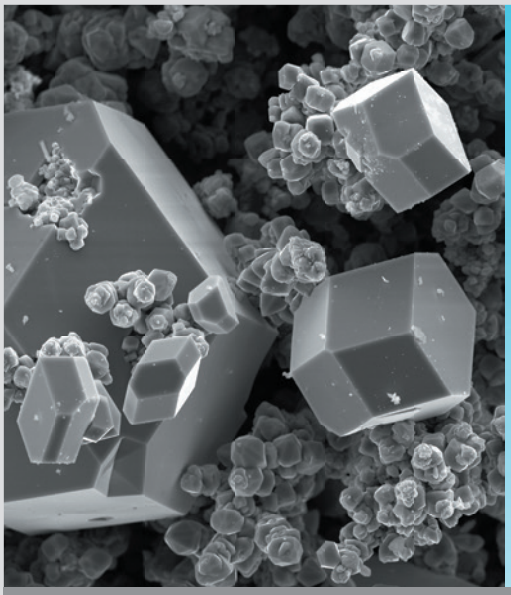

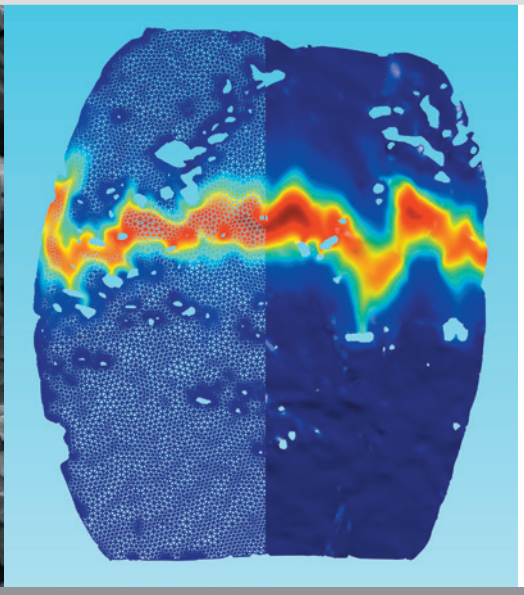

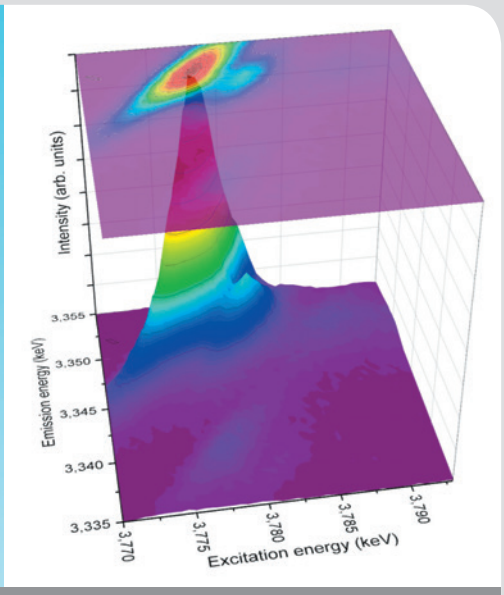

ISSN 1869-9669